Synthesis and Characterization of Triazine-Based Chemical Probes

Author: Kyle S. Cole

Synthesis and Characterization of Triazine-Based Chemical Probes

Kyle S. Cole

A dissertation

submitted to the Faculty of

the department of Chemistry

in partial fulfillment

of the requirements for the degree of

Doctor of Philosophy

Boston College
Morrissey College of Arts and Sciences
Graduate School

January 2018

SYNTHESIS AND CHARACTERIZATION OF TRIAZINE-BASED CHEMICAL PROBES

Kyle S. Cole

Advisor: Eranthie Weerapana, Ph.D.

The 1,3,5-triazine is a privileged scaffold in that it is planar and has three-fold symmetry which allows for controlled modification around the ring structure with various substituents. In this thesis, we report on two modular inhibitor libraries that center around a 1,3,5-triazine core scaffolding system, which have been shown to target protein disulfide isomerase A1 (PDIA1), glutaredoxin-3 (GLRX3), and 6-phosphofructo-1-kinase (PFKP). Protein disulfide isomerase A1 (PDIA1) is a thiol-disulfide oxidoreductase localized in the lumen of the endoplasmic reticulum (ER), and is an important folding catalyst and chaperone for proteins in the secretory pathway. PDIA1 contains two active-site domains (a and a'), each containing a Cys-Gly-His-Cys (CGHC) active-site motif. Here, we synthesize a targeted library o second-generation triazine-based inhibitors to optimize the potency and selectivity of our lead compound, RB-11-ca. Characterization of this targeted library afforded an optimized PDIA1 inhibitor, KSC-34, which covalently modifies C53 in the a site of PDIA1 and demonstrates time-dependent inhibition of the reductase activity of PDIA1 in vitro with a k_{inact}/K_I = 9.66 x 10^3 $M^{-1}s^{-1}$. Interestingly, KSC-34 treatment demonstrated that **a**-site inhibition led to decreased secretion of amyloidogenic antibody light chain, thus illustrating that site-selective inhibitors like KSC-34 provide useful tools for delineating the pathological role and therapeutic potential of PDIA1.

In 2014, our lab first reported on RB7, a dichlorotriazine-based electrophilic small

molecule which displayed extremely high reactivity and selectivity toward lysine residues in the proteome. Herein, we further on this study by investigating the unique reactivity of RB7 through the synthesis of a second-generation small molecule electrophile library and investigating proteome-wide reactivity in vitro and in situ. This library afforded KSC-46, an RB-7 analogue with p-chlorothiophenol tuning element, which provided optimal proteome reactivity to use as a scaffold for the generation of a targeted library. To take advantage of the tuned reactivity of KSC-46, a second-generation targeted library was generated to target react residues in the proteome. This library yielded two molecules, KSC-56 and KSC-65, which were identified to target glutaredoxin-3 (GLRX3) and 6-phosphofructo-1-kinase (PFKP), respectively. GLRX3 is a cytosolic, monothiol iron-sulfur cluster chaperon protein which relies on two nucleophilic cysteine residues to bind and transfer iron clusters. PFKP is known to catalyze the first irreversible step in glycolysis and regulates the flux of glucose metabolism in the cell, which makes PFKP an attract therapeutic target. KSC-56 was further characterized to bind to Cys261 in the C-terminal glutaredoxin domain of GLRX3.

For my father,
Stephen

ACKNOWLEDGEMENTS

I'd like to first begin by thanking my advisor, Eranthie Weerapana. Thank you for taking a chance and allowing me to work in your lab these past five years. I've learned a great deal and couldn't have evolved into the scientist I am today without your guidance. Thank you also for giving me the tools and resources to allow me to explore my own ideas. I truly enjoyed the opportunity and experience of working in your lab. I would also like to thank the members of my committee, Abhishek Chatterjee and Jianmin Gao. Thank you both for your advice, guidance, and help over the past years.

I'd also like to thank all of my collaborators with whom I've worked with over the years. A special thank you to Professor Luke Wiseman and Julia Grandjean for their work assessing the effects of KSC-34 treatment on the secretion of amyloidogenic light chains. Another thank you the Professor Matt Shoulders and Kenny Chen who helped with qPCR experiments to assess the activation of the unfolded protein response upon treatment with KSC-34. Another thank you to all of my other collaborators at Michigan, Case Western, and in the Chatterjee lab at BC, thank you for helping me to grow as a scientist.

To all of the members of the Weerapana lab, past and present: Nick, Alex, Yani, Julie, Shalise, Lisa, Tyler, Haley, Dan, Masahiro, Aaron, Jenny, Ari, Collin, Mattia, Eleni, Julia, Ben, and Rebecca; thank you all helping me to learn something new every day. Collin, you're the greatest undergrad anybody could ask for. You've done so much work over the last year and a half, I couldn't have done this without you. Best of luck in graduate school, I'll miss you bro. Masahiro, you're a synthesis machine. Thanks for all of the conversations and help over the years. Ari, thanks for showing me how to spatchcock a

chicken. By far the tasty thing I've learned during my time in grad school haha. I'll miss you man, never lose your humor.

To my friends and family, thank you all for the support over all of these years. I can finally answer that question "When are you getting a job?". I couldn't have done this without everyone. A special thanks to my wife, Alexandra. Thanks for sticking by me through everything. This is just as much your accomplishment as it is mine. I cannot thank you enough.

TABLE OF CONTENTS

LIST OF TABLES

LIST OF FIGURES

Chapter 2.

fluorescence intensity of the PDIA1 band. All data are normalized to RB-11-ca lead compound. Error bars represent SD for n = 3 experiments.

Figure 2.7. Characterization of PDIA1 second-generation library members. To assess cell permeability as well as selectivity of the library, probes (5 μM) were incubated with MCF-7 cells for 3 hours at 37 °C. Following cell lysis and in-gel fluorescence, KSC-34 was found to be ~8-fold more potent than the lead compound, RB-11-ca, in whole cells against PDIA1 (left panel). Coomassie gel (right panel is provided to show normalized protein abundance).

Figure 2.8. Concentration and time-dependent inhibition of PDIA1 by KSC-34, RB-11-ca, and 16F16. PDIA1 reductase activity was measured using an insulin reduction assay in a 100 μL reaction volume containing 0.5 μM PDIA1, 0.16 mM insulin, and 1 mM DTT in assay buffer. Turbidity of the insulin solution was measured over time at various concentrations and pre-incubation times with KSC-34. Error bars are calculated as SD from n = 2 experiments.

Figure 2.9. Evaluation of the site-selectivity of KSC-34. (A) Labeling of purified recombinant PDIA1 WT, C397A and C53A by KSC-34. Each recombinant PDIA1 protein (50 μg/mL) was incubated with KSC-34 (5 μM) for 1 hour, and subjected to CuAAC prior to in-gel fluorescence. (B) Structures of KSC-34 and Chloroacetamide-Rhodamine (CA-Rh). (C) PDIA1 C53A and C397A (50 μg/mL) in the background of MCF-7 lysates (1 mg/mL) were treated with increasing concentrations of KSC-34, RB-11-ca and 16F16 to quantify the selectivity for the a and a' domains. Following incubation, samples were then treated with CA-Rh) to append a fluorophore to the residual, unmodified PDIA1 active sites. Loss of fluorescence indicates inhibitor binding. ImageJ (NIH) was used to quantify the loss in fluorescence and calculate affinities for each active site. (D) Active-site selectivity for KSC-34, RB-11-ca, and 16F16. KSC-34 was found to have a 30-fold selectivity for the a domain over the a' domain, compared to RB-11-ca which exhibited a 21-fold selectivity and 16F16 which exhibited 2-fold selectivity. Error is calculated by PRISM as ± SEM from n = 3 experiments.

Figure 2.10. Evaluation of selectivity of KSC-34. PDI isoform selectivity. KSC-34 was found to only covalently modify PDIA1 over PDIA3 and PDIA4, two closely related family members.

Figure 2.11. Evaluation of proteome-wide selectivity of KSC-34. Mass spectrometry analysis of proteins enriched in KSC-34 (5 μM) and DMSO treated MCF-7 cells. The spectral count difference between KSC-34-treated and DMSO-treated samples are plotted for all proteins identified (Table 1). Errors bars show SD for n = 2 experiments.

Figure 2.12. (A) Identification of KSC-34 cellular occupancy of PDIA1. MCF-7 cells were treated with varying concentrations of KSC-34na. Following lysis, protein concentrations were normalized and subjected to treatment with KSC-34 (5

μM) to modify any residual PDIA1 a domain active site, C53. An EC_{50} of ~4 μM was calculated for KSC-34na labeling of PDIA1 in MCF-7 whole cells. All data are normalized to RB-11-ca lead compound. Error bars represent ± SD for n = 3 experiments. (B) MTT assay data in MCF-7 cells treated with varying concentrations of KSC-34. The calculated EC_{50} of KSC-34 was determined to be 82 μM. All data are normalized to vehicle treated cells. Error bars represent ± SD for n = 3 experiments.

Figure 2.13. Effects of KSC-34 on cell viability and the unfolded protein response. (A) qPCR analysis of UPR target genes following concentration-dependent treatment of MCF-7 cells with KSC-34 for 3 hours at 37 °C. Data are reported as the mean fold change (relative to DMSO) ± SEM from three biological replicates. (B) XBP1 splicing assay for MCF-7 cells treated with varying concentrations of KSC-34 for 3 hours.

Figure 2.14. Effects of KSC-34 on the unfolded protein response. qPCR analysis of UPR target genes following co-treatment of MCF-7 cells with KSC-34 (20 μM) and IRE1α inhibitor, 4μ8c. Data are reported as the mean fold change (relative to DMSO) ± SEM from three biological replicates.

Figure 2.15. Effects of KSC-34 on the unfolded protein response. (A) Activation of UPR target genes in MCF-7 cells was assessed by measuring the relative mRNA expression levels of target genes by qRT-PCR after treating with KSC-34 (20 μM) for increasing time. Transcripts were normalized to the housekeeping gene RPLP2, and all reactions were performed in technical quadruplicate. Data are reported as the mean fold change (relative to DMSO) ± SEM from three biological replicates. (B) XBP1 splicing assay for time-course experiment, where MCF-7 cells were treated with 20 μM KSC-34. Gel shows three biological replicates for each condition.

Figure 2.16. Activation of UPR target genes in A549 cells (A) or SKOV-3 cells stably expressing shPDIA1, shPDIA4 or shGFP (B). The relative mRNA expression levels of target genes were assessed by qRT-PCR after treating with increasing concentrations of KSC-34 or 5 μM of thapsigargin. Transcripts were normalized to the housekeeping gene RPLP2. (A) For A549 cells, all reactions were performed in technical quadruplicate, and data are reported as the mean fold change (relative to DMSO) ± SEM from three biological replicates. (B) For SKOV-3 cells, data are reported as mean fold change (relative to shGFP DMSO) ± SEM from reactions performed in triplicate.

Figure 2.17. KSC-34 reduces secretion of destabilized ALLC from mammalian cells. (A) Immunoblot of anti-FLAG IPs of lysates prepared from $HEK293^{DAX}$ cells transiently transfected with ^{FT}ALLC and pre-treated for 1 h with vehicle or KSC-34 (40 μM). Cells were crosslinked for 30 min with DSP (500 μM) prior to lysis. Mock transfected cells are included as a control. (B) Graph showing secreted ^{FT}ALLC (grey) and viability (blue) of $HEK293^{Trex}$ cells stably expressing ^{FT}ALLC

pretreated for 4 h with KSC-34 (40 μM). Media was conditioned for 2 h in the presence or absence of KSC-34 (40 μM) prior to quantification of secreted ^{FT}ALLC by ELISA. Viability was measured following media conditioning by Cell Titre Glo. All data are normalized to vehicle-treated cells. Error bars show SEM for n=3 experiments. ***p<0.005.

Figure 2.18. KSC-34 reduces secretion of destabilized ALLC from mammalian cells. Representative autoradiogram and quantification of the fraction [^{35}S]-labeled ^{FT}ALLC secreted from HEK293^{DAX} cells using the experimental paradigm shown. Experiments were performed in the absence or presence of KSC-34 (40 μM) added 1 h prior to labeling and then again throughout the experiment. Fraction secreted was calculated as described in Materials and Methods (64). Error bars show SEM for n=4. ***p<0.005.

Figure 2.19. KSC-34 reduces secretion of destabilized ALLC from mammalian cells. (A) Graph showing fold change mRNA levels of PDIA1 in HEK293^{DAX} cells and HEK293^{DAX} cells shRNA-depleted of PDIA1 measured by qPCR. Error bars show 95% confidence interval. (B) Graph showing secreted ^{FT}ALLC (grey) and viability (blue) of HEK293^{DAX} cells transiently expressing ^{FT}ALLC pretreated for 4 h with KSC-34 (40 μM). HEK293^{DAX} cells stably expressing PDIA1 shRNA are indicated. Media was conditioned for 2 h in the presence or absence of KSC-34 (40 μM) prior to quantification of secreted ^{FT}ALLC by ELISA. Viability was measured following media conditioning by Cell Titre Glo. All data are normalized to vehicle-treated controls. Error bars show SEM for n=3 experiments. *p<0.05. (C) Representative autoradiogram and quantification of the fraction [^{35}S]-labeled ^{FT}ALLC secreted from HEK293^{DAX} cells using the experimental paradigm shown in Figure 2-18. Experiments were performed in the absence or presence of KSC-34 (40 μM) added 1 h prior to labeling and then again throughout the experiment. Error bars show SEM for n=4 (D) Graph showing the fraction [^{35}S]-labeled ^{FT}ALLC secreted at t=4 h from HEK293^{DAX} cells transiently transfected with ^{FT}ALLC quantified using the same experimental paradigm shown in Figure 2-18. HEK293^{DAX} cells stably expressing PDIA1 shRNA are indicated. Experiments were performed in the absence or presence of KSC-34 (40 μM) added 1 h prior to labeling and then again throughout the experiment. Error bars show SEM for n=4 experiments. *p<0.05, ***p<0.005.

Chapter 3.

Figure 3.1. (A) Chemical structure of promiscuous cysteine-reactive ABPP probe, iodoacetamide-alkyne. (B) Representative structure of an ABPP probe, containing a reactive group, a linker/binding group, and a reporter element. (C) Chemical structures of various common reporter elements used in ABPP for visualization (rhodamine, and enrichment (biotin), as well as post labeling conjugation (azide and alkyne) via CuAAC.

Chapter 4.

Figure 4.3. Structures of second-generation chlorotriazine electrophiles obtained by varying the tuning element of the triazine ring.

Figure 4.4. Electrostatic potential maps demonstrating effect that electron withdrawing and electron donating groups pose on the electron distribution throughout the triazine-ring system.

Figure 4.5. Investigating the proteome reactivity of chlorotriazines. The library of chlorotriazine electrophiles were incubated in MCF7 lysates (2 mg/mL) and protein labeling by each library member (100 μM) was evaluated after CuAAC-mediated incorporation of a TAMRA fluorophore, SDS-PAGE, and in-gel fluorescence.

Figure 4.6. Effect of iodoacetamide (IAA) pre-treatment (0-10 mM) prior to labeling with IA≡ (2 μM), BBI (100 μM), and KSC-46 (100 μM). MCF7 lysates (2 mg/mL) were incubated with IA for 1 hour, followed by treatment with each probe and then subhected to CuAAC and in-gel fluorescence analysis to investigate the residue specificity of the new chlorotriazine electrophile.

Figure 4.7. (A) General chemical structure of small-molecule chlorotriazine library. (B) Chemical structures of diversity elements used in di-functionalized, chlorotriazine small-molecule probe library.

Figure 4.8. Characterization of targeted library of chlorotriazine probes *in vitro*. Library members (20 μM) were incubated with MCF7 cell lysates (2 mg/mL) in PBS, and protein labeling by each compound was evaluated after CuAAC-mediated incorporation of a TAMRA fluorophore, SDS-PAGE, and in-gel fluorescence (Left panels). Coomassie gels shown (right panels) to show equal protein loading on gels.

Figure 4.9. Characterization of targeted library of chlorotriazine probes *in situ*. Library members (20 μM) were incubated with MCF7 cells for 3 hours at 37 °C, and protein labeling by each compound was evaluated after in-gel fluorescence analysis(Left panels). Coomassie gels shown (right panels) to show equal protein loading on gels.

Figure 4.10. General chemical structures of some classes of PFKFB3 inhibitors.

Figure 4.11. (A) GLRX3 was overexpressed in HEK293T cells via transient transfection using pcDNA3.1(+). Cells were subsequently treated with KSC-56 (20 μM) for 3 hours at 37 °C, following analysis by in-gel fluorescence. Overexpression of GLRX3 was confirmed by anti-FLAG western blot. (B) GLRX3 WT, C159S, and C261S were overexpressed in HEK293T cells via transient transfection using pcDNA3.1(+). Cells were subsequently treated with KSC-56 (20 μM) for 3 hours at 37 °C, following analysis by in-gel fluorescence. Overexpression of GLRX3 was confirmed by anti-FLAG western blot.

Figure 4.12. (A) PFKP was overexpressed in HEK293T cells via transient transfection using pcDNA3.1(+). Cells were subsequently treated with KSC-65 (20 μM) for 3 hours at 37 °C, following analysis by in-gel fluorescence. Overexpression of PFKP was confirmed by anti-FLAG western blot. (B) PFKP C179S, C411S, C529S, and C641S were overexpressed in HEK293T cells via transient transfection using pcDNA3.1(+). Cells were subsequently treated with KSC-65 (20 μM) for 3 hours at 37 °C, following analysis by in-gel fluorescence. Overexpression of PFKP was confirmed by anti-FLAG western blot.

LIST OF SCHEMES

LIST OF ABBREVIATIONS

μM	micromolar
ABPP	activity-based protein profiling
ALS	amyotrophic laterl sclerosis
ATP	adenosine triphosphate
BDNB	1-bromo-2,4,dinitrobenzene
cAMP	cyclic adenosine monophosphate
CA-Rh	chloroacetamide rhodamine
CCR5	C-C chemokine receptor type 5
CD4	cluster of differentiation 4
CGHC	cysteine-glycine-histidine-cysteine
CIAPIN-1	cytokine induced apoptosis inhibitor 1
CSP	chemical shift perturbation
CuAAC	copper assisted azide-alkyne cycloaddition
CXCR4	C-X-C chemokine receptor type 4
E. coli	Escherichia coli
ED	embryonic day
ER	endoplasmic reticulum
Ero1	ER oxireductin 1
ERp27	ER protein 27 kDa
ERp29	ER protein 29 kDa
ERp57	endoplasmic reticulum resident protein 57
F1,6BP	fructose-1,6-bisphosphate
F2,6BP	fructose-2,6-bisphosphate
F6P	fructose 6-phosphate
FAD	flavin adenine nucleotide
Fe	iron
Fe/S	iron-sulfur

G1,6BP	glucose-1,6-bisphosphate
GAPDH	D-glyceraldehyde-3-phosphate dehydrogenase
GLRX3	glutaredoxin 3
GLRX5	glutaredoxin 5
gp120	envelope glycoprotein 120
Grx	glutaredoxin
GSH	glutathione
GSSG	oxidized glutathione
GST	glutathione S-transferase
GSTP1	glutathione S-transferase Pi
HD	huntington's disease
HIV-1	human immunodeficiency virus type 1
IA≡	iodoacetamide-alkyne
KDEL	lysine-aspartic acid-glutamic acid-leucine
MHC	major histocompatibility complex
mM	millimolar
NPDepo	natural products depository
P4H	prolyl-4-hydroxylase
PAMCA	propynoic acid carbamoyl methyl amide
PDI	protein disulfide isomerase
PDIA1	protein disulfide isomerase a1
PDIA3	protein disulfide isomerase a3
PDIA4	protein disulfide isomerase a4
PDIA6	protein disulfide isomerase a6
PFK-1	phosphofructokinase-1
PFKFB3	6-phosphofructo-2-kinase/fructose-2,6-biphosphatase 3
PLC	peptide-loading complex
polyQ	polyglutamine
Rh-N3	rhodamine azide
SDS-PAGE	sodium dodecyl sulfate polyacrylamide gel electrophoresis
SNAr	nucleophilic aromatic substitution

TEV	tobacco etch virus
Trx	thioredoxin

CHAPTER 1

INTRODUCTION

1.0 Introduction

Proper folding of nascent proteins in the cell is accelerated by protein folding catalysts and chaperones that inhibit protein aggregation[1-2]. A number of diseases may arise due to the accumulation of unfolded proteins in the cell[3-5], including neurodegenerative[6] and prion infections[7]. To protect against protein misfolding and aggregation, the cell uses a number of mechanisms including chaperones and folding catalysts to inhibit aggregation and increase proper folding, along with systems in place to degrade proteins that fail to properly fold[8]. Secreted and cell-surface proteins are often stabilized by the introduction of disulfide bonds[9].

Disulfide bonds are covalent bonds produced by the oxidation of two free thiols on cysteine side chains in proteins[10-11]. Disulfides usually function to stabilize tertiary protein structures via intramolecular bonds and quaternary protein structures when formed intermolecularly between two protein chains. Disulfide bonds can also play key regulatory roles as redox switches, controlling the activity of various enzymes[10-11]. Disulfide bond formation one of the crucial and key rate-limiting steps for the correct folding of nascent polypeptides[12]. Nearly one-third of all eurkaryotic proteins, including nearly ~80% of all secretory proteins, contain at least one disulfide bond in their structure[10, 13]. Early in protein folding, disulfide bond formation can be error-prone, where the wrong cysteines are covalently linked[14-15]. Another common occurrence is the correct formation of the disulfide bond, but formation occurs to quickly to allow the nascent protein to adopt its correct fold prior to disulfide bond formation[16-18]. The synthesis and folding of these disulfide bond containing proteins takes place in the lumen of the endoplasmic reticulum (ER), which is

more oxidizing than the cytosol, and is equipped with catalysts of disulfide formation and isomerization[10, 19-20].

Protein disulfide isomerase A1 (PDIA1) was discovered as the first protein folding catalyst in 1963 by two independent research groups[21-22]. PDIA1 is localized in the ER via a classic KDEL ER retention sequence[23], and accounts for approximately 0.8% of total cellular protein[24]. PDIA1 is a 57 kDa multi-domain thiol-disulfide oxidoreductase and molecular chaperone that is responsible for the catalysis of disulfide bond oxidation, reduction, and isomerization in its nascent protein substrates[25]. PDIA1 has also been implicated in binding and stabilizing the major histocompatibility complex (MHC) class I peptide-loading complex (PLC), which mediates MHC class I peptide loading[26]. PDIA1 is also the β subunit of prolyl-4-hydroxylase which catalyzes the formation of 4-hydroxyproline in collagen biosynthesis[13, 27]. Recently, PDIA1 has been found to be rapidly secreted from platelet and endothelial cells during thrombus formation *in vivo*[28-30].

1.1 The Protein Disulfide Isomerase Family

The enzymes of the protein disulfide isomerase (PDI) family are thiol-disulfide oxidoreductases that reside in the ER. The PDI family contains both thiol-reactive and thiol non-reactive members[31]. Currently, the PDIA gene family consists of 21 family members varying in length, domain arrangement, and substrate specificity, but all share one common motif – the thioredoxin-like domain (Table 1.1)[13]. All human PDIs contain at least one thioredoxin-like domain, which can be divided into two different types, catalytic (**a**) and non-catalytic (**b**). Although the family name implies isomerase functionality, not every family member has this catalytic activity. Some family members, such as ER protein 27

kDa (ERp27)[32] and ER protein 29 kDa (ERp29)[33], are comprised of only non-catalytic thioredoxin domains and therefore should only possess chaperone-like activity. The **a**-type domains usually contain a –CXXC– active site motif, although some family members contain a –SXXC– active motif. Protein disulfide isomerase-like protein of the testis (PDILT) and thioredoxin-related transmembrane protein 2 (TMX2) contain these –SXXC– motifs, and have been found to form mixed disulfides but not possess full oxidase activity[31]. Most PDIs contain multiple thioredoxin domains, and usually a combination of **a**- and **b**-type domains. The inactive domains in these PDIs are mainly responsible for the chaperone activity and substrate recruitment.

Gene Name	*Protein Size*	*Name(s)*	*TRX-like Domains*	*Catalytic-site Sequences*	*ER Retention Sequence*
PDIA1	508aa	PDI, P4HB, PHDB	a-b-b'-a'	CGHC, CGHC	KDEL
PDIA2	525aa	PDIp, PDA2	a-b-b'-a'	CGHC, CTHC	KEEL
PDIA3	505aa	ERp57, ERp60, GRP57, GRP58, P58	a-b-b'-a'	CGHC, CGHC	QEDL
PDIA4	645aa	ERp70, ERp72	a'-a-b-b'-a'	CGHC, CGHC, CGHC	KEEL
PDIA5	519aa	PDIR	b-a'-a-a'	CSMC, CGHC, CPHC	KEEL
PDIA6	440aa	ERp5, P5, TXNDC7	a'-a-b-b'-a'	CGHC, CGHC	KDEL
PDILT	584aa	PDIA7	a-b-b'-a'	SKQS, SKKC	KEEL
ERP27	273aa	PDIA8	b-b'	-	KVEL
ERP29	262aa	PDIA9, ERp28, ERp31	b	-	KEEL
ERP44	406aa	PDIA10, TXNDC4	a-b-b'	CRFS	RDEL
TMX1	280aa	PDIA11, TXNDC1	a	CPAC	-
TMX2	296aa	PDIA12, TXNDC14	a	SNDC	KKDK
TMX3	454aa	PDIA13, TXNDC10	a-b-b'	CGHC	KKKD
TMX4	349aa	PDIA14, TXNDC13	a	CPSC	RQR
TXNDC5	432aa	PDIA15, ERp46, Endo-PDI	a'-a-a'	CGHC, CGHC, CGHC	KDEL
TXNDC12	172aa	PDIA16, AGR1, ERp16, ERp18, ERp19	a	CGHC	EDEL
AGR2	175aa	PDIA17, XAG-2, HAG-2	a	CPHS	KTEL
AGR3	166aa	PDIA18, HAG-3, BCMP11	a	CQYS	QSEL
DNAJC10	793aa	PDIA19, ERdj5, JDPI	a'-b-a'-a-a'	CSHC, CPPC, CHPC, CGPC	KDEL
CASQ1	396aa	PDIB1	b-b-b'	-	-
CASQ2	399aa	PDIB2	b-b-b'	-	-

Table 1.1. Overview of the 21 proteins in the human PDI family listed with domain arrangement and active-site sequence configuration.

1.2 The Discovery of PDIA1

PDIA1 was independently discovered by two research groups led by Brunó Straub and Christian Anfinsen in 1963[21-22]. Straub found that extracts from pancreas of both chickens and pigeons were able to catalyze the reoxidation of reduced ribonuclease (RNAse). It was concluded that the extracts contain an enzyme which is able to catalyze the sulfhydryl-disulfide transformation and that this protein might play a role in the final step of protein biosynthesis[22]. Anfinsen's group found that subcellular microsomal enzyme system from rat liver was responsible for accelerating the reactivation of reduced bovine pancreatic RNAse[21]. Furthermore, the group partially purified the microsomal enzyme system responsible and demonstrated that it can catalyze dithiol-disulfide exchange reactions[34-36].

1.3 The Structure of PDIA1

The full-length, unprocessed PDIA1 consists of 508 amino acids. The N-terminal 17 amino acid signal peptide is cleaved off during processing upon translocation to the ER, leaving the mature form of PDIA1 truncated to 491 amino acids[11, 25]. PDIA1 is organized into four distinct thioredoxin-like, globular domains, **a**, **b**, **b'**, and **a'**, plus a highly acidic C-terminal extension **c** and a 19 amino acid linker between the **b'** and **a'** domains, termed **x** (Figure 1.1). The **a** and **a'** domains functionally resemble thioredoxin (Trx), and contain redox catalytic Cys-Gly-His-Cys (CGHC) active-site motifs. The **b** and **b'** domains, while resembling Trx, do not contain CGHC active-site motifs and therefore are not catalytically active. PDIA1 adopts a horseshoe shape structure where the **a** and **a'** catalytic domains face inward toward each other[37].

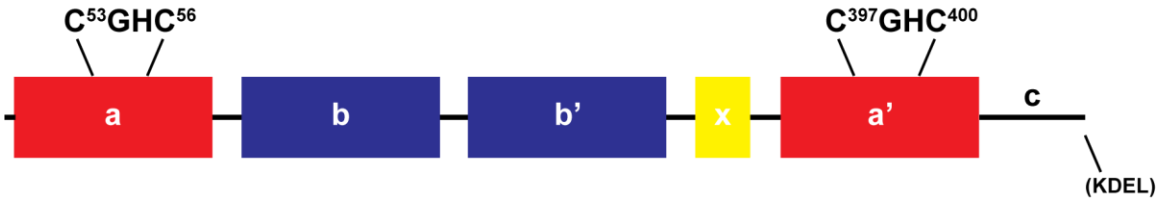

Figure 1.1. Domain organization of PDIA1. PDIA1 is comprised of four thioredoxin-like domains. The **a**-type domains contain CGHC active site motifs. PDIA1 also contains a highly acidic C-terminal extension **c** and a 19 amino acid linker between the **b'** and **a'** domains, termed **x.**

1.4 The Catalytic Domains of PDIA1

The **a** and **a'** domains share 33.6% sequence identity and contain identical CGHC active site motifs[25]. The oxidase, reductase, and isomerase activities of PDIA1 depend on the thiol groups in the active sites of the **a** and **a'** domains[38-39]. It is known that the two active sites of PDIA1 operate independently of each other. Vuori *et al.* investigated the effect of disrupting the catalytic active site in one or both domains on the catalytic activity of PDIA1. It was found that abolishing one active site cysteine in either domain resulted in a 50% loss of the oxidoreductase activity, and abolishing both active site cysteines resulted in a 100% loss in oxidoreductase activity of PDIA1[40]. Due to the fact that mutation of each active site only resulted in a loss of 50% activity, it can be concluded that each active site operates independently from each other. The secondary structure of the globular domains of PDIA1 adopt a Trx-like fold and are arranged in a β1-α1-β2-α2-β3-α3-β4-β5-α4 fashion. The residues of the catalytic active sites are positioned at the top of the second helix, α2, leaving the N-terminal cysteine partially exposed to the solvent[10].

Characterization of this active site led to the determination that the pK_a of the N-terminal cysteine lies in the range of 4.5-5.6[41-42]. Ruddock *et al* determined the pH dependence of the disulfide bond oxidation activity of PDIA1 was correlated to the pK_a of the N-terminal cysteine residue in the active site of PDIA1. The data indicated a pK_{app} of 5.6 for bovine PDIA1[41]. Kortemme et al determined the pK_a of the N-terminal active cysteine to be 4.5 for human PDI *a* by analyzing the pH dependence of ultraviolet-visible (UV/Vis) absorbance shifts or nuclear magnetic resonance (NMR) chemical shift perturbations (CSP)[42]. Furthermore, it has been demonstrated that electrostatic interactions in the active-site stabilize the thiolate anion. A link with the imidazole group of the histidine

in the CGHC motif was found to stabilize the thiolate by 1.1 kcal/mol. Further electrostatic interactions with partial positive charges at the N-terminus of the α-helix contribute 4.6 kcal/mol, up to a total of 5.7 kcal/mol stabilization of the thiolate[42]. This stabilizing effect of the thiol form of the enzyme effectively destabilizes the oxidized, disulfide bond form of the enzyme involving that same thiol group[43]. The C-terminal cysteine in the active site of PDIA1 is known to be less solvent accessible and thus has higher pK_a, effectively around 12.8[25, 44]. Lappi *et al* found that a conserved arginine, R120, moves in and out of the active site. Upon moving close to the active site, the pK_a of the C-terminal cysteine, C56, is dramatically lowered to allow formation of a thiolate anion that acts as a nucleophile on any mixed disulfide formed by C53 with and substrate, effectively reoxidizing PDIA1[44].

The **b** and **b'** domains do not contain a redox catalytic active site, and are needed primarily for spacing and substrate recruitment. The **b'** domain, which contains a large hydrophobic cavity between helices α1 and α3 to interact with unfolded protein and peptide substrates, is the major substrate binding domain of PDAI1[31, 45]. Pirneskoski *et al* demonstrated that point mutations along the substrate binding domain at positions L242, L244, F258, and I272 influenced peptide binding. Furthermore, the greatest effect was seen for the point mutation I272W. Biophysical characterization indicated no alterations in structure upon mutation of I272, revealing that the results are a direct effect on the substrate binding domain and not an observed structural effect from the mutation[46]. The **b'** domain has also been demonstrated to be essential for the assembly of prolyl-4-hydroxylase (P4H). Truncated forms of PDIA1 were overexpressed and the minimum construct found necessary for assembly was the **b'-a'** region of PDIA1, with the **a-b** region supplemented by ERp57[47].

PDIA1 has also been shown to possess chaperone activity, by inhibiting the aggregation of misfolded protein substrates at stoichiometric concentrations[48-51]. Dai and Wang demonstrated that this activity was dependent upon the **b'** domain of PDIA1. This was confirmed by expressing a mutant form of PDIA1 with 51 amino acids truncated from the C-terminal end of the **b'** domain to remove the substrate binding pocket. The mutant enzyme showed no peptide binding ability or chaperone activity against D-glyceraldehyde-3-phosphate (GAPDH), a protein with no disulfide bonds. However, the truncated protein retains most of its insulin reductase activity and isomerase activity against scrambled RNAse[52].

1.5 Thiol-Disulfide Exchange Reactions of PDIA1

PDIA1 possess two conserved CGHC active sites in the **a** and **a'** domains, in which the two cysteines can exist is the disulfide (oxidized PDIA1) or dithiol form (reduced PDIA1). These active sites are responsible for the enzymatic function, in which PDIA1 facilitates the oxidation, reduction, or isomerization or disulfide bonds within protein substrates depending on the redox state of the active site[9-10, 25]. Direct evidence for PDIA1 catalayzed thiol-disulfide exchange *in vivo* were first shown in two systems. Bulleid and Freedman demonstrated that dog pancreas microsomes, which were deficient in PDIA1, are defective in co-translational formation of disulfide bonds in γ-gliadin, a wheat storage protein. It was also shown that reconstitution of these microsomes with purified PDIA1 reversed this observed effect[53]. Second, Molinari and Helenius demonstrated that PDIA1 and other PDI-family member ERp57 (PDIA3) form mixed disulfides *in vivo* with glycoproteins in the ER of mammalian cells[54].

During the oxidation or reduction of its protein substrates, PDIA1 transfers either an oxidizing or reducing equivalent from the cysteine pairs in its active sites, which then in turn cycle between the oxidized and reduced states. The two amino acids between the cysteines in the active site in the CXXC motif contribute significantly to the reduction potential of the active site. PDIA1 has a reduction potential of -180 mV, making it one of the better oxidants in the protein disulfide isomerase family[55]. The oxidase activity of PDIA1 inserts disulfide bonds into protein substrates, which results in the pairing of two substrate thiol groups and the reduction of the PDIA1 active site (Figure 1.2). The oxidase activity of PDIA1 only require either the **a** or the **a'** domain. The catalysis has been attributed to the high reactivity of the disulfide bonds, which are approximately ~500-fold more reactive than the disulfide bond found in oxidized glutathione (GSSG)[56].

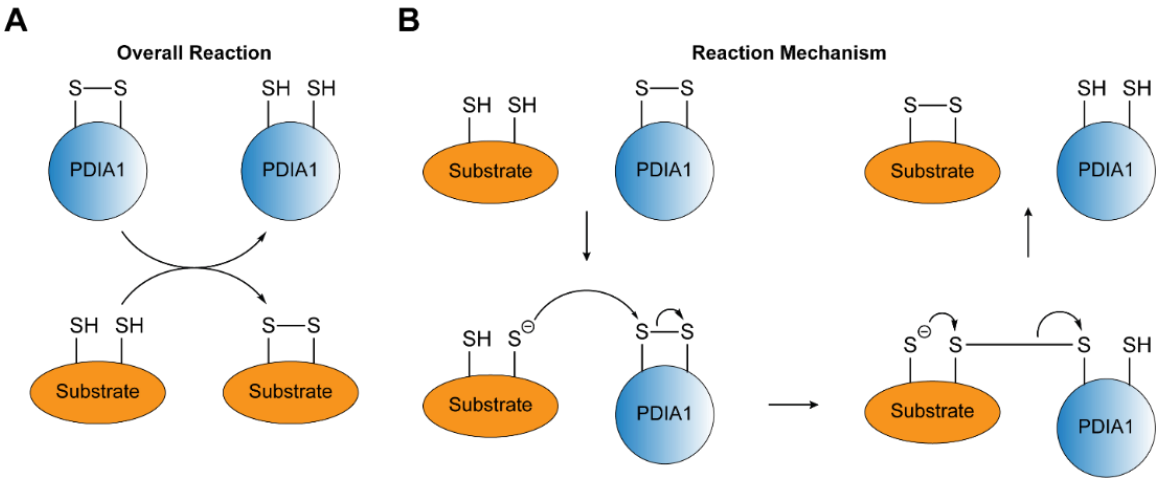

Figure 1.2. (A) The oxidase activity of PDIA1 installs disulfide bonds in protein substrates. (B) Mechanistically, a nucleophilic thiolate anion on the protein substrate attacks the disulfide bond of the of the PDIA1 active site, resulting in a mixed disulfide bond. Another cysteine within the substrate macromolecule attacks the mixed disulfide, forming the intramolecular disulfide bond on the protein substrate. PDIA1 is subsequently released, generating dithiols within the active site of PDIA1.

Reoxidation of the active sites of PDIA1 is then carried out by ER oxireductin 1 (Ero1), which is a flavin adenine nucleotide (FAD) binding oxidase[57]. Ero1 contains two distinct pairs of cysteines, one located proximal to the FAD cofactor as a CXXC motif, and the other pair located on a flexible loop[58]. Through these two pairs of cysteines, Ero1 induced reoxidation of PDIA1 is achieved via a thiol-disulfide exchange reaction with the cysteine pair located on the flexible loop of Ero1. This is subsequently followed by an electron transfer to the FAD cofactor via the cyeteine pair in the CXXC motif. The electrons are finally shuttled from the $FADH_2$ to O_2, producing one molecule of H_2O_2 and regenerating the FAD cofactor (Figure 1.3)[59].

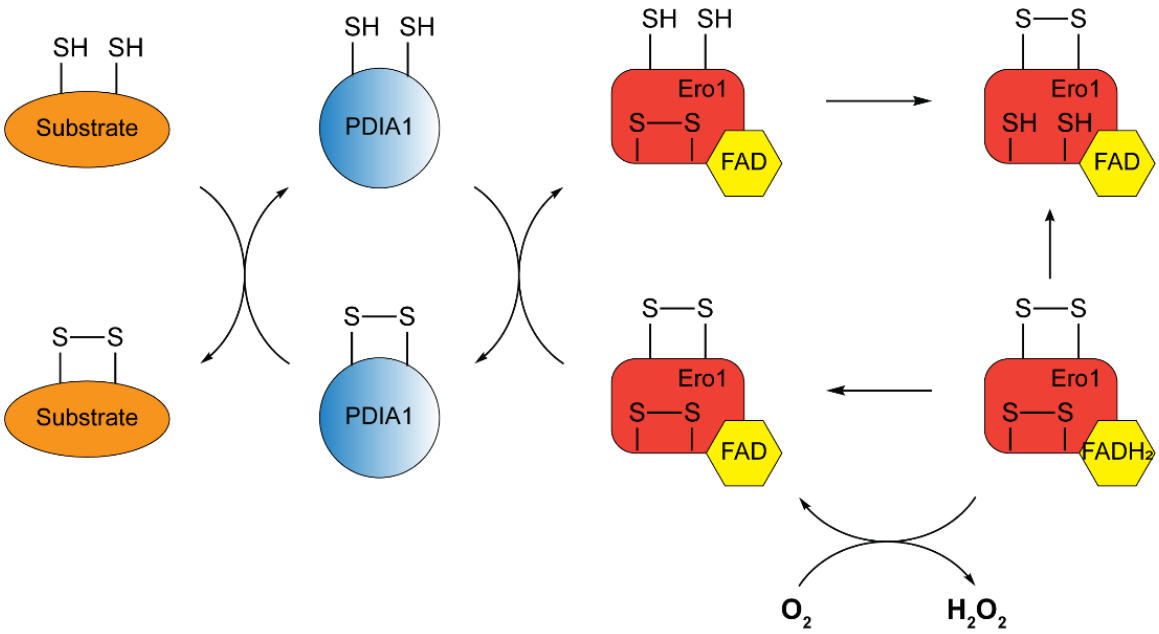

Figure 1.3. The Ero1 mediated reoxidation of PDIA1. The active site dithiols are reoxidized by Ero1, an FAD-binding oxidase. Ero1 transfers electrons from PDIA1 to FAD, and subsequently to O_2, producing one molecule of H_2O_2 and regenerating the FAD cofactor.

Due to the extremely oxidizing conditions of the endoplasmic reticulum as well as the reduction potential of the active site motifs, the active site cysteines of PDIA1 are commonly found in the oxidized (disulfide) form. Thus, PDIA1's ability to act as a reductase is less common than other members of the PDI family. Contrary to the oxidase activity, the reductase activity utilizes the reduced dithiol groups in the active site of **a** or the **a'** domain. PDIA1 will the transfer the dithiol groups to its protein substrate, and in turn oxidize its active site cysteines (Figure 1.4).

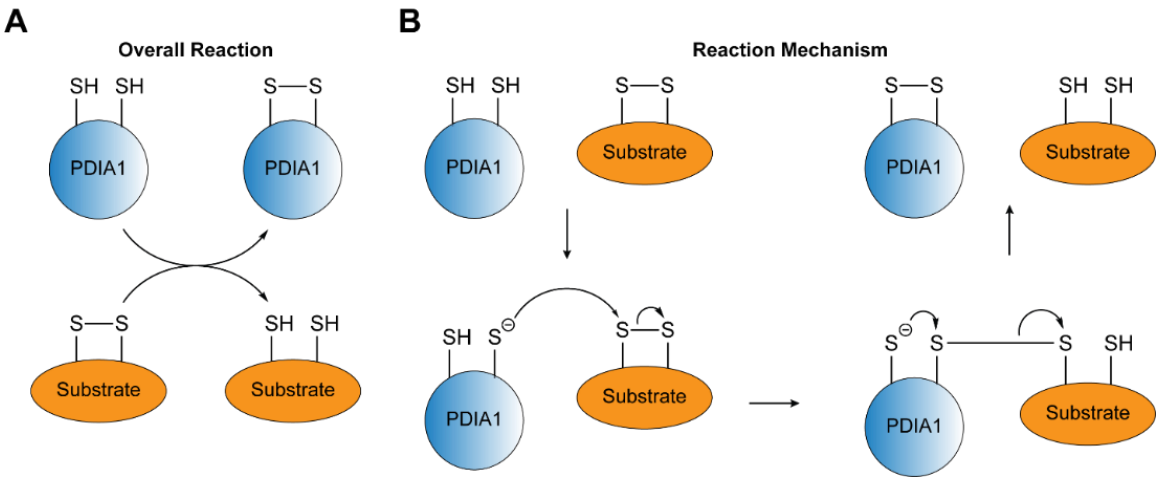

Figure 1.4. (A) The reductase activity of PDIA1 reduces disulfide bonds to dithiol groups in protein substrates. (B) Mechanistically, one of the two nucleophilic cysteines in the PDIA1 active sites, Cys53 or Cys397, will attack a substrate disulfide bond creating a mixed disulfide. After a given amount of time, the C-terminal cysteine in the active site, Cys56 or Cys400, will then be activated and attack the N-terminal cysteine. This results in oxidation of the active site of PDIA1 and release of the reduced protein substrate.

These thiol-disulfide reactions that either install or remove disulfide bonds in protein substrates proceed through the formation of transient mixed disulfide bonds between the N-terminal cysteine of the **a** or **a'** domain (Cys53 or Cys397) of PDIA1 and the protein substrate. A conserved glutamate positioned below the C-terminal cysteine (Cys56 or Cys400) forms a salt bridge and functions in proton transfer during the substrate release step in the "escape pathway"[9, 25, 31, 60]. During this step, the catalytic domains have undergone significant conformational changes, causing the pK_a of the C-terminal cysteine to drop from 12.8 to 6.1, thus becoming nucleophilic enough to attack the N-terminal cysteine of the active site[44, 61].

Interestingly, the formation of disulfide bonds early on in protein synthesis is often error prone. These errors can be the result of two incorrect cysteines being paired together to form incorrect disulfide bridges or the correct disulfides can be formed too early in protein synthesis, which impedes the protein from adopting the native conformation[62]. PDIA1 can correct these disulfides through disulfide bond isomerization, which allows the protein substrates to adopt their native conformations[9]. Mechanistically, the N-terminal cysteine of the active site attacks a cysteine in a mismatched disulfide pair forming a mixed heterodisulfide bond between the protein substrate and PDIA1 (Figure 1.5). Once this occurs, a "mechanistic decision" must occur about the fate of the covalent complex between the substrate and PDIA1. Either the original substrate cysteine can attack the heterodisulfide bond and release PDIA1 without resulting in any isomerization of the protein substrate disulfide, or another cysteine on the protein can attack the heterodisulfide bond and displace PDIA1 resulting in an isomerization through an intramolecular rearrangement within the protein substrate[63]. It is also important to note that the C-terminal

active site cysteine of PDIA1 can also react with the N-terminal cysteine and release of the substrate protein, resulting in the reduction of the original disulfide bond. In this way, the C-terminal cysteine in PDIA1 may act as a "clock" allowing the substrate a specified amount of time to succeed in an intramolecular isomerization before the substrate is just simply reduced and released from PDIA1[60]. After the "escape" of PDIA1 and subsequent reduction of the substarte disulfide bond, reoxidation of that substrate disulfide bond in an alternative configuration is also considered isomerization. Through this pathway, isomerization is considered repeated cycles of reduction and reoxidation of the substrate cysteines until it results in the correct arrangement of disulfide bonds[9].

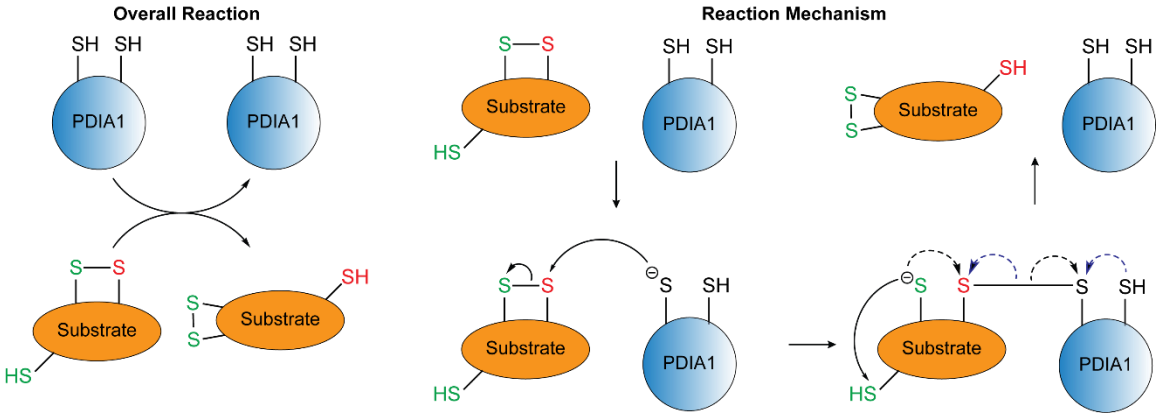

Figure 1.5. (A) The isomerase activity of PDIA1 shuffles incorrectly formed disulfide bonds to achieve properly folded substrates. (B) One of the two nucleophilic cysteines in the PDIA1 active sites, Cys53 or Cys397, will attack a substrate disulfide bond creating a mixed disulfide. At this point a decision is made to either form the correct disulfide (solid black line) or re-form the incorrect disulfide pair (dashed black line). Another option, is PDIA1 acts as a "clock" and the C-terminal active site cysteine, Cys56 or Cys400, can attack its partner and release the protein substrate as a dithiol (dashed blue arrows).

1.6 The Chaperone Activity of PDIA1

PDIA1 has also been demonstrated to possess chaperone and anti-chaperone activities at stoichiometric concentrations[48-51]. Puig and Gilbert found that at excess concentrations of PDIA1, chaperone-like activity is exhibited which prevented the aggregation of denatured lysozyme and promoted the correct folding[49]. Cai *et al*. discovered that dilution of guanidinium HCl denatured GAPDH showed only a limited extent of refolding and reactivation. It was shown that the presence of PDIA1 in the dilution mixture at near stoichiometric amounts increased refolding and reactivation, and prevented aggregation of GAPDH[48]. Song and Wang have discovered that in near stoichiometric concentrations, PDIA1 promoted the reactivation and refolding of rhodanese, a protein which is a single chain folded into two domains and contains four cysteines, but no disulfide bonds. It was also shown that PDIA1 suppressed the aggregation of rhodanese during thermal inactivation of the protein[50]. Primm *et al*. have also demonstrated this chaperone activity on two thermally and chemically denatured proteins, alcohol dehydrogenase and citrate synthase. Both of these proteins do not require disulfide bonds for correct folding, illustrating that the chaperone activity of PDIA1 does not require the active site cysteines[51].

In order to demonstrate that the chaperone-like activity of PDIA1 is not dependent on the active site cysteine residues of PDIA1, Quan *et al*. alkylated the thiol groups of reduced PDIA1 to inactivate the cysteine pairs from their isomerase activity. Next, it was demonstrated that GAPDH, a protein with no disulfide bonds, was still able to be refolded and reactivated even though the active site cysteines were inactivated[64]. Dai and Wang demonstrated that the chaperone-like activity was dependent upon the **b'** domain of PDIA1.

It was confirmed through the expression of mutant PDIA1 lacking 51 amino acids from the C-terminal end of the **b'** domain to remove the substrate binding pocket. The mutant enzyme showed no peptide binding ability or chaperone activity against GAPDH[52].

In some instances, PDIA1 demonstrates "anti-chaperone" activity, in which at sub-stoichiometric concentrations, PDIA1 will induce the aggregation of the protein substrate. Puig and Gilbert found that at concentrations of PDIA1 approximately ~10% of the substrate concentration, PDIA1 will induce aggregation of the substrate instead of promoting the refolding and reactivation. PDIA1 actively diverted the denatured lysozyme away from refolding by incorporating extensive intermolecular disulfide cross-links, resulting in large inactive aggregates[49, 65]. PDIA1 has been found to be incorporated into the insoluble aggregates, whereas other ER control proteins are not[66].

1.7 PDIA1 as a Potential Therapeutic Target

Dysregulation of the activity of PDIA1 has been implicated in a variety of diseases, including cancer[25, 67-69], neurodegenerative[70-73], and cardiovascular[74-76] diseases. The analysis of published microarray datasets indicate that the expression of PDIA1 is overexpressed (>2-fold) in a variety of cancers when compared to normal tissue, including lymphoma[77-79], brain, and CNS cancers[67-68, 80-83], ovarian[84-85], kidney[86-88], and prostate[89-90]. Increased levels of PDIA1 in a variety of cancers have also been confirmed by proteomic analyses. Upregulation of PDIA1 was observed in patients with prostate adenocarcinoma, compared to normal patients with benign prostate hyperplasia[91]. 2-DE/MALDI-TOF proteome analyses studies showed that PDIA1 is overexpressed in infiltrating ductal carcinomas in both female[92] and male[93] breast tissue when compared to the respective

adjacent non-neoplastic tissues. It was also shown that PDIA1 is upregulated in a rat model of human gastric cancer induced by methylnitrosoguanidine (MNNG)[94].

The upregulation of PDIA1 has been correlated with cancer metastasis and invasion. Patients with axillary lymph node metastatic breast tumors demonstrated significantly higher levels of PDIA1 compared to patients with normal primary breast tissue[95]. PDIA1 was also found to be overexpressed in migrating glioma cells in an *in vitro* migration assay, as well as in invasive glioma cells in both, tumor xenografts and at the invasive front of the glioblastoma[96].

Recent studies have shown that, clinically, PDIA1 might have potential for use as a biomarker for the onset of disease. It was recently reported that PDIA1 was one of the most upregulated proteins in the interstitial fluids from breast tumor patients, and could serve as a marker for early detection[97]. Anti-PDIA1 monoclonal antibodies have also been used in the clinic as a method for the *in vitro* diagnosis of colorectal cancer. PDIA1 is used in this case for early screening, therapeutic follow-up, and for prognosis determination of the disease[98].

To further this role as diagnostic tool, PDIA1 expression levels have been found to correlate with overall patient survival rates. Lower PDIA1 expression levels was observed to be correlated with significantly higher overall survival rates of patients with glioblastoma and breast cancers[67-69]. Therefore, in addition to colorectal cancer, PDIA1 can be used as a prognostic marker in cancer biopsies of other types of cancer as well. Another major clinical concern in cancer treatment associated with PDIA1 is chemoresistence in some cancers, although the exact mechanism has yet to be determined. A recent study evaluated proteome-wide differences between normal HeLa cells and

aplidin-resistant HeLa cells (Hela-R)[99]. Aplidin is a macrocyclic depsipeptide originally isolated from *Aplidium albicans*, but now obtainable through total synthesis[100]. Proteomics studies determined the HeLa-R cells to have increased expression of PDIA1 compared the the non-aplidin-resistant, normal HeLa cells. Treatment with the PDIA1 inhibitor, bacitracin, abrogated the resistance and the cells were re-senesitized to the drug[99]. It has also been demonstrated that treatment of cancer cells with PDIA1 inhibitors was found to sensitize cells toward etoposide induced apoptosis at normally subtoxic concentrations[101]. Together this data indicates the clear clinical relevance of PDIA1 and suggest that combining selective PDIA1 inhibitors with traditional anti-cancer agents could achieve a synergistic effect to overcome chemotherapeutic resistance.

Cell surface associated PDIA1 has also peaked interest in the clinic because its reductase activity has been implicated in human immunodeficiency virus type 1 (HIV-1) fusogenic events[102-105]. PDIA1 has been shown to cluster on the surface near the HIV-1 primary receptor cluster of differentiation 4 (CD4), which has separate binding sites for PDIA1 and the glycoprotein on the envelope of HIV-1, gp120[106]. Gp120 of HIV-1 first binds to CD4, followed by the reduction of at least two of nine disulfide bonds by PDIA1. This results in major conformational changes in the tertiary structure of gp120, which enhances the ability of gp120 to interact with surface receptors C-C chemokine receptor type 5 (CCR5) and C-X-C chemokine receptor type 4 (CXCR4)[102, 107]. Furthermore, gp41, another viral glycoprotein bound to gp120 undergoes rearrangement into fusogenic intermediates and allows HIV-1 to enter into host cells[107]. Taken together, there is clear clinical relevance of targeting extracellular PDIA1 in order to inhibit HIV-1 entry into host cells.

Lately, a considerable amount of evidence has implicated the oxidation state of labile disulfide bonds in critical hemostatic proteins in thrombus formation[108]. The oxidation state of these labile thiol groups has been shown to be regulated by oxidoreductases, such as PDIA1[28, 109]. Platelets have consequently been a cell type which has shown to secrete PDIA1 from the ER to the cell surface[110-111]. Cho *et al*. observed a time-dependent increase in expression of PDIA1 in murine thrombi following vessel injury. The infusion of PDIA1 inhibitor, bacitracin, or a blocking monoclonal antibody ablated thrombus formation and fibrin generation. These results indicated that PDIA1 is required *in vivo* for thrombus formation and fribrin generation[28]. Therefore, PDIA1 shows promise as a clinical target for small molecule inhibition of thrombus formation. To this end, there has been tremendous work in this field to develop selective PDIA1 inhibitors, both reversible and non-reversible.

1.8 Inhibitors of PDIA1

1.8.1 Antibiotic Inhibitors of PDIA1

The cyclic dodecapeptide antibiotic, bacitracin (Figure 1.6A), was the first ever PDIA1 inhibitor report in 1981[112]. It was demonstrated that bacitracin binds PDIA1 through disulfide bond formation between an open thiol form of the thiazoline ring and Cys314/345 in the **b'** substrate binding domain[113]. However, bacitracin was found to be nonspecific and non-potent for PDIA1, requiring high concentrations (~1 mM) to inhibit the reductase activity, with little or no inhibition of the isomerase or oxidase activity, as well as binding other proteins without or without PDIA1 activity[114].

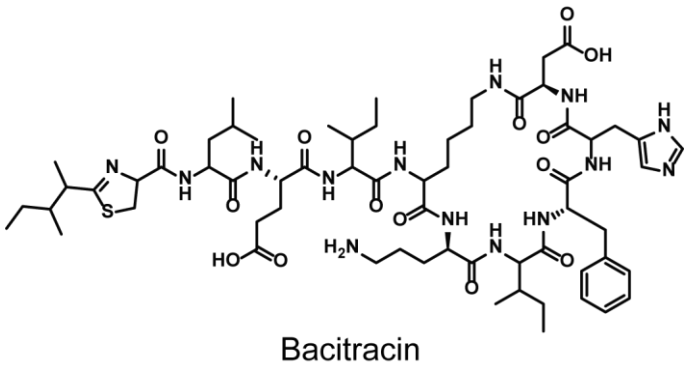

Figure 1.6. Chemical structure of the dodecapeptide PDIA1 inhibitor, bacitracin.

1.8.2 Reversible Small Molecule Inhibitors of PDIA1

Juniferdin (Figure 1.7), a sesqueterpenoid, originally isolated from the plant *Ferula junipernia* was discovered from a high-throughput screen of ~10,000 compounds of the RIKEN Natural Product Depository (NPDepo). Of all of the compounds in the library screened, only four were identified as putative PDIA1 inhibitors, and juniferdin, as the most potent, was chosen as the lead compound[115]. Structure-activity relationship studies showed that any structural alterations to the sesquiterpene ring was detrimental toward the inhibitory effect against PDIA1. Since it has been known that the PDIA1-catalyzed reduction of disulfides in gp120 is crucical for HIV-21 entry into host cells[103, 106], it was examined if juniferdin could impede HIV-1 entry by inhibiting PDIA1 activity at the cell surface[115]. Juniferdin was found to have significantly inhibited PDIA1-catalyzed reduction of HIV gp120, showing that it may inhibit HIV-1 entry into host cells[115].

Another natural product, plant metabolite identified as a PDIA1 inhibitor by means of a high throughput insulin-based turbidimetric screen of 4,900 compounds was quercetin-3-rutinoside (Figure 1.7)[116]. The inhibition of PDIA1 was found to be selective over other thiol isomerase with CXXC active site motifs. Using intravital microsocopy, it was demonstrated that quercetin-3-rutinoside blocks thrombus formation by inhibiting PDIA1, and that the infusion of recombinant PDIA1 reversed this anti-thrombotic effect[116]. Further studies have identified quercetin-3-rutinoside directly binds to the **b'x** domain of extracellular PDIA1, inducing a compact conformation, thus constricting the overall flexibility of PDIA1 and inhibiting thrombus formation[117].

Another reversible inhibitor of PDIA1 was discovered by Eirich *et al*. during a screen of a commercial compound library, and subsequent structure-activity-relationship

(SAR) studies[101]. Compounds JP04-042 and derivative PS-89 (Figure 1.7) were identified via proteomics techniques as potent and selective reversible inhibitors of PDIA1, although it also bound other isoforms PDIA3 and PDIA4. These compounds were found to sensitize Jurkat (leukemic) and MDA-MB-231 (breast) cancer cell lines to sub-toxic concentrations of etoposide (500 nM)[101]. These compounds are of great interest owing to their irreversibility, they bind to the **a** and **a'** domains to shield the active sites while exhibiting a pharmacologically more desirable mode of action than an irreversible inhibitor[101].

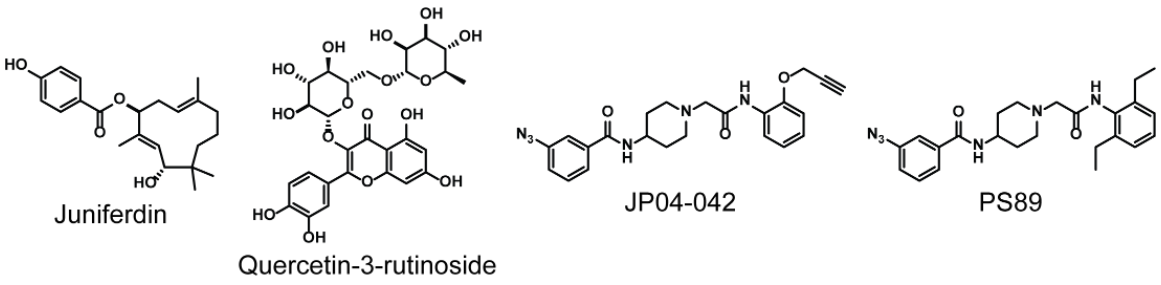

Figure 1.7. Chemical structures of reversible PDIA1 inhibitors.

1.8.3 Irreversible Inhibitors of PDIA1

In 2010, Hoffstrom *et al* identified 16F16 (Figure 1.6C) as an irreversible inhibitor of PDIA1 in a high-throughput screen of 68,887 compounds for the ability to suppress apoptosis in an *in vitro* PC12 cell-based model of Huntington's disease (HD), in which apoptosis is induced by polyglutamine (polyQ) and mediate by PDIA1[73]. 16F16 contains a chloroacetamide electrophile that covalently modifies a reactive cysteine in one of the active sites in PDIA1. Using a proteomics-amenable version of the lead compound, 16F16A, an alkyne handle allowed for CuAAC and target identification by mass spectrometry as PDIA1 and PDIA3. Within the 3-12 μM range, 16F16 displayed a dose-dependent increase in polyQ-induced apoptosis. Above 12 μM, 16F16 displayed significant cytotoxicity most likely owing to significant off-targets effects. Further, 16F16 also displayed the ability to dose-dependently rescues Aβ peptide toxicity in pyramidal neurons when PDIA1 was inhibited[73]. 16F16 and derivatives have not been radiolabeled and are being tested as new potential positron emission tomography (PET) agents for imaging PDIA1 in cancer[118].

In the result of another small screening endeavor of compounds containing vinyl sulfone/sulfonate electrofiles by Ge *et al*, **P1** was serendipitously discovered as an inhibitor of PDIA1[119]. **P1** and other library members were screened in MCF-7 cells, and *in situ* proteome reactivity profiles were analyzed, prior to compound target identification. **P1** was found to bind to PDIA1 *in situ* and is capable of killing numerous mammalian cancer cells lines, $GI_{50} \sim 4$ μM[119]. It is important to note that proteomics studies also identified other PDI family members, PDIA4 and PDIA6, as targets of P1.

It has also been previously reported that a class of propynoic acid carbamoyl methyl amides (PACMAs), which can form covalent adducts with cysteine thiol groups, have showed a broad range of cytotoxicity in a panel of human cancer cell lines[120]. Furthering on that discovery, Xu *et al*. designed a series of PACMA derivatives which displayed significant cytotoxicity in human ovarian cancers, and identified PACMA31 as a covalent modifier of PDIA1[121]. Using high-resolution mass-spectrometry and computational methods, it was predicted that PACMA31 is covalently modifying Cys397 of the **a'** domain of PDIA1[121]. It was demonstrated with circular dichroism that upon treatment with PACMA31, significant changes to the secondary structure of PDIA1 were observed, which correlated to the PACMA31 dose-dependent decrease in PDIA1 activity observed. Interestingly, PACMA31 demonstrated tumor targeting ability *in vivo* in a mouse xenograft model of human OVCAR-8 ovarian cancer. PACMA31 significantly suppressed tumor growth by up to 85% and did not exhibit adverse effects on the mice[121]. This data demonstrates the implications of targeting PDIA1 as a potential for a cancer therapeutic.

Multiple myeloma cells secrete more disulfide-bond rich proteins than any other mammalian cell, thus the inhibition of PDIA1 should increase stress in the ER beyond the point of repair and trigger apoptosis[122-123]. To streamline selection of an anti-myeloma drug candidate, 30355 compounds were screened in a mechanistically unbiased, multi-layered assay. This screen identified lead compound, CCF642, with broad anti-multiple myeloma activity. CCF642 was found to be effective *in vivo*, in part, by inhibition of PDIA1[124].

Recent interest in irreversible target binding had generated concerns over the selectivity of the molecules, mechanisms of action, and the distinct toxicity of covalent binder *in vivo*[125]. To this end, Allimuthu and Adams have recently examined the 2-

chloropropionamide electrophile functionality, a sterically hindered version of the commonly used chloroacetamide[126]. The synthesis of a library of 26 structurally diverse compounds with 2-chloropropionamides displayed low proteome reactivity of this electrophilic functionality. One molecule, S-CW3554, selectively targeted PDIA1 and showed cytotoxicity to multiple myeloma cell lines. S-CW3554 is the least reactive PDIA1 inhibitor to date, but is a candidate for optimization towards a more metabolically stable *in vivo* probe[126].

In 2013, a previous member of the Weerapana lab reprted on RB-11-ca, a cell-permeable, irreversible inhibitor of PDIA1[127]. RB-11-ca is a tri-functionalized triazine-based covalent inhibitor that contains three elements, (1) an alkyne-handle for reporter-tag conjugation via copper-catalyzed azide-alkyne cycloaddition (CuAAC); (2) an octylamine diversity element for binding specificity; and (3) an electrophilic chloroacetamide for irreversible modification of nucleophilic cysteine residues. RB-11-ca was determined to bind to PDIA1 after CuAAC-mediated conjugation of a biotin group, avidin enrichment, and subsequent target identification via LC/LC-MS/MS analysis. Through site-directed-mutagenesis, it was demonstrated that RB-11-ca selectively modifies the N-terminal cysteine in the **a** domain of PDIA1, Cys53. RB-11-ca was unique because it was the first characterized **a**-domain selective inhibitor of PDIA1[127].

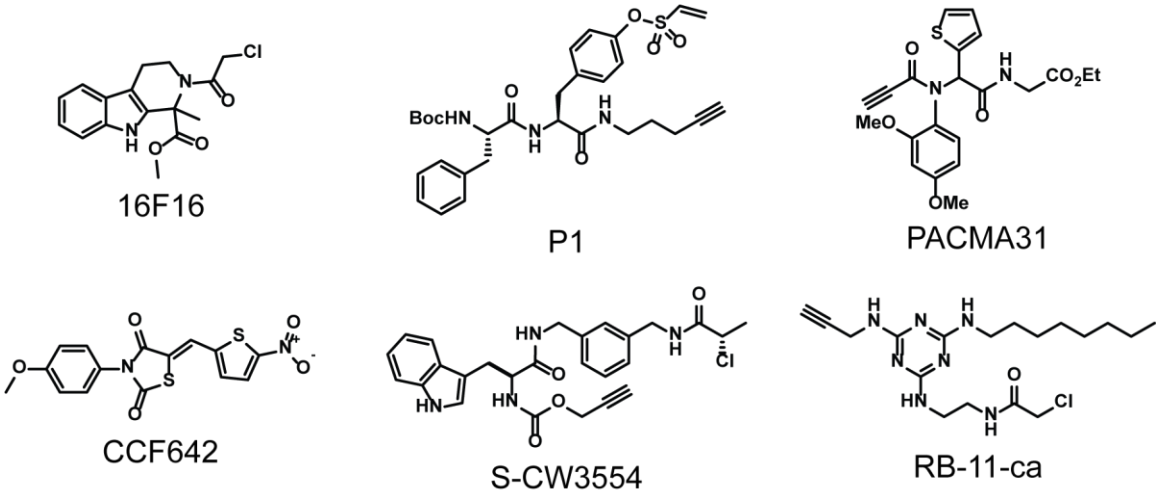

Figure 1.8. Chemical structures of irreversible inhibitors of PDIA1.

1.9 Conclusions

In conclusion, PDIA1 was the first protein folding catalyst discovered in 1963. PDIA1 is localized in the ER by a classic KDEL ER retention sequence, and accounts for approximately 0.8% of total cellular protein. PDIA1 is a 57 kDa multi-domain thiol-disulfide oxidoreductase and molecular chaperone that is responsible for disulfide bond oxidation, reduction and isomerization via two independent CXXC catalytic active site motifs. PDIA1 also possesses chaperone and anti-chaperone activity which is independent of the two catalytic active sites. The dysregulation of PDIA1 activity has been implicated in a variety of diseases including neurodegenerative, cardiovascular, and a variety of cancers. PDIA1 expression levels have also been found to correlate with patient prognosis and survival rates, as well have been of recent interest as a potential biomarker marker for disease onset and progression. To this end, there has been tremendous interest in the field to develop selective, reversible and irreversible inhibitors for PDIA1. In 2013, our lab reported on RB-11-ca, a cell permeable, irreversible inhibitor of PDIA1. RB-11-ca is a tri-functionalized triazine-based covalent inhibitor with a chloroacetamide electrophile that was found to selectively target Cys53 in the **a** domain of PDIA1. To further this study, we have since optimized a second generation of more potent and selective triazine-based covalent inhibitors of PDIA1, which will be the subject of the next chapter of this thesis.

References

1. Hartl, F. U.; Hayer-Hartl, M., Molecular chaperones in the cytosol: from nascent chain to folded protein. *Science* **2002,** *295* (5561), 1852-8.

2. Buchner, J., Supervising the fold: functional principles of molecular chaperones. *FASEB J* **1996,** *10* (1), 10-9.

3. Dobson, C. M., Protein folding and its links with human disease. *Biochem Soc Symp* **2001,** (68), 1-26.

4. Thomas, P. J.; Qu, B. H.; Pedersen, P. L., Defective protein folding as a basis of human disease. *Trends Biochem Sci* **1995,** *20* (11), 456-9.

5. Koo, E. H.; Lansbury, P. T., Jr.; Kelly, J. W., Amyloid diseases: abnormal protein aggregation in neurodegeneration. *Proc Natl Acad Sci U S A* **1999,** *96* (18), 9989-90.

6. Harper, J. D.; Lansbury, P. T., Jr., Models of amyloid seeding in Alzheimer's disease and scrapie: mechanistic truths and physiological consequences of the time-dependent solubility of amyloid proteins. *Annu Rev Biochem* **1997,** *66*, 385-407.

7. DeBurman, S. K.; Raymond, G. J.; Caughey, B.; Lindquist, S., Chaperone-supervised conversion of prion protein to its protease-resistant form. *Proc Natl Acad Sci U S A* **1997,** *94* (25), 13938-43.

8. Brodsky, J. L.; Werner, E. D.; Dubas, M. E.; Goeckeler, J. L.; Kruse, K. B.; McCracken, A. A., The requirement for molecular chaperones during endoplasmic reticulum-associated protein degradation demonstrates that protein export and import are mechanistically distinct. *J Biol Chem* **1999,** *274* (6), 3453-60.

9. Wilkinson, B.; Gilbert, H. F., Protein disulfide isomerase. *Biochim Biophys Acta* **2004,** *1699* (1-2), 35-44.

10. Appenzeller-Herzog, C.; Ellgaard, L., The human PDI family: versatility packed into a single fold. *Biochim Biophys Acta* **2008,** *1783* (4), 535-48.

11. Hatahet, F.; Ruddock, L. W., Protein disulfide isomerase: a critical evaluation of its function in disulfide bond formation. *Antioxid Redox Signal* **2009,** *11* (11), 2807-50.

12. Galligan, J. J.; Petersen, D. R., The human protein disulfide isomerase gene family. *Hum Genomics* **2012,** *6*, 6.

13. Lee, E.; Lee, D. H., Emerging roles of protein disulfide isomerase in cancer. *BMB Rep* **2017,** *50* (8), 401-410.

14. Creighton, T. E., Intermediates in the refolding of reduced ribonuclease A. *J Mol Biol* **1979,** *129* (3), 411-31.

15. Rothwarf, D. M.; Li, Y. J.; Scheraga, H. A., Regeneration of bovine pancreatic ribonuclease A: identification of two nativelike three-disulfide intermediates involved in separate pathways. *Biochemistry* **1998,** *37* (11), 3760-6.

16. Creighton, T. E., The disulfide folding pathway of BPTI. *Science* **1992,** *256* (5053), 111-4.

17. Weissman, J. S.; Kim, P. S., Reexamination of the folding of BPTI: predominance of native intermediates. *Science* **1991,** *253* (5026), 1386-93.

18. Chang, J. Y.; Li, L.; Bulychev, A., The underlying mechanism for the diversity of disulfide folding pathways. *J Biol Chem* **2000,** *275* (12), 8287-9.

19. Fassio, A.; Sitia, R., Formation, isomerisation and reduction of disulphide bonds during protein quality control in the endoplasmic reticulum. *Histochem Cell Biol* **2002,** *117* (2), 151-7.

20. Helenius, A., Quality control in the secretory assembly line. *Philos Trans R Soc Lond B Biol Sci* **2001,** *356* (1406), 147-50.

21. Goldberger, R. F.; Epstein, C. J.; Anfinsen, C. B., Acceleration of reactivation of reduced bovine pancreatic ribonuclease by a microsomal system from rat liver. *J Biol Chem* **1963,** *238*, 628-35.

22. Venetianer, P.; Straub, F. B., The enzymic reactivation of reduced ribonuclease. *Biochim Biophys Acta* **1963,** *67*, 166-8.

23. Pelham, H. R., The retention signal for soluble proteins of the endoplasmic reticulum. *Trends Biochem Sci* **1990,** *15* (12), 483-6.

24. Ferrari, D. M.; Soling, H. D., The protein disulphide-isomerase family: unravelling a string of folds. *Biochem J* **1999,** *339 (Pt 1)*, 1-10.

25. Xu, S.; Sankar, S.; Neamati, N., Protein disulfide isomerase: a promising target for cancer therapy. *Drug Discov Today* **2014,** *19* (3), 222-40.

26. Peaper, D. R.; Cresswell, P., Regulation of MHC class I assembly and peptide binding. *Annu Rev Cell Dev Biol* **2008,** *24*, 343-68.

27. Janiszewski, M.; Lopes, L. R.; Carmo, A. O.; Pedro, M. A.; Brandes, R. P.; Santos, C. X.; Laurindo, F. R., Regulation of NAD(P)H oxidase by associated protein disulfide isomerase in vascular smooth muscle cells. *J Biol Chem* **2005,** *280* (49), 40813-9.

28. Cho, J.; Furie, B. C.; Coughlin, S. R.; Furie, B., A critical role for extracellular protein disulfide isomerase during thrombus formation in mice. *J Clin Invest* **2008,** *118* (3), 1123-31.

29. Jasuja, R.; Furie, B.; Furie, B. C., Endothelium-derived but not platelet-derived protein disulfide isomerase is required for thrombus formation in vivo. *Blood* **2010,** *116* (22), 4665-74.

30. Kim, K.; Hahm, E.; Li, J.; Holbrook, L. M.; Sasikumar, P.; Stanley, R. G.; Ushio-Fukai, M.; Gibbins, J. M.; Cho, J., Platelet protein disulfide isomerase is required for thrombus formation but not for hemostasis in mice. *Blood* **2013,** *122* (6), 1052-61.

31. Kozlov, G.; Maattanen, P.; Thomas, D. Y.; Gehring, K., A structural overview of the PDI family of proteins. *FEBS J* **2010,** *277* (19), 3924-36.

32. Alanen, H. I.; Williamson, R. A.; Howard, M. J.; Hatahet, F. S.; Salo, K. E.; Kauppila, A.; Kellokumpu, S.; Ruddock, L. W., ERp27, a new non-catalytic endoplasmic reticulum-located human protein disulfide isomerase family member, interacts with ERp57. *J Biol Chem* **2006,** *281* (44), 33727-38.

33. Mkrtchian, S.; Sandalova, T., ERp29, an Unusual Redox-Inactive Member of the Thioredoxin Family. *Antioxidants & Redox Signaling* **2006,** *8* (3), 325-337.

34. Givol, D.; Delorenzo, F.; Goldberger, R. F.; Anfinsen, C. B., Disulfide Interchange and the Three-Dimensional Structure of Proteins. *Proc Natl Acad Sci U S A* **1965,** *53*, 676-84.

35. Givol, D.; Goldberger, R. F.; Anfinsen, C. B., Oxidation and Disulfide Interchange in the Reactivation of Reduced Ribonuclease. *J Biol Chem* **1964,** *239*, PC3114-16.

36. Goldberger, R. F.; Epstein, C. J.; Anfinsen, C. B., Purification and Properties of a Microsomal Enzyme System Catalyzing the Reactivation of Reduced Ribonuclease and Lysozyme. *J Biol Chem* **1964,** *239*, 1406-10.

37. Wang, C.; Li, W.; Ren, J.; Fang, J.; Ke, H.; Gong, W.; Feng, W.; Wang, C. C., Structural insights into the redox-regulated dynamic conformations of human protein disulfide isomerase. *Antioxid Redox Signal* **2013,** *19* (1), 36-45.
38. Ellgaard, L.; Ruddock, L. W., The human protein disulphide isomerase family: substrate interactions and functional properties. *EMBO Rep* **2005,** *6* (1), 28-32.
39. Hatahet, F.; Ruddock, L. W., Substrate recognition by the protein disulfide isomerases. *FEBS J* **2007,** *274* (20), 5223-34.
40. Vuori, K.; Myllyla, R.; Pihlajaniemi, T.; Kivirikko, K. I., Expression and site-directed mutagenesis of human protein disulfide isomerase in Escherichia coli. This multifunctional polypeptide has two independently acting catalytic sites for the isomerase activity. *J Biol Chem* **1992,** *267* (11), 7211-4.
41. Ruddock, L. W.; Hirst, T. R.; Freedman, R. B., pH-dependence of the dithiol-oxidizing activity of DsbA (a periplasmic protein thiol:disulphide oxidoreductase) and protein disulphide-isomerase: studies with a novel simple peptide substrate. *Biochem J* **1996,** *315 (Pt 3)*, 1001-5.
42. Kortemme, T.; Darby, N. J.; Creighton, T. E., Electrostatic interactions in the active site of the N-terminal thioredoxin-like domain of protein disulfide isomerase. *Biochemistry* **1996,** *35* (46), 14503-11.
43. Zapun, A.; Bardwell, J. C.; Creighton, T. E., The reactive and destabilizing disulfide bond of DsbA, a protein required for protein disulfide bond formation in vivo. *Biochemistry* **1993,** *32* (19), 5083-92.
44. Lappi, A. K.; Lensink, M. F.; Alanen, H. I.; Salo, K. E.; Lobell, M.; Juffer, A. H.; Ruddock, L. W., A conserved arginine plays a role in the catalytic cycle of the protein disulphide isomerases. *J Mol Biol* **2004,** *335* (1), 283-95.
45. Klappa, P.; Ruddock, L. W.; Darby, N. J.; Freedman, R. B., The b' domain provides the principal peptide-binding site of protein disulfide isomerase but all domains contribute to binding of misfolded proteins. *EMBO J* **1998,** *17* (4), 927-35.
46. Pirneskoski, A.; Klappa, P.; Lobell, M.; Williamson, R. A.; Byrne, L.; Alanen, H. I.; Salo, K. E.; Kivirikko, K. I.; Freedman, R. B.; Ruddock, L. W., Molecular characterization of the principal substrate binding site of the ubiquitous folding catalyst protein disulfide isomerase. *J Biol Chem* **2004,** *279* (11), 10374-81.

47. Pirneskoski, A.; Ruddock, L. W.; Klappa, P.; Freedman, R. B.; Kivirikko, K. I.; Koivunen, P., Domains b' and a' of protein disulfide isomerase fulfill the minimum requirement for function as a subunit of prolyl 4-hydroxylase. The N-terminal domains a and b enhances this function and can be substituted in part by those of ERp57. *J Biol Chem* **2001,** *276* (14), 11287-93.
48. Cai, H.; Wang, C. C.; Tsou, C. L., Chaperone-like activity of protein disulfide isomerase in the refolding of a protein with no disulfide bonds. *J Biol Chem* **1994,** *269* (40), 24550-2.
49. Puig, A.; Gilbert, H. F., Protein disulfide isomerase exhibits chaperone and anti-chaperone activity in the oxidative refolding of lysozyme. *J Biol Chem* **1994,** *269* (10), 7764-71.
50. Song, J. L.; Wang, C. C., Chaperone-like activity of protein disulfide-isomerase in the refolding of rhodanese. *Eur J Biochem* **1995,** *231* (2), 312-6.
51. Primm, T. P.; Walker, K. W.; Gilbert, H. F., Facilitated protein aggregation. Effects of calcium on the chaperone and anti-chaperone activity of protein disulfide-isomerase. *J Biol Chem* **1996,** *271* (52), 33664-9.
52. Dai, Y.; Wang, C., A mutant truncated protein disulfide isomerase with no chaperone activity. *J Biol Chem* **1997,** *272* (44), 27572-6.
53. Bulleid, N. J.; Freedman, R. B., Defective co-translational formation of disulphide bonds in protein disulphide-isomerase-deficient microsomes. *Nature* **1988,** *335* (6191), 649-51.
54. Molinari, M.; Helenius, A., Glycoproteins form mixed disulphides with oxidoreductases during folding in living cells. *Nature* **1999,** *402* (6757), 90-3.
55. Araki, K.; Inaba, K., Structure, mechanism, and evolution of Ero1 family enzymes. *Antioxid Redox Signal* **2012,** *16* (8), 790-9.
56. Walker, K. W.; Gilbert, H. F., Oxidation of kinetically trapped thiols by protein disulfide isomerase. *Biochemistry* **1995,** *34* (41), 13642-50.
57. Frand, A. R.; Kaiser, C. A., Ero1p oxidizes protein disulfide isomerase in a pathway for disulfide bond formation in the endoplasmic reticulum. *Mol Cell* **1999,** *4* (4), 469-77.

58. Gross, E.; Kastner, D. B.; Kaiser, C. A.; Fass, D., Structure of Ero1p, source of disulfide bonds for oxidative protein folding in the cell. *Cell* **2004,** *117* (5), 601-10.
59. Gross, E.; Sevier, C. S.; Heldman, N.; Vitu, E.; Bentzur, M.; Kaiser, C. A.; Thorpe, C.; Fass, D., Generating disulfides enzymatically: reaction products and electron acceptors of the endoplasmic reticulum thiol oxidase Ero1p. *Proc Natl Acad Sci U S A* **2006,** *103* (2), 299-304.
60. Walker, K. W.; Gilbert, H. F., Scanning and escape during protein-disulfide isomerase-assisted protein folding. *J Biol Chem* **1997,** *272* (14), 8845-8.
61. Karala, A. R.; Lappi, A. K.; Ruddock, L. W., Modulation of an active-site cysteine pKa allows PDI to act as a catalyst of both disulfide bond formation and isomerization. *J Mol Biol* **2010,** *396* (4), 883-92.
62. van Lith, M.; Karala, A. R.; Bown, D.; Gatehouse, J. A.; Ruddock, L. W.; Saunders, P. T.; Benham, A. M., A developmentally regulated chaperone complex for the endoplasmic reticulum of male haploid germ cells. *Mol Biol Cell* **2007,** *18* (8), 2795-804.
63. Walker, K. W.; Lyles, M. M.; Gilbert, H. F., Catalysis of oxidative protein folding by mutants of protein disulfide isomerase with a single active-site cysteine. *Biochemistry* **1996,** *35* (6), 1972-80.
64. Quan, H.; Fan, G.; Wang, C. C., Independence of the chaperone activity of protein disulfide isomerase from its thioredoxin-like active site. *J Biol Chem* **1995,** *270* (29), 17078-80.
65. Sideraki, V.; Gilbert, H. F., Mechanism of the antichaperone activity of protein disulfide isomerase: facilitated assembly of large, insoluble aggregates of denatured lysozyme and PDI. *Biochemistry* **2000,** *39* (5), 1180-8.
66. Puig, A.; Gilbert, H. F., Anti-chaperone behavior of BiP during the protein disulfide isomerase-catalyzed refolding of reduced denatured lysozyme. *J Biol Chem* **1994,** *269* (41), 25889-96.
67. Network, T. C. G. A. R., Comprehensive genomic characterization defines human glioblastoma genes and core pathways. *Nature* **2008,** *455* (7216), 1061-8.
68. Shai, R.; Shi, T.; Kremen, T. J.; Horvath, S.; Liau, L. M.; Cloughesy, T. F.; Mischel, P. S.; Nelson, S. F., Gene expression profiling identifies molecular subtypes of gliomas. *Oncogene* **2003,** *22* (31), 4918-23.

69. van de Vijver, M. J.; He, Y. D.; van't Veer, L. J.; Dai, H.; Hart, A. A.; Voskuil, D. W.; Schreiber, G. J.; Peterse, J. L.; Roberts, C.; Marton, M. J.; Parrish, M.; Atsma, D.; Witteveen, A.; Glas, A.; Delahaye, L.; van der Velde, T.; Bartelink, H.; Rodenhuis, S.; Rutgers, E. T.; Friend, S. H.; Bernards, R., A gene-expression signature as a predictor of survival in breast cancer. *N Engl J Med* **2002,** *347* (25), 1999-2009.

70. Uehara, T.; Nakamura, T.; Yao, D.; Shi, Z. Q.; Gu, Z.; Ma, Y.; Masliah, E.; Nomura, Y.; Lipton, S. A., S-nitrosylated protein-disulphide isomerase links protein misfolding to neurodegeneration. *Nature* **2006,** *441* (7092), 513-7.

71. Unterberger, U.; Hoftberger, R.; Gelpi, E.; Flicker, H.; Budka, H.; Voigtlander, T., Endoplasmic reticulum stress features are prominent in Alzheimer disease but not in prion diseases in vivo. *J Neuropathol Exp Neurol* **2006,** *65* (4), 348-57.

72. Hoozemans, J. J.; van Haastert, E. S.; Eikelenboom, P.; de Vos, R. A.; Rozemuller, J. M.; Scheper, W., Activation of the unfolded protein response in Parkinson's disease. *Biochem Biophys Res Commun* **2007,** *354* (3), 707-11.

73. Hoffstrom, B. G.; Kaplan, A.; Letso, R.; Schmid, R. S.; Turmel, G. J.; Lo, D. C.; Stockwell, B. R., Inhibitors of protein disulfide isomerase suppress apoptosis induced by misfolded proteins. *Nat Chem Biol* **2010,** *6* (12), 900-6.

74. Shibata, E.; Ejima, K.; Nanri, H.; Toki, N.; Koyama, C.; Ikeda, M.; Kashimura, M., Enhanced protein levels of protein thiol/disulphide oxidoreductases in placentae from pre-eclamptic subjects. *Placenta* **2001,** *22* (6), 566-72.

75. Severino, A.; Campioni, M.; Straino, S.; Salloum, F. N.; Schmidt, N.; Herbrand, U.; Frede, S.; Toietta, G.; Di Rocco, G.; Bussani, R.; Silvestri, F.; Piro, M.; Liuzzo, G.; Biasucci, L. M.; Mellone, P.; Feroce, F.; Capogrossi, M.; Baldi, F.; Fandrey, J.; Ehrmann, M.; Crea, F.; Abbate, A.; Baldi, A., Identification of protein disulfide isomerase as a cardiomyocyte survival factor in ischemic cardiomyopathy. *J Am Coll Cardiol* **2007,** *50* (11), 1029-37.

76. Laurindo, F. R.; Fernandes, D. C.; Amanso, A. M.; Lopes, L. R.; Santos, C. X., Novel role of protein disulfide isomerase in the regulation of NADPH oxidase activity: pathophysiological implications in vascular diseases. *Antioxid Redox Signal* **2008,** *10* (6), 1101-13.

77. Basso, K.; Margolin, A. A.; Stolovitzky, G.; Klein, U.; Dalla-Favera, R.; Califano, A., Reverse engineering of regulatory networks in human B cells. *Nat Genet* **2005,** *37* (4), 382-90.
78. Compagno, M.; Lim, W. K.; Grunn, A.; Nandula, S. V.; Brahmachary, M.; Shen, Q.; Bertoni, F.; Ponzoni, M.; Scandurra, M.; Califano, A.; Bhagat, G.; Chadburn, A.; Dalla-Favera, R.; Pasqualucci, L., Mutations of multiple genes cause deregulation of NF-kappaB in diffuse large B-cell lymphoma. *Nature* **2009,** *459* (7247), 717-21.
79. Piccaluga, P. P.; Agostinelli, C.; Califano, A.; Rossi, M.; Basso, K.; Zupo, S.; Went, P.; Klein, U.; Zinzani, P. L.; Baccarani, M.; Dalla Favera, R.; Pileri, S. A., Gene expression analysis of peripheral T cell lymphoma, unspecified, reveals distinct profiles and new potential therapeutic targets. *J Clin Invest* **2007,** *117* (3), 823-34.
80. Rickman, D. S.; Bobek, M. P.; Misek, D. E.; Kuick, R.; Blaivas, M.; Kurnit, D. M.; Taylor, J.; Hanash, S. M., Distinctive molecular profiles of high-grade and low-grade gliomas based on oligonucleotide microarray analysis. *Cancer Res* **2001,** *61* (18), 6885-91.
81. Gutmann, D. H.; Hedrick, N. M.; Li, J.; Nagarajan, R.; Perry, A.; Watson, M. A., Comparative gene expression profile analysis of neurofibromatosis 1-associated and sporadic pilocytic astrocytomas. *Cancer Res* **2002,** *62* (7), 2085-91.
82. Sun, L.; Hui, A. M.; Su, Q.; Vortmeyer, A.; Kotliarov, Y.; Pastorino, S.; Passaniti, A.; Menon, J.; Walling, J.; Bailey, R.; Rosenblum, M.; Mikkelsen, T.; Fine, H. A., Neuronal and glioma-derived stem cell factor induces angiogenesis within the brain. *Cancer Cell* **2006,** *9* (4), 287-300.
83. Bredel, M.; Bredel, C.; Juric, D.; Harsh, G. R.; Vogel, H.; Recht, L. D.; Sikic, B. I., Functional network analysis reveals extended gliomagenesis pathway maps and three novel MYC-interacting genes in human gliomas. *Cancer Res* **2005,** *65* (19), 8679-89.
84. Bonome, T.; Levine, D. A.; Shih, J.; Randonovich, M.; Pise-Masison, C. A.; Bogomolniy, F.; Ozbun, L.; Brady, J.; Barrett, J. C.; Boyd, J.; Birrer, M. J., A gene signature predicting for survival in suboptimally debulked patients with ovarian cancer. *Cancer Res* **2008,** *68* (13), 5478-86.
85. Welsh, J. B.; Zarrinkar, P. P.; Sapinoso, L. M.; Kern, S. G.; Behling, C. A.; Monk, B. J.; Lockhart, D. J.; Burger, R. A.; Hampton, G. M., Analysis of gene expression

profiles in normal and neoplastic ovarian tissue samples identifies candidate molecular markers of epithelial ovarian cancer. *Proc Natl Acad Sci U S A* **2001,** *98* (3), 1176-81.
86. Yusenko, M. V.; Kuiper, R. P.; Boethe, T.; Ljungberg, B.; van Kessel, A. G.; Kovacs, G., High-resolution DNA copy number and gene expression analyses distinguish chromophobe renal cell carcinomas and renal oncocytomas. *BMC Cancer* **2009,** *9*, 152.
87. Beroukhim, R.; Brunet, J. P.; Di Napoli, A.; Mertz, K. D.; Seeley, A.; Pires, M. M.; Linhart, D.; Worrell, R. A.; Moch, H.; Rubin, M. A.; Sellers, W. R.; Meyerson, M.; Linehan, W. M.; Kaelin, W. G., Jr.; Signoretti, S., Patterns of gene expression and copy-number alterations in von-hippel lindau disease-associated and sporadic clear cell carcinoma of the kidney. *Cancer Res* **2009,** *69* (11), 4674-81.
88. Jones, J.; Otu, H.; Spentzos, D.; Kolia, S.; Inan, M.; Beecken, W. D.; Fellbaum, C.; Gu, X.; Joseph, M.; Pantuck, A. J.; Jonas, D.; Libermann, T. A., Gene signatures of progression and metastasis in renal cell cancer. *Clin Cancer Res* **2005,** *11* (16), 5730-9.
89. Welsh, J. B.; Sapinoso, L. M.; Su, A. I.; Kern, S. G.; Wang-Rodriguez, J.; Moskaluk, C. A.; Frierson, H. F., Jr.; Hampton, G. M., Analysis of gene expression identifies candidate markers and pharmacological targets in prostate cancer. *Cancer Res* **2001,** *61* (16), 5974-8.
90. Singh, D.; Febbo, P. G.; Ross, K.; Jackson, D. G.; Manola, J.; Ladd, C.; Tamayo, P.; Renshaw, A. A.; D'Amico, A. V.; Richie, J. P.; Lander, E. S.; Loda, M.; Kantoff, P. W.; Golub, T. R.; Sellers, W. R., Gene expression correlates of clinical prostate cancer behavior. *Cancer Cell* **2002,** *1* (2), 203-9.
91. Alaiya, A. A.; Al-Mohanna, M.; Aslam, M.; Shinwari, Z.; Al-Mansouri, L.; Al-Rodayan, M.; Al-Eid, M.; Ahmad, I.; Hanash, K.; Tulbah, A.; Bin Mahfooz, A.; Adra, C., Proteomics-based signature for human benign prostate hyperplasia and prostate adenocarcinoma. *Int J Oncol* **2011,** *38* (4), 1047-57.
92. Chahed, K.; Kabbage, M.; Ehret-Sabatier, L.; Lemaitre-Guillier, C.; Remadi, S.; Hoebeke, J.; Chouchane, L., Expression of fibrinogen E-fragment and fibrin E-fragment is inhibited in the human infiltrating ductal carcinoma of the breast: the two-dimensional electrophoresis and MALDI-TOF-mass spectrometry analyses. *Int J Oncol* **2005,** *27* (5), 1425-31.

93. Chahed, K.; Kabbage, M.; Hamrita, B.; Guillier, C. L.; Trimeche, M.; Remadi, S.; Ehret-Sabatier, L.; Chouchane, L., Detection of protein alterations in male breast cancer using two dimensional gel electrophoresis and mass spectrometry: the involvement of several pathways in tumorigenesis. *Clin Chim Acta* **2008,** *388* (1-2), 106-14.
94. Chen, J.; Kahne, T.; Rocken, C.; Gotze, T.; Yu, J.; Sung, J. J.; Chen, M.; Hu, P.; Malfertheiner, P.; Ebert, M. P., Proteome analysis of gastric cancer metastasis by two-dimensional gel electrophoresis and matrix assisted laser desorption/ionization-mass spectrometry for identification of metastasis-related proteins. *J Proteome Res* **2004,** *3* (5), 1009-16.
95. Thongwatchara, P.; Promwikorn, W.; Srisomsap, C.; Chokchaichamnankit, D.; Boonyaphiphat, P.; Thongsuksai, P., Differential protein expression in primary breast cancer and matched axillary node metastasis. *Oncol Rep* **2011,** *26* (1), 185-91.
96. Goplen, D.; Wang, J.; Enger, P. O.; Tysnes, B. B.; Terzis, A. J.; Laerum, O. D.; Bjerkvig, R., Protein disulfide isomerase expression is related to the invasive properties of malignant glioma. *Cancer Res* **2006,** *66* (20), 9895-902.
97. Gromov, P.; Gromova, I.; Bunkenborg, J.; Cabezon, T.; Moreira, J. M.; Timmermans-Wielenga, V.; Roepstorff, P.; Rank, F.; Celis, J. E., Up-regulated proteins in the fluid bathing the tumour cell microenvironment as potential serological markers for early detection of cancer of the breast. *Mol Oncol* **2010,** *4* (1), 65-89.
98. Ataman-Onal, Y.; Beaulieu, C.; Busseret, S.; Charrier, J. P.; Choquet-Kastylevsky, G.; Rolland, D. Protein disulfide isomerase assay method for the in vitro diagnosis of colorectal cancer. 20110104701, 2011.
99. Gonzalez-Santiago, L.; Alfonso, P.; Suarez, Y.; Nunez, A.; Garcia-Fernandez, L. F.; Alvarez, E.; Munoz, A.; Casal, J. I., Proteomic analysis of the resistance to aplidin in human cancer cells. *J Proteome Res* **2007,** *6* (4), 1286-94.
100. Sakai, R.; Rinehart, K. L.; Kishore, V.; Kundu, B.; Faircloth, G.; Gloer, J. B.; Carney, J. R.; Namikoshi, M.; Sun, F.; Hughes, R. G., Jr.; Garcia Gravalos, D.; de Quesada, T. G.; Wilson, G. R.; Heid, R. M., Structure--activity relationships of the didemnins. *J Med Chem* **1996,** *39* (14), 2819-34.
101. Eirich, J.; Braig, S.; Schyschka, L.; Servatius, P.; Hoffmann, J.; Hecht, S.; Fulda, S.; Zahler, S.; Antes, I.; Kazmaier, U.; Sieber, S. A.; Vollmar, A. M., A small molecule

inhibits protein disulfide isomerase and triggers the chemosensitization of cancer cells. *Angew Chem Int Ed Engl* **2014,** *53* (47), 12960-5.

102. Gallina, A.; Hanley, T. M.; Mandel, R.; Trahey, M.; Broder, C. C.; Viglianti, G. A.; Ryser, H. J., Inhibitors of protein-disulfide isomerase prevent cleavage of disulfide bonds in receptor-bound glycoprotein 120 and prevent HIV-1 entry. *J Biol Chem* **2002,** *277* (52), 50579-88.

103. Barbouche, R.; Miquelis, R.; Jones, I. M.; Fenouillet, E., Protein-disulfide isomerase-mediated reduction of two disulfide bonds of HIV envelope glycoprotein 120 occurs post-CXCR4 binding and is required for fusion. *J Biol Chem* **2003,** *278* (5), 3131-6.

104. Markovic, I.; Stantchev, T. S.; Fields, K. H.; Tiffany, L. J.; Tomic, M.; Weiss, C. D.; Broder, C. C.; Strebel, K.; Clouse, K. A., Thiol/disulfide exchange is a prerequisite for CXCR4-tropic HIV-1 envelope-mediated T-cell fusion during viral entry. *Blood* **2004,** *103* (5), 1586-94.

105. Pierson, T. C.; Doms, R. W.; Pohlmann, S., Prospects of HIV-1 entry inhibitors as novel therapeutics. *Rev Med Virol* **2004,** *14* (4), 255-70.

106. Ryser, H. J.; Levy, E. M.; Mandel, R.; DiSciullo, G. J., Inhibition of human immunodeficiency virus infection by agents that interfere with thiol-disulfide interchange upon virus-receptor interaction. *Proc Natl Acad Sci U S A* **1994,** *91* (10), 4559-63.

107. Ryser, H. J.; Fluckiger, R., Progress in targeting HIV-1 entry. *Drug Discov Today* **2005,** *10* (16), 1085-94.

108. Chen, V. M.; Hogg, P. J., Allosteric disulfide bonds in thrombosis and thrombolysis. *J Thromb Haemost* **2006,** *4* (12), 2533-41.

109. Morishima, S.; Ogawa, S.; Matsubara, A.; Kawase, T.; Nannya, Y.; Kashiwase, K.; Satake, M.; Saji, H.; Inoko, H.; Kato, S.; Kodera, Y.; Sasazuki, T.; Morishima, Y.; Japan Marrow Donor, P., Impact of highly conserved HLA haplotype on acute graft-versus-host disease. *Blood* **2010,** *115* (23), 4664-70.

110. Chen, K.; Lin, Y.; Detwiler, T. C., Protein disulfide isomerase activity is released by activated platelets. *Blood* **1992,** *79* (9), 2226-8.

111. Essex, D. W.; Chen, K.; Swiatkowska, M., Localization of protein disulfide isomerase to the external surface of the platelet plasma membrane. *Blood* **1995,** *86* (6), 2168-73.
112. Roth, R. A., Bacitracin: an inhibitor of the insulin degrading activity of glutathione-insulin transhydrogenase. *Biochem Biophys Res Commun* **1981,** *98* (2), 431-8.
113. Dickerhof, N.; Kleffmann, T.; Jack, R.; McCormick, S., Bacitracin inhibits the reductive activity of protein disulfide isomerase by disulfide bond formation with free cysteines in the substrate-binding domain. *FEBS J* **2011,** *278* (12), 2034-43.
114. Karala, A. R.; Ruddock, L. W., Bacitracin is not a specific inhibitor of protein disulfide isomerase. *FEBS J* **2010,** *277* (11), 2454-62.
115. Khan, M. M.; Simizu, S.; Lai, N. S.; Kawatani, M.; Shimizu, T.; Osada, H., Discovery of a small molecule PDI inhibitor that inhibits reduction of HIV-1 envelope glycoprotein gp120. *ACS Chem Biol* **2011,** *6* (3), 245-51.
116. Jasuja, R.; Passam, F. H.; Kennedy, D. R.; Kim, S. H.; van Hessem, L.; Lin, L.; Bowley, S. R.; Joshi, S. S.; Dilks, J. R.; Furie, B.; Furie, B. C.; Flaumenhaft, R., Protein disulfide isomerase inhibitors constitute a new class of antithrombotic agents. *J Clin Invest* **2012,** *122* (6), 2104-13.
117. Lin, L.; Gopal, S.; Sharda, A.; Passam, F.; Bowley, S. R.; Stopa, J.; Xue, G.; Yuan, C.; Furie, B. C.; Flaumenhaft, R.; Huang, M.; Furie, B., Quercetin-3-rutinoside Inhibits Protein Disulfide Isomerase by Binding to Its b'x Domain. *J Biol Chem* **2015,** *290* (39), 23543-52.
118. Gao, M.; Yang, Q.; Wang, M.; Miller, K. D.; Sledge, G. W.; Zheng, Q. H., Synthesis of radiolabeled protein disulfide isomerase (PDI) inhibitors as new potential PET agents for imaging of the enzyme PDI in neurological disorders and cancer. *Appl Radiat Isot* **2013,** *74*, 61-9.
119. Ge, J.; Zhang, C. J.; Li, L.; Chong, L. M.; Wu, X.; Hao, P.; Sze, S. K.; Yao, S. Q., Small molecule probe suitable for in situ profiling and inhibition of protein disulfide isomerase. *ACS Chem Biol* **2013,** *8* (11), 2577-85.
120. Yamada, R.; Cao, X.; Butkevich, A. N.; Millard, M.; Odde, S.; Mordwinkin, N.; Gundla, R.; Zandi, E.; Louie, S. G.; Petasis, N. A.; Neamati, N., Discovery and

preclinical evaluation of a novel class of cytotoxic propynoic acid carbamoyl methyl amides (PACMAs). *J Med Chem* **2011,** *54* (8), 2902-14.

121. Xu, S.; Butkevich, A. N.; Yamada, R.; Zhou, Y.; Debnath, B.; Duncan, R.; Zandi, E.; Petasis, N. A.; Neamati, N., Discovery of an orally active small-molecule irreversible inhibitor of protein disulfide isomerase for ovarian cancer treatment. *Proc Natl Acad Sci U S A* **2012,** *109* (40), 16348-53.

122. Vincenz, L.; Jager, R.; O'Dwyer, M.; Samali, A., Endoplasmic reticulum stress and the unfolded protein response: targeting the Achilles heel of multiple myeloma. *Mol Cancer Ther* **2013,** *12* (6), 831-43.

123. Masciarelli, S.; Sitia, R., Building and operating an antibody factory: redox control during B to plasma cell terminal differentiation. *Biochim Biophys Acta* **2008,** *1783* (4), 578-88.

124. Vatolin, S.; Phillips, J. G.; Jha, B. K.; Govindgari, S.; Hu, J.; Grabowski, D.; Parker, Y.; Lindner, D. J.; Zhong, F.; Distelhorst, C. W.; Smith, M. R.; Cotta, C.; Xu, Y.; Chilakala, S.; Kuang, R. R.; Tall, S.; Reu, F. J., Novel Protein Disulfide Isomerase Inhibitor with Anticancer Activity in Multiple Myeloma. *Cancer Res* **2016,** *76* (11), 3340-50.

125. Nakayama, S.; Atsumi, R.; Takakusa, H.; Kobayashi, Y.; Kurihara, A.; Nagai, Y.; Nakai, D.; Okazaki, O., A zone classification system for risk assessment of idiosyncratic drug toxicity using daily dose and covalent binding. *Drug Metab Dispos* **2009,** *37* (9), 1970-7.

126. Allimuthu, D.; Adams, D. J., 2-Chloropropionamide As a Low-Reactivity Electrophile for Irreversible Small-Molecule Probe Identification. *ACS Chem Biol* **2017,** *12* (8), 2124-2131.

127. Banerjee, R.; Pace, N. J.; Brown, D. R.; Weerapana, E., 1,3,5-Triazine as a modular scaffold for covalent inhibitors with streamlined target identification. *J Am Chem Soc* **2013,** *135* (7), 2497-500.

CHAPTER 2

CHARACTERIZATION OF AN A-SITE SELECTIVE PROTEIN DISULFIDE ISOMERASE A1 INHIBITOR

UPR activation data was collected by Kenny Chen, working under Prof. Matt Shoulders in the Chemistry Department at MIT. ALLC secretion data was collected by Julia Grandjean, working under Prof. R. Luke Wiseman in the Department of Molecular Medicine at The Scripps Research Institute.

2.0 Abstract

Protein disulfide isomerase A1 (PDIA1) is a thiol-disulfide oxidoreductase localized in the lumen of the endoplasmic reticulum (ER), and is an important folding catalyst and chaperone for proteins in the secretory pathway. PDIA1 contains two active-site domains (**a** and **a'**), each containing a Cys-Gly-His-Cys (CGHC) active-site motif. The two active-site domains share only 37% sequence identity, and several studies point to the functional nonequivalence of these two regions. Numerous inhibitors for PDIA1 have been reported, yet the selectivity of these inhibitors toward the **a** and **a'** sites have been poorly characterized. We previously identified a cysteine-reactive PDIA1 inhibitor, RB-11-ca, which demonstrates **a**-site selectivity. Here, we synthesize a targeted library to optimize the potency and selectivity of RB-11-ca. Characterization of this targeted library afforded an optimized PDIA1 inhibitor, KSC-34, which covalently modifies C53 in the **a** site of PDIA1, and demonstrates 30-fold selectivity for the **a** site over the **a'** site. KSC-34 shows time-dependent inhibition of the reductase activity of PDIA1 *in vitro* with a $k_{inact}/K_I = 9.66 \times 10^3$ $M^{-1}s^{-1}$. KSC-34 is highly selective for PDIA1 over members of the PDI family, as well as other cellular cysteine-containing proteins. PDIA1 inhibition by KSC-34 has minimal sustained effects on the cellular unfolded protein response (UPR), indicating that **a**-site inhibition does not globally induce protein-folding associated ER stress. KSC-34 treatment significantly decreases secretion of a destabilized, amyloidogenic antibody light chain, illustrating the ability of **a**-site selective PDIA1 inhibitors to minimize pathogenic amyloidogenic extracellular proteins that rely on high PDIA1 activity for proper folding and secretion. Given the poor understanding of the contribution of each PDIA1 active site to the (patho)physiological functions of PDIA1, site-selective inhibitors like KSC-34

provide useful tools for delineating the pathological role and therapeutic potential of PDIA1.

2.1 Introduction

Proper folding of nascent proteins in the cell is accelerated by chaperones that serve to stabilize protein domains and overall structure. One such family of protein-folding catalysts comprise dithiol-disulfide oxidoreductases of the protein disulfide isomerase (PDI) family. The PDI family is primarily located in the endoplasmic reticulum (ER), and includes 21 proteins with at least one thioredoxin-like domain. PDIs contain two different types of thioredoxin-like domains, catalytic (**a**) and non-catalytic (**b**)[1-2]. The catalytic **a** domains of the PDIs are responsible for catalyzing the oxidation, reduction, and isomerization of disulfide bonds in nascent proteins. The non-catalytic **b** domains are rigid spacers between the catalytic domains that are involved in recognizing and recruiting unfolded protein substrates[1].

Protein disulfide isomerase A1 (PDIA1)[3-4] was the first PDI family member to be discovered[5-6]. PDIA1 is a 57 kDa oxidoreductase and molecular chaperone that localizes in the lumen of the ER, and accounts for roughly 0.8% of total cellular protein[7]. PDIA1 catalyzes the oxidation, reduction, and isomerization of disulfide bonds between cysteine residues on its protein substrates. PDIA1 is organized into four globular domains, **a**, **b**, **b'**, and **a'**, as well as a highly acidic C-terminal extension with a KDEL ER-retention sequence (Figure 2.1)[3-4]. The **a** and **a'** domains functionally resemble thioredoxin, and contain redox catalytic Cys-Gly-His-Cys (CGHC) active-site motifs. It is known that the **a** and **a'**

domains operate independently of each other because mutation of either active-site cysteine eliminated 50% of the catalytic activity of PDIA1 *in vitro*, while mutations in both active sites completely abolished activity[8]. The non-catalytic domains, **b** and **b'**, are primarily for spacing and substrate recruitment. The **b'** domain is the major substrate binding site of PDIA1, containing a large hydrophobic cavity between helices α1 and α3 to interact with unfolded protein substrates[1, 9]. PDIA1 has also been shown to possess chaperone activity, by inhibiting the aggregation of misfolded protein substrates at stoichiometric concentrations[10-13]. The chaperone activity of PDIA1 is independent of the two catalytic CGHC active-site motifs, but dependent on the non-catalytic **b** sites[14]. This was confirmed by truncation of the C-terminal **b'** domain of PDIA1, which abolished all chaperone activity without significantly impacting isomerase activity[15].

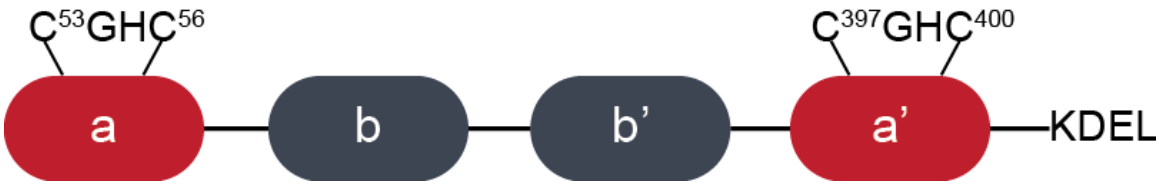

Figure 2.1. Domain organization of PDIA1. PDIA1 comprises two active-site **a**-type domains that contain a CGHC active-site motif, together with two **b**-domains implicated in substrate recognition and binding.

The dysregulation of PDIA1 activity has been implicated in a variety of diseases, including cancer[3, 16-18], cardiovascular[19-21], and neurodegenerative[22-25] diseases. Gene-expression profiles indicate that PDIA1 is overexpressed (>2-fold) in a wide variety of cancers, including lymphoma[26-28], brain, and CNS cancers[16-17, 29-32], ovarian[33-34], kidney[35-37], and prostate[38-39]. Furthermore, expression levels of PDIA1 have been correlated with overall patient survival rates in brain and breast cancers, whereby patients with lower expression levels of PDIA1 have significantly higher survival rates[3, 16-18]. PDIA1 is retained in the ER through a C-terminal KDEL retention signal sequence, however, the presence of PDIA1 in the extracellular milieu is well documented[3, 40-41]. Extracellular PDIA1 is involved in many biological processes such as platelet activation, thrombus formation, and viral infection. For example, PDIA1 can catalyze the reduction of structural disulfides on gp120, which results in a major conformational change, allowing the HIV virus to interact with the cell surface[40].

The demonstrated role of increased PDIA1 activity in various diseases has spurred the development of a variety of small-molecule inhibitors targeting PDIA1. Juniferdin, discovered in a high-throughput screen of natural products, was found to inhibit extracellular PDIA1-mediated disulfide-bond reduction of gp120, thus inhibiting HIV entry into host cells[40]. Quercetin-3-rutinoside has been shown to bind to the **b'x** region of extracellular PDIA1 to induce a compact conformation, thus constricting the overall flexibility of PDIA1, and inhibiting thrombus formation[42]. T8 and derivative JP04-042 were reported to sensitize cancer cells to sub-toxic concentrations of etoposide through inhibition of PDIA1 by reversible binding near the active sites[43]. Another reversible inhibitor of PDIA1, LOC14, was identified from a high-throughput screen of ~10,000

compounds, and reversibly binds PDIA1 to induce an oxidized conformation. This LOC14-induced oxidative conformation has been shown to be neuroprotective in PC12 cells expressing mutant huntingtin protein[44]. PACMA31 is an irreversible PDIA1 inhibitor that reacts through a propynoic acid carbamoyl methyl amide moiety, and suppresses tumor growth in a mouse xenograft model of ovarian cancer[45]. S-CW3554 possesses a 2-chloropropionamide reactive group, and has been shown to be cytotoxic to various multiple myeloma cell lines[46]. 16F16, an irreversible inhibitor that reacts with PDIA1 via a chloroacetamide electrophile, prevents neuronal cell death in a cell-based model of Huntington's disease[25]. Lastly, P1, an irreversible inhibitor, which reacts via a vinyl-sulfone electrophile, demonstrated anti-proliferative effects in a variety of cancers[47].

In 2013, we reported RB-11-ca (Figure 2.2A), a cell-permeable, irreversible inhibitor of PDIA1[48]. RB-11-ca is a tri-functionalized triazine-based covalent inhibitor that contains an alkyne-handle for reporter-tag conjugation via copper-catalyzed azide-alkyne cycloaddition (CuAAC), an octylamine diversity element for binding specificity, and an electrophilic chloroacetamide for irreversible modification of proximal cysteine residues. PDIA1 was identified as the primary target of RB-11-ca after CuAAC-mediated conjugation of a biotin group, avidin enrichment, and subsequent target identification via LC/LC-MS/MS. The specific cysteine residue targeted by RB-11-ca was determined using cysteine-to-alanine mutants of each cysteine residue within the CXXC motifs of the two **a** domains. RB-11-ca was confirmed to bind to C53, the N-terminal cysteine in the **a** domain of PDIA1[48]. RB-11-ca was therefore unique in that it was the first characterized **a**-domain selective inhibitor reported for PDIA1.

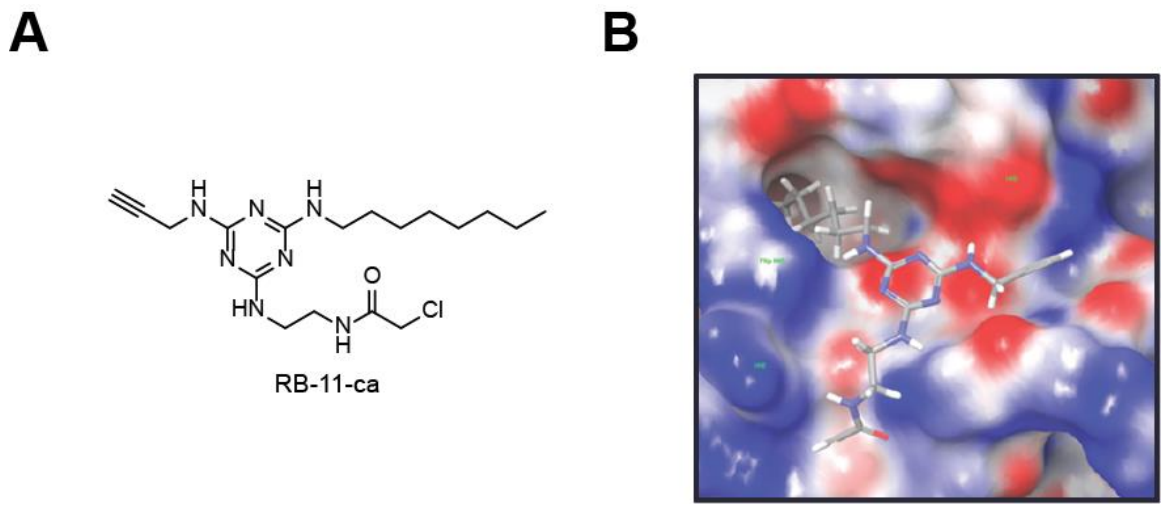

Figure 2.2. (A) Chemical structure of RB-11-ca, a previously reported a-site inhibitor of PDIA1. RB-11-ca contains a central triazine scaffold, a chloroacetamide reactive group for covalent cysteine modification, an alkyne bioorthogonal handle for CuAAC, and an octylamine diversity element. (B) Predicted binding pose of RB-11-ca in a domain active site of PDIA1 by the covalent docking algorithm from Schrodinger, Inc.

Herein we report on KSC-34, an optimized PDIA1 inhibitor, which demonstrates a 30-fold selectivity for the **a** domain over the **a'** domain. KSC-34 also displays high selectivity for PDIA1 in complex proteomes with minimal engagement of other members of the PDI family. Given the critical role of PDIA1 in normal protein homeostasis, PDIA1 inhibitors that shut down both active sites demonstrate high cytotoxicity. By selectively inhibiting a single active-site domain of PDIA1, we hypothesized that basal PDIA1 activity could be maintained to minimize cytotoxicity, whilst selectively inhibiting pathogenic functions that are dependent on elevated PDIA1 activity. We demonstrate that **a**-site selective PDIA1 inhibition shows negligible toxicity, and minimal induction of sustained cellular protein-folding stress as demonstrated by low activation of the unfolded protein response (UPR). PDIA1 inhibition by KSC-34 has the potential to display targeted effects on the secretion of pathogenic proteins that utilize PDIA1 for folding and secretion. In particular, antibody light chains contain a disulfide bond within the hydrophobic core of the protein, and the folding of antibody light chains has been shown to involve PDIA1 activity[49]. Dysregulated light-chain secretion from a clonal expansion of plasma cells can lead to immunoglobulin light-chain amyloidosis[50]. Here we demonstrate that KSC-34 treatment decreases secretion of a destabilized, amyloidogenic antibody light chain at non-toxic concentrations. Together, we identify a potent and selective PDIA1 inhibitor that uniquely targets the **a** active-site domain of PDIA1 with the ability to affect the secretion of pathogenic proteins whose folding involves PDIA1 activity.

2.2 Results and Discussion

2.2.1 Generation of a targeted library of RB-11-ca analogs

In previous published studies, we identified a cysteine-reactive triazine-based compound, RB-11-ca, as an **a**-site selective covalent modifier of PDIA1[48]. In order to further optimize the selectivity and potency of RB-11-ca, we sought to develop a second-generation library of triazine-based covalent inhibitors for PDIA1. To gain deeper insight into the binding mode of our lead compound, RB-11-ca (Figure 2.2A), within the **a** domain of PDIA1, we embarked on some preliminary docking studies. Only one high-resolution crystal structure of full-length PDIA1 is available[51], and this structure was utilized to predict a binding model for RB-11-ca using the Covalent Dock workflow from Schrodinger, Inc (New York, NY) (Figure 2.2B)[52]. In the predicted binding pose, RB-11-ca is covalently bound to the N-terminal cysteine (C53) of the CGHC active-site motif within the **a** domain, and the octylamine diversity element interacts with a large hydrophobic pocket at the domain periphery. Based on this predicted binding mode of RB-11-ca, we hypothesized that variations to the octylamine diversity element could likely enhance the predicted interactions with the observed hydrophobic pocket, and serve to improve the potency of the compound. Therefore, a second-generation library of 15 compounds (Figure 2.3) was synthesized according to previous methods with minor modifications (Scheme S1)[48]. These second-generation compounds contain diversity elements that possess hydrocarbons of varying lengths, cyclic, branched, and benzyl-functionalized hydrocarbons.

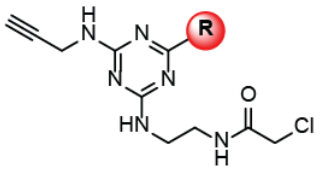

Compound	R	Compound	R
KSC-4	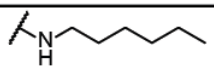	KSC-13	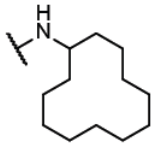
KSC-5	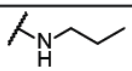		
KSC-6	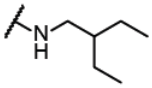	KSC-14	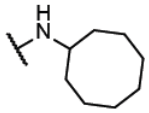
KSC-7	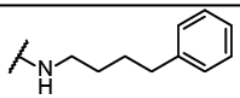	KSC-23	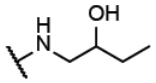
KSC-9	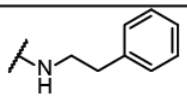	KSC-24	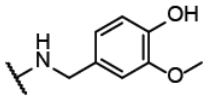
KSC-10	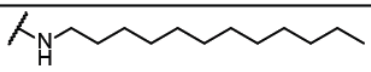		
KSC-11	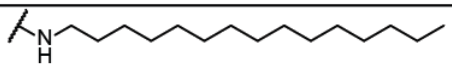	KSC-26	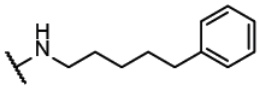
KSC-12	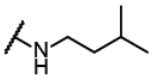		
KSC-25	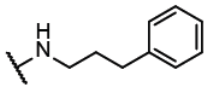	KSC-34	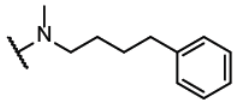

Figure 2.3. Structures of second-generation PDIA1 inhibitors obtained by varying the diversity element of RB-11-ca.

2.2.2 Identification of KSC-34 as a potent and selective covalent modifier of PDIA1

To streamline the selection of an optimized PDIA1 inhibitor, we first screened for compounds with improved covalent modification of PDIA1 using a gel-based fluorescence screening platform. Given that the extent of covalent modification of active-site cysteines directly correlate with PDIA1 inhibition, screening for improved covalent modifiers acts as a proxy for increased PDIA1 inhibition. In the first screening step, covalent modification of purified, recombinant PDIA1 was evaluated to identify compounds that demonstrated increased covalent modification of PDIA1 relative to RB-11-ca. Briefly, PDIA1 (50 μg/mL) was incubated with RB-11-ca and second-generation library members (5 μM) for 1 hour. After incubation, covalent modification of PDIA1 was monitored by appending a tetramethylrhodamine (TAMRA) fluorophore to the alkyne group of each compound using CuAAC[53-54], followed by in-gel fluorescence to quantify the amount of compound-bound PDIA1 (Figure 2-4). Seven library members (KSC-4, 7, 10, 11, 24, 26 and 34) that possessed equal or greater potency compared to RB-11-ca were advanced to the next round of selection.

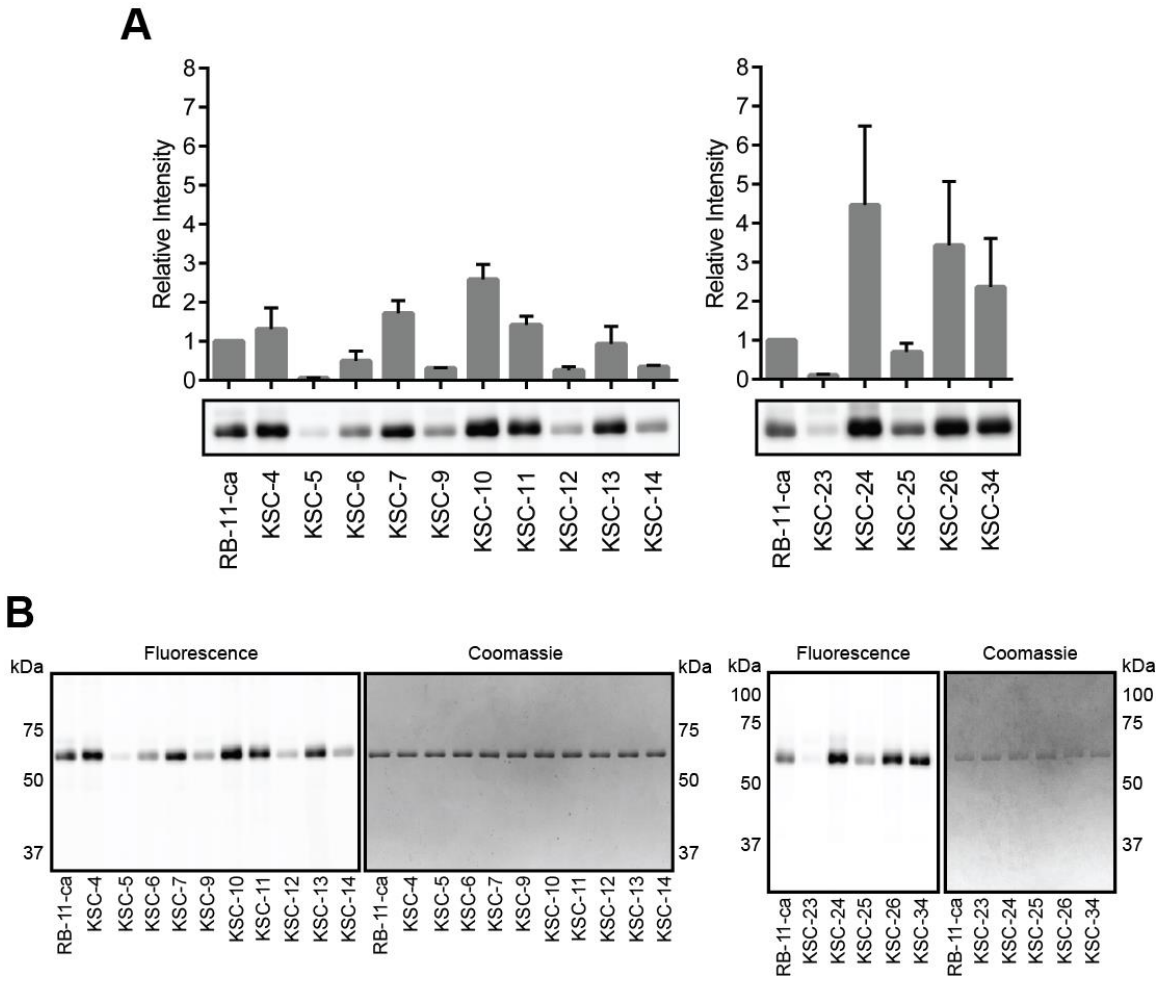

Figure 2.4. Characterization of PDIA1 second-generation library members (A) Library members (5 μM) were incubated with purified recombinant PDIA1 (50 μg/mL) in PBS, and protein labeling by each compound was evaluated after CuAAC-mediated incorporation of a TAMRA fluorophore, SDS-PAGE, and in-gel fluorescence. Library members with equal or great potency than RB-11-ca progressed to the next step of the assay. (B) Complete gel images illustrating only recombinant PDIA1 used in assay. ImageJ (NIH, Bethesda, MD) was used to quantify the fluorescence intensity of the PDIA1 band. All data are normalized to RB-11-ca lead compound. Error bars represent SD for n = 3 experiments.

In the second screening step, library members were assessed against purified, recombinant PDIA1 (50 μg/mL) in the background of MCF-7 cell lysates (1 mg/mL) to evaluate whether other cellular proteins interfere with the ability of each compound to covalently modify PDIA1 (Figure 2-5). Four library members (KSC-7, 24, 26, and 34) possessed equal or greater potency to RB-11-ca, and thus were advanced to the next stage. In the third screening step, library members were evaluated in MCF-7 lysates (2 mg/mL) for their ability to covalently modify endogenous PDIA1 (Figure 2-6). This analysis afforded three library members (KSC-24, 26 and 34) that had equal or greater potency toward PDIA1 compared to RB-11-ca. Of these, the two most potent library members, KSC-24 and KSC-34, were advanced to the final stage.

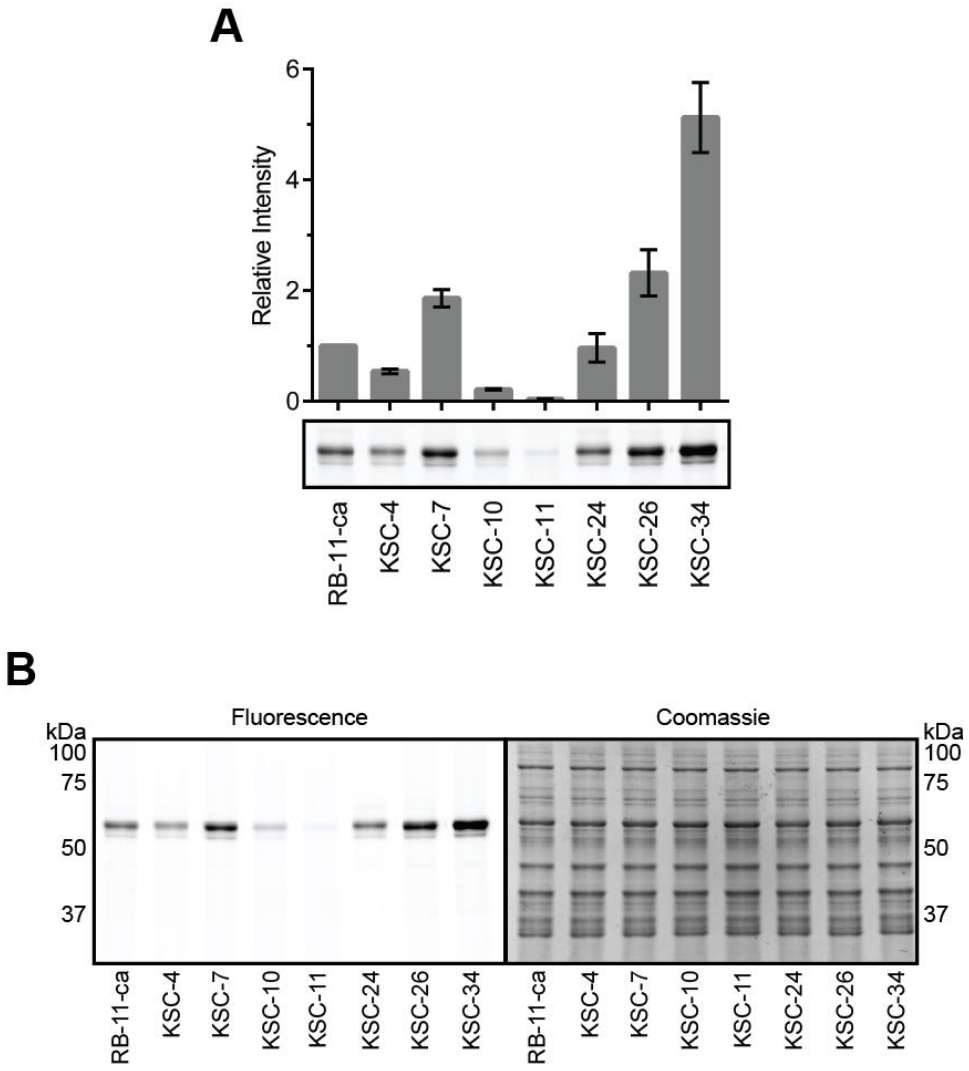

Figure 2.5. Characterization of PDIA1 second-generation library members. (A) Library members were assessed against purified, recombinant PDIA1 (50 μg/mL) in the background of MCF-7 cell lysates (1 mg/mL) to evaluate whether other cellular proteins interfere with the ability of each compound to covalently modify PDIA1. (B) Complete gels for part (A) illustrating proteome-wide selectivity of second-generation library members. ImageJ (NIH, Bethesda, MD) was used to quantify the fluorescence intensity of the PDIA1 band. All data are normalized to RB-11-ca lead compound. Error bars represent SD for n = 3 experiments.

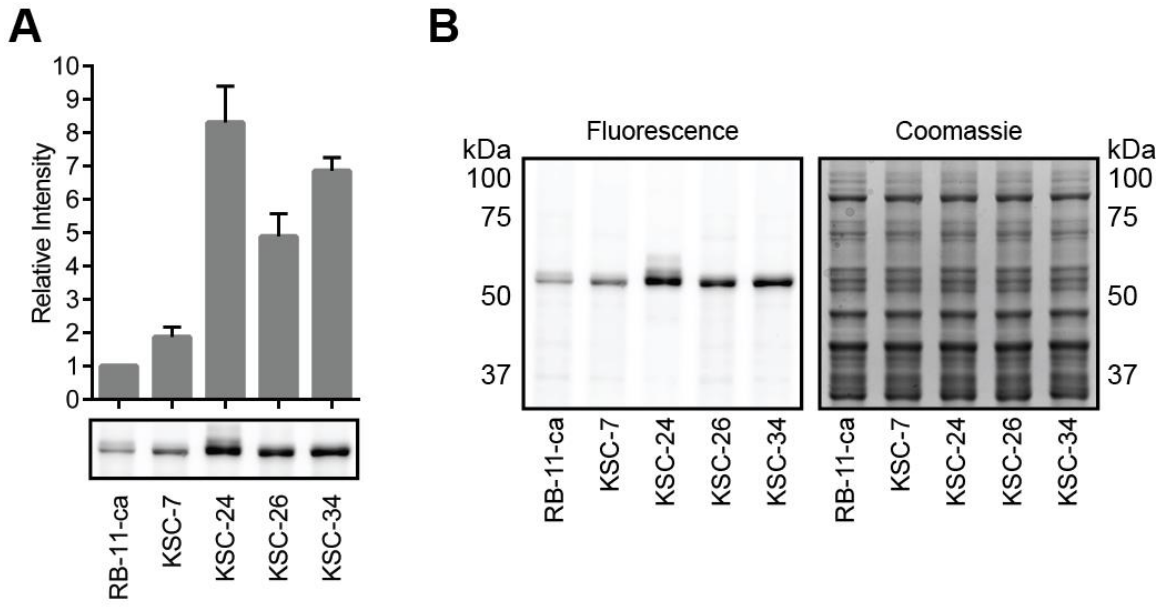

Figure 2.6. Characterization of PDIA1 second-generation library members. (A) In-gel fluorescence studies of library members (5 μM) incubated with MCF-7 cell lysate (2 mg/mL) to assess potency and selectivity for endogenous PDIA1 in a complex proteome. (B) Complete gel images for analysis used in part (A) demonstrating proteome-wide selectivity of second generation library members in a complex proteome. ImageJ (NIH, Bethesda, MD) was used to quantify the fluorescence intensity of the PDIA1 band. All data are normalized to RB-11-ca lead compound. Error bars represent SD for n = 3 experiments.

In the fourth and final step of this multilayered assay, the cell permeability and ability of the compounds to engage with ER-localized PDIA1 directly in living cells was assessed. MCF-7 cells were treated with compound for 3 hours at 37 °C, followed by in-gel fluorescence analysis (Figure 2-7). KSC-34, which contains a (4-phenylbutyl)methylamine diversity element, was found to covalently modify PDIA1 directly in living cells with approximately 8-fold increased potency compared to RB-11-ca. The presence of a single robust fluorescent band at ~60 kD demonstrates the high potency and selectivity of KSC-34 for covalent modification of PDIA1 within the background of other highly abundant cysteine-containing proteins.

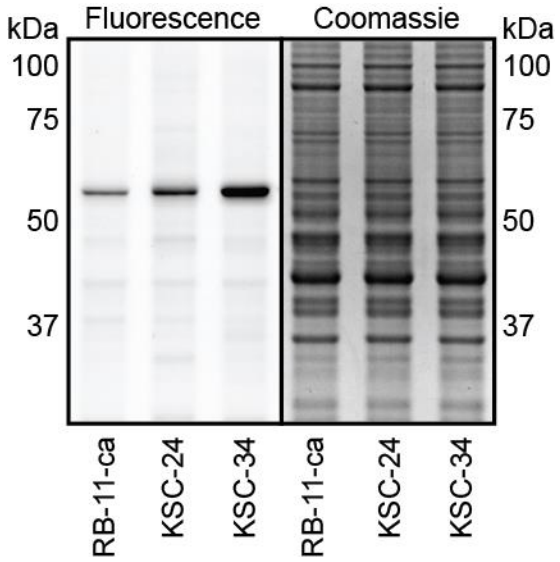

Figure 2.7. Characterization of PDIA1 second-generation library members. To assess cell permeability as well as selectivity of the library, probes (5 μM) were incubated with MCF-7 cells for 3 hours at 37 °C. Following cell lysis and in-gel fluorescence, KSC-34 was found to be ~8-fold more potent than the lead compound, RB-11-ca, in whole cells against PDIA1 (left panel). Coomassie gel (right panel is provided to show normalized protein abundance).

2.2.3 KSC-34 demonstrates time-dependent inhibition of PDIA1 *in vitro*

To confirm that improved covalent modification of PDIA1 by KSC-34 correlated with increased inhibitory potency, we utilized an *in vitro* insulin turbidity assay that monitors PDI reductase activity[55]. The reduction of disulfide bonds in insulin results in aggregation of the insulin β chain causing a measurable increase in turbidity. Due to the covalent nature of RB-11-ca and KSC-34, PDIA1-induced insulin aggregation was monitored upon treatment with each inhibitor at varying concentrations and pre-incubation times. We also compared RB-11-ca and KSC-34 to the commercially available PDIA1 inhibitor, 16F16[25], which also contains a chloroacetamide electrophile for covalent modification of PDIA1, similar to our triazine-based compounds. KSC-34 inhibited PDIA1 in a concentration and time-dependent manner, with a k_{inact}/K_I = 9.66 x 10^3 M^{-1} s^{-1} (Figure 2-8), which is ~3-fold more potent than RB-11-ca (k_{inact}/K_I = 3.35 x 10^3 M^{-1} s^{-1}), and 38-fold more potent than the commercial PDIA1 inhibitor 16F16 (k_{inact}/K_I = 2.52 x 10^2 M^{-1} s^{-1}).

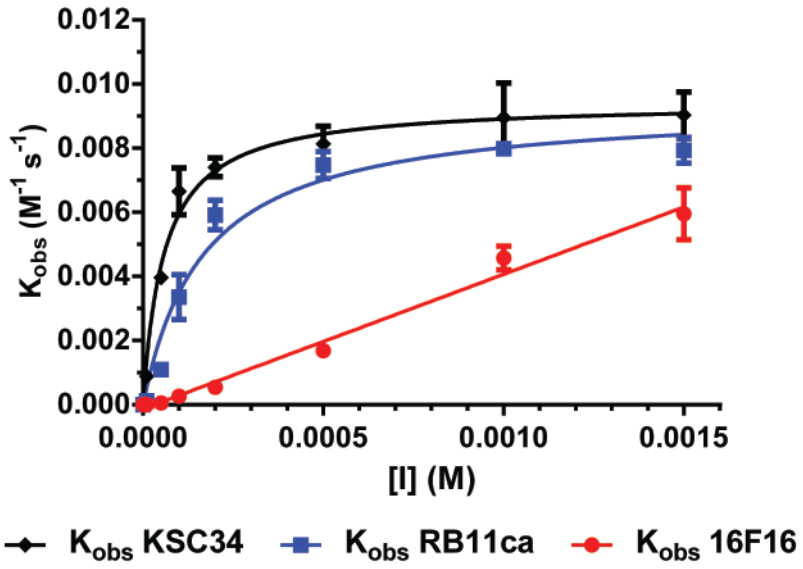

Figure 2.8. Concentration and time-dependent inhibition of PDIA1 by KSC-34, RB-11-ca, and 16F16. PDIA1 reductase activity was measured using an insulin reduction assay in a 100 µL reaction volume containing 0.5 µM PDIA1, 0.16 mM insulin, and 1 mM DTT in assay buffer. Turbidity of the insulin solution was measured over time at various concentrations and pre-incubation times with KSC-34. Error bars are calculated as SD from n = 2 experiments.

2.2.4 KSC-34 is a highly selective covalent modifier of PDIA1

Upon confirmation of the ability of KSC-34 to covalently modify and inhibit PDIA1 activity, we sought to determine the selectivity of KSC-34 for the **a** and **a'** active sites of PDIA1. Given that our first-generation compound RB-11-ca was **a**-site selective, we expected KSC-34 to bind in a similar fashion. Site-selectivity was assessed by recombinantly expressing wild-type PDIA1 (WT) and cysteine-to-alanine mutants of each of the two active-site nucleophilic residues (C53A and C397A). Each recombinant PDIA1 protein (50 μg/mL) was incubated with KSC-34 (5 μM) for 1 hour, and subjected to CuAAC prior to in-gel fluorescence (Figure 2-9A). The absence of fluorescence in the C53A sample indicates that the binding of KSC-34 to PDIA1 is reliant on the presence of C53. Therefore, KSC-34 maintains selectivity for C53 in the **a** domain of PDIA1 with minimal binding to C397 in the **a'** domain. To further quantify the selectivity for the **a** and **a'** domains, IC_{50} values were obtained for binding to each active site (Figure 2-9D). To attain IC_{50} values, PDIA1 C53A and C397A (50 μg/mL), in the background of MCF-7 lysates (1 mg/mL), were treated with increasing concentrations of KSC-34, RB-11-ca and 16F16. Following incubation, samples were then treated with chloroacetamide-rhodamine (CA-Rh) (8 μM, Figure 2-9B), to append a fluorophore to residual, unmodified active-site cysteines in each PDIA1 mutant. Loss in CA-Rh labeling of each active-site mutant is indicative of inhibitor binding, and informs on the affinity of each compound to the **a** and **a'** domains. KSC-34 demonstrated a 30-fold selectivity for the **a** domain over the **a'** domain, whereas RB-11-ca demonstrated a 21-fold **a**-domain and 16F16 demonstrated a 2-fold selectivity for the **a**-domain over the **a'** domain. KSC-34 is therefore the most selective and potent **a**-site inhibitor of PDIA1 reported to date.

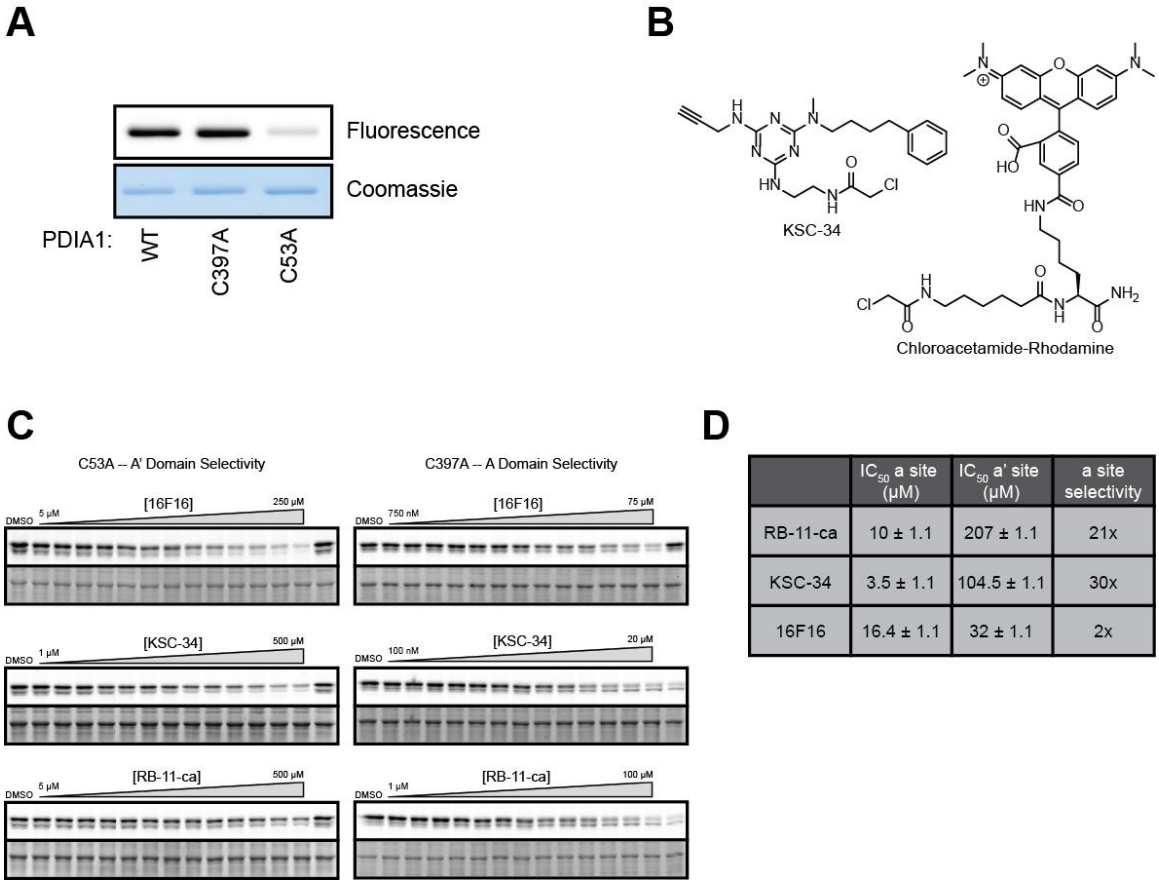

D

	IC_{50} a site (µM)	IC_{50} a' site (µM)	a site selectivity
RB-11-ca	10 ± 1.1	207 ± 1.1	21x
KSC-34	3.5 ± 1.1	104.5 ± 1.1	30x
16F16	16.4 ± 1.1	32 ± 1.1	2x

Figure 2.9. Evaluation of the site-selectivity of KSC-34. (A) Labeling of purified recombinant PDIA1 WT, C397A and C53A by KSC-34. Each recombinant PDIA1 protein (50 µg/mL) was incubated with KSC-34 (5 µM) for 1 hour, and subjected to CuAAC prior to in-gel fluorescence. (B) Structures of KSC-34 and Chloroacetamide-Rhodamine (CA-Rh). (C) PDIA1 C53A and C397A (50 µg/mL) in the background of MCF-7 lysates (1 mg/mL) were treated with increasing concentrations of KSC-34, RB-11-ca and 16F16 to quantify the selectivity for the a and a' domains. Following incubation, samples were then treated with CA-Rh) to append a fluorophore to the residual, unmodified PDIA1 active sites. Loss of fluorescence indicates inhibitor binding. ImageJ (NIH) was used to quantify the loss in fluorescence and calculate affinities for each active site. (D) Active-site selectivity for KSC-34, RB-11-ca, and 16F16. KSC-34 was found to have a 30-fold selectivity for the a domain over the a' domain, compared to RB-11-ca which exhibited a 21-fold selectivity and 16F16 which exhibited 2-fold selectivity. Error is calculated by PRISM as ± SEM from n = 3 experiments.

Owing to structural similarity amongst PDI family members, we next assessed the selectivity of KSC-34 for PDIA1 relative to two other PDI family members, PDIA3 and PDIA4, which display 34% and 36% similarity to PDIA1, respectively. Briefly, PDIA1, PDIA3 and PDIA4 (50 µg/mL) were incubated in the presence or absence of MCF-7 lysates (1 mg/mL), and subjected to CuAAC, and in-gel fluorescence (Figure 2-10). As indicated by the absence of fluorescence in the PDIA3 and PDIA4 samples, KSC-34 is selective for PDIA1 over other PDI family members. The band observed in the cell-lysate samples for PDIA3 and PDIA4 is the endogenous PDIA1 in the MCF-7 cell lysates, further confirming the selectivity of KSC-34, in that the presence of a large excess of PDIA3 and PDIA4 does not affect the targeting of PDIA1 by KSC-34.

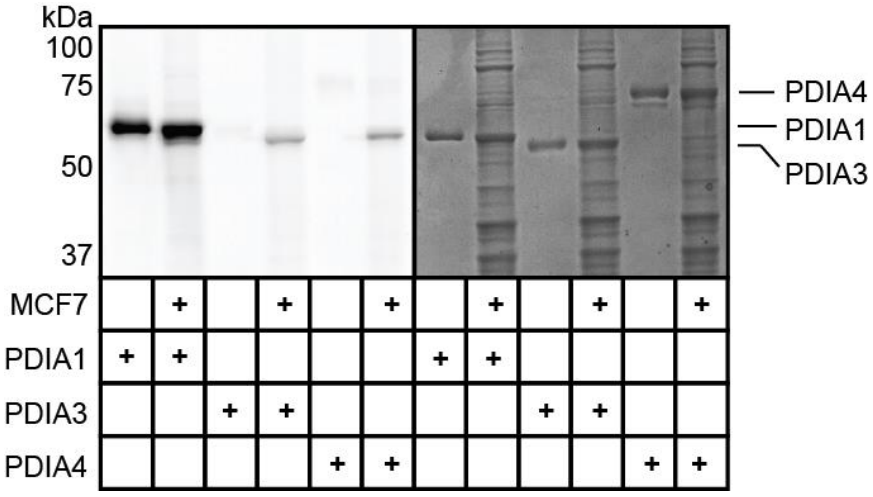

Figure 2.10. Evaluation of selectivity of KSC-34. PDI isoform selectivity. KSC-34 was found to only covalently modify PDIA1 over PDIA3 and PDIA4, two closely related family members.

To more comprehensively assess the selectivity of KSC-34 across other cellular PDIs, as well as any proteins bearing highly reactive cysteine residues, the protein targets of KSC-34 were globally investigated. To achieve this, MCF-7 cells were incubated with KSC-34 (5 μM) or DMSO. Upon cell lysis, KSC-34-labeled proteins were then appended to biotin-azide using CuAAC, enriched on streptavidin beads, subjected to on-bead tryptic digestion, and subsequent LC/LC-MS/MS analysis. Spectral counts (number of fragmentation spectra) generated for each protein in the KSC-34-treated samples were compared to the DMSO control (Figure 2-11, Table 1). In KSC-34-treated samples, an average of ~2000 spectral counts were matched to PDIA1 (with an average of ~5 spectral counts in the DMSO control). Importantly, the second most enriched protein was prostaglandin E synthase 2 (PTGES2), which was identified with an average of ~120 spectral counts in the KSC-34-treated sample, significantly lower than that for PDIA1. PDIA6 was the only other PDI that was enriched by KSC-34, albeit with low spectral counts of ~20. KSC-34 is therefore highly selective for PDIA1 over other PDIs, as well as cellular proteins bearing reactive cysteines that could potentially be modified by the chloroacetamide electrophile on KSC-34.

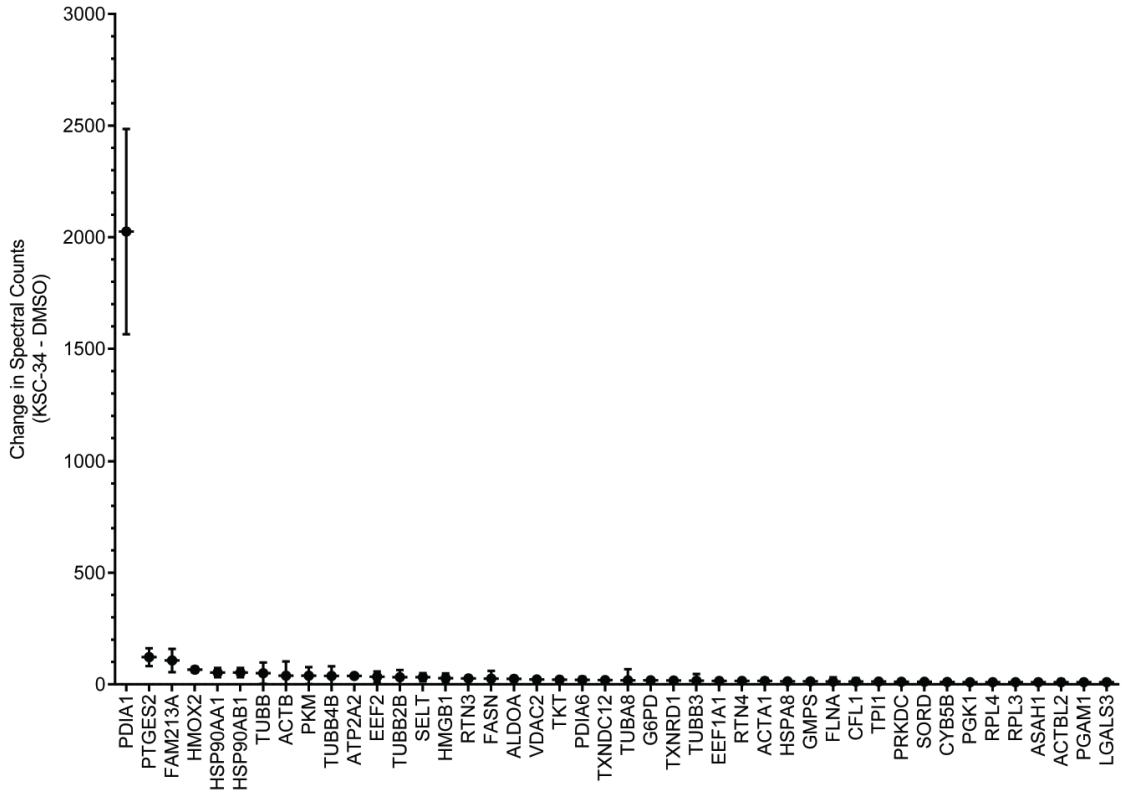

Figure 2.11. Evaluation of proteome-wide selectivity of KSC-34. Mass spectrometry analysis of proteins enriched in KSC-34 (5 μM) and DMSO treated MCF-7 cells. The spectral count difference between KSC-34-treated and DMSO-treated samples are plotted for all proteins identified (Table 1). Errors bars show SD for n = 2 experiments.

Protein	UniProt ID	DMSO_1	DMSO_2	Average DMSO	KSC-34_5uM_1	KSC-34_5uM_2	Average 5 uM KSC-34	Change in Spectral Count (KSC-34 - DMSO)
P4HB	P07237	9	0	5	1704	2355	2030	2025
PTGES2	Q9H7Z7	0	0	0	94	150	122	122
FAM213A	Q9BRX8	0	0	0	70	143	107	107
HMOX2	P30519	0	0	0	57	75	66	66
HSP90AA1	P07900	31	13	22	63	87	75	53
HSP90AB1	P08238	40	23	32	72	96	84	53
TUBB	P07437	62	82	72	89	154	122	50
ACTB	P60709	215	144	180	190	247	219	39
PKM	P14618	48	46	47	59	113	86	39
TUBB4B	P68371	63	92	78	89	142	116	38
ATP2A2	P16615	5	2	4	34	48	41	38
EEF2	P13639	21	15	18	35	69	52	34
TUBB2B	Q9BVA1	49	64	57	67	110	89	32
SELT	P62341	0	0	0	19	45	32	32
HMGB1	P09429	0	8	4	18	46	32	28
RTN3	O95197	0	0	0	20	34	27	27
FASN	P49327	64	43	54	57	101	79	26
ALDOA	P04075	19	14	17	34	49	42	25
VDAC2	P45880	2	0	1	16	30	23	22
TKT	P29401	8	8	8	24	33	29	21
PDIA6	Q15084	3	3	3	13	33	23	20
TXNDC12	O95881	0	0	0	21	17	19	19
TUBA8	Q9NY65	62	0	31	31	66	49	18
G6PD	P11413	3	2	3	15	25	20	18
TXNRD1	Q16881	0	2	1	10	26	18	17
TUBB3	Q13509	44	76	60	62	90	76	16
EEF1A1	P68104	41	29	35	44	56	50	15
RTN4	Q9NQC3	0	0	0	10	20	15	15
ACTA1	P68133	52	55	54	78	58	68	15
HSPA8	P11142	22	19	21	32	36	34	14
GMPS	P49915	0	0	0	13	14	14	14
FLNA	P21333	67	56	62	63	86	75	13
CFL1	P23528	3	20	12	30	18	24	13
TPI1	P60174	5	10	8	14	26	20	13
SORD	Q00796	0	2	1	14	12	13	12
PRKDC	P78527	7	6	7	14	23	19	12
CYB5B	O43169	0	0	0	5	16	11	11
PGK1	P00558	8	10	9	17	21	19	10
ASAH1	Q13510	0	0	0	9	11	10	10
RPL4	P36578	11	5	8	13	23	18	10
RPL3	P39023	4	0	2	9	15	12	10
PGAM1	P18669	0	0	0	10	9	10	10
ACTBL2	Q562R1	17	0	9	15	21	18	10
LGALS3	P17931	0	0	0	7	12	10	10
GPI	P06744	4	5	5	12	15	14	9

Table 2.1. Mass spectrometry data for KSC-34 treated MCF-7 cells. The proteins shown are sorted by the spectral count difference between the KSC-34 treated and the DMSO treated samples.

2.2.5 Inhibition of PDIA1 has minimal effects on the cellular unfolded protein response

Given the critical role of PDIA1 in disulfide-bond formation on nascent proteins in the ER, complete loss of PDIA1 activity will likely result in the accumulation of unfolded or misfolded proteins in the ER. Misfolded protein accumulation in the ER typically activates a series of complex stress-responsive signaling pathways known as the unfolded protein response (UPR)[56-58]. UPR activation involves three different pathways, which implicate inositol-requiring 1α (IRE1α), PKR-like ER kinase (PERK), and activating transcription factor-6α (ATF6α)[59-60]. Initial consequences of UPR activation include inhibition of translation, and increased ER protein-folding capacity. Chronic and sustained ER stress will eventually trigger cellular apoptosis. We sought to investigate the effects of KSC-34-mediated **a**-site inhibition of PDIA1 on each of these three arms of the UPR.

First, we identified an optimal concentration range of KSC-34 to utilize in our UPR assays, which would provide maximal PDIA1 target engagement with minimal toxicity. To quantify PDIA1 target occupancy at varying concentrations of KSC-34, we first synthesized a non-alkyne containing analog, KSC-34na, with identical PDIA1 binding properties to KSC-34, but lacking the biorthogonal handle for further functionalization with reporter tags (Figure 2-12A). To determine PDIA1 occupancy in cells, MCF-7 cells were treated with varying concentrations of KSC-34na. Following cell lysis, protein concentrations were normalized, and the lysates were incubated with KSC-34 (5 μM) to covalently modify any residual, non-inhibitor bound **a**-site C53 on PDIA1. In-gel fluorescence measurements were used to quantify the amount of PDIA1 that was not occupied by KSC-34na at each concentration. These measurements provided an EC_{50} of 4

μM for KSC-34na labeling of PDIA1 in MCF-7 cells, and demonstrated that complete occupation of C53 of PDIA1 in cells occurs at concentrations less than ~10 μM. To determine toxicity of KSC-34 at these same concentrations, MTT cell-viability assays were performed in MCF-7 cells, generating an EC_{50} value of 82 μM (Figure 2-12B), which underscores the relatively low toxicity of **a**-site selective PDIA1 inhibitors in MCF-7 cells.

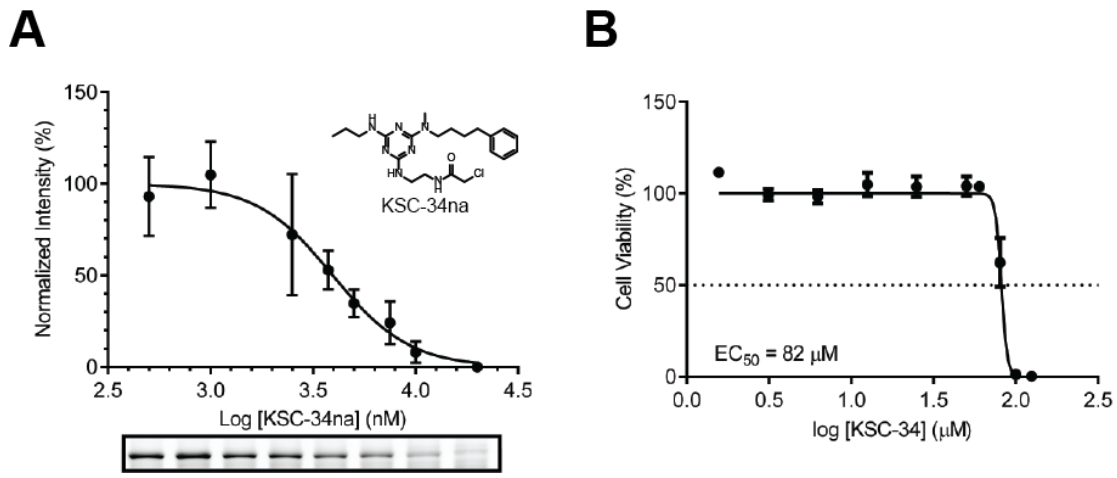

Figure 2.12. (A) Identification of KSC-34 cellular occupancy of PDIA1. MCF-7 cells were treated with varying concentrations of KSC-34na. Following lysis, protein concentrations were normalized and subjected to treatment with KSC-34 (5 μM) to modify any residual PDIA1 a domain active site, C53. An EC_{50} of ~4 μM was calculated for KSC-34na labeling of PDIA1 in MCF-7 whole cells. All data are normalized to RB-11-ca lead compound. Error bars represent ± SD for n = 3 experiments. (B) MTT assay data in MCF-7 cells treated with varying concentrations of KSC-34. The calculated EC_{50} of KSC-34 was determined to be 82 μM. All data are normalized to vehicle treated cells. Error bars represent ± SD for n = 3 experiments.

Upon identifying non-toxic concentrations of KSC-34 for cellular studies, quantitative transcriptional-profiling methods were utilized to monitor activation of known UPR target genes. Briefly, MCF-7 cells were treated with DMSO, thapsigargin (Tg) (5 μM), and varying concentrations of KSC-34 (4-40 μM) for 3 hours at 37 °C. Tg is a sesquiterpene lactone that induces ER stress by inhibiting sarcoplasmic/endoplasmic reticulum calcium ATPase (SERCA). Treated cells were then subjected to qPCR analysis for mRNA encoding known downstream targets preferentially regulated by each of the three arms of the UPR, including *SEC24D* and *ERDJ4* (IRE1α-regulated), *BIP* and *HYOU1* (IRE1α and ATF6-regulated), *CHOP* and *GADD34* (PERK-regulated) and, *GRP94* (ATF6-regulated). KSC-34 treatment showed no significant activation of the PERK and ATF6 arms of the UPR (Figure 2-13A). Interestingly, a small but reproducible increase in *SEC24D* and *ERDJ4* mRNA levels was observed (~2-fold) at >20 μM concentrations of KSC-34, suggesting selective activation of the IRE1α arm under these conditions, consistent with minor induction of *XBP1* splicing upon KSC-34 treatment (Figure 2-13B). Treatment with an IRE1α inhibitor, 4μ8c, confirmed that the observed effects on *SEC24D*, *ERDJ4*, *BIP*, and *HYOU1* were mediated directly through IRE1α (Figure 2-14). Further characterization determined that IRE1α activation only occurs within a short timeframe (<6 hours), since longer incubation times led to a loss in upregulation of IRE1α-dependent transcripts (Figure 2-15). Evaluation of other cell lines demonstrated that this effect is cell type-dependent, as no significant effects were observed in SKOV-3 and A549 cells (Figure 2-16). Together, these data suggest that **a**-site inhibition of PDIA1 by KSC-34 has minimal effects on activation of the PERK and ATF6 arms of the UPR, with some short-lived, and cell line-dependent effects on the IRE1α arm.

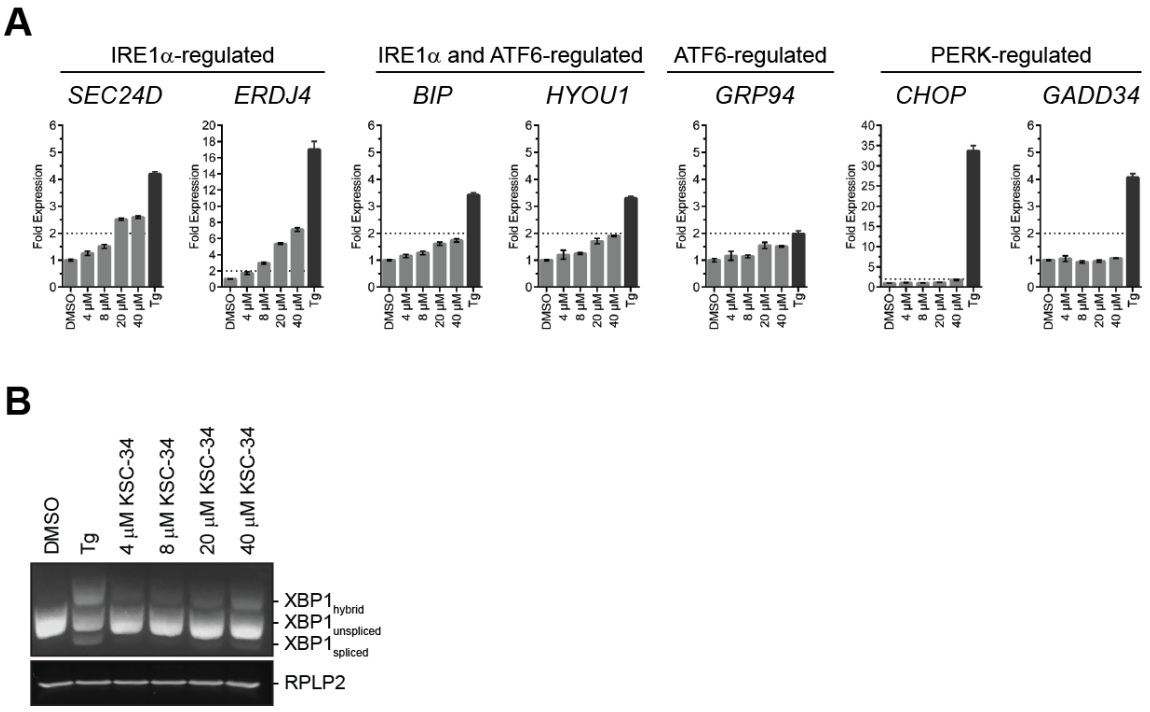

Figure 2.13. Effects of KSC-34 on cell viability and the unfolded protein response. (A) qPCR analysis of UPR target genes following concentration-dependent treatment of MCF-7 cells with KSC-34 for 3 hours at 37 °C. Data are reported as the mean fold change (relative to DMSO) ± SEM from three biological replicates. (B) XBP1 splicing assay for MCF-7 cells treated with varying concentrations of KSC-34 for 3 hours.

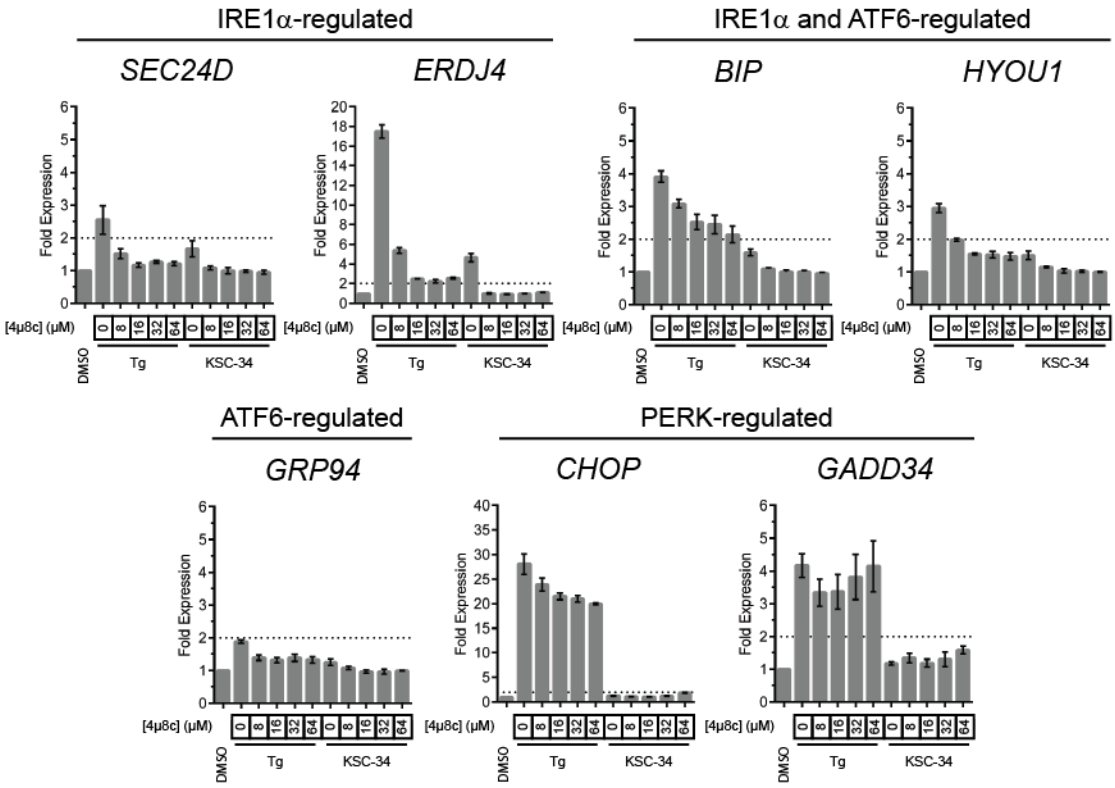

Figure 2.14. Effects of KSC-34 on the unfolded protein response. qPCR analysis of UPR target genes following co-treatment of MCF-7 cells with KSC-34 (20 μM) and IRE1α inhibitor, 4μ8c. Data are reported as the mean fold change (relative to DMSO) ± SEM from three biological replicates.

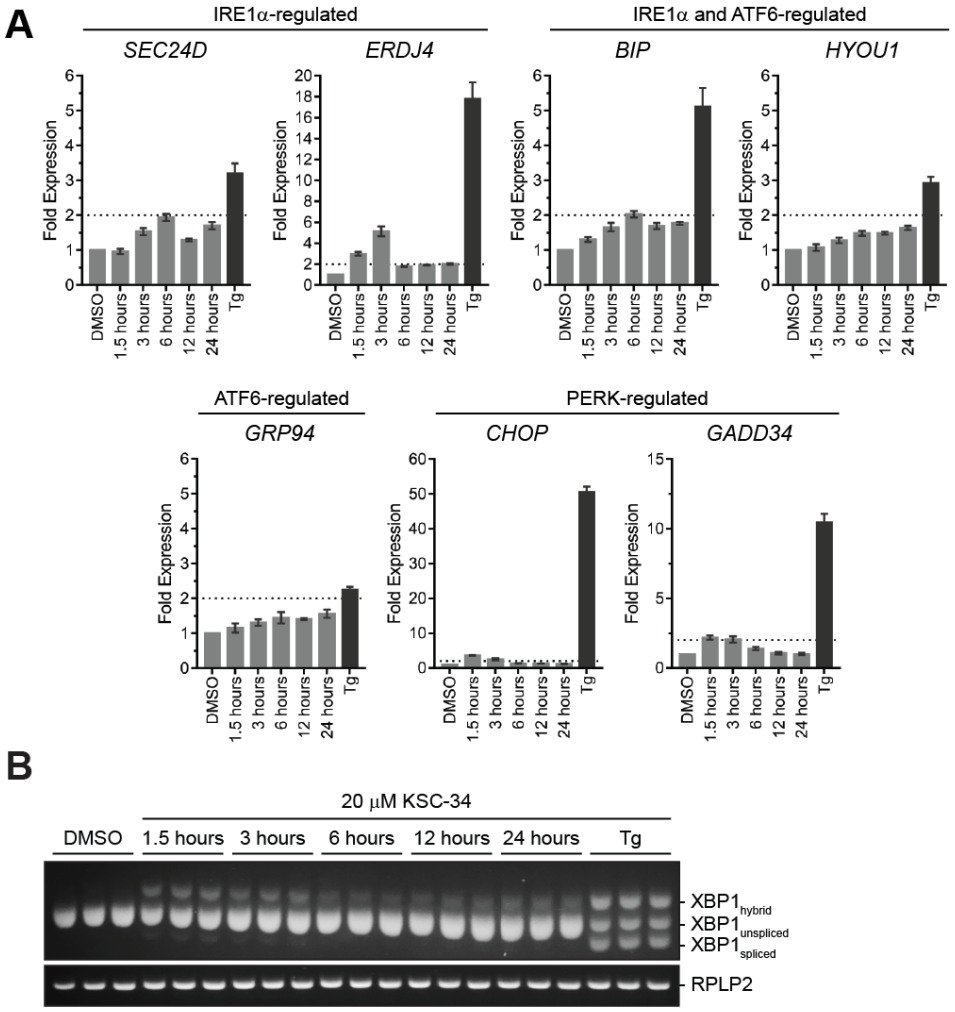

Figure 2.15. Effects of KSC-34 on the unfolded protein response. (A) Activation of UPR target genes in MCF-7 cells was assessed by measuring the relative mRNA expression levels of target genes by qRT-PCR after treating with KSC-34 (20 μM) for increasing time. Transcripts were normalized to the housekeeping gene RPLP2, and all reactions were performed in technical quadruplicate. Data are reported as the mean fold change (relative to DMSO) ± SEM from three biological replicates. (B) XBP1 splicing assay for time-course experiment, where MCF-7 cells were treated with 20 μM KSC-34. Gel shows three biological replicates for each condition.

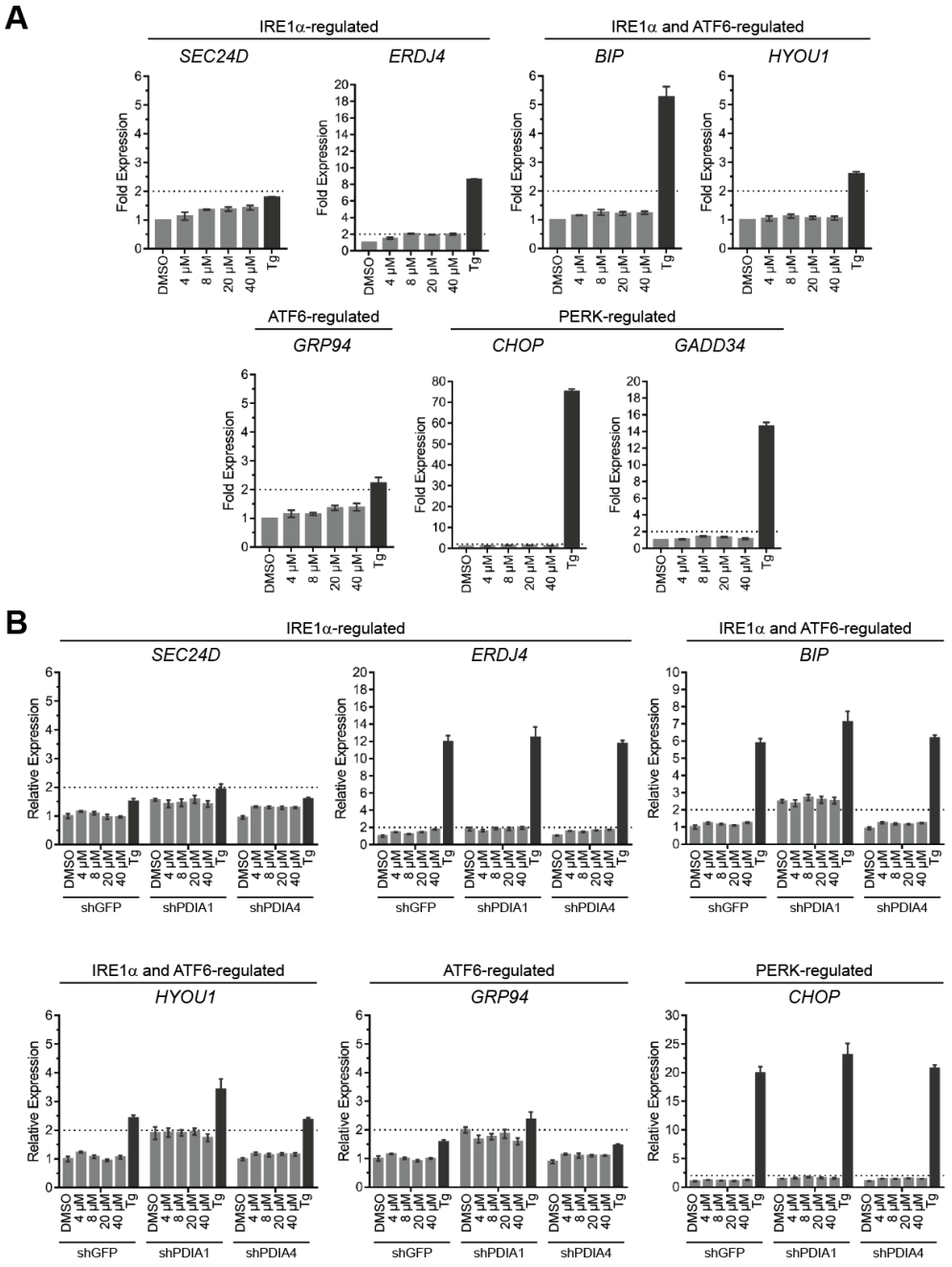

Figure 2.16. Activation of UPR target genes in A549 cells (A) or SKOV-3 cells stably expressing shPDIA1, shPDIA4 or shGFP (B). The relative mRNA expression levels of target genes were assessed by qRT-PCR after treating with increasing concentrations of KSC-34 or 5 μM of thapsigargin. Transcripts were normalized to the housekeeping gene RPLP2. (A) For A549 cells, all reactions were performed in technical quadruplicate, and data are reported as the mean fold change (relative to DMSO) ± SEM from three biological

replicates. (B) For SKOV-3 cells, data are reported as mean fold change (relative to shGFP DMSO) ± SEM from reactions performed in triplicate.

2.2.6 PDIA1 Inhibition by KSC-34 decreases secretion of an amyloidogenic light chain

PDIA1 influences the folding of disulfide-containing secretory proteins including antibody light chains[49, 61-63]. Therefore, we sought to evaluate the functional consequence of KSC-34-mediated inhibition of PDIA1 in cell-culture models expressing the destabilized, disease-associated antibody light chain ALLC[64]. We first performed co-immunoprecipitation (co-IP) experiments to determine how KSC-34-dependent inhibition of PDIA1 influences its interaction with flag-tagged ALLC (^{FT}ALLC) in HEK293^{DAX} cells[58]. PDIA1 was enriched in ^{FT}ALLC IPs in the absence of KSC-34, confirming that PDIA1 interacts with this destabilized light chain in mammalian cells (Figure 2-17A). The addition of KSC-34 disrupted this interaction, shown by a decrease in the co-isolation of PDIA1 with ^{FT}ALLC (Figure 2-17A). However, the closely related ER protein PDIA4 co-purifies with ^{FT}ALLC in cells treated with or without KSC-34, demonstrating that this compound does not influence the interaction between these proteins. These results show that KSC-34 selectively disrupts the interaction between ^{FT}ALLC and PDIA1, demonstrating the high selectivity of KSC-34 for PDIA1 under these cellular conditions.

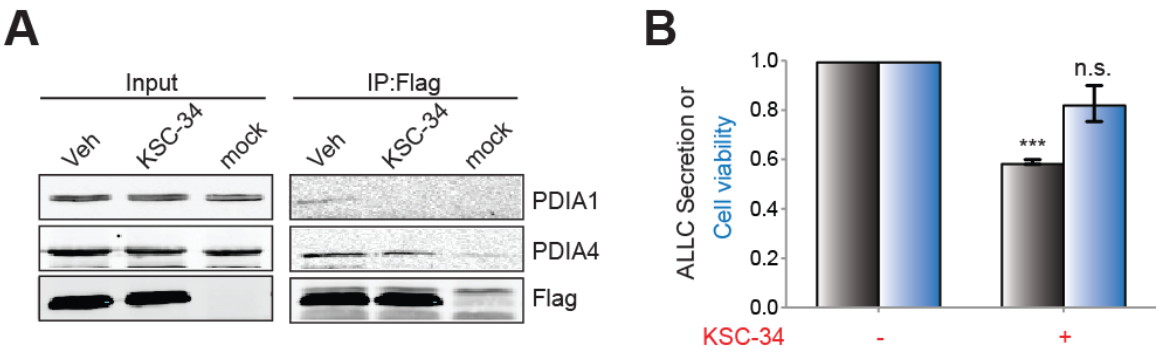

Figure 2.17. KSC-34 reduces secretion of destabilized ALLC from mammalian cells. (A) Immunoblot of anti-FLAG IPs of lysates prepared from HEK293^{DAX} cells transiently transfected with ^{FT}ALLC and pre-treated for 1 h with vehicle or KSC-34 (40 µM). Cells were crosslinked for 30 min with DSP (500 µM) prior to lysis. Mock transfected cells are included as a control. (B) Graph showing secreted ^{FT}ALLC (grey) and viability (blue) of HEK293^{Trex} cells stably expressing ^{FT}ALLC pretreated for 4 h with KSC-34 (40 µM). Media was conditioned for 2 h in the presence or absence of KSC-34 (40 µM) prior to quantification of secreted ^{FT}ALLC by ELISA. Viability was measured following media conditioning by Cell Titre Glo. All data are normalized to vehicle-treated cells. Error bars show SEM for n=3 experiments. ***p<0.005.

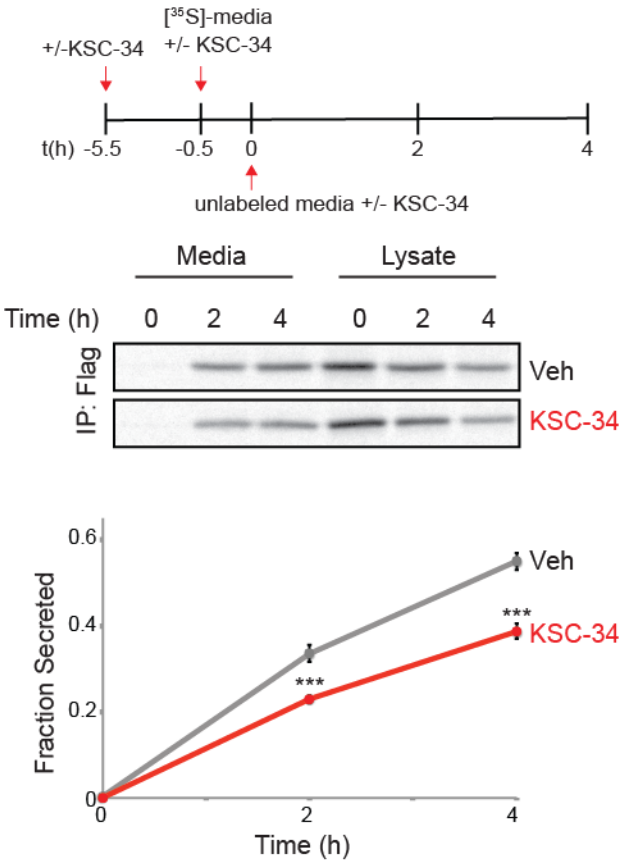

Figure 2.18. KSC-34 reduces secretion of destabilized ALLC from mammalian cells. Representative autoradiogram and quantification of the fraction [^{35}S]-labeled ^{FT}ALLC secreted from HEK293^{DAX} cells using the experimental paradigm shown. Experiments were performed in the absence or presence of KSC-34 (40 μM) added 1 h prior to labeling and then again throughout the experiment. Fraction secreted was calculated as described in Materials and Methods (64). Error bars show SEM for n=4. ***p<0.005.

Next, we determined whether KSC-34-dependent inhibition of PDIA1 influences ALLC secretion. We treated HEK293^{Trex} cells stably expressing ^{FT}ALLC with KSC-34, and monitored secretion by ELISA. Treatment with KSC-34 reduced levels of ^{FT}ALLC in the conditioned media by 40%, as compared to vehicle (Figure 2-17B). This treatment did result in a modest 20% reduction in cellular viability, however this decrease is not sufficient to account for the observed changes in secreted ^{FT}ALLC. To further define the impact of KSC-34 on ^{FT}ALLC secretion, we monitored the fraction of newly-synthesized ^{FT}ALLC secreted from HEK293^{DAX} cells treated with or without KSC-34 using [^{35}S] metabolic labeling (Figure 2-18). Pretreatment with KSC-34 reduced the fraction of [^{35}S]-labeled ^{FT}ALLC secreted by 30%, confirming the results observed by ELISA (Figure 2-18). Next, we sought to determine the PDIA1-dependence of these effects on LC secretion utilizing HEK293^{DAX} cells stably expressing *PDIA1* shRNA. We confirmed *PDIA1* knockdown in these cells by qPCR (Fig. S9A). Depletion of *PDIA1* attenuated the KSC-34-dependent reduction in ^{FT}ALLC secretion measured by ELISA (Figure 6D) and [^{35}S] metabolic labeling (Figure 6E and Fig. S9B). This shows that KSC-34 decreases destabilized ALLC secretion through a mechanism dependent on PDIA1. These data support the utility of **a**-site selective PDIA1 inhibitors to selectively affect secretion of amyloidogenic proteins like destabilized antibody light chains.

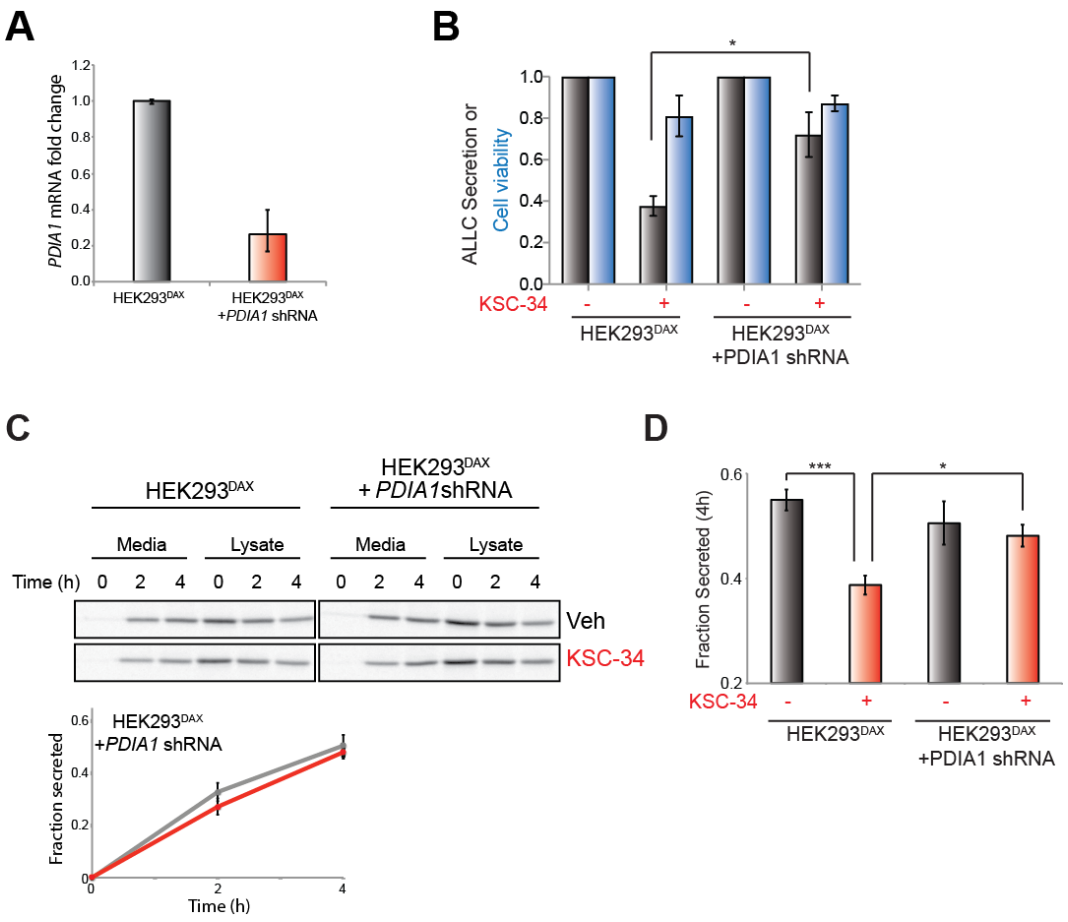

Figure 2.19. KSC-34 reduces secretion of destabilized ALLC from mammalian cells. (A) Graph showing fold change mRNA levels of PDIA1 in HEK293^{DAX} cells and HEK293^{DAX} cells shRNA-depleted of PDIA1 measured by qPCR. Error bars show 95% confidence interval. (B) Graph showing secreted ^{FT}ALLC (grey) and viability (blue) of HEK293^{DAX} cells transiently expressing ^{FT}ALLC pretreated for 4 h with KSC-34 (40 μM). HEK293^{DAX} cells stably expressing PDIA1 shRNA are indicated. Media was conditioned for 2 h in the presence or absence of KSC-34 (40 μM) prior to quantification of secreted ^{FT}ALLC by ELISA. Viability was measured following media conditioning by Cell Titre Glo. All data are normalized to vehicle-treated controls. Error bars show SEM for n=3 experiments. *p<0.05. (C) Representative autoradiogram and quantification of the fraction [^{35}S]-labeled ^{FT}ALLC secreted from HEK293^{DAX} cells using the experimental paradigm shown in Figure 2-18. Experiments were performed in the absence or presence of KSC-34 (40 μM) added 1 h prior to labeling and then again throughout the experiment. Error bars show SEM for n=4 (D) Graph showing the fraction [^{35}S]-labeled ^{FT}ALLC secreted at t=4 h from HEK293^{DAX} cells transiently transfected with ^{FT}ALLC quantified using the same experimental paradigm shown in Figure 2-18. HEK293^{DAX} cells stably expressing PDIA1 shRNA are indicated. Experiments were performed in the absence or presence of KSC-34

(40 μM) added 1 h prior to labeling and then again throughout the experiment. Error bars show SEM for n=4 experiments. *$p<0.05$, ***$p<0.005$.

2.3 Conclusions

In conclusion, we report the discovery and characterization of KSC-34, a potent and selective inhibitor of PDIA1. KSC-34 was identified from a targeted library of compounds generated around an initial lead compound, RB-11-ca. KSC-34 contains a (4-phenylbutyl)methylamine diversity element for optimized binding to the **a** domain of PDIA1 with a chloroacetamide electrophile for covalent modification of C53 on PDIA1. Notably, the presence of a bioorthogonal alkyne handle on KSC-34 and derivatives, facilitated the rapid screening of these compounds for potency and selectivity both *in vitro* against purified PDIs, as well as directly in living cells. Importantly, despite the prominent reactivity of the chloroacetamide electrophile on KSC-34, extremely high selectivity is observed for PDIA1 within a complex proteome. The high inhibitory potency of KSC-34 was confirmed in an *in vitro* insulin-reduction assay, where KSC-34 proved to be approximately 38-fold more potent than the commercially available PDIA1 inhibitor 16F16. Importantly, KSC-34 is unique in that it displays selective binding to the **a** domain of PDIA1, and is the most site-selective PDIA1 inhibitor reported to date. KSC-34 treatment generally results in minimal sustained activation of the UPR, although some low cell-specific, short-lived effects were observed with the IRE1α arm in MCF-7 cells. Lastly, the ability of KSC-34 to reduce the extracellular pathogenic load of amyloidogenic antibody light-chain is demonstrated, highlighting the potential of site-selective PDIA1 inhibitors to have therapeutic value by selectively downregulating a subset of PDIA1 functions in cells. The development of KSC-34 validates the potential to selectively, and potently pharmacologically modulate individual thioredoxin-like active-site domains within a single member of the PDI family. KSC-34 is a useful tool compound to further

interrogate the cellular functions of the **a** domain of PDIA1, and additionally, to explore the therapeutic value of site-selective PDI inhibitors.

2.4 Materials and Methods

2.4.1 General Information

All materials were obtained from Sigma-Aldrich, Fisher Scientific, Combi-Blocks, or Oakwood Chemicals, unless otherwise noted. Phosphate buffered saline (PBS) buffer, RPMI 1640 media, Trypsin-EDTA and Anti-Anti were purchased from Fisher Scientific (Pittsburgh, PA). Fetal bovine serum was purchased from Atlanta Biologicals (Flowery Branch, GA). All protein concentrations were determined using the DC Protein Assay kit from Bio-Rad (Hercules, CA). Analytical thin layer chromatography (TLC) was performed on EMD Millipore F254 glass-backed TLC plates (250 μm, Billerica, MA). All compounds were visualized on TLC under UV light and by potassium permanganate staining. Column chromatography was carried out using forced flow of solvent on Sorbent Technologies (Norcross, GA) standard grade silica gel, 40-63 μm particle size, 60 Å pore size. Proton and carbon NMR spectra were carried out on Varian (Palo Alto, CA) 500 MHz and 600 MHz NMR spectrometers. Chemical shifts (δ) are reported in parts per million (ppm) with chemical shifts reported to internal standards: $CDCl_3$ (7.26 ppm for 1H, 77.23 ppm for ^{13}C), $(CD_3)_2CO$ (2.05 ppm for ^{1}H, 29.92 ppm for ^{13}C), CD_3OD (3.31 ppm for ^{1}H, 49.15 ppm for ^{13}C). Coupling constants (J) are reported in Hertz (Hz) and multiplicities are abbreviated as singlet (s), doublet (d), triplet (t), multiplet (m), doublet of doublets (dd), and doublet of triplets (dt). High resolution Mass Spectra (HRMS) were obtained at the Mass Spectrometry Facility at Boston College (Chestnut Hill, MA).

2.4.2 Covalent Docking Studies

Covalent docking calculations were performed by the covalent docking workflow[52] by Schrodinger, Inc. For the calculations, the experimental structure of PDIA1 in its reduced state was used (PDB ID: 4EKZ)[51]. A two-dimensional structure was prepared in ChemDraw (Perkin-Elmer) and then converted to 3D and energy minimized with default settings with LigPrep (Schrodinger). Prior to calculations, RB-11-ca was manually positioned in the a domain active site of PDIA1 near the catalytic cysteine, for use in automatic grid determination. The ligand was then docked using a nucleophilic substitution reaction at position C53 with default pose-prediction settings.

2.4.3 Cell culture and preparation of MCF-7 cell lysates

MCF-7 cells were cultured at 37 °C under an atmosphere of 5% CO_2 in RPMI 1640 media (Corning) supplemented with 10% fetal bovine serum (FBS, Atlanta Biologicals) and 25 µg/mL of Amphotericin B, 10,000 units/mL of penicillin, and 10,000 µg/mL streptomycin (Gibco Anti-Anti). The cells were then harvested and the pellets washed with phosphate buffered saline (PBS). After washing, the pellets were resuspended in an appropriate amount of PBS and then sonicated with an ultrasonic tip sonicator (Cole Parmer, Vernon Hills, IL). The lysates were separated by centrifugation at 45,000 rpm for 45 minutes at 4 °C to obtain soluble and insoluble lysate fractions. The soluble fraction was collected and the pellet discarded. Protein concentrations were determined using the DC Protein Assay kit (Bio-Rad, Hercules, CA).

2.4.4 Fluorescent Gel Analysis

For recombinant PDI labeling gels, purified protein (50 µL, 50 µg mL^{-1}) in PBS was treated with probe (1 µL of 50x stock in DMSO) for one hour. For endogenous PDI labeling gels, MCF-7 cell lysates (50 µL, 2 mg mL^{-1}) in PBS were treated with probe (1 µL of 50x stock in DMSO) for one hour. Rhodamine-azide (25 µM, 100x stock in DMSO, Click Chemistry Tools), was then appended to probe-labeled proteins via CuAAC; TCEP (1 mM, 50x stock in water), TBTA (100 µM, 17x stock in t-BuOH:DMSO 4:1), and copper (II) sulfate (1 mM, 50x stock in water) were added to the cell lysate. Samples were then incubated at room temperature for one hour to allow for the cycloaddition reaction to occur. An equal volume of SDS-PAGE loading buffer (2x, reducing) was added to each reaction and 20 µL of this solution was separated on a 10% SDS-PAGE gel. Gels were visualized for rhodamine fluorescence on a ChemiDoc MP imaging system (BioRad, Hercules, CA). Gels were then coomassie stained following a standard procedure and visualized on the same imager.

2.4.5 *In situ* labeling experiments

MCF-7 cells were grown to ~90% confluence in 10 cm tissue culture plates. Growth media was removed and replaced with 5 mL RPMI. Probes in an appropriate DMSO stock was then added to the media to achieve the desired labeling concentration and incubated at 37 °C under an atmosphere of 5% CO_2 for 3 hours. Cells were then harvested and were then prepared as lysates as described above.

2.4.6 KSC-34 cellular occupancy experiments

MCF-7 cells were labeled dose-dependently with the non-alkyne analogue, KSC-34na, and prepared as above. After normalizing protein concentrations to 2 mg/mL across samples, each sample was then treated with 5 μM KSC-34 for 1 hour at room temperature. Samples were then subjected to click chemistry to append a fluorophore for fluorescent-gel analysis. Gels were visualized for rhodamine fluorescence on a ChemiDoc MP imaging system (BioRad, Hercules, CA). Gels were then coomassie stained following a standard procedure and visualized on the same imager. ImageJ was used to quantify the loss of fluorescence intensity of the PDIA1 band and an EC_{50} value for cellular occupancy was determined using PRISM.

2.4.7 PDIA1 active site selectivity experiments

In order to determine the active site preference for each probe, mutant recombinant PDIA1, C53A or C397A (50 μg/mL), was spiked into MCF-7 lysate (1 mg/mL) followed by dose-dependent increases of KSC-34, RB-11-ca or 16F16. Following incubation, samples were then incubated with Chloroacetamide-Rhodamine (8 μM, Figure 2-9B), to append a fluorophore to any unlabeled PDIA1. ImageJ was used to quantify the loss of fluorescence intensity of the PDIA1 band and IC_{50} values for each active site were determined using PRISM.

2.4.8 PDI isoform selectivity experiments

In order to determine the selectivity of KSC-34 for PDIA1 over other PDI family members, an in-gel fluorescence experiment was performed comparing labeling of PDIA1 with KSC-34 to PDIA3 and PDIA4. The PDIs (50 μg/mL) in PBS either in the absence or presence of an MCF-7 lysate background (1 mg/mL) were treated with KSC-34 (5 μM) for one hour at room temperature. Following treatment, rhodamine-azide was appended with click-chemistry for fluorescent-gel analysis. Gels were visualized for rhodamine fluorescence on a ChemiDoc MP imaging system (BioRad, Hercules, CA). Gels were then coomassie stained following a standard procedure and visualized on the same imager.

2.4.9 PDIA1 Insulin Reduction Activity Assay

PDIA1 WT (5 μM) in PBS was aliquoted as 25 μL samples. Inhibitor or DMSO (0.5 μL of 50x) were added to each sample to achieve a final concentration between 0 μM and 1,500 μM for either 5, 15, 30, 45, or 60 minutes. The samples were briefly vortexed and then 10 μL was taken from each sample and added to the assay plate. Fresh assay buffer (100 mM K_2HPO_4, 2 mM EDTA, pH 7.0) was prepared and 70 μL was aliquoted per well. Bovine insulin (Sigma-Aldrich, 10 μL, 10x, 1.6 mM) was also added to the wells. Following a brief shake in the plate reader, DTT (10 μL, 10x, 10 mM) was added to initiate the activity assay. A sample without PDIA1 and a sample without DTT were used as blank controls. This results in final concentrations in this assay of PDIA1 WT (0.5 μM), Insulin (0.16 mM), and DTT (1 mM). The assay plate was read for absorbance at 650 nm every 20 seconds for 30 minutes, with shaking between reads.

For data analysis, each well was normalized to the – PDIA1 sample at each time point. The linear portion (400 – 800 sec) of the absorbance vs time plot was used to monitor

a loss in PDIA1 activity. Linear regressions for each pre-incubation time point at each [Inhibitor] were performed to determine the rates of the reactions (5 slopes, 5 different pre-incubation times) for each [Inhibitor]. For each [Inhibitor], the Rate of Activity vs Pre-incubation time was plotted. This was determined by normalizing the reaction rates of each sample to samples without inhibitor, to give % Rate of Control vs Pre-incubation time. A one-phase decay nonlinear regression was performed for each [Inhibitor] to produce a rate constant for inhibition, k_{obs}. These rate constants were plotted as k_{obs} vs [Inhibitor], and another nonlinear regression was performed to calculate K_I and k_{inact}.

2.4.10 KSC-34 Mass Spectrometry Sample Preparation and Data Analysis

MCF-7 cells were grown to ~90% confluence in 15 cm tissue culture plates. Growth media was removed and replaced with 10 mL RPMI. KSC-34 (10 µL, 1000x stock) or DMSO was then added to the media to achieve the desired labeling concentration and incubated at 37 °C under an atmosphere of 5% CO_2 for 3 hours. Cells were then harvested and were then prepared as lysates as described above.

KSC-34 labeled MCF-7 cell lysates (500 µL, 2 mg mL^{-1}) in PBS were subjected to click chemistry. Biotin azide (200 µM from 100x stock in DMSO), TCEP (1 mM, 50x stock in water), TBTA (100 µM, 17x stock in t-BuOH:DMSO 4:1), and copper (II) sulfate (1 mM, 50x stock in water) were added to the cell lysate. Samples were incubated at room temperature for 1 hour to allow for the cycloaddition reaction to occur. Samples were then centrifuged for 10 minutes at 4 °C to pellet the precipitated proteins. Protein pellets were then resuspended in cold methanol by tip sonication followed by centrifugation. Following a second methanol wash, pelleted proteins were solubilized in a 1.2% SDS/PBS solution

via tip sonication and incubation at 85 °C for 5 minutes. Samples were then diluted with 5 mL PBS to lower the concentration of SDS to 0.2%. Next, samples were incubated with 100 µL streptavidin agarose beads (Thermo Fisher Scientific, Waltham, MA) at 4 °C for 16 hours. Samples were then washed with 0.2% SDS/PBS (5 mL), PBS (3 x 5 mL), and water (3 x 5 mL). The streptavidin agarose beads were pelleted between each wash step by centrifugation (1,400 g, 3 minutes).

The beads were suspended in a solution of 6 M Urea/PBS (500 µL) and 10 mM dithiothreitol (DTT, 20x stock in water), followed by incubation at 65 °C for 20 minutes. Next, iodoacetamide (20 mM, from 50x stock in water) was added to each sample and incubated at room temperature for 30 minutes. The beads were pelleted (1,400 g, 3 minutes) and resuspended in 200 µL of 2 M Urea/PBS, 1 mM $CaCl_2$ (100x stock in water), and 2 µg trypsin (Promega, Madison, WI). On-bead trypsin digestion was allowed to proceed overnight at 37 °C with agitation. The beads were pelleted (1,400 g, 3 min) and the supernatant collected. The beads were washed with water (2 x 50 µL) and the washes were combined with the supernatant. Formic acid (15 µL, Thermo Fisher Scientific, Waltham, MA) was then added to each sample and the samples were stored at -20 °C until mass spectrometry analysis.

LC/LC-MS/MS analysis was performed on an LTQ Orbitrap Discovery mass spectrometer (Thermo Fisher Scientific, Waltham, MA) coupled to an Agilent 1200 series HPLC (Agilent Technologies, Santa Clara, CA). Tryptic digests were pressure loaded onto a 250 µm fused silica desalting column packed with 4 cm of Aqua C18 reversed phase resin (Phenomenex, Torrance, CA). Peptides were then eluted onto a biphasic 100 µm fused silica column with a 5 µm tip, packed with 10 cm of C18 and 4 cm of Partisphere

SCX (Whatman, Pittsburgh, PA). Elution of the peptides from the desalting column into the biphasic column occurred using a gradient of 5-100% Buffer B in Buffer A (Buffer A: 95% water, 5% acetonitrile, 0.1% formic acid; Buffer B: 20% water, 80% acetonitrile, 0.1% formic acid). The peptides were eluted from the SCX onto the C18 resin and then into the mass spectrometer using four salt pushes[65]. The flow rate of buffer through the fused silica column was set to 0.25 μL min^{-1} and the spray voltage was set 2.75 kV. One full MS scan (400 – 1800 MW) was followed by 8 data dependent scans of the n^{th} most intense ions with dynamic exclusion enabled.

Two biological replicates each of KSC-34 (5 μM) or DMSO treated MCF-7 cells were subjected to LC/LC-MS/MS analysis as outlined above. The generated tandem MS data was searched using the SEQUEST algorithm against the human UniProt database. A static modification of +57.0215 on cysteine was added to account for alkylation of cysteine residues with iodoacetamide. The SEQUEST output files were then filtered using DTASelect v2.0 to generate a list of proteins identified with a false-discovery rate of < 5%. The resulting peptides were then further filtered to display proteins identified in KSC-34 treated samples with an average of 10 spectral counts or greater across the biological replicates. For each of these proteins, the change in spectral counts between KSC-34 treated samples and DMSO samples was calculated and the data was ranked by those proteins displaying the highest change in spectral counts in the KSC-34 treated samples relative to the DMSO treated samples.

2.4.11 UPR Assays and Cell Culture

MCF7 cells were cultured in RPMI-1640 supplemented with glutamine, penicillin/streptomycin, and 10% fetal bovine serum (FBS). Cells were treated with the indicated concentrations of KSC-34 (see Results section) at the indicated time points, with 0.1% DMSO serving as negative control. To induce global ER stress, the sarco/endoplasmic reticulum Ca^{2+}-ATPase inhibitor thapsigargin was used at 5 μM for three hours. To inhibit IRE1 activity, cells were co-treated with 4μ8C (purchased from Sigma-Aldrich) at the indicated concentrations for three hours.

2.4.12 Quantitative RT-PCR

The relative mRNA expression levels of target genes were measured by quantitative RT-PCR (see Table 1 for a list of primers used). Cells were lysed in tissue culture plates, and total RNA was extracted using the Omega E.Z.N.A. Total RNA Kit I according to the manufacturer's instructions. RNA concentrations were quantified and normalized to 1 μg total RNA for cDNA reverse transcription. Using the Applied Biosystems High-Capacity cDNA Reverse Transcription Kit, cDNA was synthesized in a Bio-Rad T100 Thermal Cycler. LightCycler 480 SYBR Green I Master reaction mix (Roche), appropriate primers (purchased from Sigma-Aldrich), and cDNA were used for amplification in a LightCycler 480 Instrument II (Roche) in the MIT BioMicro Center. Primer integrity was assessed by thermal melt to ensure homogeneity. Transcripts were normalized to the housekeeping gene *RPLP2*, and all reactions were performed in quadruplicate. Experiments were repeated in biological triplicate. Data were analyzed using the ΔΔCt method and presented as mean fold change.

2.4.13 XBP1 Splicing Assay

cDNA synthesized from total RNA (as above) was amplified using the Q5 High-Fidelity DNA Polymerase (NEB) according to the manufacturer's instructions with the appropriate *XBP1* primers (Table 2). Five microliters of the resultant reaction were separated on 2.5% agarose gels stained with GelGreen (Biotium).

Table 2.2. Primers used for qPCR and XBP1 splicing assays.

Transcript	Forward	Reverse
BIP	5'- GCCTGTATTTCTAGACCTGCC-3'	5′-TTCATCTTGCCAGCCAGTTG-3′
CHOP	5′-GGAGCTGGAAGCCTGGTATG-3′	5′-GCCAGAGAAGCAGGGTCAAG-3′
ERDJ4	5'-CTGTATGCTGATTGGTAGAGTCAA-3'	5'-AGTAGACAAAGGCATCATTTCCAA-3'
GADD34	5'-TGGTAGAAGCTGGCCTGGAG-3'	5'-GGGAACTGCTGGTTTTCAGC-3'
GRP94	5'-GGCCAGTTTGGTGTCGGTTT-3'	5'-CGTTCCCCGTCCTAGAGTGTT-3'
HYOU1	5′-GCAGACCTGTTGGCACTGAG-3′	5′-TCACGATCACCGGTGTTTTC-3′
RPLP2	5′-CCATTCAGCTCACTGATAACCTTG-3′	5′-CGTCGCCTCCTACCTGCT-3′
SEC24D	5′-AGCAGACTGTCCTGGGAAGC-3′	5'-TTTGTTTGGGGCTGGAAAAG-3′
XBP1	5'-CCTTGTAGTTGAGAACCAGG-3'	5'-GGGGCTTGGTATATATGTGG-3'

2.4.14 Cell culture and transfections

HEK293^{TREX}, HEK293^{DAX},[58] and HEK293^{DAX} *PDIA1* shRNA cells were cultured in High-Glucose Dulbecco's Modified Eagle's Medium (DMEM) supplemented with glutamine, penicillin/streptomycin and 10% fetal bovine serum. *PDIA1* shRNA knockdown cells were additionally cultured with 5ug/ml puromycin. HEK293^{DAX} cells were transfected with ^{FT}ALLC.pcDNA3.1 using calcium phosphate, as previously described.[64, 66] All cells were cultured under typical tissue culture conditions (37°C, 5% CO2).

2.4.15 Cytotoxicity assays

HEK293^{TREX} and HEK293^{DAX} cells were plated at 5,000 cells/well in a poly-D-lysine coated transparent, flat-bottomed 96 well plate. Cells were pretreated for 4 hours with KSC-34 or DMSO vehicle. This media was replaced with fresh media containing KSC-34 or vehicle and conditioned for 2 hours. Cell metabolic activity was measured using the CellTiter-Glo assay (Promega). CellTiter-Glo reagent was added to cell culture media at a 1:1 ratio and incubated for 2 min on an orbital shaker to induce cell lysis. The plate was then incubated at room temperature for 10 min to stabilize the luminescent signal and read on a Tecan F200 Pro microplate reader.

2.4.16 [^{35}S] Metabolic labeling experiments

HEK293^{DAX} cells plated on poly-D-lysine coated dishes were metabolically labeled in DMEM-Cys/-Met (Corning CellGro, Mediatech Inc., Manassas, VA) supplemented with glutamine, penicillin/streptomycin, 10% dialyzed fetal bovine serum, and EasyTag EXPRESS [^{35}S] Protein Labeling Mix (Perkin Elmer) for 30 min. Cells were washed twice with complete media and incubated in pre-warmed DMEM. At the indicated time, media was collected and lysates were prepared in RIPA buffer with fresh protease inhibitor cocktail (Roche). FLAG-tagged ALLC was immunopurified using M1 anti-FLAG agarose beads (Sigma Aldrich) and washed four times with RIPA buffer. The immunoisolates were then eluted by boiling in Laemmli buffer and separated on SDS-PAGE. The gels were then dried, exposed to phosphorimager plates (GE Healthcare, Pittsburgh, PA), and imaged with a Typhoon imager. Band intensities were quantified by densitometry in ImageQuant. Fraction secreted was calculated using the equation: fraction secreted = [extracellular [^{35}S]-

^{FT}ALLC signal at t / (extracellular [^{35}S]-^{FT}ALLC signal at t=0 + intracellular [^{35}S]-^{FT}ALLC signal at t=0)].

2.4.17 Immunoprecipitation and SDS-PAGE

For immunoprecipitations, cells were washed with PBS then incubated with with 0.5 mM of the cell permeable reversible crosslinker Dithiobis(succinimidiyl propionate) (DSP) for 30 min at room temperature. The reaction was quenched by addition of 100 mM Tris pH 7.5. Lysates were then prepared in RIPA buffer and cleared by centrifugation at 10000 x *g* for 15 min. Proteins were immunopurified using using M1 anti-FLAG agarose beads (Sigma Aldrich). After four washes in RIPA buffer, proteins were eluted by boiling in Laemmli buffer + 100 mM DTT and samples were separated by SDS-PAGE and transferred to nitrocellulose membranes. Blots were probed with the following primary antibodies: monoclonal mouse M2 anti-FLAG (1:500, Sigma Aldrich), rabbit polyclonal anti-PDIA1 (1:1000, GeneTex GTX101468, Irvine, CA), rabbit polyclonal anti-PDIA4 (1:1000, Proteintech Group 14712-1-AP, Rosemont, IL).

2.4.18 Light chain ELISA

HEK293^{TREX} stably expressing ^{FT}ALLC or transfected HEK293^{DAX} cells were plated at 10,000 cells/well in a poly-D-lysine coated transparent, flat-bottomed 96 well plate. Triplicate wells were pretreated for 4 hours with 40µM KSC-34 or vehicle. Wells were washed twice with 100µL media and then fresh media with 40µM KSC-34 or vehicle was added for 2-hour conditioning. Conditioned media was harvested into a 96-well plate. Free LC concentrations were determined by ELISA in 96-well plates (Immulon 4HBX,

Thermo Fisher). Wells were coated overnight at 37 ºC with sheep polyclonal free λ LC antibody (Bethyl Laboratories, A80-127A) at a 1:500 dilution in 50 mM sodium carbonate (pH 9.6). In between all incubation steps, the plates were rinsed extensively with Tris-buffered saline containing 0.05% Tween-20 (TBST). Plates were blocked with 5% non-fat dry milk in TBST for 1 hr at 37ºC. Media analytes were diluted between 5 – 200 fold in 5% non-fat dry milk in TBST and 100 µL of each sample was added to individual wells. Light chain standards ranging from 3 – 300 ng/mL were prepared from purified human Bence Jones λ light chain (Bethyl Laboratories, P80-127). Plates were incubated at 37 ºC for 1.5 hr while shaking. Finally, HRP-conjugated goat anti-human λ light chain antibody (Bethyl Laboratories, A80-116P) was added at a 1:5,000 in 5% non-fat dry milk in TBST, followed by a 1.5 hr incubation of the plates at 37 ºC. The detection was carried out with 2,2'-azinobis(3-ethylbenzothiazoline-6-sulfonic acid) (ABTS, 0.18 mg/mL) and 0.03% hydrogen peroxide in 100 mM sodium citrate pH 4.0. Detection solution (100 µL) was added to each well and the plates were incubated at room temperature. The absorbance was recorded at 405 nm and the values for the LC standards were fitted to a 4-parameter logistic function. Light chain concentrations were averaged from 3 independent replicates under each treatment and then normalized to vehicle conditions.

2.4.19 Quantitative RT-PCR

Cells were treated as described at 37°C, washed with Dulbecco's phosphate-buffered saline, and then RNA was extracted using the RNeasy Mini Kit (Qiagen). qPCR reactions were performed on cDNA prepared from 500 ng of total cellular RNA using the QuantiTect Reverse Transcription Kit (Qiagen). The FastStart Universal SYBR Green

Master Mix (Roche), cDNA, and appropriate human primers for *PDIA1 (*TCTTCATCGACAGCGACCAC and ATCCTCTCTGCCGTCAGCTC) purchased from Integrated DNA Technologies were used for amplifications (45 cycles of 1 min at 95°C, 10 s at 95°C, 30 sec at 60°C) in an ABI 7900HT Fast Real Time PCR machine. Transcripts were normalized to the housekeeping gene *GAPDH* and all measurements were performed in triplicate. Data were analyzed using the RQ Manager and DataAssist 2.0 softwares (ABI, Foster City, CA).

2.4.20 Synthetic Methods and Characterization

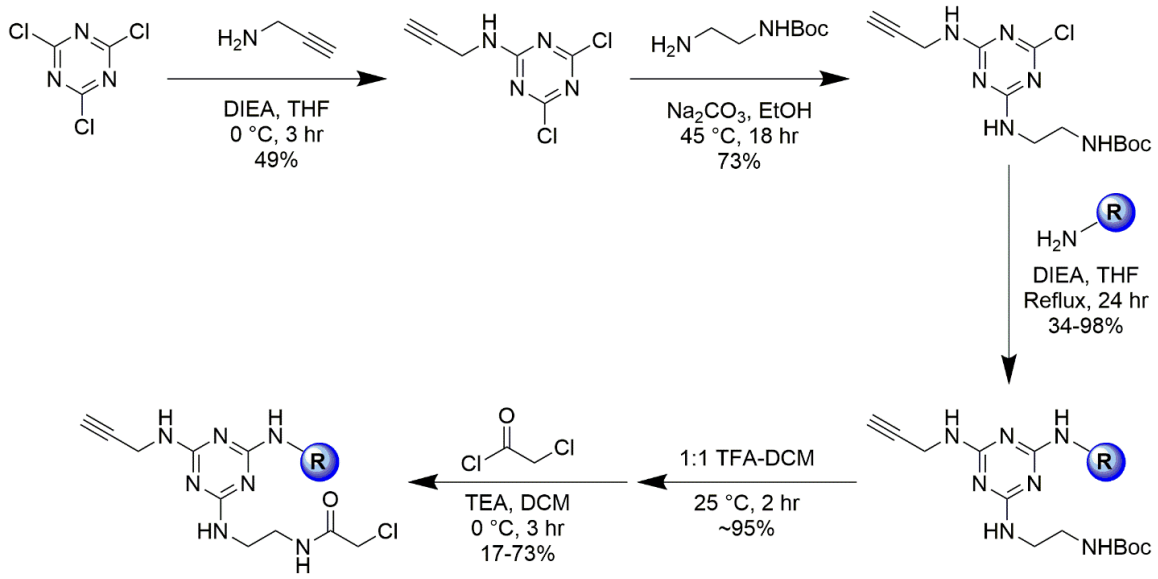

Scheme 2.1. General synthetic route for triazine-based covalent PDIA1 inhibitors.

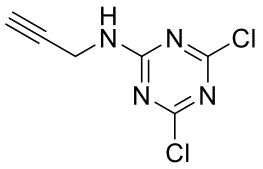

BBI

4,6-dichloro-N-(prop-2-yn-1-yl)-1,3,5-triazin-2-amine (BBI): To an ice cold solution of cyanuric chloride (1.0 eq, 151.1 mg, 0.8194 mmol) and diisopropylethylamine (1.1 eq, 116.5 mg, 0.9013 mmol) in tetrahydrofuran (THF) (0.055 M, 15 mL), propargylamine (1.2 eq, 54.2 mg, 0.9832 mmol) was added dropwise. The reaction mixture was allowed to stir at 0 °C for 3 hours. The solvent was removed *in vacuo* and the crude product was purified via flash chromatography to give the desired product **BBI** as a white solid (82.2 mg, 49%). ^{1}H NMR (600 MHz, Acetone-d_6) δ 8.30 (s, 1H), 4.43 – 4.15 (m, 2H), 2.79 (t, J = 2.6 Hz, 1H). ^{13}C NMR (151 MHz, Acetone-d_6) δ 171.32, 170.63, 166.91, 79.56, 73.13, 31.35. HRMS for BBI: m/z calcd. 202.9813; obsd. 201.9901.

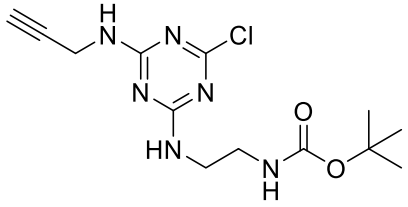

BBII

***tert*-butyl(2-((4-chloro-6-(prop-2-yn-1-ylamino)-1,3,5-triazin-2-yl)amino)ethyl)carbamate (BBII):** To a solution of **BBI** (1.0 eq, 79.4 mg, 0.3911 mmol) and sodium carbonate (2.2 eq, 91.2 mg, 0.8604 mmol) in ethanol (0.08 M, 5 mL), N-Boc-

ethylenediamine (1.1eq, 68.9 mg, 0.4302 mmol) was added dropwise at room temperature. The solution was then allowed to warm to 45 °C while stirring and continued to stir for 18 hours. After the reaction was complete, 15 mL of water was added and the reaction was extracted with ethyl acetate (3 x 15 mL). The organic layer was washed with brine and dried with $MgSO_4$, then the solvent was removed *in vacuo*. The crude product was purified via flash chromatography to afford the desired to product, **BBII** as a white solid (93.2 mg, 73%). ^{1}H NMR (600 MHz, DMSO-d_6) δ 8.12 (dt, J = 44.7, 5.8 Hz, 1H), 8.01 – 7.54 (m, 1H), 6.82 (dt, J = 11.4, 5.9 Hz, 1H), 4.17 – 3.92 (m, 2H), 3.31 – 3.19 (m, 2H), 3.18 – 3.00 (m, 2H), 2.50 (p, J = 1.8 Hz, 1H), 1.36 (d, J = 1.9 Hz, 9H). ^{13}C NMR (151 MHz, DMSO-d_6) δ 168.38, 168.12, 167.78, 165.36, 164.79, 155.57, 80.87, 77.61, 72.91, 29.63, 28.21. HRMS for BBII: m/z calcd. 327.1258; obsd. 327.1345.

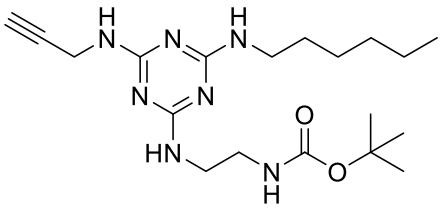

KSC-4-int

***tert*-butyl(2-((4-(hexylamino)-6-(prop-2-yn-1-ylamino)-1,3,5-triazin-2-yl)amino)ethyl)carbamate (KSC-4-int):** To a solution of **BBII** (1.0 eq, 92.8 mg, 0.2840 mmol) and diisopropylethylamine (2.5 eq, 91.8 mg, 0.7100 mmol) in THF (0.04 M, 8 mL), hexylamine (2.5 eq, 71.8 mg, 0.7100 mmol) was added dropwise at room temperature. The solution was then allowed to heat to reflux while stirring and continued to reflux for 24 hours. After the reaction was complete, the solvent was removed *in vacuo*. The crude

product was purified via flash chromatography to afford the desired to product, **KSC-4-int** as an oil (107.2 mg, 96%). ^{1}H NMR (500 MHz, Chloroform-*d*) δ 6.01 – 4.66 (m, 4H), 4.16 (s, 2H), 3.60 – 3.16 (m, 6H), 2.27 – 2.12 (m, 1H), 1.52 (q, *J* = 7.4 Hz, 2H), 1.42 (d, *J* = 2.0 Hz, 9H), 1.37 – 1.25 (m, 6H), 0.87 (dt, *J* = 6.9, 3.3 Hz, 3H). ^{13}C NMR (151 MHz, Chloroform-*d*) δ 166.54, 165.75, 156.33, 81.00, 79.27, 71.01, 41.53, 40.84, 40.70, 31.67, 30.44, 29.82, 28.52, 26.73, 22.71, 14.22, 14.15. HRMS for KSC-4-int: m/z calcd. 392.2696; obsd. 392.2774.

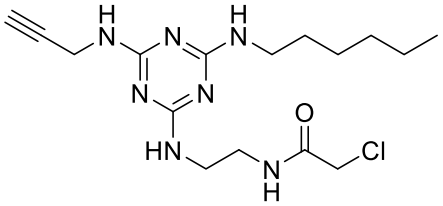

KSC-4

2-chloro-N-(2-((4-(hexylamino)-6-(prop-2-yn-1-ylamino)-1,3,5-triazin-2-yl)amino)ethyl)acetamide (KSC-4): KSC-4-int was deprotected using a 50% solution of TFA/DCM (4 mL) at 25 °C for 2 hours. The solvent was removed *in vacuo* and the crude product remained on the vacuum overnight to remove any excess TFA. Then, to an ice cold solution of deprotected amine (1.0 eq, 39.9 mg, 0.1369 mmol) and triethylamine (1.5 eq, 20.8 mg, 0.2054 mmol) in DCM (0.03 M, 5 mL), chloroacetyl chloride (1.2 eq, 18.6 mg, 0.1643 mmol) in DCM (2 mL) was added dropwise over 30 min. The reaction was stirred at 0 °C for 3 hours. After the reaction was complete, the solvent was removed *in vacuo* and the crude product was purified by flash chromatography to give the desired product **KSC-4** (26.3 mg, 52%). ^{1}H NMR (600 MHz, Chloroform-*d*) δ 4.21 (s, 2H), 4.03 (s, 2H),

3.74 – 3.43 (m, 2H), 3.39 (s, 2H), 2.23 (s, 1H), 1.56 (s, 2H), 1.31 (dd, *J* = 16.3, 9.6 Hz, 6H), 1.25 (d, *J* = 2.4 Hz, 2H), 0.88 (t, *J* = 6.7 Hz, 3H). ^{13}C NMR (151 MHz, Chloroform-*d*) δ 166.86, 163.97, 117.49, 115.56, 79.67, 71.63, 42.71, 41.06, 39.81, 31.60, 30.43, 29.83, 29.55, 26.64, 22.69, 14.15. HRMS for KSC-4: m/z calcd. 368.1887; obsd. 368.1966.

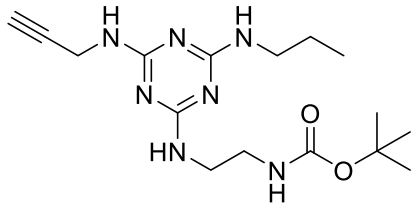

KSC-5-int

***tert*-butyl(2-((4-(prop-2-yn-1-ylamino)-6-(propylamino)-1,3,5-triazin-2-yl)amino)ethyl)carbamate (KSC-5-int):** To a solution of **BBII** (1.0 eq, 44.0 mg, 0.1346 mmol) and diisopropylethylamine (2.4 eq, 41.8 mg, 0.3231 mmol) in THF (0.03 M, 5 mL), propylamine (2.4 eq, 19.1 mg, 0.3231 mmol) was added dropwise at room temperature. The solution was then allowed to heat to reflux while stirring and continued to reflux for 24 hours. After the reaction was complete, the solvent was removed *in vacuo*. The crude product was purified via flash chromatography to afford the desired to product, **KSC-5-int** as an oil (37.4 mg, 80%). ^{1}H NMR (600 MHz, Chloroform-*d*) δ 4.24 – 4.06 (m, 2H), 3.47 (s, 2H), 3.29 (s, 4H), 2.20 (t, *J* = 2.5 Hz, 1H), 1.56 (q, *J* = 7.5 Hz, 2H), 1.41 (s, 9H), 0.93 (t, *J* = 7.4 Hz, 3H). ^{13}C NMR (151 MHz, Chloroform-*d*) δ 166.70, 166.15, 165.69, 156.32, 81.03, 79.27, 71.00, 42.60, 41.67, 40.68, 30.47, 28.53, 23.11, 11.58. HRMS for KSC-5-int: m/z calcd. 350.2226; obsd. 350.2324.

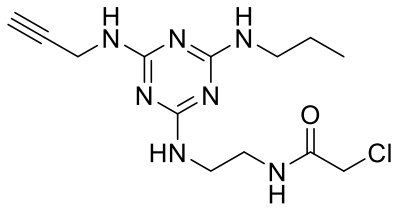

KSC-5

2-chloro-N-(2-((4-(prop-2-yn-1-ylamino)-6-(propylamino)-1,3,5-triazin-2-yl)amino)ethyl)acetamide (KSC-5): KSC-5-int was deprotected using a 50% solution of TFA/DCM (4 mL) at 25 °C for 2 hours. The solvent was removed *in vacuo* and the crude product remained on the vacuum overnight to remove any excess TFA. Then, to an ice cold solution of deprotected amine (1.0 eq, 31.3 mg, 0.1256 mmol) and triethylamine (1.5 eq, 19.0 mg, 0.1884 mmol) in DCM (0.025 M, 5 mL), chloroacetyl chloride (1.2 eq, 17.0 mg, 0.1507 mmol) in DCM (2 mL) was added dropwise over 30 min. The reaction was stirred at 0 °C for 3 hours. After the reaction was complete, the solvent was removed *in vacuo* and the crude product was purified by flash chromatography to give the desired product **KSC-5** (23.5 mg, 58%). ^{1}H NMR (500 MHz, Chloroform-*d*) δ 4.30 – 4.12 (m, 2H), 4.04 (s, 2H), 3.73 – 3.22 (m, 6H), 2.30 – 2.21 (m, 1H), 1.35 – 1.15 (m, 2H), 0.95 (d, *J* = 7.8 Hz, 3H). ^{13}C NMR (151 MHz, Acetone-d_6) δ 167.50, 163.27, 152.84, 76.67, 74.19, 72.96, 51.02, 45.41, 43.36, 41.60, 40.25, 39.27, 37.53, 24.38, 23.33, 14.36, 11.23. HRMS for KSC-5: m/z calcd. 326.1418; obsd. 326.1487.

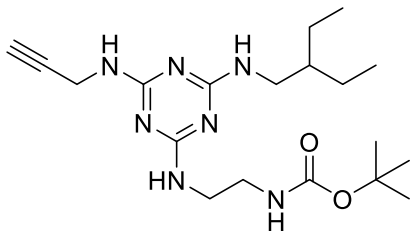

KSC-6-int

***tert*-butyl(2-((4-((2-ethylbutyl)amino)-6-(prop-2-yn-1-ylamino)-1,3,5-triazin-2-yl)amino)ethyl)carbamate (KSC-6-int):** To a solution of **BBII** (1.0 eq, 47.1 mg, 0.1441 mmol) and diisopropylethylamine (2.4 eq, 44.7 mg, 0.3459 mmol) in THF (0.03 M, 5 mL), 2-ethylbutylamine (2.4 eq, 35.0 mg, 0.3459 mmol) was added dropwise at room temperature. The solution was then allowed to heat to reflux while stirring and continued to reflux for 24 hours. After the reaction was complete, the solvent was removed *in vacuo*. The crude product was purified via flash chromatography to afford the desired to product, **KSC-6-int** as an oil (46.4 mg, 82%). ^{1}H NMR (600 MHz, Chloroform-*d*) δ 4.17 (s, 2H), 3.48 (s, 2H), 3.29 (s, 4H), 2.20 (t, *J* = 2.6 Hz, 1H), 1.42 (s, 9H), 1.33 (p, *J* = 7.2 Hz, 4H), 1.25 (d, *J* = 2.7 Hz, 1H), 0.89 (t, *J* = 7.4 Hz, 6H). ^{13}C NMR (151 MHz, Chloroform-*d*) δ 166.38, 165.59, 156.32, 81.00, 79.29, 71.01, 43.15, 41.71, 41.27, 40.70, 30.52, 29.83, 23.92, 14.25, 11.15. HRMS for KSC-6-int: m/z calcd. 392.2696; obsd. 392.2778.

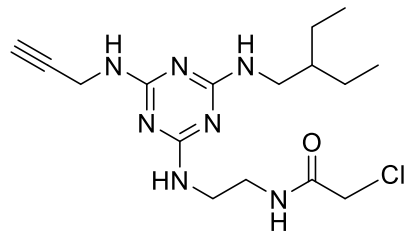

KSC-6

2-chloro-N-(2-((4-((2-ethylbutyl)amino)-6-(prop-2-yn-1-ylamino)-1,3,5-triazin-2-yl)amino)ethyl)acetamide (KSC-6): KSC-6-int was deprotected using a 50% solution of TFA/DCM (4 mL) at 25 °C for 2 hours. The solvent was removed *in vacuo* and the crude product remained on the vacuum overnight to remove any excess TFA. Then, to an ice cold solution of deprotected amine (1.0 eq, 34.5 mg, 0.1185 mmol) and triethylamine (1.5 eq, 18.0 mg, 0.1778 mmol) in DCM (0.025 M, 5 mL), chloroacetyl chloride (1.2 eq, 16.1 mg, 0.1422 mmol) in DCM (2 mL) was added dropwise over 30 min. The reaction was stirred at 0 °C for 3 hours. After the reaction was complete, the solvent was removed *in vacuo* and the crude product was purified by flash chromatography to give the desired product **KSC-6** (31.0 mg, 71%). ^{1}H NMR (500 MHz, Chloroform-*d*) δ 4.28 – 4.10 (m, 2H), 4.04 (s, 2H), 3.71 – 3.22 (m, 4H), 2.32 – 2.20 (m, 1H), 1.42 – 1.30 (m, 10H), 1.25 (d, *J* = 2.4 Hz, 3H). ^{13}C NMR (151 MHz, Acetone-d_6) δ 167.50, 163.27, 152.84, 76.67, 74.19, 72.96, 51.02, 45.41, 43.36, 41.60, 40.25, 39.27, 37.53, 24.38, 23.33, 14.36, 11.23. HRMS for KSC-6: m/z calcd. 368.1887; obsd. 368.1976.

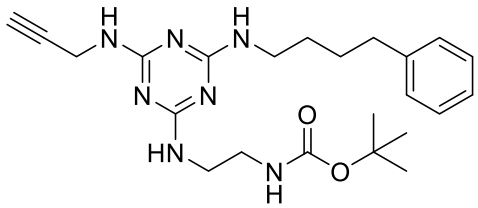

KSC-7-int

***tert*-butyl(2-((4-((4-phenylbutyl)amino)-6-(prop-2-yn-1-ylamino)-1,3,5-triazin-2-yl)amino)ethyl)carbamate (KSC-7-int):** To a solution of **BBII** (1.0 eq, 53.9 mg, 0.1649 mmol) and diisopropylethylamine (2.4 eq, 51.1 mg, 0.3956 mmol) in THF (0.03 M, 5 mL),

4-phenylbutylamine (2.4 eq, 59.0 mg, 0.3956 mmol) was added dropwise at room temperature. The solution was then allowed to heat to reflux while stirring and continued to reflux for 24 hours. After the reaction was complete, the solvent was removed *in vacuo*. The crude product was purified via flash chromatography to afford the desired to product, **KSC-7-int** as an oil (70.7 mg, 98%). ^{1}H NMR (600 MHz, Chloroform-*d*) δ 7.30 – 7.23 (m, 2H), 7.17 (t, *J* = 8.1 Hz, 3H), 4.31 – 3.99 (m, 2H), 3.53 – 3.13 (m, 6H), 2.63 (t, *J* = 7.6 Hz, 2H), 2.19 (s, 1H), 1.67 (q, *J* = 7.8 Hz, 2H), 1.58 (t, *J* = 7.8 Hz, 2H), 1.42 (s, 9H). ^{13}C NMR (151 MHz, Chloroform-*d*) δ 166.15, 156.31, 142.34, 128.52, 125.88, 81.01, 79.29, 71.02, 41.61, 40.71, 40.61, 35.69, 30.49, 29.83, 29.54, 28.81, 28.54, 14.33, 1.15. HRMS for KSC-7-int: m/z calcd. 440.2696; obsd. 440.2739.

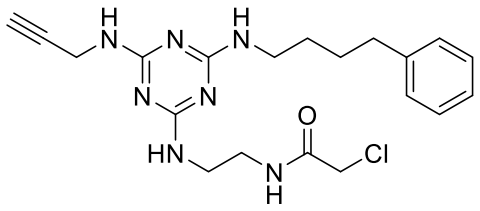

KSC-7

2-chloro-N-(2-((4-((4-phenylbutyl)amino)-6-(prop-2-yn-1-ylamino)-1,3,5-triazin-2-yl)amino)ethyl)acetamide (KSC-7): KSC-7-int was deprotected using a 50% solution of TFA/DCM (4 mL) at 25 °C for 2 hours. The solvent was removed *in vacuo* and the crude product remained on the vacuum overnight to remove any excess TFA. Then, to an ice cold solution of deprotected amine (1.0 eq, 54.6 mg, 0.1608 mmol) and triethylamine (1.5 eq, 24.4 mg, 0.2412 mmol) in DCM (0.03 M, 5 mL), chloroacetyl chloride (1.2 eq, 21.8 mg, 0.1930 mmol) in DCM (2 mL) was added dropwise over 30 min. The reaction was stirred

at 0 °C for 3 hours. After the reaction was complete, the solvent was removed *in vacuo* and the crude product was purified by flash chromatography to give the desired product **KSC-7** (47.9 mg, 72%). ^{1}H NMR (500 MHz, Chloroform-*d*) δ 7.31 – 7.24 (m, 2H), 7.23 – 7.10 (m, 3H), 4.29 – 4.09 (m, 2H), 4.06 (s, 2H), 3.71 – 3.31 (m, 4H), 2.71 – 2.56 (m, 1H), 1.65 (d, *J* = 16.0 Hz, 4H), 1.41 – 1.17 (m, 4H). ^{13}C NMR (126 MHz, Chloroform-*d*) δ 167.00, 141.93, 128.52, 126.04, 78.42, 72.40, 53.56, 42.72, 41.52, 40.83, 40.01, 39.34, 35.54, 31.33, 30.30, 29.84, 28.63, 22.83. HRMS for KSC-7: m/z calcd. 416.1887; obsd. 416.1963.

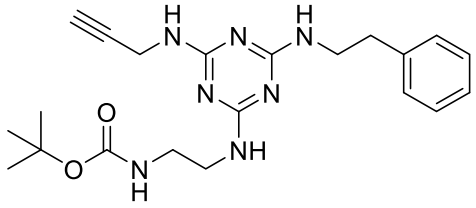

KSC-9-int

***tert*-butyl(2-((4-(phenethylamino)-6-(prop-2-yn-1-ylamino)-1,3,5-triazin-2-yl)amino)ethyl)carbamate (KSC-9-int):** To a solution of **BBII** (1.0 eq, 92.8 mg, 0.2840 mmol) and diisopropylethylamine (4.0 eq, 146.8 mg, 1.1359 mmol) in THF (0.05 M, 5 mL), 2-phenethylamine hydrochloride (4.0 eq, 137.7 mg, 1.1359 mmol) was added dropwise at room temperature. The solution was then allowed to heat to reflux while stirring and continued to reflux for 24 hours. After the reaction was complete, the solvent was removed *in vacuo*. The crude product was purified via flash chromatography to afford the desired to product, **KSC-9-int** as an oil (57.1 mg, 49%). ^{1}H NMR (500 MHz, Chloroform-*d*) δ 7.29 (t, *J* = 7.6 Hz, 2H), 7.20 (d, *J* = 7.2 Hz, 3H), 5.82 – 4.91 (m, 4H), 4.15 (d, *J* = 17.4 Hz, 2H), 3.74 – 3.38 (m, 4H), 3.29 (s, 2H), 2.86 (t, *J* = 7.4 Hz, 2H), 2.19

(s, 1H), 1.41 (s, 9H). ^{13}C NMR (126 MHz, Chloroform-*d*) δ 166.87, 166.31, 165.96, 156.58, 139.64, 129.17, 126.70, 81.29, 79.56, 71.27, 42.43, 40.95, 36.40, 30.71, 30.06, 28.78, 23.06. HRMS for KSC-9-int: m/z calcd. 412.2383; obsd. 412.2461.

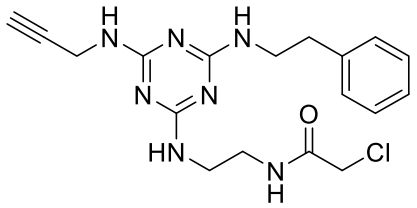

KSC-9

2-chloro-N-(2-((4-(phenethylamino)-6-(prop-2-yn-1-ylamino)-1,3,5-triazin-2-yl)amino)ethyl)acetamide (KSC-9): KSC-9-int was deprotected using a 50% solution of TFA/DCM (4 mL) at 25 °C for 2 hours. The solvent was removed *in vacuo* and the crude product remained on the vacuum overnight to remove any excess TFA. Then, to an ice cold solution of deprotected amine (1.0 eq, 125.5 mg, 0.4030 mmol) and triethylamine (1.3 eq, 53.0 mg, 0.5239 mmol) in DCM (0.08 M, 5 mL), chloroacetyl chloride (1.3 eq, 59.2 mg, 0.5239 mmol) in DCM (2 mL) was added dropwise over 30 min. The reaction was stirred at 0 °C for 3 hours. After the reaction was complete, the solvent was removed *in vacuo* and the crude product was purified by flash chromatography to give the desired product **KSC-9** (26.9 mg, 17%). ^{1}H NMR (500 MHz, Chloroform-*d*) δ 7.46 – 7.28 (m, 3H), 7.25 – 7.18 (m, 2H), 4.23 (m, 2H), 4.16 – 3.98 (m, 2H), 3.79 – 3.45 (m, 6H), 2.90 (dt, *J* = 17.7, 8.8 Hz, 2H), 2.36 – 2.22 (m, 1H). ^{13}C NMR (126 MHz, Chloroform-*d*) δ 174.40, 156.18, 137.95, 128.60, 126.62, 101.36, 72.19, 49.42, 42.32, 39.84, 39.20, 35.38, 31.04, 30.06, 29.60, 14.01. HRMS for KSC-9: m/z calcd. 388.1574; obsd. 388.1653.

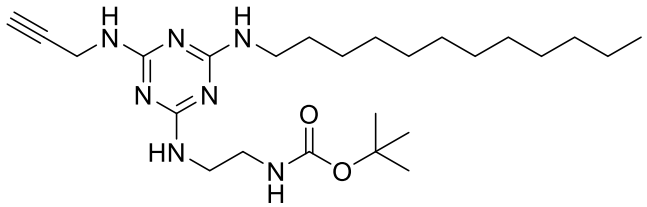

KSC-10-int

***tert*-butyl(2-((4-(dodecylamino)-6-(prop-2-yn-1-ylamino)-1,3,5-triazin-2-yl)amino)ethyl)carbamate (KSC-10-int):** To a solution of **BBII** (1.0 eq, 51.6 mg, 0.1580 mmol) and diisopropylethylamine (2.5 eq, 51.1 mg, 0.3950 mmol) in THF (0.03 M, 5 mL), dodecylamine (2.5 eq, 73.2 mg, 0.3950 mmol) was added dropwise at room temperature. The solution was then allowed to heat to reflux while stirring and continued to reflux for 24 hours. After the reaction was complete, the solvent was removed *in vacuo*. The crude product was purified via flash chromatography to afford the desired to product, **KSC-10-int** as an oil (53.5 mg, 71%). ^{1}H NMR (500 MHz, Chloroform-*d*) δ 5.78 – 4.84 (m, 4H), 4.15 (s, 2H), 3.57 – 3.18 (m, 6H), 2.20 (t, *J* = 2.5 Hz, 1H), 1.59 – 1.46 (m, 2H), 1.41 (s, 9H), 1.37 – 1.17 (m, 18H), 0.87 (t, *J* = 6.9 Hz, 3H). ^{13}C NMR (151 MHz, Chloroform-*d*) δ 165.93, 156.55, 134.07, 129.61, 93.58, 81.10, 79.53, 71.29, 41.78, 41.09, 32.26, 30.74, 30.08, 30.01, 29.97, 29.94, 29.73, 29.69, 28.75, 27.29, 23.03, 14.46, 1.36. HRMS for KSC-10-int: m/z calcd. 476.3635; obsd. 476.3692.

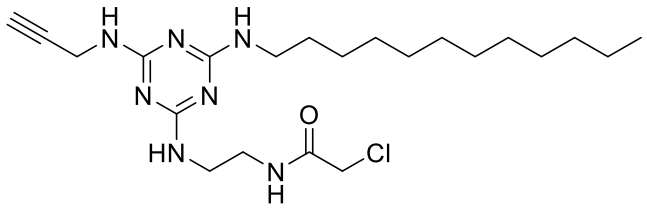

KSC-10

2-chloro-N-(2-((4-(dodecylamino)-6-(prop-2-yn-1-ylamino)-1,3,5-triazin-2-yl)amino)ethyl)acetamide (KSC-10): KSC-10-int was deprotected using a 50% solution of TFA/DCM (4 mL) at 25 °C for 2 hours. The solvent was removed *in vacuo* and the crude product remained on the vacuum overnight to remove any excess TFA. Then, to an ice cold solution of deprotected amine (1.0 eq, 24.6 mg, 0.0656 mmol) and triethylamine (2.0 eq, 23.3 mg, 0.1310 mmol) in DCM (0.01 M, 5 mL), chloroacetyl chloride (2.0 eq, 14.8 mg, 0.1310 mmol) in DCM (2 mL) was added dropwise over 30 min. The reaction was stirred at 0 °C for 3 hours. After the reaction was complete, the solvent was removed *in vacuo* and the crude product was purified by flash chromatography to give the desired product **KSC-10** (19.1 mg, 64%). ^{1}H NMR (600 MHz, Chloroform-*d*) δ 4.28 – 4.16 (m, 2H), 4.09 (s, 2H), 3.72 – 3.48 (m, 4H), 3.47 – 3.27 (m, 2H), 2.39 – 2.16 (m, 1H), 1.70 – 1.46 (m, 2H), 1.40 – 1.06 (m, 18H), 0.87 (t, *J* = 7.0 Hz, 3H). ^{13}C NMR (151 MHz, Chloroform-*d*) δ 167.40, 163.20, 156.28, 155.49, 117.09, 115.16, 72.23, 72.05, 71.93, 71.84, 42.35, 40.88, 39.93, 31.81, 31.09, 30.28, 29.53, 29.25, 28.88, 26.59, 22.59, 14.01. HRMS for KSC-10: m/z calcd. 452.2826; obsd. 452.2898.

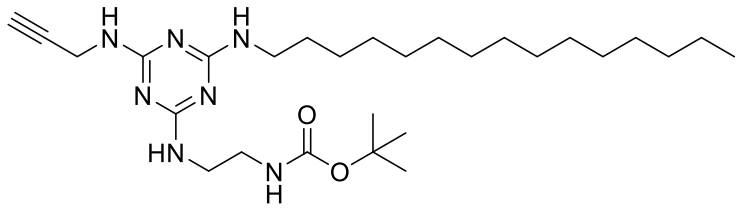

KSC-11-int

***tert*-butyl(2-((4-(pentadecylamino)-6-(prop-2-yn-1-ylamino)-1,3,5-triazin-2-yl)amino)ethyl)carbamate (KSC-11-int):** To a solution of **BBII** (1.0 eq, 50.9 mg, 0.1560 mmol) and diisopropylethylamine (2.5 eq, 50.9 mg, 0.3890 mmol) in THF (0.03 M, 5 mL), pentadecylamine (2.5 eq, 88.6 mg, 0.3890 mmol) was added at room temperature. The solution was then allowed to heat to reflux while stirring and continued to reflux for 24 hours. After the reaction was complete, the solvent was removed *in vacuo*. The crude product was purified via flash chromatography to afford the desired to product, **KSC-11-int** as an oil (59.6 mg, 74%). ^{1}H NMR (600 MHz, Chloroform-*d*) δ 4.13 (d, *J* = 15.5 Hz, 2H), 3.43 (d, *J* = 25.5 Hz, 2H), 3.37 – 3.06 (m, 4H), 2.19 (d, *J* = 2.5 Hz, 1H), 1.58 – 1.46 (m, 2H), 1.40 (s, 9H), 1.23 (s, 26H), 0.85 (t, *J* = 7.0 Hz, 3H). ^{13}C NMR (151 MHz, Chloroform-*d*) δ 166.78, 166.28, 165.90, 156.52, 81.35, 79.36, 71.13, 41.73, 41.00, 40.80, 38.48, 32.21, 30.56, 30.08, 29.98, 29.94, 29.91, 29.83, 29.70, 29.65, 29.54, 28.70, 27.28, 27.15, 22.97, 22.85, 14.40, 1.29. HRMS for KSC-11-int: m/z calcd. 518.4104; obsd. 518.4182.

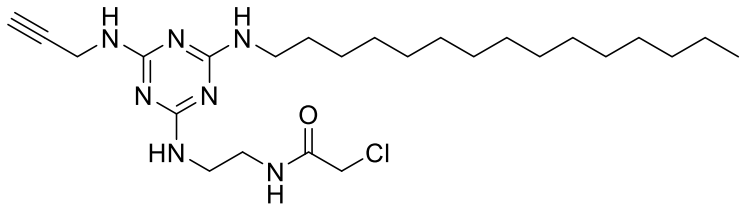

KSC-11

2-chloro-N-(2-((4-(pentadecylamino)-6-(prop-2-yn-1-ylamino)-1,3,5-triazin-2-yl)amino)ethyl)acetamide (KSC-11): KSC-11-int was deprotected using a 50% solution of TFA/DCM (4 mL) at 25 °C for 2 hours. The solvent was removed *in vacuo* and the crude product remained on the vacuum overnight to remove any excess TFA. Then, to an ice cold solution of deprotected amine (1.0 eq, 20.3 mg, 0.0487 mmol) and triethylamine (2.0 eq, 9.9 mg, 0.0973 mmol) in DCM (0.01 M, 5 mL), chloroacetyl chloride (2.0 eq, 11.0 mg, 0.0973 mmol) in DCM (2 mL) was added dropwise over 30 min. The reaction was stirred at 0 °C for 3 hours. After the reaction was complete, the solvent was removed *in vacuo* and the crude product was purified by flash chromatography to give the desired product **KSC-11** (17.6 mg, 73%). ^{1}H NMR (500 MHz, Chloroform-*d*) δ 4.21 (s, 2H), 4.04 (d, *J* = 3.8 Hz, 2H), 3.70 – 3.24 (m, 6H), 2.24 (s, 1H), 1.56 (s, 2H), 1.25 (s, 24H), 0.87 (t, *J* = 6.9 Hz, 3H). ^{13}C NMR (151 MHz, Chloroform-*d*) δ 170.10, 166.38, 158.26, 119.83, 117.90, 81.15, 79.88, 79.67, 79.45, 74.96, 74.67, 45.09, 44.19, 43.60, 42.65, 41.97, 34.56, 33.82, 33.00, 32.33, 31.99, 31.62, 29.32, 25.32, 16.74. HRMS for KSC-11: m/z calcd. 494.3296; obsd. 494.3394.

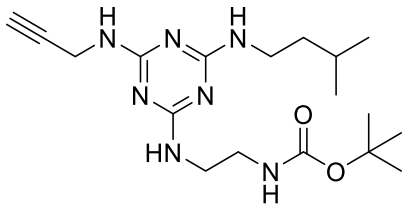

KSC-12-int

***tert*-butyl(2-((4-(isopentylamino)-6-(prop-2-yn-1-ylamino)-1,3,5-triazin-2-yl)amino)ethyl)carbamate (KSC-12-int):** To a solution of **BBII** (1.0 eq, 52.0 mg, 0.1590 mmol) and diisopropylethylamine (2.5 eq, 51.0 mg, 0.3980 mmol) in THF (0.03 M, 5 mL), isoamylamine (2.5 eq, 35.0 mg, 0.3980 mmol) was added dropwise at room temperature. The solution was then allowed to heat to reflux while stirring and continued to reflux for 24 hours. After the reaction was complete, the solvent was removed *in vacuo*. The crude product was purified via flash chromatography to afford the desired to product, **KSC-12-int** as an oil (49.5 mg, 83%). ^{1}H NMR (600 MHz, Chloroform-*d*) δ 4.16 (s, 2H), 3.58 – 3.17 (m, 6H), 2.20 (t, *J* = 2.5 Hz, 1H), 1.63 (dq, *J* = 13.5, 6.7 Hz, 1H), 1.41 (s, 11H), 0.91 (d, *J* = 6.6 Hz, 6H). ^{13}C NMR (151 MHz, Chloroform-*d*) δ 166.00, 156.34, 80.99, 79.31, 71.01, 41.60, 40.72, 39.02, 38.85, 30.48, 28.54, 25.81, 22.71, 22.65. HRMS for KSC-12-int: m/z calcd. 378.2539; obsd. 378.2608.

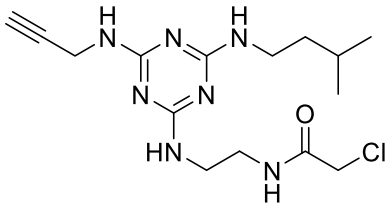

KSC-12

2-chloro-N-(2-((4-(isopentylamino)-6-(prop-2-yn-1-ylamino)-1,3,5-triazin-2-yl)amino)ethyl)acetamide (KSC-12): KSC-12-int was deprotected using a 50% solution of TFA/DCM (4 mL) at 25 °C for 2 hours. The solvent was removed *in vacuo* and the crude product remained on the vacuum overnight to remove any excess TFA. Then, to an ice cold solution of deprotected amine (1.0 eq, 36.4 mg, 0.1310 mmol) and triethylamine (2.0 eq, 26.5 mg, 0.2620 mmol) in DCM (0.025 M, 5 mL), chloroacetyl chloride (2.0 eq, 29.5 mg, 0.2620 mmol) in DCM (2 mL) was added dropwise over 30 min. The reaction was stirred at 0 °C for 3 hours. After the reaction was complete, the solvent was removed *in vacuo* and the crude product was purified by flash chromatography to give the desired product **KSC-12** (18.2 mg, 40%). ^{1}H NMR (500 MHz, Chloroform-*d*) δ 4.18 m, 2H), 4.05 (s, 2H), 3.56 (s, 2H), 3.52 (m, 1H), 3.46 (s, 2H), 2.27 (t, *J* = 10.7 Hz, 1H), 1.64 (s, 2H), 1.55 – 1.37 (m, 2H), 0.94 (t, *J* = 8.1 Hz, 6H). ^{13}C NMR (151 MHz, Chloroform-*d*) δ 183.42, 166.94, 163.75, 115.53, 114.73, 42.76, 40.04, 39.56, 37.95, 31.25, 30.54, 30.30, 29.85, 25.82, 22.53. HRMS for KSC-12: m/z calcd. 354.1731; obsd. 354.1791.

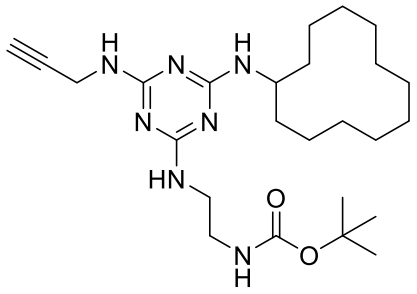

KSC-13-int

***tert*-butyl(2-((4-(cyclododecylamino)-6-(prop-2-yn-1-ylamino)-1,3,5-triazin-2-yl)amino)ethyl)carbamate (KSC-13-int):** To a solution of **BBII** (1.0 eq, 193.3 mg,

0.5915 mmol) and diisopropylethylamine (4.0 eq, 305.8 mg, 2.3661 mmol) in THF (0.1 M, 5 mL), cyclododecylamine hydrochloride (4.0 eq, 433.8 mg, 2.3661 mmol) was added at room temperature. The solution was then allowed to heat to reflux while stirring and continued to reflux for 24 hours. After the reaction was complete, the solvent was removed *in vacuo*. The crude product was purified via flash chromatography to afford the desired to product, **KSC-13-int** as an oil (136.6 mg, 49%). ^{1}H NMR (500 MHz, Chloroform-*d*) δ 4.25 – 4.08 (m, 2H), 3.46 (s, 2H), 3.28 (s, 2H), 2.20 (t, *J* = 2.4 Hz, 1H), 1.86 (m, 2H), 1.71 – 1.62 (m, 2H), 1.55 (m, 18H), 1.41 (d, *J* = 2.5 Hz, 9H), 1.29 – 1.21 (m, 1H). ^{13}C NMR (126 MHz, Chloroform-*d*) δ 166.29, 165.61, 156.26, 81.32, 79.04, 70.90, 55.66, 47.69, 46.07, 41.47, 40.41, 33.27, 31.17, 30.26, 29.36, 28.41, 24.30, 23.80, 23.60, 23.46, 21.88, 21.39, 18.45. HRMS for KSC-13-int: m/z calcd. 474.3478; obsd. 474.3557.

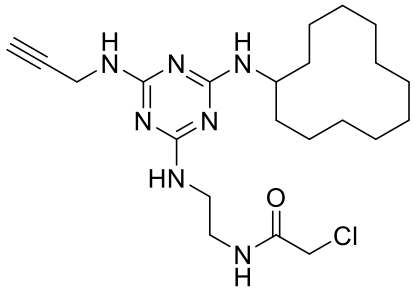

KSC-13

2-chloro-N-(2-((4-(cyclododecylamino)-6-(prop-2-yn-1-ylamino)-1,3,5-triazin-2-yl)amino)ethyl)acetamide (KSC-13): KSC-13-int was deprotected using a 50% solution of TFA/DCM (4 mL) at 25 °C for 2 hours. The solvent was removed *in vacuo* and the crude product remained on the vacuum overnight to remove any excess TFA. Then, to an ice cold solution of deprotected amine (1.0 eq, 107.7 mg, 0.2883 mmol) and triethylamine (1.3 eq,

37.9 mg, 0.3748 mmol) in DCM (0.06 M, 5 mL), chloroacetyl chloride (1.3 eq, 42.3 mg, 0.3748 mmol) in DCM (2 mL) was added dropwise over 30 min. The reaction was stirred at 0 °C for 3 hours. After the reaction was complete, the solvent was removed *in vacuo* and the crude product was purified by flash chromatography to give the desired product **KSC-13** (36.0 mg, 28%). ^{1}H NMR (500 MHz, Chloroform-*d*) δ 4.32 – 4.15 (m, 3H), 4.07 (s, 2H), 3.77 – 3.42 (m, 4H), 2.04 (t, 1H), 1.59 – 1.05 (m, 22H). ^{13}C NMR (126 MHz, Chloroform-*d*) δ 163.04, 155.11, 124.89, 117.45, 115.15, 78.69, 72.14, 60.57, 47.78, 42.53, 39.88, 30.88, 30.63, 30.37, 29.85, 24.01, 23.76, 23.38, 23.08, 21.89, 21.68, 14.33. HRMS for KSC-13: m/z calcd. 450.2670; obsd. 450.2748.

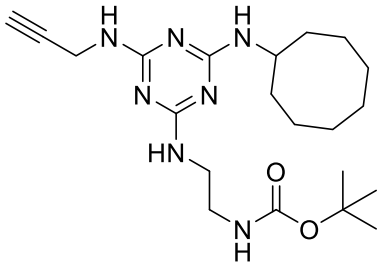

KSC-14-int

***tert*-butyl(2-((4-(cyclooctylamino)-6-(prop-2-yn-1-ylamino)-1,3,5-triazin-2-yl)amino)ethyl)carbamate (KSC-14-int):** To a solution of **BBII** (1.0 eq, 188.5 mg, 0.5768 mmol) and diisopropylethylamine (4.0 eq, 298.2 mg, 2.3073 mmol) in THF (0.06 M, 10 mL), cyclooctylamine (4.0 eq, 293.6 mg, 2.3073 mmol) was added dropwise at room temperature. The solution was then allowed to heat to reflux while stirring and continued to reflux for 24 hours. After the reaction was complete, the solvent was removed *in vacuo*. The crude product was purified via flash chromatography to afford the desired to product,

KSC-14-int as an oil (158.3 mg, 66%). ^{1}H NMR (500 MHz, Chloroform-*d*) δ 4.12 (s, 2H), 3.44 (s, 2H), 3.24 (s, 2H), 2.17 (d, *J* = 2.6 Hz, 1H), 1.87 – 1.73 (m, 2H), 1.56 – 1.42 (m, 13H), 1.36 (s, 9H). ^{13}C NMR (126 MHz, Chloroform-*d*) δ 166.37, 165.62, 164.90, 156.24, 81.22, 79.02, 70.88, 50.04, 41.56, 40.42, 32.48, 30.27, 28.40, 27.19, 25.83, 23.87. HRMS for KSC-14-int: m/z calcd. 418.2852; obsd. 418.2931.

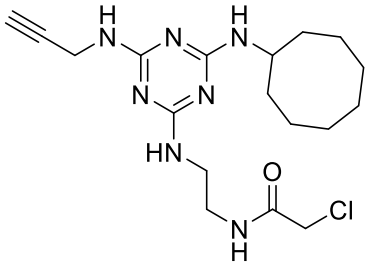

KSC-14

2-chloro-N-(2-((4-(cyclooctylamino)-6-(prop-2-yn-1-ylamino)-1,3,5-triazin-2-yl)amino)ethyl)acetamide (KSC-14): KSC-14-int was deprotected using a 50% solution of TFA/DCM (4 mL) at 25 °C for 2 hours. The solvent was removed *in vacuo* and the crude product remained on the vacuum overnight to remove any excess TFA. Then, to an ice cold solution of deprotected amine (1.0 eq, 120.3 mg, 0.3791 mmol) and triethylamine (1.3 eq, 49.9 mg, 0.4927 mmol) in DCM (0.08 M, 5 mL), chloroacetyl chloride (1.3 eq, 55.6 mg, 0.4927 mmol) in DCM (2 mL) was added dropwise over 30 min. The reaction was stirred at 0 °C for 3 hours. After the reaction was complete, the solvent was removed *in vacuo* and the crude product was purified by flash chromatography to give the desired product **KSC-14** (47.6 mg, 31%). ^{1}H NMR (500 MHz, Chloroform-*d*) δ 4.24 – 3.99 (m, 4H), 3.71 – 3.49 (m, 4H), 2.57 – 2.53 (m, 1H), 2.44 (s, 1H), 1.76 – 1.44 (m, 14H). ^{13}C NMR (126 MHz,

Chloroform-*d*) δ 163.62, 144.81, 142.28, 129.95, 128.43, 125.89, 70.64, 51.58, 39.68, 35.79, 32.27, 30.85, 29.84, 28.84, 27.02, 25.13, 23.87, 21.76. HRMS for KSC-14: m/z calcd. 394.2044; obsd. 394.2122.

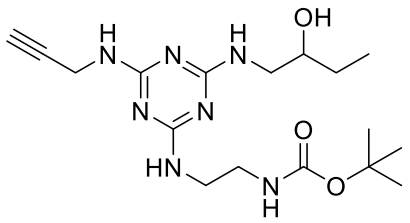

KSC-23-int

***tert*-butyl(2-((4-((2-hydroxybutyl)amino)-6-(prop-2-yn-1-ylamino)-1,3,5-triazin-2-yl)amino)ethyl)carbamate (KSC-23-int):** To a solution of **BBII** (1.0 eq, 53.4 mg, 0.1634 mmol) and diisopropylethylamine (4.0 eq, 84.5 mg, 0.6536 mmol) in THF (0.03 M, 5 mL), racemic 1-aminobutan-2-ol (4.0 eq, 58.3 mg, 0.6536 mmol) was added dropwise at room temperature. The solution was then allowed to heat to reflux while stirring and continued to reflux for 24 hours. After the reaction was complete, the solvent was removed *in vacuo*. The crude product was purified via flash chromatography to afford the desired to product, **KSC-23-int** as an oil (48.8 mg, 79%). ^{1}H NMR (600 MHz, Chloroform-*d*) δ 5.57 (m, 2H), 4.08 (dd, *J* = 13.1, 6.6 Hz, 2H), 3.50 (m, 3H), 3.30 – 2.92 (m, 3H), 2.18 (d, *J* = 2.6 Hz, 1H), 1.48 – 1.39 (m, 1H), 1.36 (s, 9H), 0.90 (t, *J* = 7.6 Hz, 3H). ^{13}C NMR (151 MHz, Chloroform-*d*) δ 166.03, 165.31, 156.35, 80.79, 79.21, 73.07, 70.98, 60.42, 46.53, 40.65, 30.38, 28.42, 27.78, 14.20, 10.06. HRMS for KSC-23-int: m/z calcd. 380.2332; obsd. 380.2419.

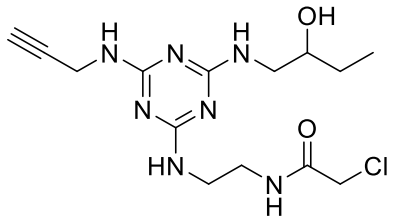

KSC-23

2-chloro-N-(2-((4-((2-hydroxybutyl)amino)-6-(prop-2-yn-1-ylamino)-1,3,5-triazin-2-yl)amino)ethyl)acetamide (KSC-23): KSC-23-int was deprotected using a 50% solution of TFA/DCM (4 mL) at 25 °C for 2 hours. The solvent was removed *in vacuo* and the crude product remained on the vacuum overnight to remove any excess TFA. Then, to an ice cold solution of deprotected amine (1.0 eq, 45.6 mg, 0.1632 mmol) and triethylamine (2.0 eq, 32.3 mg, 0.3200 mmol) in DCM (0.04 M, 4 mL), chloroacetyl chloride (2.0 eq, 36.1 mg, 0.3200 mmol) in DCM (2 mL) was added dropwise over 30 min. The reaction was stirred at 0 °C for 3 hours. After the reaction was complete, the solvent was removed *in vacuo* and the crude product was purified by flash chromatography to give the desired product **KSC-23** (23.4 mg, 40%). ^{1}H NMR (600 MHz, Chloroform-*d*) δ 4.28 – 4.10 (m, 2H), 4.06 (s, 2H), 3.98 – 3.69 (m, 1H), 3.68 – 3.48 (m, 4H), 2.38 – 2.20 (m, 1H), 1.76 (ddq, *J* = 22.3, 15.2, 7.5 Hz, 2H), 1.34 – 1.14 (m, 3H), 0.98 (dt, *J* = 20.8, 8.1 Hz, 3H). ^{13}C NMR (151 MHz, Chloroform-*d*) δ 171.18, 167.42, 163.46, 156.28, 117.10, 115.17, 113.45, 72.14, 60.34, 42.33, 29.61, 24.38, 14.09, 9.14. HRMS for KSC-23: m/z calcd. 356.1524; obsd. 356.1601.

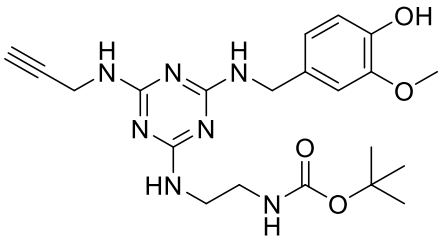

KSC-24-int

***tert*-butyl(2-((4-((4-hydroxy-3-methoxybenzyl)amino)-6-(prop-2-yn-1-ylamino)-1,3,5-triazin-2-yl)amino)ethyl)carbamate (KSC-24-int):** To a solution of **BBII** (1.0 eq, 132.8 mg, 0.4064 mmol) and diisopropylethylamine (2.0 eq, 105.0 mg, 0.8128 mmol) in THF (0.08 M, 5 mL), vanillylamine hydrochloride (2.0 eq, 124.5 mg, 0.8128 mmol) was added at room temperature. The solution was then allowed to heat to reflux while stirring and continued to reflux for 24 hours. After the reaction was complete, the solvent was removed *in vacuo*. The crude product was purified via flash chromatography to afford the desired to product, **KSC-24-int** as a solid (61.7 mg, 34%). ^{1}H NMR (600 MHz, Chloroform-*d*) δ 6.84 – 6.79 (m, 1H), 6.77 (s, 2H), 4.44 (s, 2H), 4.13 (s, 2H), 3.75 (s, 3H), 3.45 (s, 2H), 3.25 (s, 2H), 2.18 (s, 1H), 1.41 (s, 9H). ^{13}C NMR (151 MHz, Chloroform-*d*) δ 165.49, 156.10, 146.77, 144.92, 130.74, 120.53, 114.72, 110.53, 79.12, 70.87, 60.29, 55.77, 44.52, 41.31, 40.51, 30.24, 29.58, 28.29, 14.09. HRMS for KSC-24-int: m/z calcd. 444.2281; obsd. 444.2364.

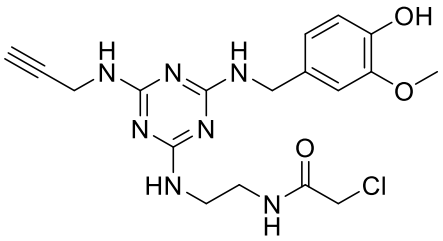

KSC-24

2-chloro-N-(2-((4-((4-hydroxy-3-methoxybenzyl)amino)-6-(prop-2-yn-1-ylamino)-1,3,5-triazin-2-yl)amino)ethyl)acetamide (KSC-24): KSC-24-int was deprotected using a 50% solution of TFA/DCM (4 mL) at 25 °C for 2 hours. The solvent was removed *in vacuo* and the crude product remained on the vacuum overnight to remove any excess TFA. Then, to an ice cold solution of deprotected amine (1.0 eq, 29.7 mg, 0.0865 mmol) and triethylamine (1.5 eq, 13.1 mg, 0.1298 mmol) in DCM (0.04 M, 2 mL), chloroacetyl chloride (1.2 eq, 11.7 mg, 0.1040 mmol) in DCM (2 mL) was added dropwise over 30 min. The reaction was stirred at 0 °C for 3 hours. After the reaction was complete, the solvent was removed *in vacuo* and the crude product was purified by flash chromatography to give the desired product **KSC-24** (8.0 mg, 22%). ^{1}H NMR (600 MHz, DMSO-d_6) δ 6.92 (s, 1H), 6.71 (d, J = 21.5 Hz, 2H), 4.34 (s, 2H), 4.02 (m, 3H), 3.73 (s, 4H), 3.26 – 2.97 (m, 4H), 2.08 (s, 1H). ^{13}C NMR (151 MHz, DMSO-d_6) δ 166.04, 147.27, 145.27, 119.64, 115.09, 111.80, 55.57, 42.63, 33.64, 31.27, 30.68, 29.34, 28.99, 28.71, 28.52, 24.47, 22.07, 13.94. HRMS for KSC-24: m/z calcd. 420.1473; obsd. 420.1543.

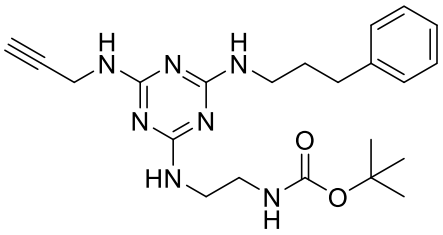

KSC-25-int

***tert*-butyl(2-((4-((3-phenylpropyl)amino)-6-(prop-2-yn-1-ylamino)-1,3,5-triazin-2-yl)amino)ethyl)carbamate (KSC-25-int):** To a solution of **BBII** (1.0 eq, 130.3 mg, 0.3999 mmol) and diisopropylethylamine (2.0 eq, 103.4 mg, 0.7999 mmol) in THF (0.08 M, 5 mL), 3-phenyl-1-propylamine (2.0 eq, 108.2 mg, 0.7999 mmol) was added dropwise at room temperature. The solution was then allowed to heat to reflux while stirring and continued to reflux for 24 hours. After the reaction was complete, the solvent was removed *in vacuo*. The crude product was purified via flash chromatography to afford the desired to product, **KSC-25-int** as a solid (72.6 mg, 43%). ^{1}H NMR (500 MHz, Chloroform-*d*) δ 7.29 – 7.23 (m, 2H), 7.19 – 7.13 (m, 3H), 4.24 – 4.06 (m, 2H), 3.52 – 3.40 (m, 2H), 3.40 – 3.31 (m, 4H), 3.27 (s, 2H), 2.65 (t, *J* = 7.8 Hz, 2H), 2.20 (t, *J* = 2.5 Hz, 1H), 1.41 (s, 9H). ^{13}C NMR (126 MHz, Chloroform-*d*) δ 166.13, 165.65, 156.29, 141.73, 128.46, 128.42, 125.92, 81.10, 79.20, 70.96, 41.54, 40.60, 40.27, 33.24, 31.44, 30.97, 30.35, 28.49. HRMS for KSC-25-int: m/z calcd. 426.2539; obsd. 426.2617.

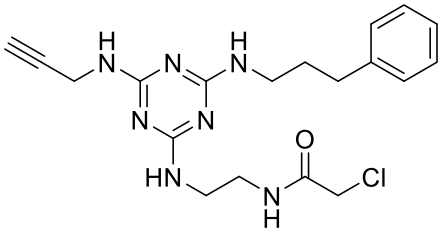

KSC-25

2-chloro-N-(2-((4-((3-phenylpropyl)amino)-6-(prop-2-yn-1-ylamino)-1,3,5-triazin-2-yl)amino)ethyl)acetamide (KSC-25): KSC-25-int was deprotected using a 50% solution of TFA/DCM (4 mL) at 25 °C for 2 hours. The solvent was removed *in vacuo* and the crude product remained on the vacuum overnight to remove any excess TFA. Then, to an ice cold solution of deprotected amine (1.0 eq, 55.5 mg, 0.1705 mmol) and triethylamine (3.0 eq, 51.8 mg, 0.5116 mmol) in DCM (0.08 M, 2 mL), chloroacetyl chloride (3.0 eq, 57.8 mg, 0.5116 mmol) in DCM (2 mL) was added dropwise over 30 min. The reaction was stirred at 0 °C for 3 hours. After the reaction was complete, the solvent was removed *in vacuo* and the crude product was purified by flash chromatography to give the desired product **KSC-25** (36.9 mg, 54%). ^{1}H NMR (600 MHz, Chloroform-*d*) δ 7.26 (d, *J* = 5.7, 3.9 Hz, 2H), 7.17 (t, *J* = 5.8 Hz, 3H), 4.25 – 4.08 (m, 2H), 4.07 (s, 2H), 3.54 (s, 2H), 3.49 (s, 2H), 3.46 – 3.32 (m, 2H), 2.77 – 2.56 (m, 2H), 2.28 – 2.18 (m, 1H), 1.91 (dt, *J* = 25.9, 7.4 Hz, 2H). ^{13}C NMR (151 MHz, Chloroform-*d*) δ 163.23, 156.22, 141.12, 128.50, 126.15, 117.25, 115.34, 78.63, 72.26, 42.41, 40.48, 40.24, 32.95, 31.15, 30.29, 29.83, 8.40. HRMS for KSC-25: m/z calcd. 402.1731; obsd. 402.1809.

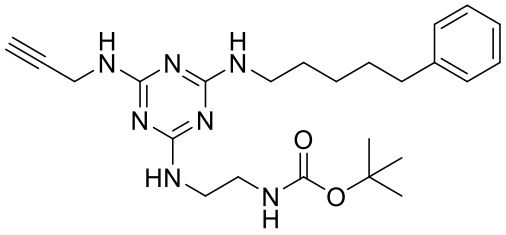

KSC-26-int

***tert*-butyl(2-((4-((5-phenylpentyl)amino)-6-(prop-2-yn-1-ylamino)-1,3,5-triazin-2-yl)amino)ethyl)carbamate (KSC-26-int):** To a solution of **BBII** (1.0 eq, 57.0 mg, 0.1744 mmol) and diisopropylethylamine (2.0 eq, 45.1 mg, 0.3489 mmol) in THF (0.03 M, 5 mL), 5-phenyl-1-pentylamine (2.0 eq, 57.0 mg, 0.3489 mmol) was added at room temperature. The solution was then allowed to heat to reflux while stirring and continued to reflux for 24 hours. After the reaction was complete, the solvent was removed *in vacuo*. The crude product was purified via flash chromatography to afford the desired to product, **KSC-26-int** as a solid (47.3 mg, 60%). ^{1}H NMR (600 MHz, Chloroform-*d*) δ 7.26 (p, *J* = 5.2, 4.0 Hz, 2H), 7.16 (d, *J* = 7.9 Hz, 3H), 4.29 – 4.02 (m, 2H), 3.45 (s, 2H), 3.30 (d, *J* = 31.8 Hz, 4H), 2.66 – 2.50 (m, 2H), 2.18 (d, *J* = 20.0 Hz, 1H), 1.71 – 1.50 (m, 4H), 1.41 (d, *J* = 6.0 Hz, 11H). ^{13}C NMR (151 MHz, Chloroform-*d*) δ 166.08, 156.31, 142.60, 128.47, 128.38, 125.77, 81.05, 79.26, 70.99, 41.58, 40.69, 35.96, 31.28, 30.43, 29.76, 28.53, 26.67, 22.75, 21.16, 14.31. HRMS for KSC-26-int: m/z calcd. 454.2852; obsd. 454.2932.

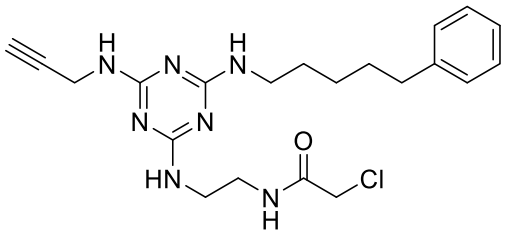

KSC-26

2-chloro-N-(2-((4-((5-phenylpentyl)amino)-6-(prop-2-yn-1-ylamino)-1,3,5-triazin-2-yl)amino)ethyl)acetamide (KSC-26): KSC-26-int was deprotected using a 50% solution of TFA/DCM (4 mL) at 25 °C for 2 hours. The solvent was removed *in vacuo* and the crude product remained on the vacuum overnight to remove any excess TFA. Then, to an ice cold

solution of deprotected amine (1.0 eq, 36.2 mg, 0.1024 mmol) and triethylamine (4.0 eq, 46.2 mg, 0.4096 mmol) in DCM (0.05 M, 2 mL), chloroacetyl chloride (4.0 eq, 41.4 mg, 0.4096 mmol) in DCM (2 mL) was added dropwise over 30 min. The reaction was stirred at 0 °C for 3 hours. After the reaction was complete, the solvent was removed *in vacuo* and the crude product was purified by flash chromatography to give the desired product **KSC-26** (18.9 mg, 43%). ^{1}H NMR (500 MHz, Chloroform-*d*) δ 7.29 (s, 2H), 7.22 – 7.14 (m, 3H), 4.27 – 4.17 (m, 2H), 4.05 (s, 2H), 3.66 – 3.49 (m, 4H), 3.46 – 3.30 (m, 2H), 2.62 (dt, *J* = 12.6, 6.1 Hz, 2H), 2.26 (t, *J* = 2.5 Hz, 1H), 1.64 (dd, *J* = 17.7, 9.6 Hz, 6H). ^{13}C NMR (126 MHz, Chloroform-*d*) δ 200.82, 139.88, 138.15, 128.77, 128.71, 126.15, 77.67, 77.41, 77.16, 51.65, 42.93, 36.13, 31.34, 30.11, 29.30, 26.70. HRMS for KSC-26: m/z calcd. 430.2044; obsd. 430.2122.

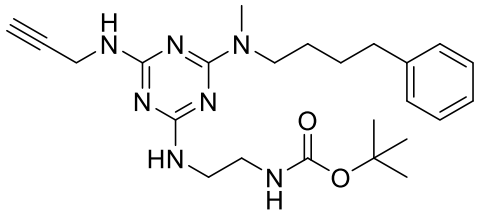

KSC-34-int

***tert*-butyl(2-((4-(methyl(4-phenylbutyl)amino)-6-(prop-2-yn-1-ylamino)-1,3,5-triazin-2-yl)amino)ethyl)carbamate (KSC-34-int):** To a solution of **BBII** (1.0 eq, 105.8 mg, 0.3238 mmol) and diisopropylethylamine (2.0 eq, 83.7 mg, 0.6475 mmol) in THF (0.06 M, 5 mL), N-methyl-4-phenyl-1-butylamine hydrochloride (2.0 eq, 129.3 mg, 0.6475 mmol) was added at room temperature. The solution was then allowed to heat to reflux while stirring and continued to reflux for 24 hours. After the reaction was complete, the

solvent was removed *in vacuo*. The crude product was purified via flash chromatography to afford the desired to product, **KSC-34-int** as a solid (100.8 mg, 69%). ^{1}H NMR (600 MHz, Chloroform-*d*) δ 7.31 – 7.20 (m, 2H), 7.20 – 7.11 (m, 3H), 5.27 (m, 3H), 4.11 (q, *J* = 7.1 Hz, 2H), 3.49 (d, *J* = 69.7 Hz, 4H), 3.27 (s, 2H), 3.04 (s, 3H), 2.64 (q, *J* = 6.7, 5.2 Hz, 2H), 2.24 – 2.08 (m, 1H), 1.62 (d, *J* = 7.8 Hz, 4H), 1.41 (s, 9H). ^{13}C NMR (151 MHz, Chloroform-*d*) δ 171.16, 165.19, 156.23, 142.46, 128.46, 128.33, 125.76, 79.05, 70.72, 60.43, 40.63, 35.74, 34.35, 30.37, 29.75, 28.71, 28.48, 27.10, 21.09, 14.26. HRMS for KSC-34-int: m/z calcd. 454.2852; obsd. 454.2941.

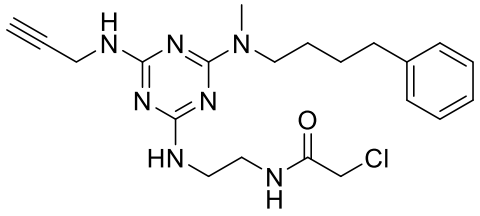

KSC-34

2-chloro-N-(2-((4-(methyl(4-phenylbutyl)amino)-6-(prop-2-yn-1-ylamino)-1,3,5-triazin-2-yl)amino)ethyl)acetamide (KSC-34): KSC-34-int was deprotected using a 50% solution of TFA/DCM (4 mL) at 25 °C for 2 hours. The solvent was removed *in vacuo* and the crude product remained on the vacuum overnight to remove any excess TFA. Then, to an ice cold solution of deprotected amine (1.0 eq, 100.8 mg, 0.2852 mmol) and triethylamine (1.3 eq, 37.5 mg, 0.3707 mmol) in DCM (0.15 M, 2 mL), chloroacetyl chloride (1.3 eq, 41.9 mg, 0.3707 mmol) in DCM (2 mL) was added dropwise over 30 min. The reaction was stirred at 0 °C for 3 hours. After the reaction was complete, the solvent was removed *in vacuo* and the crude product was purified by flash chromatography to give

the desired product **KSC-34** (35.3 mg, 29%). ^{1}H NMR (600 MHz, Chloroform-*d*) δ 7.28 (dt, *J* = 7.9, 4.0 Hz, 2H), 7.21 – 7.13 (m, 3H), 4.30 – 3.97 (m, 4H), 3.75 – 3.44 (m, 6H), 3.15 (d, *J* = 3.3 Hz, 3H), 2.65 (t, *J* = 7.0, 3.3 Hz, 2H), 2.10 (s, 1H), 1.74 – 1.58 (m, 4H). ^{13}C NMR (151 MHz, Chloroform-*d*) δ 162.98, 162.01, 154.53, 141.82, 128.33, 128.29, 125.85, 117.03, 115.10, 78.28, 71.44, 49.59, 49.38, 42.18, 35.51, 30.85, 30.18, 29.64, 28.43, 26.75, 26.64. HRMS for KSC-34: m/z calcd. 430.2044; obsd. 430.2102.

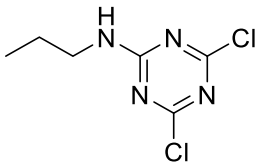

BBIna

4,6-dichloro-N-propyl-1,3,5-triazin-2-amine (BBIna): To an ice cold solution of cyanuric chloride (1.0 eq, 521.0 mg, 2.8252 mmol) and diisopropylethylamine (1.1 eq, 401.6 mg, 3.1077 mmol) in tetrahydrofuran (THF) (0.043 M, 65.4 mL), propylamine (1.2 eq, 200.4 mg, 3.3903 mmol) was added dropwise. The reaction mixture was allowed to stir at 0 °C for 3 hours. The solvent was removed *in vacuo* and the crude product was purified via flash chromatography to give the desired product **BBIna** as a white solid (534.6 mg, 91%). ^{1}H NMR (600 MHz, Chloroform-*d*) δ 6.75 (d, *J* = 6.4 Hz, 1H), 3.58 – 3.20 (m, 2H), 1.63 (h, *J* = 7.4 Hz, 2H), 0.94 (t, *J* = 7.4 Hz, 3H). ^{13}C NMR (151 MHz, Chloroform-*d*) δ 171.05, 169.64, 165.90, 43.30, 22.46, 11.26. HRMS for BBIna: m/z calcd. 207.0126; obsd. 207.0204.

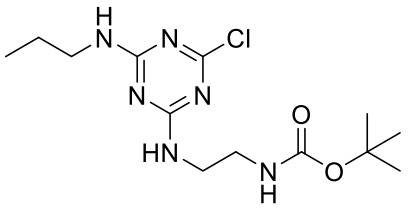

BBIIna

tert-butyl(2-((4-chloro-6-(propylamino)-1,3,5-triazin-2-yl)amino)ethyl)carbamate (BBIIna): To a solution of **BBIna** (1.0 eq, 534.6 mg, 2.5820 mmol) and sodium carbonate (2.2 eq, 602 mg, 5.68 mmol) in ethanol (0.09 M, 30 mL), N-Boc-ethylenediamine (1.1eq, 445 mg, 2.84 mmol) was added dropwise at room temperature. The solution was then allowed to warm to 45 °C while stirring and continued to stir for 18 hours. After the reaction was complete, 15 mL of water was added and the reaction was extracted with ethyl acetate (3 x 15 mL). The organic layer was washed with brine and dried with $MgSO_4$, then the solvent was removed *in vacuo*. The crude product was purified via flash chromatography to afford the desired to product, **BBIIna** as a white solid (695.1 mg, 81%). ^{1}H NMR (500 MHz, Chloroform-*d*) δ 6.05 (d, *J* = 100.2 Hz, 1H), 5.80 – 5.40 (m, 1H), 5.38 – 4.72 (m, 1H), 3.64 – 3.43 (m, 2H), 3.43 – 3.24 (m, 4H), 1.69 – 1.52 (m, 2H), 1.43 (s, 9H), 1.04 – 0.85 (m, 3H). ^{13}C NMR (126 MHz, Chloroform-*d*) δ 197.31, 166.14, 156.46, 96.43, 46.67, 43.17, 41.04, 28.77, 24.63, 22.96, 11.78. HRMS for BBIIna: m/z calcd. 331.1571; obsd. 331.1649.

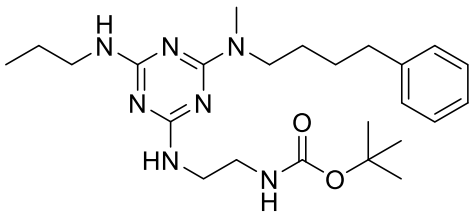

KSC-34na-int

tert-butyl(2-((4-(methyl(4-phenylbutyl)amino)-6-(propylamino)-1,3,5-triazin-2-yl)amino)ethyl)carbamate (KSC-34na-int): To a solution of **BBIIna** (1.0 eq, 30.2 mg, 0.0913 mmol) and diisopropylethylamine (4.0 eq, 47.2 mg, 0.3652 mmol) in THF (0.02 M, 5 mL), N-methyl-4-phenyl-1-butylamine hydrochloride (2.0 eq, 36.5 mg, 0.1826 mmol) was added at room temperature. The solution was then allowed to heat to reflux while stirring and continued to reflux for 24 hours. After the reaction was complete, the solvent was removed *in vacuo*. The crude product was purified via flash chromatography to afford the desired to product, **KSC-34na-int** as a solid (23.6 mg, 57%). ^{1}H NMR (600 MHz, Chloroform-*d*) δ 7.29 – 7.24 (m, 3H), 7.19 – 7.15 (m, 3H), 5.76 (s, 1H), 4.96 (s, 1H), 4.76 (s, 1H), 3.56 (s, 2H), 3.47 (s, 2H), 3.29 (s, 3H), 3.04 (s, 3H), 2.77 – 2.48 (m, 2H), 1.67 – 1.58 (m, 2H), 1.42 (s, 9H), 1.26 (d, *J* = 1.4 Hz, 4H), 0.94 (t, *J* = 7.4 Hz, 3H). ^{13}C NMR (151 MHz, Chloroform-*d*) δ 157.23, 146.95, 145.10, 131.04, 130.91, 128.33, 79.86, 79.65, 79.44, 47.28, 45.14, 43.19, 38.33, 32.35, 31.32, 31.07, 29.73, 25.73, 14.16. HRMS for KSC-34na-int: m/z calcd. 458.3165; obsd. 458.32435.

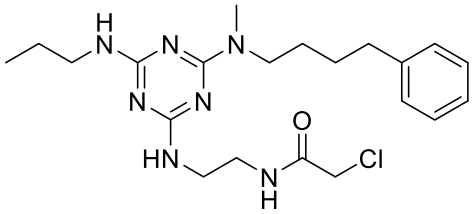

KSC-34na

2-chloro-N-(2-((4-(methyl(4-phenylbutyl)amino)-6-(propylamino)-1,3,5-triazin-2-yl)amino)ethyl)acetamide (KSC-34na): KSC-34na-int was deprotected using a 50% solution of TFA/DCM (4 mL) at 25 °C for 2 hours. The solvent was removed *in vacuo* and the crude product remained on the vacuum overnight to remove any excess TFA. Then, to an ice cold solution of deprotected amine (1.0 eq, 81.8 mg, 0.2288 mmol) and triethylamine (3.0 eq, 69.5 mg, 0.6864 mmol) in DCM (0.02 M, 10 mL), chloroacetyl chloride (3.0 eq, 77.5 mg, 0.6864 mmol) in DCM (2 mL) was added dropwise over 30 min. The reaction was stirred at 0 °C for 3 hours. After the reaction was complete, the solvent was removed *in vacuo* and the crude product was purified by flash chromatography to give the desired product **KSC-34na** (95.5 mg, 96%). ^{1}H NMR (500 MHz, Chloroform-*d*) δ 7.28 (t, *J* = 7.7 Hz, 2H), 7.20 (d, *J* = 7.3 Hz, 1H), 7.16 (t, *J* = 6.7 Hz, 2H), 3.71 – 3.47 (m, 6H), 3.39 – 3.28 (m, 2H), 3.13 (s, 3H), 2.70 – 2.58 (m, 2H), 1.74 – 1.50 (m, 6H), 1.25 (s, 2H), 0.94 (dt, *J* = 12.9, 7.5 Hz, 3H). ^{13}C NMR (126 MHz, Chloroform-*d*) δ 166.09, 141.94, 128.55, 128.43, 126.11, 78.00, 49.50, 42.75, 39.91, 39.35, 35.72, 35.64, 35.36, 29.86, 28.68, 26.95, 22.58, 11.46, 1.18. HRMS for KSC-34na: m/z calcd. 434.2357; obsd. 434.2435.

References

1. Kozlov, G.; Maattanen, P.; Thomas, D. Y.; Gehring, K., A structural overview of the PDI family of proteins. *FEBS J* **2010,** *277* (19), 3924-36.
2. Appenzeller-Herzog, C.; Ellgaard, L., The human PDI family: versatility packed into a single fold. *Biochim Biophys Acta* **2008,** *1783* (4), 535-48.
3. Xu, S.; Sankar, S.; Neamati, N., Protein disulfide isomerase: a promising target for cancer therapy. *Drug Discov Today* **2014,** *19* (3), 222-40.
4. Hatahet, F.; Ruddock, L. W., Protein disulfide isomerase: a critical evaluation of its function in disulfide bond formation. *Antioxid Redox Signal* **2009,** *11* (11), 2807-50.
5. Goldberger, R. F.; Epstein, C. J.; Anfinsen, C. B., Acceleration of reactivation of reduced bovine pancreatic ribonuclease by a microsomal system from rat liver. *J Biol Chem* **1963,** *238*, 628-35.
6. Venetianer, P.; Straub, F. B., The enzymic reactivation of reduced ribonuclease. *Biochim Biophys Acta* **1963,** *67*, 166-8.
7. Freedman, R. B., Native Disulfide Band Formation in Protein-Biosynthesis - Evidence for the Role of Protein Disulfide Isomerase. *Trends in Biochemical Sciences* **1984,** *9* (10), 438-441.
8. Vuori, K.; Myllyla, R.; Pihlajaniemi, T.; Kivirikko, K. I., Expression and site-directed mutagenesis of human protein disulfide isomerase in Escherichia coli. This multifunctional polypeptide has two independently acting catalytic sites for the isomerase activity. *J Biol Chem* **1992,** *267* (11), 7211-4.
9. Klappa, P.; Ruddock, L. W.; Darby, N. J.; Freedman, R. B., The b' domain provides the principal peptide-binding site of protein disulfide isomerase but all domains contribute to binding of misfolded proteins. *EMBO J* **1998,** *17* (4), 927-35.
10. Puig, A.; Gilbert, H. F., Protein disulfide isomerase exhibits chaperone and anti-chaperone activity in the oxidative refolding of lysozyme. *J Biol Chem* **1994,** *269* (10), 7764-71.
11. Primm, T. P.; Walker, K. W.; Gilbert, H. F., Facilitated protein aggregation. Effects of calcium on the chaperone and anti-chaperone activity of protein disulfide-isomerase. *J Biol Chem* **1996,** *271* (52), 33664-9.

12. Cai, H.; Wang, C. C.; Tsou, C. L., Chaperone-like activity of protein disulfide isomerase in the refolding of a protein with no disulfide bonds. *J Biol Chem* **1994,** *269* (40), 24550-2.
13. Song, J. L.; Wang, C. C., Chaperone-like activity of protein disulfide-isomerase in the refolding of rhodanese. *Eur J Biochem* **1995,** *231* (2), 312-6.
14. Quan, H.; Fan, G.; Wang, C. C., Independence of the chaperone activity of protein disulfide isomerase from its thioredoxin-like active site. *J Biol Chem* **1995,** *270* (29), 17078-80.
15. Dai, Y.; Wang, C., A mutant truncated protein disulfide isomerase with no chaperone activity. *J Biol Chem* **1997,** *272* (44), 27572-6.
16. Network, T. C. G. A. R., Comprehensive genomic characterization defines human glioblastoma genes and core pathways. *Nature* **2008,** *455* (7216), 1061-8.
17. Shai, R.; Shi, T.; Kremen, T. J.; Horvath, S.; Liau, L. M.; Cloughesy, T. F.; Mischel, P. S.; Nelson, S. F., Gene expression profiling identifies molecular subtypes of gliomas. *Oncogene* **2003,** *22* (31), 4918-23.
18. van de Vijver, M. J.; He, Y. D.; van't Veer, L. J.; Dai, H.; Hart, A. A.; Voskuil, D. W.; Schreiber, G. J.; Peterse, J. L.; Roberts, C.; Marton, M. J.; Parrish, M.; Atsma, D.; Witteveen, A.; Glas, A.; Delahaye, L.; van der Velde, T.; Bartelink, H.; Rodenhuis, S.; Rutgers, E. T.; Friend, S. H.; Bernards, R., A gene-expression signature as a predictor of survival in breast cancer. *N Engl J Med* **2002,** *347* (25), 1999-2009.
19. Shibata, E.; Ejima, K.; Nanri, H.; Toki, N.; Koyama, C.; Ikeda, M.; Kashimura, M., Enhanced protein levels of protein thiol/disulphide oxidoreductases in placentae from pre-eclamptic subjects. *Placenta* **2001,** *22* (6), 566-72.
20. Severino, A.; Campioni, M.; Straino, S.; Salloum, F. N.; Schmidt, N.; Herbrand, U.; Frede, S.; Toietta, G.; Di Rocco, G.; Bussani, R.; Silvestri, F.; Piro, M.; Liuzzo, G.; Biasucci, L. M.; Mellone, P.; Feroce, F.; Capogrossi, M.; Baldi, F.; Fandrey, J.; Ehrmann, M.; Crea, F.; Abbate, A.; Baldi, A., Identification of protein disulfide isomerase as a cardiomyocyte survival factor in ischemic cardiomyopathy. *J Am Coll Cardiol* **2007,** *50* (11), 1029-37.
21. Laurindo, F. R.; Fernandes, D. C.; Amanso, A. M.; Lopes, L. R.; Santos, C. X., Novel role of protein disulfide isomerase in the regulation of NADPH oxidase activity:

pathophysiological implications in vascular diseases. *Antioxid Redox Signal* **2008,** *10* (6), 1101-13.

22. Uehara, T.; Nakamura, T.; Yao, D.; Shi, Z. Q.; Gu, Z.; Ma, Y.; Masliah, E.; Nomura, Y.; Lipton, S. A., S-nitrosylated protein-disulphide isomerase links protein misfolding to neurodegeneration. *Nature* **2006,** *441* (7092), 513-7.

23. Unterberger, U.; Hoftberger, R.; Gelpi, E.; Flicker, H.; Budka, H.; Voigtlander, T., Endoplasmic reticulum stress features are prominent in Alzheimer disease but not in prion diseases in vivo. *J Neuropathol Exp Neurol* **2006,** *65* (4), 348-57.

24. Hoozemans, J. J.; van Haastert, E. S.; Eikelenboom, P.; de Vos, R. A.; Rozemuller, J. M.; Scheper, W., Activation of the unfolded protein response in Parkinson's disease. *Biochem Biophys Res Commun* **2007,** *354* (3), 707-11.

25. Hoffstrom, B. G.; Kaplan, A.; Letso, R.; Schmid, R. S.; Turmel, G. J.; Lo, D. C.; Stockwell, B. R., Inhibitors of protein disulfide isomerase suppress apoptosis induced by misfolded proteins. *Nat Chem Biol* **2010,** *6* (12), 900-6.

26. Basso, K.; Margolin, A. A.; Stolovitzky, G.; Klein, U.; Dalla-Favera, R.; Califano, A., Reverse engineering of regulatory networks in human B cells. *Nat Genet* **2005,** *37* (4), 382-90.

27. Compagno, M.; Lim, W. K.; Grunn, A.; Nandula, S. V.; Brahmachary, M.; Shen, Q.; Bertoni, F.; Ponzoni, M.; Scandurra, M.; Califano, A.; Bhagat, G.; Chadburn, A.; Dalla-Favera, R.; Pasqualucci, L., Mutations of multiple genes cause deregulation of NF-kappaB in diffuse large B-cell lymphoma. *Nature* **2009,** *459* (7247), 717-21.

28. Piccaluga, P. P.; Agostinelli, C.; Califano, A.; Rossi, M.; Basso, K.; Zupo, S.; Went, P.; Klein, U.; Zinzani, P. L.; Baccarani, M.; Dalla Favera, R.; Pileri, S. A., Gene expression analysis of peripheral T cell lymphoma, unspecified, reveals distinct profiles and new potential therapeutic targets. *J Clin Invest* **2007,** *117* (3), 823-34.

29. Rickman, D. S.; Bobek, M. P.; Misek, D. E.; Kuick, R.; Blaivas, M.; Kurnit, D. M.; Taylor, J.; Hanash, S. M., Distinctive molecular profiles of high-grade and low-grade gliomas based on oligonucleotide microarray analysis. *Cancer Res* **2001,** *61* (18), 6885-91.

30. Gutmann, D. H.; Hedrick, N. M.; Li, J.; Nagarajan, R.; Perry, A.; Watson, M. A., Comparative gene expression profile analysis of neurofibromatosis 1-associated and sporadic pilocytic astrocytomas. *Cancer Res* **2002,** *62* (7), 2085-91.
31. Sun, L.; Hui, A. M.; Su, Q.; Vortmeyer, A.; Kotliarov, Y.; Pastorino, S.; Passaniti, A.; Menon, J.; Walling, J.; Bailey, R.; Rosenblum, M.; Mikkelsen, T.; Fine, H. A., Neuronal and glioma-derived stem cell factor induces angiogenesis within the brain. *Cancer Cell* **2006,** *9* (4), 287-300.
32. Bredel, M.; Bredel, C.; Juric, D.; Harsh, G. R.; Vogel, H.; Recht, L. D.; Sikic, B. I., Functional network analysis reveals extended gliomagenesis pathway maps and three novel MYC-interacting genes in human gliomas. *Cancer Res* **2005,** *65* (19), 8679-89.
33. Bonome, T.; Levine, D. A.; Shih, J.; Randonovich, M.; Pise-Masison, C. A.; Bogomolniy, F.; Ozbun, L.; Brady, J.; Barrett, J. C.; Boyd, J.; Birrer, M. J., A gene signature predicting for survival in suboptimally debulked patients with ovarian cancer. *Cancer Res* **2008,** *68* (13), 5478-86.
34. Welsh, J. B.; Zarrinkar, P. P.; Sapinoso, L. M.; Kern, S. G.; Behling, C. A.; Monk, B. J.; Lockhart, D. J.; Burger, R. A.; Hampton, G. M., Analysis of gene expression profiles in normal and neoplastic ovarian tissue samples identifies candidate molecular markers of epithelial ovarian cancer. *Proc Natl Acad Sci U S A* **2001,** *98* (3), 1176-81.
35. Yusenko, M. V.; Kuiper, R. P.; Boethe, T.; Ljungberg, B.; van Kessel, A. G.; Kovacs, G., High-resolution DNA copy number and gene expression analyses distinguish chromophobe renal cell carcinomas and renal oncocytomas. *BMC Cancer* **2009,** *9*, 152.
36. Beroukhim, R.; Brunet, J. P.; Di Napoli, A.; Mertz, K. D.; Seeley, A.; Pires, M. M.; Linhart, D.; Worrell, R. A.; Moch, H.; Rubin, M. A.; Sellers, W. R.; Meyerson, M.; Linehan, W. M.; Kaelin, W. G., Jr.; Signoretti, S., Patterns of gene expression and copy-number alterations in von-hippel lindau disease-associated and sporadic clear cell carcinoma of the kidney. *Cancer Res* **2009,** *69* (11), 4674-81.
37. Jones, J.; Otu, H.; Spentzos, D.; Kolia, S.; Inan, M.; Beecken, W. D.; Fellbaum, C.; Gu, X.; Joseph, M.; Pantuck, A. J.; Jonas, D.; Libermann, T. A., Gene signatures of progression and metastasis in renal cell cancer. *Clin Cancer Res* **2005,** *11* (16), 5730-9.
38. Welsh, J. B.; Sapinoso, L. M.; Su, A. I.; Kern, S. G.; Wang-Rodriguez, J.; Moskaluk, C. A.; Frierson, H. F., Jr.; Hampton, G. M., Analysis of gene expression

identifies candidate markers and pharmacological targets in prostate cancer. *Cancer Res* **2001,** *61* (16), 5974-8.

39. Singh, D.; Febbo, P. G.; Ross, K.; Jackson, D. G.; Manola, J.; Ladd, C.; Tamayo, P.; Renshaw, A. A.; D'Amico, A. V.; Richie, J. P.; Lander, E. S.; Loda, M.; Kantoff, P. W.; Golub, T. R.; Sellers, W. R., Gene expression correlates of clinical prostate cancer behavior. *Cancer Cell* **2002,** *1* (2), 203-9.

40. Khan, M. M.; Simizu, S.; Lai, N. S.; Kawatani, M.; Shimizu, T.; Osada, H., Discovery of a small molecule PDI inhibitor that inhibits reduction of HIV-1 envelope glycoprotein gp120. *ACS Chem Biol* **2011,** *6* (3), 245-51.

41. Jiang, X. M.; Fitzgerald, M.; Grant, C. M.; Hogg, P. J., Redox control of exofacial protein thiols/disulfides by protein disulfide isomerase. *J Biol Chem* **1999,** *274* (4), 2416-23.

42. Lin, L.; Gopal, S.; Sharda, A.; Passam, F.; Bowley, S. R.; Stopa, J.; Xue, G.; Yuan, C.; Furie, B. C.; Flaumenhaft, R.; Huang, M.; Furie, B., Quercetin-3-rutinoside Inhibits Protein Disulfide Isomerase by Binding to Its b'x Domain. *J Biol Chem* **2015,** *290* (39), 23543-52.

43. Eirich, J.; Braig, S.; Schyschka, L.; Servatius, P.; Hoffmann, J.; Hecht, S.; Fulda, S.; Zahler, S.; Antes, I.; Kazmaier, U.; Sieber, S. A.; Vollmar, A. M., A small molecule inhibits protein disulfide isomerase and triggers the chemosensitization of cancer cells. *Angew Chem Int Ed Engl* **2014,** *53* (47), 12960-5.

44. Kaplan, A.; Gaschler, M. M.; Dunn, D. E.; Colligan, R.; Brown, L. M.; Palmer, A. G., 3rd; Lo, D. C.; Stockwell, B. R., Small molecule-induced oxidation of protein disulfide isomerase is neuroprotective. *Proc Natl Acad Sci U S A* **2015,** *112* (17), E2245-52.

45. Xu, S.; Butkevich, A. N.; Yamada, R.; Zhou, Y.; Debnath, B.; Duncan, R.; Zandi, E.; Petasis, N. A.; Neamati, N., Discovery of an orally active small-molecule irreversible inhibitor of protein disulfide isomerase for ovarian cancer treatment. *Proc Natl Acad Sci U S A* **2012,** *109* (40), 16348-53.

46. Allimuthu, D.; Adams, D. J., 2-Chloropropionamide As a Low-Reactivity Electrophile for Irreversible Small-Molecule Probe Identification. *ACS Chem Biol* **2017,** *12* (8), 2124-2131.

47. Ge, J.; Zhang, C. J.; Li, L.; Chong, L. M.; Wu, X.; Hao, P.; Sze, S. K.; Yao, S. Q., Small molecule probe suitable for in situ profiling and inhibition of protein disulfide isomerase. *ACS Chem Biol* **2013,** *8* (11), 2577-85.
48. Banerjee, R.; Pace, N. J.; Brown, D. R.; Weerapana, E., 1,3,5-Triazine as a modular scaffold for covalent inhibitors with streamlined target identification. *J Am Chem Soc* **2013,** *135* (7), 2497-500.
49. Mayer, M.; Kies, U.; Kammermeier, R.; Buchner, J., BiP and PDI cooperate in the oxidative folding of antibodies in vitro. *J Biol Chem* **2000,** *275* (38), 29421-5.
50. Gertz, M. A., Immunoglobulin light chain amyloidosis: 2016 update on diagnosis, prognosis, and treatment. *Am J Hematol* **2016,** *91* (9), 947-56.
51. Wang, C.; Li, W.; Ren, J.; Fang, J.; Ke, H.; Gong, W.; Feng, W.; Wang, C. C., Structural insights into the redox-regulated dynamic conformations of human protein disulfide isomerase. *Antioxid Redox Signal* **2013,** *19* (1), 36-45.
52. Zhu, K.; Borrelli, K. W.; Greenwood, J. R.; Day, T.; Abel, R.; Farid, R. S.; Harder, E., Docking covalent inhibitors: a parameter free approach to pose prediction and scoring. *J Chem Inf Model* **2014,** *54* (7), 1932-40.
53. Speers, A. E.; Adam, G. C.; Cravatt, B. F., Activity-based protein profiling in vivo using a copper(i)-catalyzed azide-alkyne [3 + 2] cycloaddition. *J Am Chem Soc* **2003,** *125* (16), 4686-7.
54. Speers, A. E.; Cravatt, B. F., Profiling enzyme activities in vivo using click chemistry methods. *Chem Biol* **2004,** *11* (4), 535-46.
55. Holmgren, A., Thioredoxin catalyzes the reduction of insulin disulfides by dithiothreitol and dihydrolipoamide. *J Biol Chem* **1979,** *254* (19), 9627-32.
56. Schroder, M.; Kaufman, R. J., The mammalian unfolded protein response. *Annu Rev Biochem* **2005,** *74*, 739-89.
57. Hetz, C., The unfolded protein response: controlling cell fate decisions under ER stress and beyond. *Nat Rev Mol Cell Biol* **2012,** *13* (2), 89-102.
58. Shoulders, M. D.; Ryno, L. M.; Genereux, J. C.; Moresco, J. J.; Tu, P. G.; Wu, C.; Yates, J. R., 3rd; Su, A. I.; Kelly, J. W.; Wiseman, R. L., Stress-independent activation of XBP1s and/or ATF6 reveals three functionally diverse ER proteostasis environments. *Cell Rep* **2013,** *3* (4), 1279-92.

59. Cawley, K.; Deegan, S.; Samali, A.; Gupta, S., Assays for detecting the unfolded protein response. *Methods Enzymol* **2011,** *490*, 31-51.
60. Walter, P.; Ron, D., The unfolded protein response: from stress pathway to homeostatic regulation. *Science* **2011,** *334* (6059), 1081-6.
61. Borth, N.; Mattanovich, D.; Kunert, R.; Katinger, H., Effect of increased expression of protein disulfide isomerase and heavy chain binding protein on antibody secretion in a recombinant CHO cell line. *Biotechnol Prog* **2005,** *21* (1), 106-11.
62. Lilie, H.; McLaughlin, S.; Freedman, R.; Buchner, J., Influence of protein disulfide isomerase (PDI) on antibody folding in vitro. *J Biol Chem* **1994,** *269* (19), 14290-6.
63. Roth, R. A.; Pierce, S. B., In vivo cross-linking of protein disulfide isomerase to immunoglobulins. *Biochemistry* **1987,** *26* (14), 4179-82.
64. Cooley, C. B.; Ryno, L. M.; Plate, L.; Morgan, G. J.; Hulleman, J. D.; Kelly, J. W.; Wiseman, R. L., Unfolded protein response activation reduces secretion and extracellular aggregation of amyloidogenic immunoglobulin light chain. *Proc Natl Acad Sci U S A* **2014,** *111* (36), 13046-51.
65. Weerapana, E.; Speers, A. E.; Cravatt, B. F., Tandem orthogonal proteolysis-activity-based protein profiling (TOP-ABPP)--a general method for mapping sites of probe modification in proteomes. *Nat Protoc* **2007,** *2* (6), 1414-25.
66. Plate, L.; Cooley, C. B.; Chen, J. J.; Paxman, R. J.; Gallagher, C. M.; Madoux, F.; Genereux, J. C.; Dobbs, W.; Garza, D.; Spicer, T. P.; Scampavia, L.; Brown, S. J.; Rosen, H.; Powers, E. T.; Walter, P.; Hodder, P.; Wiseman, R. L.; Kelly, J. W., Small molecule proteostasis regulators that reprogram the ER to reduce extracellular protein aggregation. *Elife* **2016,** *5*.

CHAPTER 3

THE TUNABILITY OF RESIDUE SPECIFIC ELECTROPHILES

3.0 Introduction

Functional amino acids that display heightened levels of nucleophilicity tend to play roles in catalysis and regulation. The chemical modification of these nucleophiles is crucial for various applications from irreversible inhibitor development to activity-based protein profiling (ABPP). ABPP has become a powerful chemical proteomic strategy to directly characterize enzymatic functionality directly in native biological systems, on a global scale[1]. ABPP relies on the design of active-site directed covalent probes to interrogate various families of enzymes in complex proteomes, meanwhile providing a quantitative, chemical readout of the functional state of the individuals enzymes in that particular enzyme family[1]. Current ABPP scaffolds utilize a wide variety of chemical scaffolds, general electrophiles, natural products and mechanism-based inhibitors. It is also important to note that because the activity of an enzyme is regulated by a variety of posttranslational modifications and molecular mechanisms[2-4], activity-based probes report can report on the structure and reactivity of an enzyme active site in the context of the cell.

The use of covalent small molecules in drug design and ABPP relies on selective, protein-reactive electrophiles. To date there have been many reported, well characterized electrophiles including, haloacetamides[5-7], maleimides[7], and α,β-unsaturated ketones[5] which have all shown selectivity for cysteine thiols. Other electrophiles which have shown diverse reactivities toward other amino acids are sulfonate esters (aspartate, glutamate, and tyrosine)[5], acyl phophates (lysine)[8], sulfonyl fluorides (serine and tyrosine)[9-10], and fluorophosphonates (serine)[11]. Many of these electrophiles demonstrate high reactivity and functional group specificity, covalently modifiying proteins without the presence of a binding motif. Interestingly, there are other protein-reactive electrophiles including

epoxysuccinates[12], spiroepoxides[13], carbamates[14], acyloxymethyl ketones[15], phenoxymethyl ketones[16], and β-lactams[14], which require the presence of a binding motif to facilitate the covalent conjugation of these electrophiles toward nucleophilic proteins of interest.

3.1 Activity-Based Protein Profiling

Recent advances in genomic technologies, such as chromosomal translocation and gene amplification, have provided insights into relative gene expression levels inside the cell[17-18].Other genomic technologies, such as transcriptional profiling and RNA-interference-based gene silencing (RNAi) probe gene expressional level to deduce protein function, yet cannot fully realize the multitude of post translational modifications that regulate protein activity inside the cell. ABPP is a powerful chemical proteomic approach to directly interrogate protein functionality in the context on the cell. ABPP relies on active-site directed covalent probes to interrogate various enzyme families within the proteome, and to provide a chemical readout of the functional state of those enzymes within that family[1].

3.1.1 ABPP Probe Design Features

Fundamentally, ABPP probes are small-molecules that covalently label the active site(s) of a given enzyme or enzyme family. An ideal electrophilic ABPP probe would target a large subset of enzymes, as to provide a global view of the functional state of that particular enzyme family. However, some probes, like iodoacetamide-alkyne (IA≡, Figure 3.1A), are extremely-promiscuous and label hundreds to thousands of nucleophilic cysteine

residues. Most ABPP probes reach a desired balance between coverage and promiscuity by combining reactive groups and binding groups that target conserved structural features in an enzyme active site(s) (Figure 3.1B)[1]. ABPP probes can contain two different classes of reactive groups, general electrophiles that modify nucleophilic residues or photoreactive groups that label proximal residues upon irradiation with UV light. The third and final element that ABPP probes must possess is a reporter element, to facilitate protein target characterization upon labeling. Reporter elements can include fluorophores for visualization, a biotin group for enrichment, or a biorthogonal handle, such as an azide or alkyne, for use in copper assisted azide-alkyne cycloaddition (CuAAC) reactions, "click chemistry" (Figure 3.1C).

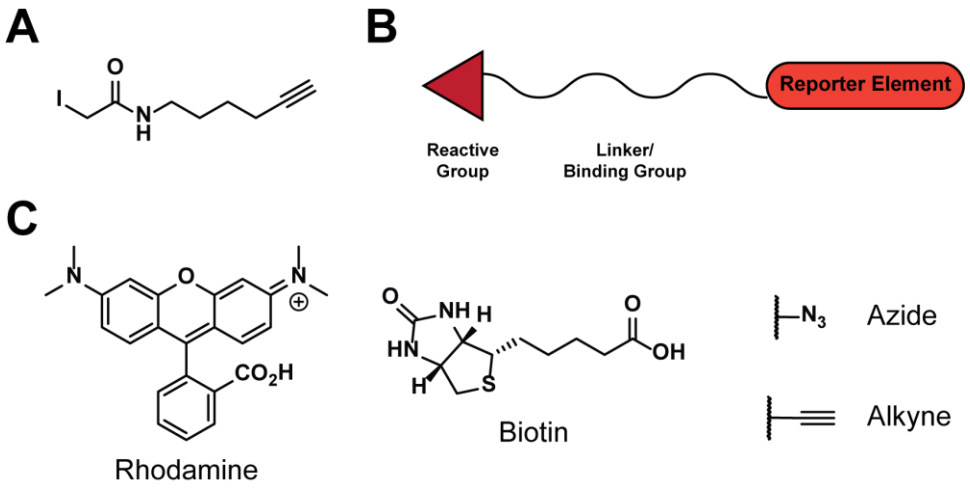

Figure 3-1. (A) Chemical structure of promiscuous cysteine-reactive ABPP probe, iodoacetamide-alkyne. (B) Representative structure of an ABPP probe, containing a reactive group, a linker/binding group, and a reporter element. (C) Chemical structures of various common reporter elements used in ABPP for visualization (rhodamine, and enrichment (biotin), as well as post labeling conjugation (azide and alkyne) via "click" chemistry.

3.2 The Tunability of Reactive Aryl Halides

The selective covalent modification of amino acid side chains requires the appropriate selection of an electrophile with the suitable affinity for the specific amino acid of interest. Toward this end, there are numerous electrophiles with high reactivity and selectivity for specific residues, and some electrophiles with disparate reactivity profiles in the context of the proteome. Due to the widespread application for covalent electrophiles with distinct and tunable reactivity profiles, in 2014, our lab reported on the reactivity and tenability of various aryl chloride-based electrophiles[19]. Arylation of the nucleophilic residue with these electrophiles proceeds via a nucleophilic aromatic substitution (S_NAr) mechanism, similar to that during the conjugation of glutathione to activated aryl groups by glutathione *S*-tranferases (GSTs)[20].

Previous members of the Weerapana lab, Alex Shannon and Ranjan Banerjee, synthesized a panel of alkyne-functionalized aryl chloride-based electrophiles and systematically evaluated the reactivity and selectivity of these compounds in the context of the proteome[19]. Initial studies began by investigating the reactivity of a panel of chloronitrobenzene (CNB) electrophiles. It was hypothesized that these electrophiles react via an S_NAR mechanism and thus the rate limiting step would be the formation of the Meisenheimer complex[21-22]. Therefore, it was hypothesized that the reactivity of these aryl halide electrophiles can be tuned by varying the position of the electron withdrawing nitro substituent on the aromatic ring[19]. To test this hypothesis, four CNBs were synthesized varying the nitro electron withdrawing group (EWG) in the ortho (ERW1 and ERW2), meta (RB1), and para (RB2) position. (Figure 3-2A).

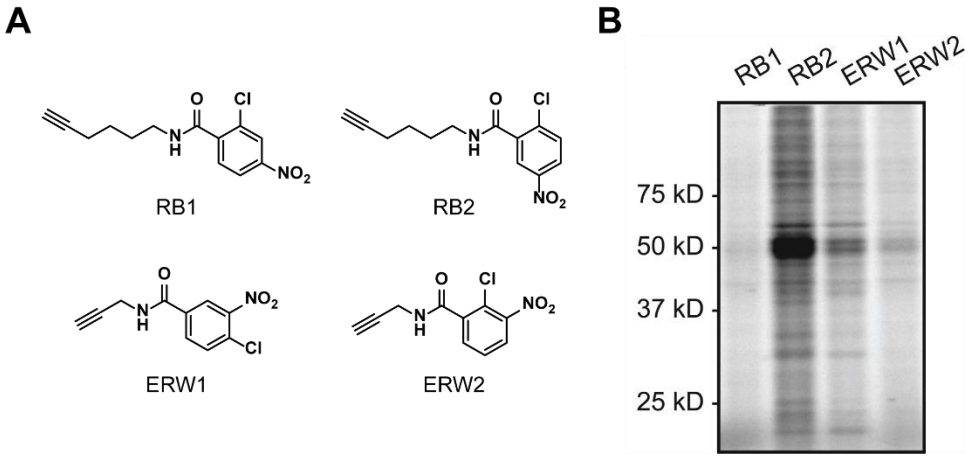

Figure 3-2. (A) Chemical structures of the panel of alkyne-functionalized chloronitrobenzene probes evaluated. (B) In-gel fluorescence study of the reactivity of CNBs in complex proteomes, after incorporation of rhodamine-azide (Rh-N_3) using CuAAC.

To evaluate the reactivity of this panel of CNBs in complex proteomes, each probe was incubated in HeLa cell lysates at 100 μM for 1 hr, followed by the conjugation of rhodamine-azide (Rh-N_3) using CuAAC. Following the separation of proteins on gel via SDS-PAGE, visualization of probe labeled proteins was performed using in-gel fluorescence (Figure 3-2B). As originally hypothesized, RB2 was the most reactive compound amongst the panel, owing to the nitro substituent in the para position and the increased resonance stabilization of the Meisenheimer complex. As indicated by the gel, shifting the EWG to the ortho position, as in ERW1 and ERW2, still showed reactivity, although much lower than RB2. Also, it can be seen that shifting the EWG to the meta position completely abrogates the reactivity of the probe. This study demonstrates that the proteome reactivity of CNBs can be finely adjusted by means of modulating the electronics and sterics of the aryl ring system[19].

To further this exploration into the reactivity and selectivity of aryl halide electrophiles, the panel was then expanded to include a fluoronitrobenzene (ERW3), chloropyridines (RB3 and RB4), chloropyrimidines (RB5 and RB6), and a dichlorotriazine (RB7) (Figure 3-3A)[19]. In this instance, the reactivity of these compounds will be determined by the resonance stabilization realized by the nitrogen(s) in the aromatic ring system. Upon evaluation of this panel of compounds in a proteome, it was found that the fluoronitrobenzene, ERW3, exhibitied similar labeling to RB2 (Figure 3-3B). It was also shown that the chloropyridines, RB3 and RB4, and the chloropyrimidines (RB6 and RB6) all exhibited significantly decreased reactivity compared to that of RB2 as demonstrated by in-gel fluorescence (Figure 3-3B). Interestingly, the dichlorotriaizine showed extremely

potent labeling of the proteome compared to RB2, demonstrating the increased resonance and stabilization of the Meisenheimer complex[19, 21].

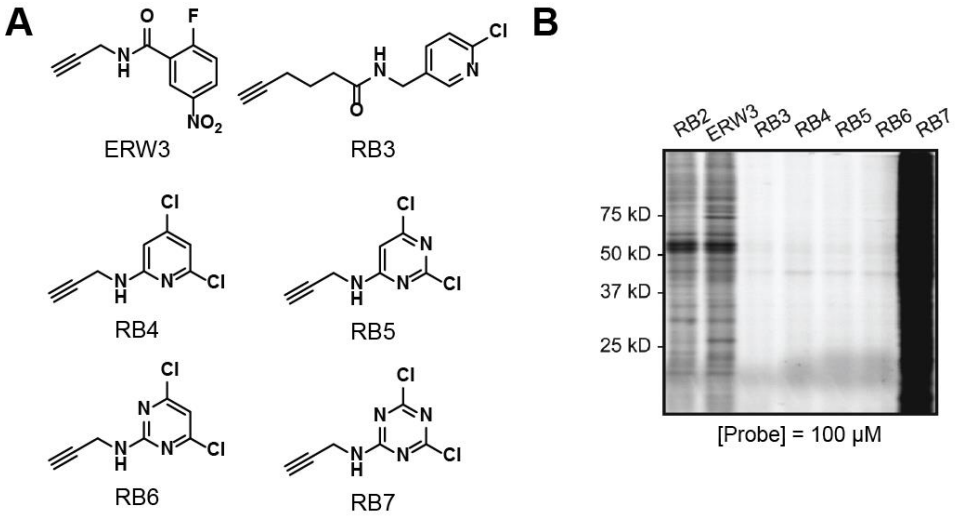

Figure 3-3. (A) Chemical structures of the panel of alkyne-functionalized fluoronitrobenzene, chloropyridine, chloropyrimidine, and dichlorotriazine probes evaluated. (B) In-gel fluorescence study of the reactivity of aryl halide probes in HeLa lysates at 100 µM, followed by incorporation of rhodamine-azide (Rh-N_3) using CuAAC and separation using SDS-PAGE.[19]

Initial screening efforts of the small panel of compounds identified RB2, ERW3, and RB7 as aryl halides with high reactivity in the proteome. However, RB7 was significantly more potent than RB2 and ERW3 (Figure 3-3B) and thus could not be directly compared to the latter at the screening concentration of 100 μM. In order to gain clarity on these electrophiles and to evaluate labeling patterns, Shannon *et al* decreased the probe concentrations of RB7 to 5 μM and RB2 and ERW3 to 20 μM, in order to better evaluate the probes directly to each other (Figure 3-4A)[19]. As shown in the in-gel fluorescence study with equipotent labeling, the dichlorotriazine, RB7, displays a distinct labeling pattern compared to that of the chloronitrobenzenes, RB2 and ERW3, suggesting that RB7 is targeting a distinct sub-population of proteins compared to the CNBs[19]. *p*-Chloronitrobenzene compounds have recently been used in compounds that modify proteins with nucleophilic cysteine residues, including peroxisome proliferator-activated receptor (PPARγ)[23] and β-tubulin[24]. To investigate if these compounds were labeling nucleophilic cysteine residues, as expected of the CNBs, a competition-based assay with the highly reactive, cysteine-selective electrophile, iodoacetamide (IA) was performed. To do this, lysates were either treated with vehicle (DMSO) or IA (2 mM) to cap the nucleophilic cysteine residues, followed by labeling with the panel of electrophilic compounds RB2 (20 μM), ERW3 (20 μM), or RB7 (1 μM) (Figure 3-4B). As indicated from the assay, labeling by RB2 and ERW3 was completely abolished by pre-treatment with IA to cap the nucleophilic cysteine residues in the proteome[19]. This suggests that these two electrophilic compounds selectively modify cysteine residues in a complex proteome. Interestingly, RB7 labeling of the proteome remained intact of pre-treatment with IA, suggesting that RB7 is labeling nucleophilic residues other than cysteine.

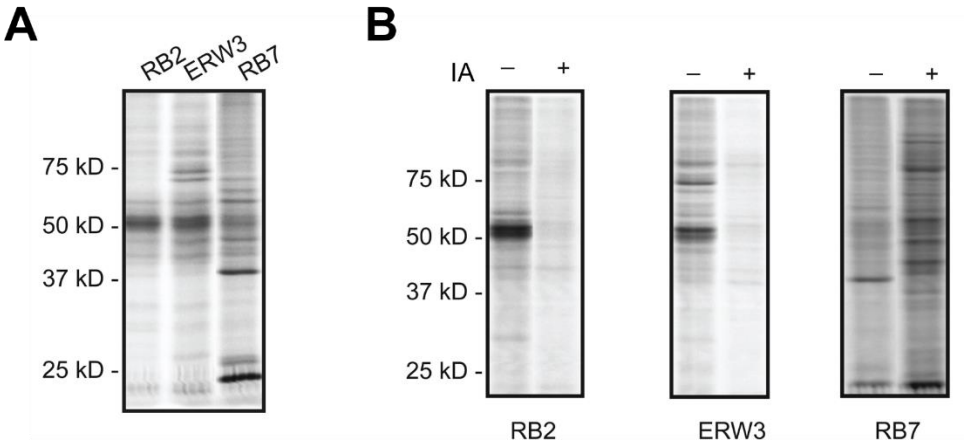

Figure 3-4. (A) In-gel fluorescence studies comparing probe labeling patterns of RB2 (20 μM), ERW3 (20 μM), and RB7 (20 μM). (B) Competition assay with IA comparing probe labeling of RB2, ERW3, and RB7 prior to treatment with IA[19].

To confirm the cysteine selectivity of RB2 and to identify the preferential labeling of RB7, a mass-spectrometry-based platform was employed to identify the site of labeling within the complex proteome, tandem orthogonal proteolysis activity-based protein profiling (TOP-ABPP). TOP-ABPP is a chemo-proteomic method which allows for the parallel characterization of probe-labeled proteins and for the sites of probe modification. This approach uses "click" chemistry to append a multifunctional tag onto alkyne-functionalized probes which contains a biotin group for avidin enrichmentand a tobacco etch virus (TEV) protease cleavage site for selective release of the probe modified peptides. Following labeling and enrichment on streptavidin beads, protein targets are then digested and identified before releasing the probe-modified peptides from the beads for site-of-labeling identification[25-26]. HeLa lysates were treated with RB2 and RB7 at 100 μM an analyzed by TOP-ABPP methodologies. The resulting MS2 fragmentation data were subsequently search for probe modifications on all nucleophilic amino acids including cysteine, aspartate, glutamate, histidine, lysine, serine, threonine, and tyrosine using the SEQUEST search algorithm[19, 27]. It was confirmed that RB2 predominantly labels cysteine residues, while RB7 shows extreme reactivity towards nucleophilic lysine residues with minimal cysteine modification.

3.3 A Dichlorotriazine-based Inhibitor of GSTP1, LAS-17

To further explore the unique reactivity of the dichlorotriazine electrophile that Shannon *et al*. reported, in 2016 our lab reported on a library of covalent inhibitors based on the dichlorotriazine electrophilic functionality[28]. The small-molecules in this library contained the following functionalities: (1) an alkyne handle for bio-orthogonal reporter

tag conjugation; (2) a diversity element to direct the probes to different subsets of the proteome; and (3) a dichlorotriazine electrophile (Figure 3.5A). Crawford and Weerapana synthesized a small library of 20 compounds with diversity elements containing various hydrocarbons, aromatic groups, as well as different L- and D-amino acids (Figure 3.5B)[28].

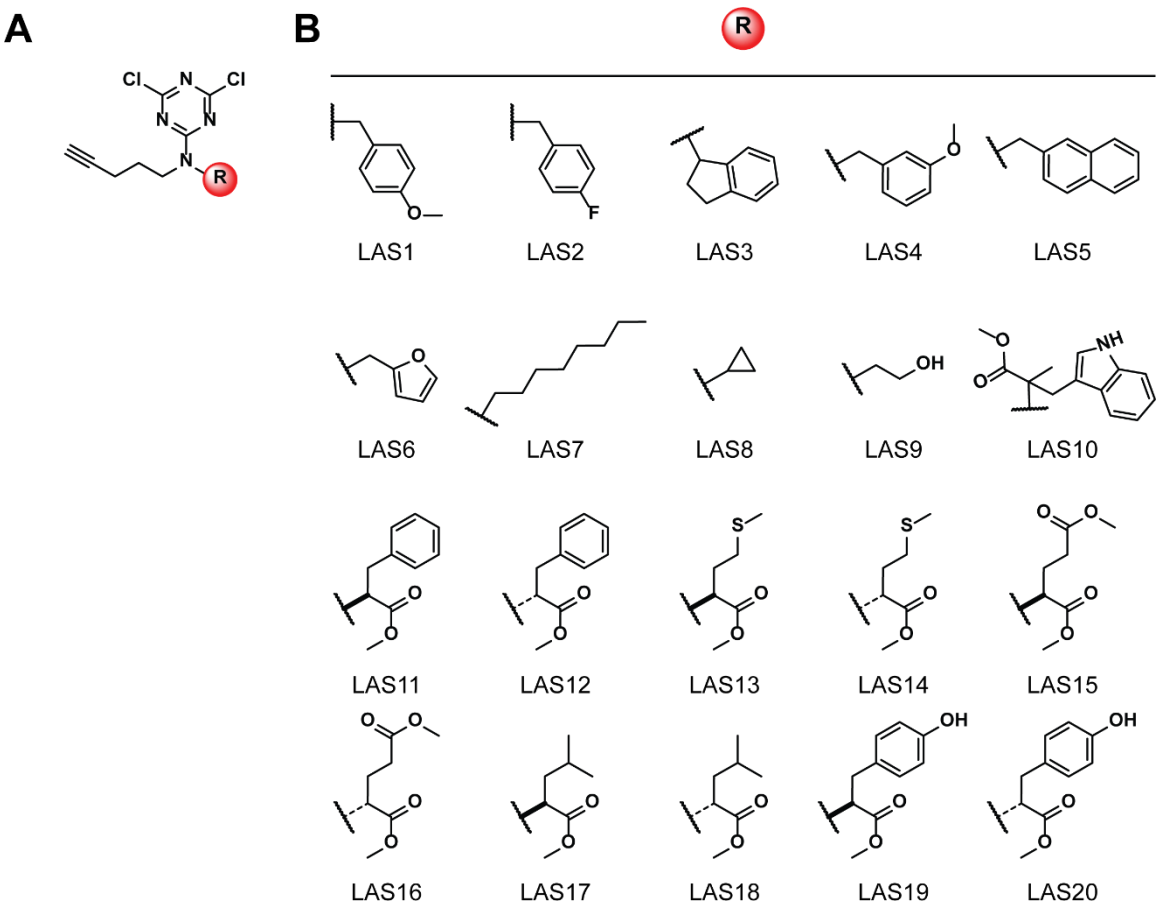

Figure 3.5. (A) General chemical structure of small-molecule probes. Each probe contains three elements: (1) an alkyne handle for bio-orthogonal reporter tag conjugation; (2) a diversity element to direct the probes to different subsets of the proteome; and (3) a dichlorotriazine electrophile. (B) Chemical structures of diversity elements used in dichlorotriazine small-molecule probe library.

Initial screening efforts focused on evaluating the reactivity and selectivity of the small-molecule probes in a complex proteome. Briefly, HeLa cell lysates (2 mg/mL) were treated with 1 μM of each probe for 1 hour, followed by the conjugation of rhodamine-azide (Rh-N_3) using "click" chemistry. Following the separation of the proteins by SDS-PAGE, visualization of probe-labeled proteins was performed by in-gel fluorescence. These in-gel fluorescence screening studies demonstrated that several library members covalently labeled proteins in the complex proteome. LAS17 (Figure 3.6A), which contains a L-leucine methyl ester diversity element, was found to selectively labeled a low-molecular weight protein, ~25 kDa (Figure 3.6B)[28]. Furthermore, to assess the cell permeability and selectivity of LAS17 *in situ*, HeLa cells were treated with LAS17 (Figure 3.6C). Following treatment with probe (1 μM) for 1 hour, cells were subjected to lysis and reporter tag conjugation. After subsequent SDS-PAGE separation and in-gel fluorescence analysis, the presence of a single robust fluorescent band at ~25 kDa, which demonstrated the high reactivity and selectivity of LAS17 for covalent modification of this protein target within the context of the complex proteome.

To more comprehensively assess the reactivity and selectivity of LAS17 in the complex proteome, the protein target of LAS17 were globally investigated. In order to do this, HeLa cells were treated with LAS17 (1 μM) or DMSO. Upon cell lysis, LAS17-labeled proteins were then appended to biotin-azide using CuAAC, enriched on streptavidin beads, subjected to on-bead tryptic digestion, and subsequent LC/LC-MS/MS analysis. Spectral counts for proteins identified in the LAS17 samples were then compared to the DMSO treated samples, and indicated that the protein target of LAS17 is glutathione *S*-transferase Pi (GSTP1) (Figure 3.6D).

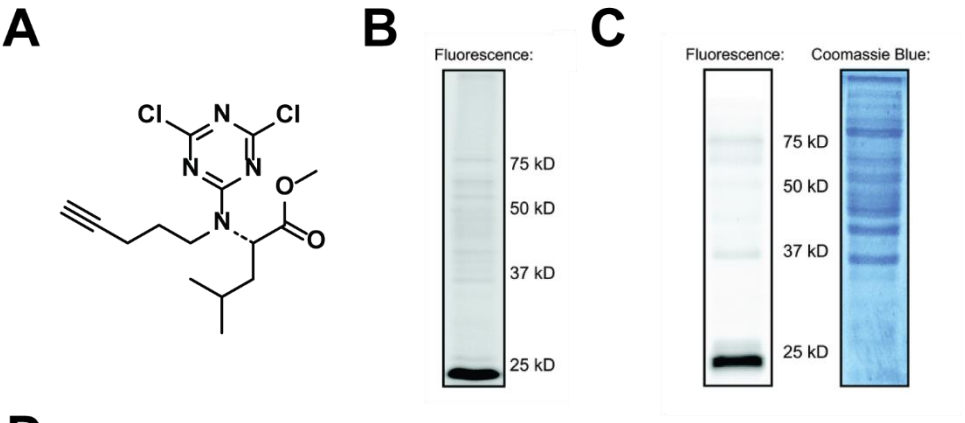

D

Protein	Mol Weight (Da)	DMSO	LAS17
GSTP1 Glutathione S-transferase P	23342	0	24
HSP90AB1 Heat shock protein HSP 90-beta	83264	4	24
TKT Transketolase	67878	3	23
TUBA4A Tubulin alpha-4A chain	49924	4	22
PKM Pyruvate kinase isozymes M1/M2	57937	6	22
EEF1A1 Elongation factor 1-alpha 1	50141	5	20
FLNA Filamin-A	280737	6	20
TUBB Tubulin beta chain	49671	6	19
PGK1 Phosphoglycerate kinase 1	44615	1	14
HSP90AA1 Heat shock protein HSP 90-alpha	84660	0	12

Figure 3.6. (A) Chemical structure of LAS17. (B) In-gel fluorescence studies of LAS17 (1 μM) incubated with HeLa cell lysate (2 mg/mL) to assess potency and selectivity for endogenous proteins in a complex proteome. (C) HeLa cells were treated with LAS17 (1 μM) and subjected to in-gel fluorescence analysis to assess the cell permeability and selectivity of LAS17 *in situ*. (D) HeLa cell lysates treated with LAS17 (1 μM) or DMSO were subjected to CuAAC with biotin-azide, enriched on streptavidin beads, and subsequent LC/LC-MS/MS analysis. The top 10 proteins with the greatest difference in average spectral counts among three trials for DMSO and LAS17 treated samples are listed.

GSTP1 is the most ubiquitous member of the GST protein superfamily and is primarily responsible for the conjugation of glutathione (GSH) to exogenous electrophiles as a mechanism of cellular detoxification[29]. Interestingly, most of the dichlorotriazine library labels a protein of similar molecular weight to that of GSTP1. Owing to the hyper-reactivity of the dichlorotriazine electrophile, as demonstrated by Shannon *et al*., it can be hypothesized that GSTP1 is reacting with these probes to detoxify the cellular environment, thus demonstrating a need to modulate the reactivity of this electrophile so it can be more useful in a cellular context. High expression levels of GSTP1 have also been implicated to play a role in chemotherapeutic resistance[30], and a variety of different cancers including breast, colon, and ovarian cancers have shown to have elevated levels GSTP1 relative to healthy tissue[31].

To validate the protein target of LAS17, GSTP1, identified by LC/LC-MS/MS, human GSTP1 with an N-terminal 6X His-tag was recombinantly overexpressed and purified from *E. coli*. The purified protein was subsequently treated with LAS17 (1 μM) and subjected to in-gel fluorescence analysis (Figure 3.7A). The presence of a robust fluorescent band demonstrates that LAS17 does in fact covalently modify GSTP1, confirming the mass spectrometry findings[28].

To interrogate whether the covalent linkage of LAS17 to GSTP1 correlated with any inhibitory effect, an *in vitro* activity assay was performed in which the transfer of glutathione (GSH) to 1-bromo-2,4,dinitrobenzene (BDNB) spectrophotometrically[28]. It was demonstrated that LAS17 could inhibit GSTP1 activity in a concentration-dependent manner (Figure 3.7B). Owning to the covalent nature of the small-moleucle inhibitor, time-

dependent inhibition of GSTP1 was also monitored (data not shown), affording a second-order rate constant of inactivation (k_{inact}/K_I) of 31,200 M^{-1} s^{-1}.

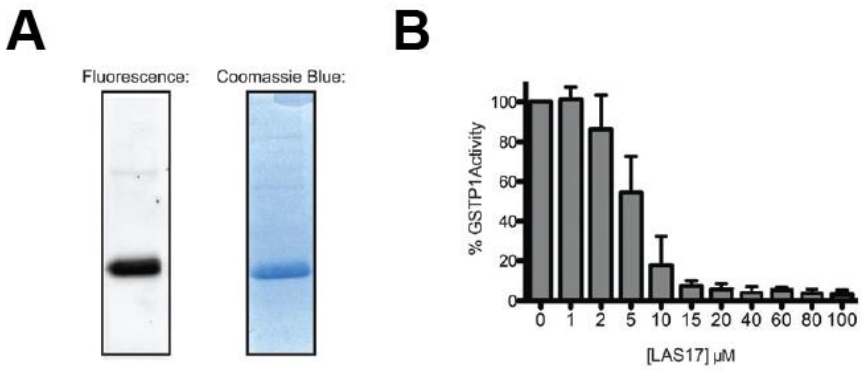

Figure 3.7. (A) Purified, recombinant GSTP1 was treated with LAS17 (1 µM) and evaluated by in-gel fluorescence. (B) *In vitro* GSTP1 activity assay data demonstrate that LAS17 inhibits GSTP1 activity in a concentration-dependent manner[28].

3.4 Conclusions

In summary, functional amino acids in the cell tend to have a heightened sense of nucleophilicity responsible for roles in catalysis and regulation of cellular processes. Recent advances in genomic technologies such as transcriptional profiling and RNAi attempt to probe at the gene expression level to deteremine the functions of these nucleophilic residues and their corresponding proteins. However, due to the myriad of post-translational modifications and mechanisms, genomic approaches cannot fully realize the functional state of a given protein in a complex proteome. These technological advances have given rise to ABPP, which is a powerful chemical proteomic method that uses small-molecule covalent probes to directly interrogate the functionality of a given protein/protein family. Due to the covalent nature of the small-molecule probes used, ABPP can directly report on the structure and reactivity of an enzyme active site in the context of a complex proteome. In order to perturb to a wide variety of protein reactivities in the proteome, ABPP relies on the use of selective, protein-reactive electrophiles. To date there have been many reported, well characterized electrophiles targeting a variety of nucleophilic amino acids with disparate reactivity profiles. In 2014, our lab demonstrated that a small panel of aryl halide electrophiles could possess a range of proteome reactivity, and selectivity for nucleophilic residues. RB2 was found to be a potent, selective electrophile against cysteine residues and RB7 was found to extremely reactive and selective towards lysine residues in a complex proteome. Interestingly, it was also demonstrated that the reactivity profiles of these types of aryl halides can be tuned by varying the electronics and sterics of the aryl ring system. Modulation of the electronics of the aryl ring to stabilize the S_NAR transition state complex increases or decreases the reactivity of the probe based on the position of the

EWG. In 2016, our lab furthered the investigation of the dichlorotriazine electrophiles and reported on a panel of inhibitors that contained that electrophilic functionality. One small-molecule, LAS17, was found to potenltly and selectively label GSTP1 in the context of the complex proteome. Further studies demonstrated that LAS17 inhibited GSTP1 activity in a concentration- and time-dependent manner. The primary role of GSTP1 in the cell is to conjugate glutathione to exogenous electrophiles as a mechanism of cellular detoxification, indicating the dichlorotriazine motif is too reactive for use as a probe scaffold. As such, modulation of the dichlorotriazine ring system to further optimize the electronics and tune the electrophilicity will be the subject of the next chapter of this thesis.

1. Cravatt, B. F.; Wright, A. T.; Kozarich, J. W., Activity-based protein profiling: from enzyme chemistry to proteomic chemistry. *Annu Rev Biochem* **2008,** *77*, 383-414.
2. Khan, A. R.; James, M. N., Molecular mechanisms for the conversion of zymogens to active proteolytic enzymes. *Protein Sci* **1998,** *7* (4), 815-36.
3. Kobe, B.; Kemp, B. E., Active site-directed protein regulation. *Nature* **1999,** *402* (6760), 373-6.
4. Zhou, Y.; Wynia-Smith, S. L.; Couvertier, S. M.; Kalous, K. S.; Marletta, M. A.; Smith, B. C.; Weerapana, E., Chemoproteomic Strategy to Quantitatively Monitor Transnitrosation Uncovers Functionally Relevant S-Nitrosation Sites on Cathepsin D and HADH2. *Cell Chem Biol* **2016,** *23* (6), 727-37.
5. Weerapana, E.; Simon, G. M.; Cravatt, B. F., Disparate proteome reactivity profiles of carbon electrophiles. *Nat Chem Biol* **2008,** *4* (7), 405-7.
6. Weerapana, E.; Wang, C.; Simon, G. M.; Richter, F.; Khare, S.; Dillon, M. B.; Bachovchin, D. A.; Mowen, K.; Baker, D.; Cravatt, B. F., Quantitative reactivity profiling predicts functional cysteines in proteomes. *Nature* **2010,** *468* (7325), 790-5.
7. Shin, N. Y.; Liu, Q.; Stamer, S. L.; Liebler, D. C., Protein targets of reactive electrophiles in human liver microsomes. *Chem Res Toxicol* **2007,** *20* (6), 859-67.
8. Patricelli, M. P.; Szardenings, A. K.; Liyanage, M.; Nomanbhoy, T. K.; Wu, M.; Weissig, H.; Aban, A.; Chun, D.; Tanner, S.; Kozarich, J. W., Functional interrogation of the kinome using nucleotide acyl phosphates. *Biochemistry* **2007,** *46* (2), 350-8.
9. Gu, C.; Shannon, D. A.; Colby, T.; Wang, Z.; Shabab, M.; Kumari, S.; Villamor, J. G.; McLaughlin, C. J.; Weerapana, E.; Kaiser, M.; Cravatt, B. F.; van der Hoorn, R. A., Chemical proteomics with sulfonyl fluoride probes reveals selective labeling of functional tyrosines in glutathione transferases. *Chem Biol* **2013,** *20* (4), 541-8.
10. Shannon, D. A.; Gu, C.; McLaughlin, C. J.; Kaiser, M.; van der Hoorn, R. A.; Weerapana, E., Sulfonyl fluoride analogues as activity-based probes for serine proteases. *Chembiochem* **2012,** *13* (16), 2327-30.
11. Kidd, D.; Liu, Y.; Cravatt, B. F., Profiling serine hydrolase activities in complex proteomes. *Biochemistry* **2001,** *40* (13), 4005-15.

12. Greenbaum, D.; Medzihradszky, K. F.; Burlingame, A.; Bogyo, M., Epoxide electrophiles as activity-dependent cysteine protease profiling and discovery tools. *Chem Biol* **2000,** *7* (8), 569-81.

13. Evans, M. J.; Morris, G. M.; Wu, J.; Olson, A. J.; Sorensen, E. J.; Cravatt, B. F., Mechanistic and structural requirements for active site labeling of phosphoglycerate mutase by spiroepoxides. *Mol Biosyst* **2007,** *3* (7), 495-506.

14. Bachovchin, D. A.; Ji, T.; Li, W.; Simon, G. M.; Blankman, J. L.; Adibekian, A.; Hoover, H.; Niessen, S.; Cravatt, B. F., Superfamily-wide portrait of serine hydrolase inhibition achieved by library-versus-library screening. *Proc Natl Acad Sci U S A* **2010,** *107* (49), 20941-6.

15. Kato, D.; Boatright, K. M.; Berger, A. B.; Nazif, T.; Blum, G.; Ryan, C.; Chehade, K. A.; Salvesen, G. S.; Bogyo, M., Activity-based probes that target diverse cysteine protease families. *Nat Chem Biol* **2005,** *1* (1), 33-8.

16. Verdoes, M.; Oresic Bender, K.; Segal, E.; van der Linden, W. A.; Syed, S.; Withana, N. P.; Sanman, L. E.; Bogyo, M., Improved quenched fluorescent probe for imaging of cysteine cathepsin activity. *J Am Chem Soc* **2013,** *135* (39), 14726-30.

17. Hanahan, D.; Weinberg, R. A., The hallmarks of cancer. *Cell* **2000,** *100* (1), 57-70.

18. Vogelstein, B.; Kinzler, K. W., Cancer genes and the pathways they control. *Nat Med* **2004,** *10* (8), 789-99.

19. Shannon, D. A.; Banerjee, R.; Webster, E. R.; Bak, D. W.; Wang, C.; Weerapana, E., Investigating the proteome reactivity and selectivity of aryl halides. *J Am Chem Soc* **2014,** *136* (9), 3330-3.

20. Ji, X.; Armstrong, R. N.; Gilliland, G. L., Snapshots along the reaction coordinate of an SNAr reaction catalyzed by glutathione transferase. *Biochemistry* **1993,** *32* (48), 12949-54.

21. Miller, J., The S_N Mechanism in Aromatic Compounds. Part XXVII.[1] A Quantitative Approach to Aromatic Nucleophilic Substitution. *J Am Chem Soc* **1963,** *85* (11), 1628-1635.

22. Bernasconi, C. F., *Chimia* **1980,** *34*.

23. Leesnitzer, L. M.; Parks, D. J.; Bledsoe, R. K.; Cobb, J. E.; Collins, J. L.; Consler, T. G.; Davis, R. G.; Hull-Ryde, E. A.; Lenhard, J. M.; Patel, L.; Plunket, K. D.; Shenk, J. L.; Stimmel, J. B.; Therapontos, C.; Willson, T. M.; Blanchard, S. G., Functional consequences of cysteine modification in the ligand binding sites of peroxisome proliferator activated receptors by GW9662. *Biochemistry* **2002,** *41* (21), 6640-50.
24. Banerjee, R.; Pace, N. J.; Brown, D. R.; Weerapana, E., 1,3,5-Triazine as a modular scaffold for covalent inhibitors with streamlined target identification. *J Am Chem Soc* **2013,** *135* (7), 2497-500.
25. Speers, A. E.; Cravatt, B. F., A tandem orthogonal proteolysis strategy for high-content chemical proteomics. *J Am Chem Soc* **2005,** *127* (28), 10018-9.
26. Weerapana, E.; Speers, A. E.; Cravatt, B. F., Tandem orthogonal proteolysis-activity-based protein profiling (TOP-ABPP)--a general method for mapping sites of probe modification in proteomes. *Nat Protoc* **2007,** *2* (6), 1414-25.
27. Eng, J. K.; McCormack, A. L.; Yates, J. R., An approach to correlate tandem mass spectral data of peptides with amino acid sequences in a protein database. *J Am Soc Mass Spectrom* **1994,** *5* (11), 976-89.
28. Crawford, L. A.; Weerapana, E., A tyrosine-reactive irreversible inhibitor for glutathione S-transferase Pi (GSTP1). *Mol Biosyst* **2016,** *12* (6), 1768-71.
29. Nebert, D. W.; Vasiliou, V., Analysis of the glutathione S-transferase (GST) gene family. *Hum Genomics* **2004,** *1* (6), 460-4.
30. Townsend, D. M.; Tew, K. D., The role of glutathione-S-transferase in anti-cancer drug resistance. *Oncogene* **2003,** *22* (47), 7369-75.
31. Schnekenburger, M.; Karius, T.; Diederich, M., Regulation of epigenetic traits of the glutathione S-transferase P1 gene: from detoxification toward cancer prevention and diagnosis. *Front Pharmacol* **2014,** *5*, 170.

CHAPTER 4

INVESTIGATING THE REACTIVITY AND SELECTIVITY OF CHLOROTRIAZINE ELECTROPHILES IN A COMPLEX PROTEOME

4.1 Introduction

The use of the covalent modifications of proteins by small molecules has numerous applications in drug design[1-3], imaging[4], and activity-based protein profiling[5-6]. The modifications on proteins occur at sites of heightened nucleophilicity, which tend to be functional amino acids that play a role in catalysis or the regulation of cellular processes. Activity-based protein profiling (ABPP) is a powerful chemical proteomic technique that relies on potent, selective electrophiles to directly interrogate the functional state of an enzyme or enzyme family in a biological system. To date, may electrophiles have demonstrated high reactivity and functional group specificity including haloacetamides[7-9], α,β-unsaturated ketones[7], and maleimides[9] which have all shown selectivity for cysteine residues. Additional electrophiles have also been discovered which target other nucleophilic residues in the proteome, such as sulfonate esters which react with aspartates, glutamates, and tyrosines[7]; acyl phosphates which has been shown to react with lysines in the kinome[10]; sulfonyl fluorides which react with serines and tyrosines[11-12]; and fluorophosphonates which have been shown to react with nucleophilic serines in serine hydrolases[13]. Many of the aforementioned electrophilic groups demonstrate high reactivity, and as such can react with nucleophilic amino acids in the proteome without the presence of a binding element to position the electrophile on the protein of interest. Other electrophiles, while still reactive enough to modify proteins in a complex proteome, require the presence of a binding motif to facilitate the reaction. These functional groups include epoxysuccinates which covalently bind to cysteine proteases[14]; spiroepoxides, which have been shown to label the glycolytic enzyme, phosphoglycerate mutase[15]; carbamates and β-lactams, which have been used in profiling the serine hydrolase family[16]; acyloxymethyl

ketones, which have been shown to label diverse cysteine proteases[17]; and phenoxymethyl ketones, which have been used in labeling cysteine containing cathepsin proteases[18].

Previous reports from our lab have looked at the reactivity and selectivity of aryl halides in the complex proteome. Shannon *et al*. synthesized a panel of aryl halide electrophiles to investigate proteome reactivity and residue specificity[19]. These studies initially looked at a small subset of chloronitrobenzene (CNB) derivatives, varying the position of the electron withdrawing nitro substituent. As originally hypothesized, the CNB with the nitro in the *para* position had the highest reactivity in the proteome, presumably through the resonance stabilization of the Meisenheimer-complex[20-21]. Shifting the nitro group to the *meta* position destabilizes the Meisenheimer-complex and thus the reactivity of RB1 is completely abrogated. Further investigation of another panel of aryl halides containing a fluoronitrobenzene, chloropyridines, chloropyrimidines, and a dichlorotriazine. Interestingly, the dichlorotriazine electrophile, RB7 (Figure 4.1), demonstrated hyper reactivity in the complex proteome via in-gel fluorescence analysis. RB7 also displayed a unique action in that it was identified to label predominantly lysine residues in the complex proteome by LC/LC-MS/MS analysis, with little cysteine modification[19]. This study was vital in showing that the reactivity of aryl halide compounds that react with proteins through an S_NAR mechanism can be tuned by modulating the electronics of the aromatic ring.

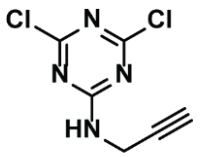

RB7

Figure 4.1. Chemical structure of dichlorotriazine compound, RB7.

Furthering on the unique reactivity of the dichlorotriazine, Crawford *et al*. reported in 2016 on a probe library based on the dichlorotriazine electrophilic motif[22]. A panel of 20 dichlorotriazine-based probes were synthesized each containing a varied diversity element to direct the probe to a different subset of the proteome, as well as an alkyne handle for subsequent reporter tag conjugation via CuAAC. Initial screening of the library in HeLa cell lysates afforded, LAS17, which has an L-leucine methyl ester diversity element, to be potent and selective for a low molecular weight protein. Subsequent identification through proteomic approaches identified the protein target of LAS17 to be glutathione *S*-tranferase Pi (GSTP1)[22]. GSTP1 is the most ubiquitous member of the GST protein superfamily, and is primarily responsible for conjugation glutathione to exogenous electrophiles to detoxify the cellular environment[23]. Owing to the hyper reactivity of the dichlorotriazine electrophilic motif, it was interesting that most of the library member synthesized by Crawford *et al*. seemed to label a low molecular band, assumed to be GSTP1. Therefore, the reactivity of these electrophiles needs to be tuned down so the cell does not target them for deactivation, and this can presumably be done by varying the electron withdrawing (EWG) and electron donating groups (EDG) on the triazine ring to modulate the electronics.

Nucleophilic aromatic substitution (S_NAR) reactions are an important class of synthetic organic reactions and their mechanisms have been well investigated[20-21, 24-25]. The reaction follows a simple, two-step addition-elimination mechanism (Figure 4.2). Simple aryl halide moieties are activated through the placement of strong EWG on the aromatic ring in the *ortho*- or *para*- positions. The presence of the EWG helps to stabilize the Meisenheimer complex, which is a charged reaction intermediate that is formed by the

nucleophilic attack on the aromatic ring. Absence of EWG groups on the aromatic ring prohibit this reaction intermediate from forming, thus inhibiting the reaction from proceeding. Therefore, it can be hypothesized that variation of the EWG on the aromatic ring can tune the reactivity of the electrophile through modulation of the electronics of the ring system. Subsequently, the study of this chapter will be to tune the reactivity of the dichlorotriazine electrophile previously studied in our lab by varying EWG and EDG groups on the triazine ring to modulate the reactivity of the electrophile.

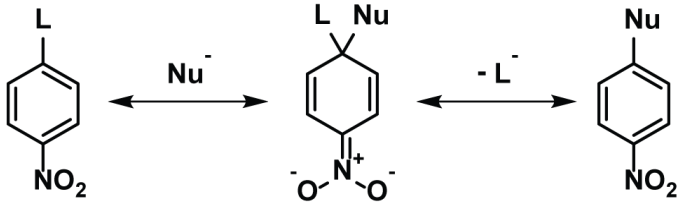

Figure 4.2. The S_NAR reaction mechanism. L = leaving group. Nu = Nucleophile.

4.2 Results and Discussion

4.2.1 Generation of a Library of Chlorotriazine Electrophiles

In a previous study, we identified a dichlorotriazine-based electrophile, RB7, with high proteome reactivity and selectivity towards nucleophilic lysine residues[19]. Currently, the dichlorotriazine electrophile is too reactive to use as a scaffold to target functional residues. In order to optimize the potency and selectivity of RB7 (Figure 4.1), we sought to develop a second generation of chlorotriazine electrophiles. These electrophiles are expected to react via an S_NAR mechanism, whereby the rate limiting step is the formation of the Meisenheimer-complex[20-21]. Therefore, as shown in previous studies by Shannon *et al.*[19], we should be able to tune the reactivity by varying electron withdrawing groups (EWG) and electron donating groups (EDG) in the position of one chlorine atom, thus generating a chlorotriazine electrophile. With this in mind, a second-generation chlorotriazine library was synthesized with EWG and EDG tuning elements in th containing hydrocarbons, branched hydrocarbons, benzyl-functionalized hydrocarbons, amines, functionalized-mercaptans, and functionalized-thiophenols (Figure 4.3). To gain deeper insight into the electronics of the triazine ring of RB7, we enlisted some preliminary computational calculations. Electrostatic potential maps (ESPs) were generated with Gaussian 09[26] to view electron density modulation at the electrophilic carbon position as the EWG/EDG was varied (Figure 4.4). The electron density maps demonstrate by computation that by varying the strength of the EWG and EDG in the para position, we can modulate the electronics of the triazine ring, and therefore should be able to tune the reactivity of the chlorotriazine electrophile based on the “tuning element” chosen.

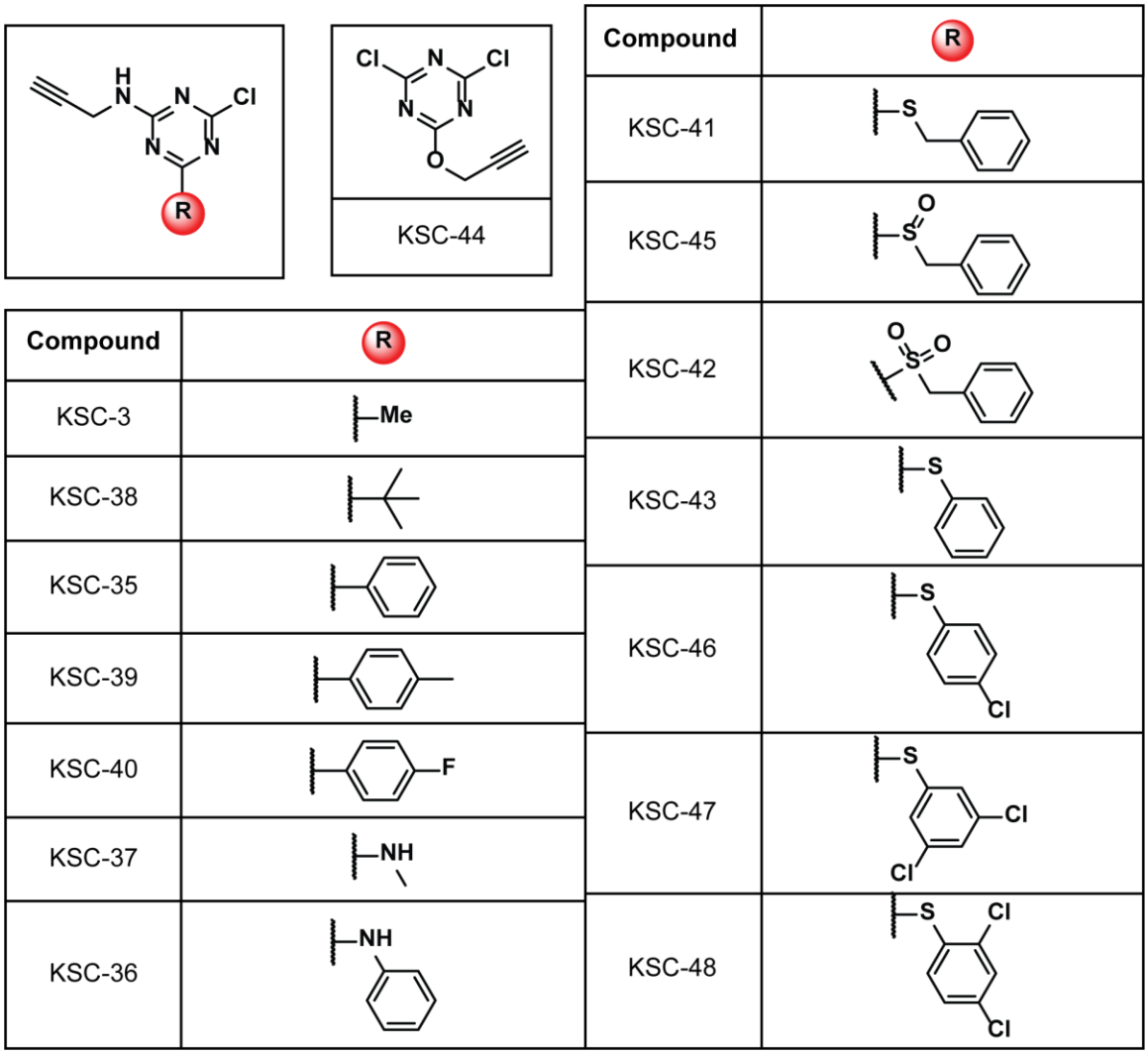

Figure 4.3. Structures of second-generation chlorotriazine electrophiles obtained by varying the tuning element of the triazine ring.

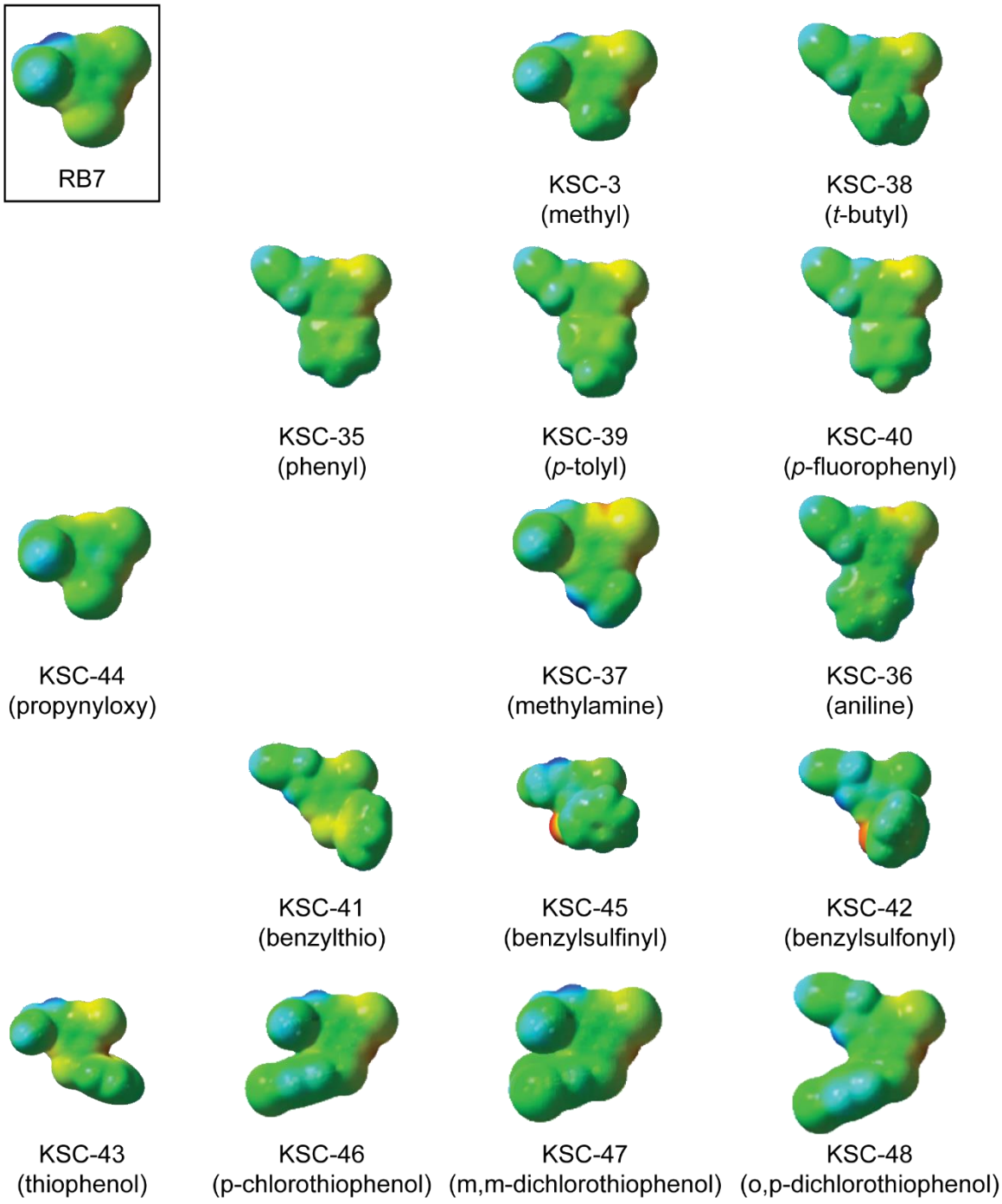

Figure 4.4. Electrostatic potential maps demonstrating effect that electron withdrawing and electron donating groups pose on the electron distribution throughout the triazine-ring system.

4.2.2 Identification of KSC-46 as an Optimized Chlorotriazine Scaffold

To streamline the selection of an optimized electrophilic scaffold, we screened the proteome reactivity of the library of chlorotriazines and RB7 using a gel-based fluorescence screening platform. Briefly, MCF7 cell lysates (2 mg/mL) were incubated with each probe (100 μM) for 1 hour. After incubation, the reactivity of each probe was monitored by appending a tetramethylrhodamine (TAMRA) fluorophore to the alkyne group of each compound using CuAAC[27-28], separating the proteins on SDS-PAGE, and visualizing protein labeling using in-gel fluorescence (Figure 4.5). As indicated by the computational calculations, electrophiles containing tuning elements with alkyl, benzyl, or amino groups did not withdraw enough electron density from the triazine ring, and thus had poor proteome reactivity. As anticipated from the calculations, the sulfur containing tuning elements (KSC-41, 42, 43, 46, 47, 48) had the appropriate range of electron withdrawing ability to tune the reactivity of the electrophile. Furthermore, KSC-46 which contains a *p*-chlorothiophenol tuning element was found to be the optimal electrophile for use as a scaffold.

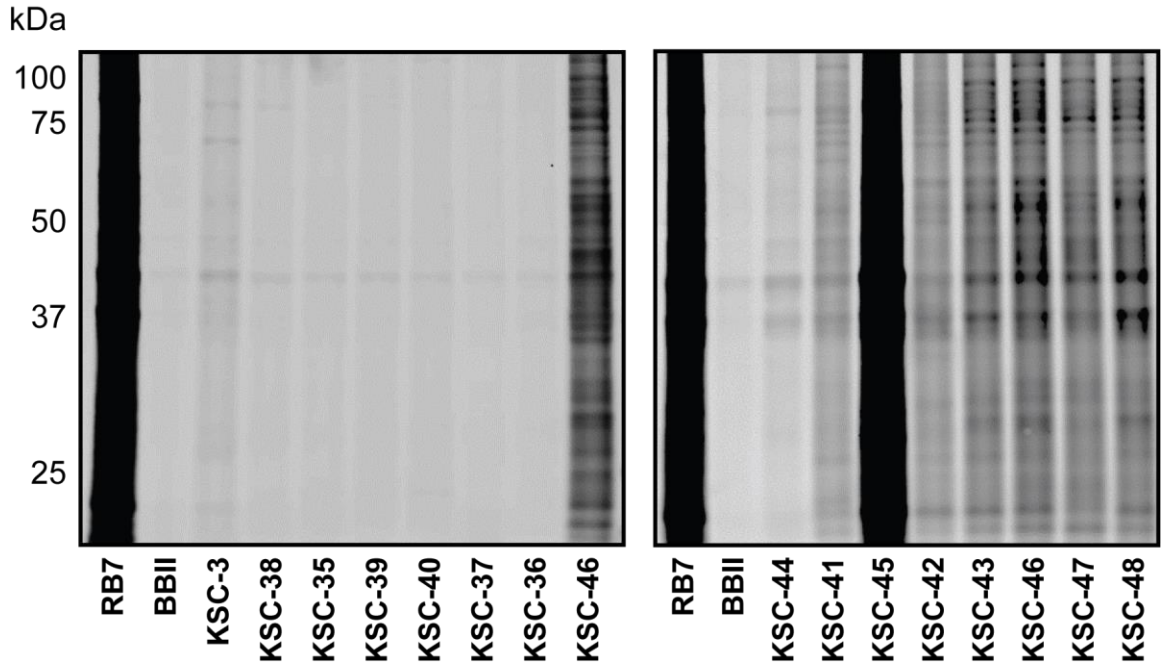

Figure 4.5. Investigating the proteome reactivity of chlorotriazines. The library of chlorotriazine electrophiles were incubated in MCF7 lysates (2 mg/mL) and protein labeling by each library member (100 μM) was evaluated after CuAAC-mediated incorporation of a TAMRA fluorophore, SDS-PAGE, and in-gel fluorescence.

4.2.3 Interrogation of Cysteine Reactivity of KSC-46

Previously, RB7 was found to be extremely potent and selective toward lysine residues. To investigate if KSC-46 maintains this amino acid specificity, we performed a competition assay with a highly know reactive cysteine-specific electrophile, iodoacetamide (IA). KSC-46 was compared to RB7 and also IA≡, a known promiscuous cysteine-reactive electrophile. To achieve this competition, MCF7 lysates were pretreated with IA (0 – 10 mM) for 1 hour, followed by treatment with KSC-46 (100 μM), RB7 (100 μM) or IA≡ (2 μM) for 1 hour (Figure 4.6). As expected, pretreatment with IA completely abrogates labeling of cysteine residues by IA≡ yet does not affect labeling of RB7 which is labeling predominantly lysine residues. Interestingly, KSC-46 labeling initially decreases upon IA pretreatment, indicating KSC-46 covalently binds cysteine residues. However, labeling is not completely abolished until high concentrations of IA. These data thereby indicate that KSC-46 does not selectively label lysine residues like the dichlorotriazines, RB7, and that it binds other nucleophilic residues in the complex proteome.

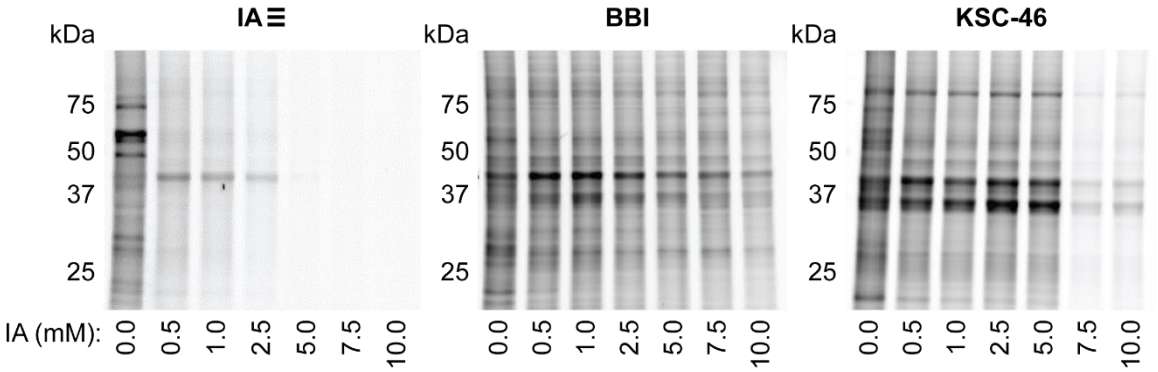

Figure 4.6. Effect of iodoacetamide (IAA) pre-treatment (0-10 mM) prior to labeling with IA≡ (2 μM), BBI (100 μM), and KSC-46 (100 μM). MCF7 lysates (2 mg/mL) were incubated with IA for 1 hour, followed by treatment with each probe and then subhected to CuAAC and in-gel fluorescence analysis to investigate the residue specificity of the new chlorotriazine electrophile.

4.2.4 Generation of a Library of Chlorotriazine Probes using the KSC-46 Electrophilic Scaffold

With the electronics of the triazine ring optimized, using the *p*-chlorothiophenol tuning element to generate KSC-46, we turn to utilize this tuned reactivity through the development of a small-molecule probe library to covalently target functional residues in a complex proteome. Our library of small-molecule probes each contain four distinct elements (Figure 4.7A): (1) a *p*-chlorothiophenol tuning element to optimize the reactivity of the chlorotriazine electrophile, (2) a chlorotriazine reactive group for covalent modification, (3) an alkyne handle for downstream reporter tag conjugation via CuAAC, and (4) varaiable diversity element to direct the probes to different subsets of the proteome. The diversity elements chosen were varied across the library and incorporate a multitude of physicochemical properties to direct the probes to different subsets of the proteome (Figure 4.7B). Detailed information regarding the synthesis of library members can be found in the experimental section (Scheme 4.1, 4.2)

A

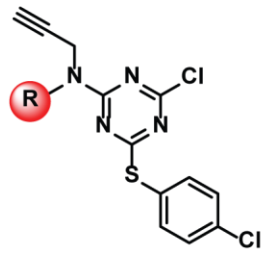

B

Compound	R	Compound	R
KSC-50	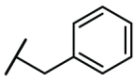	KSC-60	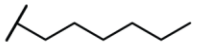
KSC-52	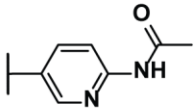	KSC-61	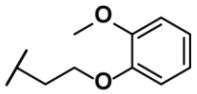
KSC-53	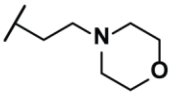	KSC-62	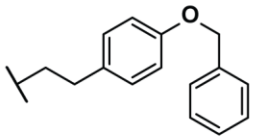
KSC-55	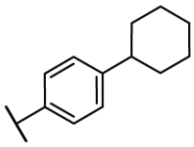	KSC-63	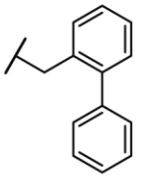
KSC-56	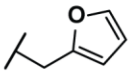	KSC-64	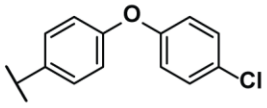
KSC-57	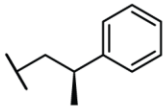	KSC-65	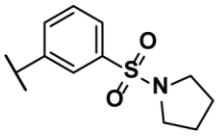
KSC-58	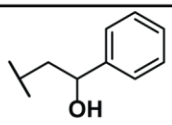	KSC-66	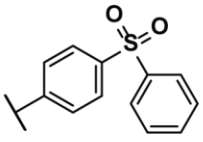
KSC-59	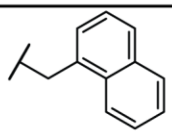		

Figure 4.7. (A) General chemical structure of small-molecule chlorotriazine library. (B) Chemical structures of diversity elements used in di-functionalized, chlorotriazine small-molecule probe library.

4.2.5 Assessing the Potency and Selectivity of Chlorotriazine Library

Our first goal was to assess the reactivity and selectivity of these di-functionalized triazine compounds in MCF7 cell lysates using a gel-based screening platform. Briefly, MCF7 cell lysates (2 mg/mL) were incubated with each probe (10 μM) for 1 hour. After incubation, the reactivity and selectivity of each probe was monitored by appending a TAMRA fluorophore to the alkyne group of each compound using CuAAC, followed by visualization by in-gel fluorescence. This small molecule library demonstrated covalent attachment to target proteins in the complex proteome (Figure 4.8), however, these small-molecules proved to not possess much selectivity *in vitro*. Previous studies have established that the *in* vitro reactivity and selectivity of a given electrophile, is not indicative of the in cell reactivity and selectivity of the electrophile.

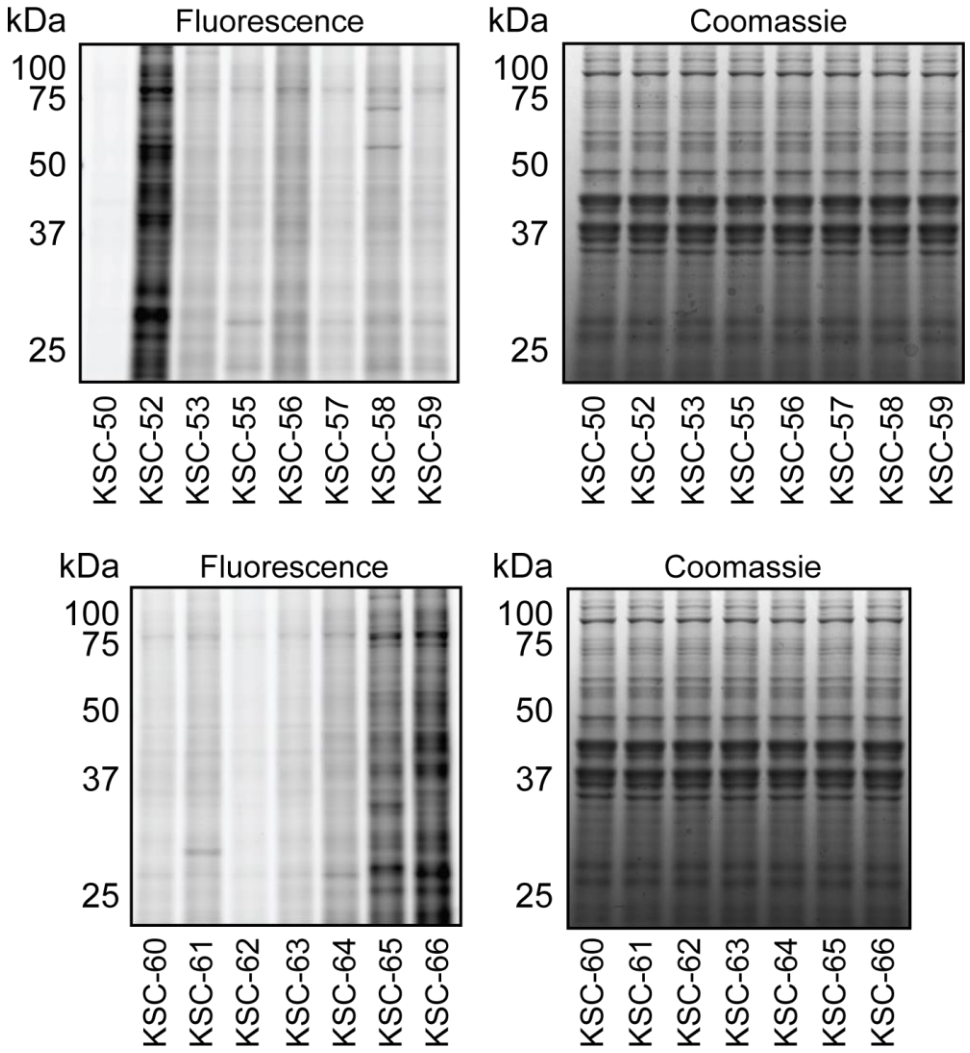

Figure 4.8. Characterization of targeted library of chlorotriazine probes *in vitro*. Library members (20 μM) were incubated with MCF7 cell lysates (2 mg/mL) in PBS, and protein labeling by each compound was evaluated after CuAAC-mediated incorporation of a TAMRA fluorophore, SDS-PAGE, and in-gel fluorescence (Left panels). Coomassie gels shown (right panels) to show equal protein loading on gels.

With this in mind, we next decided to assess to potency, selectivity, and cell permeability of this library *in situ* in MCF7 cells using the same gel-based screening platform. Briefly, MCF7 cells were treated with each probe for 3 hours at 37 °C, followed by in-gel fluorescence analysis (Figure 4.9). KSC-56, which contains a furfurylamine diversity element, demonstrated high selectivity toward a single protein target ~39 kDa. Interestingly, KSC-65, which contains a phenylsulfonylpyrrolidine diversity element, demonstrated high selectivity toward a protein target ~75 kDa. These studies highlight the cell permeability of the chlorotriazine compounds and their ability to selectively target proteins in the complex proteome by varying the diversity element on the electrophilic scaffold.

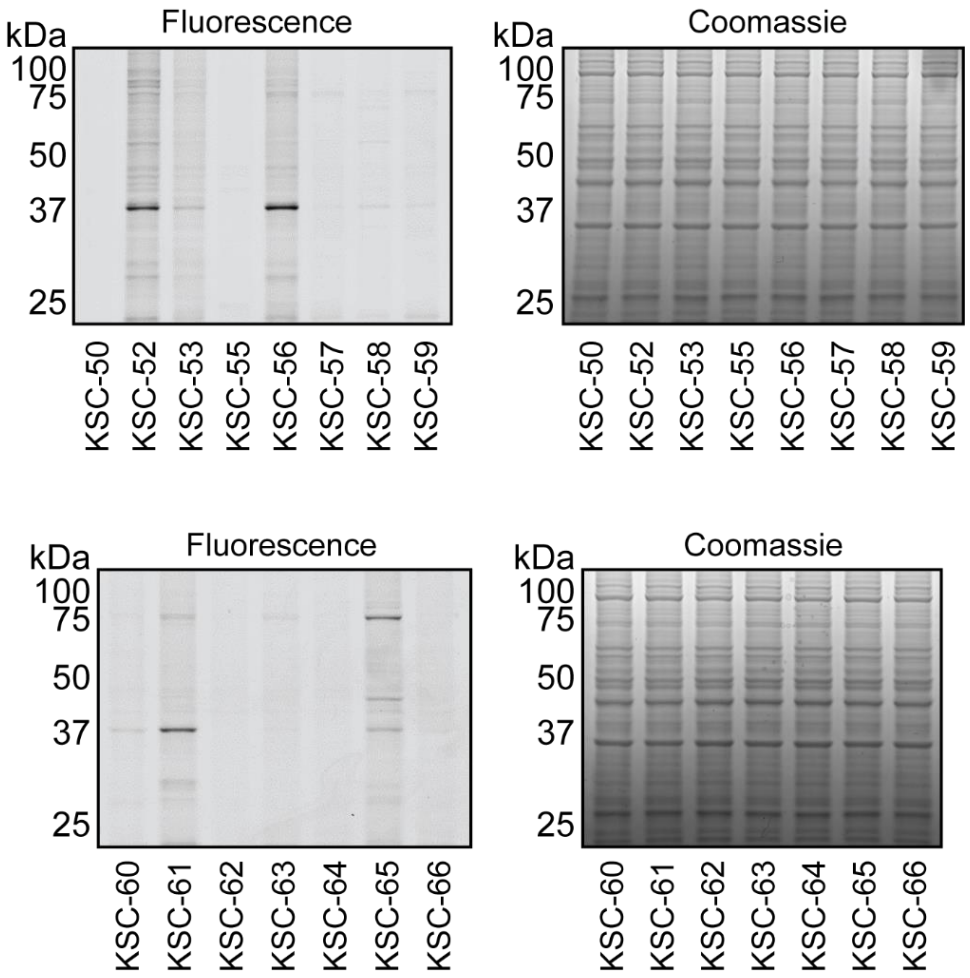

Figure 4.9. Characterization of targeted library of chlorotriazine probes *in situ*. Library members (20 μM) were incubated with MCF7 cells for 3 hours at 37 °C, and protein labeling by each compound was evaluated after in-gel fluorescence analysis(Left panels). Coomassie gels shown (right panels) to show equal protein loading on gels.

4.2.6 Identification of the Protein targets of KSC-56 and KSC-65

We follow up on target identification for these two compounds in our library, KSC-56 and KSC-65, which demonstrated high selectivity toward a single protein target in MCF7 cells. To achieve this, we employed a mass spectrometry-based method in which MCF7 cells were incubated with DMSO, KSC-56 (20 μM), or KSC-65 (20 μM). Upon cell lysis, probe-labeled proteins were then appended to biotin-azide using CuAAC, enriched on streptavidin beads, subjected to on-bead tryptic digestion, and subsequent LC/LC-MS/MS analysis. Spectral counts (number of fragmentation spectra) generated for each protein for the probe-labeled samples were compared to the DMSO control sample (Tables 4-1, 4-2, Appendix Tables 4-1, 4-2). In the KSC-56-treated samples, mass spectrometry studies identified the ~39 kDa target of this probe as glutaredoxin-3 (GLRX3). In the KSC-56-treated samples, an average of ~305 spectral counts were matched to GLRX3 (with an average of ~5 spectral counts in the DMSO control). In the KSC-65-treated samples, mass spectrometry studies identified the ~75 kDa target of this probe as 6-phospofructokinase, platelet type (PFKP). In the KSC-65-treated samples, an average of ~398 spectral counts were matched to PFKP (with an average of ~33 spectral counts in the DMSO control). It is important to note that other proteins in the proteome were enriched by each probe, indicating that these probes merely are lead compounds for further optimization.

Protein	Description	pI	Length(aa)	Mass(Da)	DMSO Avg	KSC56 Avg	Change in Spectral Counts (KSC-56 -DMSO)
GLRX3	GLRX3 Glutaredoxin-3	5.4	335	37432	0	312	312
ACTB	ACTB Actin, cytoplasmic 1	5.5	375	41737	28	188	160
ALDOA	ALDOA Fructose-bisphosphate aldolase A	8.1	364	39420	10	84	74
PCBP1	PCBP1 Poly(rC)-binding protein 1	7.1	356	37498	1	58	57
Uncharacterized	Uncharacterized protein	5.7	379	40447	0	51	51
PCBP2	PCBP2 Poly(rC)-binding protein 2	6.8	365	38580	0	30	30
HMOX2	HMOX2 Heme oxygenase 2	5.4	316	36033	0	29	29
ACTA1	ACTA1 Actin, alpha skeletal muscle	5.4	377	42051	0	28	28
ACTA2	ACTA2 Actin, aortic smooth muscle	5.4	377	42009	0	28	28
GAPDH	GAPDH Glyceraldehyde-3-phosphate dehydrogenase	8.5	335	36053	6	23	17
AIP	AIP AH receptor-interacting protein	6.3	330	37636	0	12	12
CRKL	CRKL Crk-like protein	6.7	303	33777	0	12	12
PRMT1	PRMT1 Protein arginine N-methyltransferase 1	5.4	361	41516	0	11	11
MDH2	MDH2 Malate dehydrogenase, mitochondrial	8.7	338	35503	7	12	6

Table 4.1. Mass Spectrometry data for KSC-56 treated samples. The proteins shown are those that fell within the required molecular weight range of 33-43 kDa and is sorted by the spectral count difference between the KSC-56 treated and the DMSO (no probe) samples. Full data set is displayed in the appendix.

ID	Protein	Description	pI	Length(aa)	Mass(Da)	DMSO Avg	KSC65 Avg	Change in Spectral Counts (KSC-65 - DMSO)
Q01813	PFKP	PFKP 6-phosphofructokinase type C	7.6	784	85596	2	546	545
P08238	HSP90AB1	HSP90AB1 Heat shock protein HSP 90-beta	5	724	83264	11	203	192
P05165	PCCA	PCCA Propionyl-CoA carboxylase alpha chain, mit	7.5	728	80059	94	264	170
Q96RQ3	MCCC1	MCCC1 Methylcrotonoyl-CoA carboxylase subuni	7.8	725	80473	157	321	164
P07900	HSP90AA1	HSP90AA1 Heat shock protein HSP 90-alpha	5	732	84660	7	153	146
P13639	EEF2	EEF2 Elongation factor 2	6.8	858	95338	17	81	64
P17858	PFKL	PFKL 6-phosphofructokinase, liver type	7.5	780	85018	3	55	52
P14625	HSP90B1	HSP90B1 Endoplasmin	4.8	803	92469	4	23	19
P34932	HSPA4	HSPA4 Heat shock 70 kDa protein 4	5.2	840	94331	3	10	7

Table 4.2. Mass Spectrometry data for KSC-65 treated samples. The proteins shown are those that fell within the required molecular weight range of 75-95 kDa and is sorted by the spectral count difference between the KSC-65 treated and the DMSO (no probe) samples. Full data set is displayed in the appendix.

4.2.7 Glutaredoxin 3

Cells contain hundreds of proteins that require iron cofactors for activity in the form of heme iron-sulfur (Fe/S) clusters, and ferrous/ferric ions, yet the pathways that distribute these cofactors remain incompletely defined[29]. Recent studies in both baker's yeast and in vertebrates demonstrate that there are many proteins involved in the biogenesis and cellular distribution cytosolic Fe/S clusters[30-31]. One class of proteins has been implicated in the trafficking of both Fe/S clusters and Fe ions in the cell, the monothiol glutaredoxins (Grxs)[32-36]. Two different classes of Grxs have been identified, dithiol (–CPYC–) and monothiol (–CGFS–)[37]. Dithiol Grxs have been shown to reduce protein disulfides and mixed-disulfides with glutathione, regulating protein function function[37]. The functions of monothiol Grxs hasn't been as well characterized. Although monothiol Grxs contain the functional residues necessary to catalyze the reduction of mixed disulfide bonds between GSH and substrate proteins, most of them lack this enzymatic activity entirely[38].

Monothiol Grxs can be further categorized into two sub-groups, single domain monothiols Grxs and multidomain monothiol Grxs. Single domain monothiol Grxs consist of only one Grx domain. Multidomain monothiol Grxs consist of one N-terminal thioredoxin (Trx)-like domain and one to three C-terminal monothiol Grx domains[37, 39]. In humans, two monothiol Grxs are present, GLRX3 and GLRX5[40]. GLRX5 is located in the mitochondria and acts as a [2Fe-2S] cluster transfer protein in the ISC machinery[41]. GLRX3, located in the cytoplasm, consists of three domains: one N-terminal Trx-like domains and two C-terminal Grx domains, each of which are able to bind a glutathione-coordinated [2Fe-2S] cluster via dimerization[29, 40, 42].

Recent interest in the biochemical characterization of GLRX3 has demonstrated that GLRX3-deficient human cells show a severe dysregulation of cytosolic iron metabolism through iron-regulatory protein 1 (IRP1), which in turn up-regulated the expression of the iron importer, transferrin receptor (TfR), and down-regulated the expression of the iron storage protein, ferritin[43]. In another study, Banci *et al*. demonstrated that GLRX3 can have a functional role in cytosolic [2Fe-2S] cluster trafficking through the transfer of clusters to its binding partner anamorsin, (CIAPIN-1)[42]. It was also demonstrated through electron paramagnetic resonance studies (EPR) and chemical shift perturbation assays that the association between the two partner proteins occurs between the N-terminal domains, and that the transfer mechanism was facilitated by a protein-protein complex between the N-terminal domains[42]. Furthermore, Frey *et al*. demonstrated that GLRX3 and BolA-like protein 2 (BOLA2) form a complex in human cells which is dependent upon the bridging of a coordinating [2Fe-2S] cluster[29]. Studies indicates that GLRX3-[2Fe-2S]-BOLA2 complexes can serves as a rapidly expandable pool of Fe/S clusters, based on cellular iron availability. Finally, Fe/S coordination by GLRX3-BOLA2 did not depend on anamorsin, alternatively the GLRX3-BOL2 bound anamorsin and facilitated Fe/S transfer which demonstrate the chaperone ability of the GLRX3-BOLA2 complex[29].

Initially, GLRX3 was described as an interacting partner of protein kinase C-Θ (PKCΘ). In T cells, GLRX3 inhibited the activiation of c-Jun N-terminal kinase and subsequently the activation of transcription factors AP-1 and Nf-κB[44]. Further investigation between GLRX3 signal transduction and iron availability is needed to demonstrate therapeutic potential. Clinically, GLRX3 has been found to be upregulated in

animal models of cardiac hypertrophy, and the overexpression of GLRX3 protected from cardiac hypertrophy[45-46]. Heterozygous $Grx^{+/-}$ mice are much more predisposed to developing cardiac hypertrophy than homozygous $Grx^{+/+}$ mice[45]. Interestingly, GLRX3 has also proven essential for embryonic development in mice. Homozygous $Grx^{-/-}$ mice die between embryonic days (ED) 12.5 and 14.5[45]. It is worth noting that ED 12.5 indicates the beginning of erythropoiesis in the fetal liver[43].

4.2.8 Phosphofructokinase-1

6-phosphofructo-1-kinase (PFK-1) is the key rate-limiting regulatory enzyme of glycolysis which catalyzes the phosphorylation of fructose 6-phosphate (F6P) to fructose-1,6-bisphosphate (F1,6BP)[47]. Localizing at the beginning of the glycolytic pathway and catalyzing an irreversible, adenosine triphosphate (ATP)-dependent reaction make this enzyme a key regulator. In mammalian cells, PFK-1 exists in three isoforms: muscle (PFKM), liver (PFKL), and platelet (PFKP)[48]. The genes for each isoform are located on different chromosomes and display tissue specific expression. Interestingly, in muscle tissue only PFKM is present, but in all other tissues, all three isoforms are present in tissue specific ratios[48]. PFK-1 activity is finely regulated by more than 20 allosteric regulators including adenine nucleotides, cyclic adenosine monophosphate (cAMP), citrate, acyl-CoA, F1,6BP, and glucose-1,6-bisphosphate (G1,6BP). The most potent modulator of PFK-1 activity is ATP, which directly inhibits PFK-1 in order to cause negative feedback when cellular energy is abundant[49]. In 1980, fructose-2,6-bisphosphate (F2,6BP) was discovered as an allosteric activator of PFK-1[50]. F2,6BP allosterically activates PFK-1 by inducing a conformational equilibrium shift from a low affinity state to a high affinity state

for its substrate, F6P[50]. F2,6BP can relieve inhibition of PFK-1 by ATP, thus allowing cells to maintain a high glycolytic flux even in elevated physiological concentrations of ATP[51].

Recent biochemical characterization has demonstrated that PFK-1 assembles into a tetrameric structure in a concentration- and ligand-dependent manner. Furthermore, allosteric activators of PFK-1 have been shown to promote the formation of the tetrameric complex, whereas allosteric inhibitors favor the formation of an inactive dimeric form[52-53]. Recent studies by Webb *et al*, have demonstrated through site-directed-mutagenesis that PFKP-F649L particles form dimers, and lose ~98% of the catalytic activity compared to the WT PFKP, which forms a tertrameric complex[54]. Crystal structures of the two complexes suggest that an electrostatic interaction between R613 of one subunit and E657 of the adjacent subunit are important for the enzymatic function. This salt bridge was only present in WT PFKP tetramers and not in the PFKP-F649L dimers[54].

Cancer cells rely on aerobic glycolysis to provide the energy and building blocks required to support the rapid proliferation[55]. Accordingly, PFK-1 activity has been demonstrated to be increased in a variety of cancers and primary tumors[56], and the expression of PFK-1 has been shown to be upregulated in breast[57] and liver[57] cancers. Due to this role of PFK-1 upregulation in cancer metabolism, it has since become a target for therapeutic intervention, albeit by indirectly targeting the bifunctional enzyme, 6-phosphofructo-2-kinase/fructose-2,6-bisphosphatase-3 (PFKFB3)[58]. PFKBF3 posseses both kinase and phosphatase functionality, and it is responsible for converting F6P to F2,6PBP, the major allosteric activator of PFK-1[47]. Therefore, targeting PFKFB3 could significantly inhibit the glycotlytic pathway. To this end, there have been many advances in the design and development of PFKFB3 inhibitors with IC_{50} values in the low nanomolar

range. These derivatives include a variety of different classes of compounds including benzopyrans, naphthalene, heteroaryl and bisarylsulfonamides, and pyridinyl derivatives (Figure 4.10)[59-65]. To date, no selective, direct inhibitors of PFK-1 have been reported.

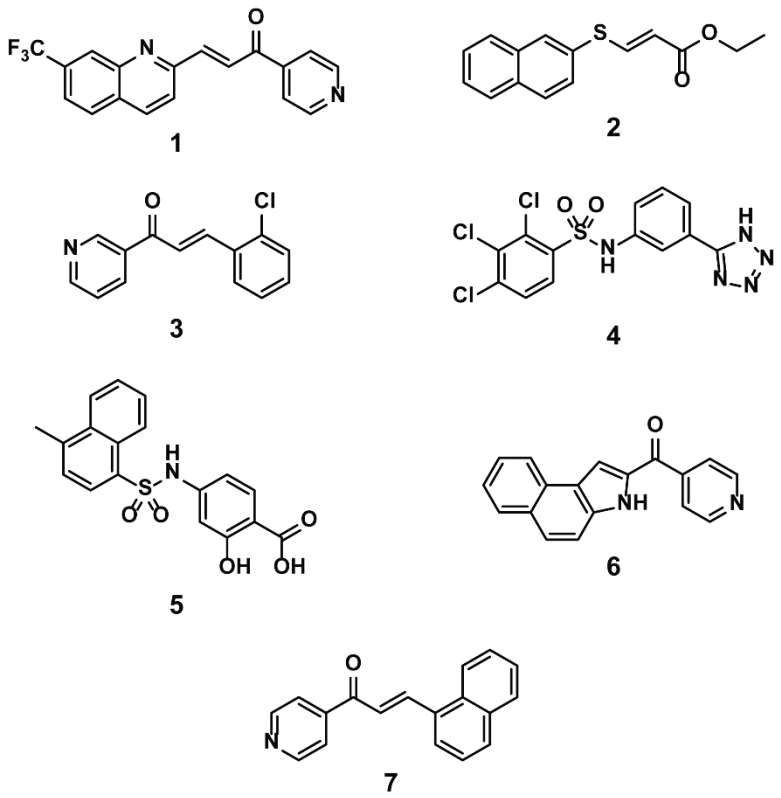

Figure 4.10. General chemical structures of some classes of PFKFB3 inhibitors.

4.2.9 Validation of GLRX3 as the Protein Target of KSC-56 and Identification of the Site-of-Labeling

In order to verify the protein target of KSC-56 identified by mass spectrometry, GLRX3, we overexpressed the wild-type form of the protein with a C-terminal FLAG-tag using transient transfection in HEK293T cells using pcDNA3.1(+). Briefly, HEK293T cells overexpressing GLRX3 were treated with DMSO or KSC-56 (20 μM) for 3 hours at 37 °C. Following cell lysis, a fluorophore was appended to probe-labeled proteins via CuAAC and visualized with in-gel fluorescence. The presence of a fluorescent band in the GLRX3-FLAG overexpressed sample, which is absent in the mock-transfected control confirms that GLRX3 is the protein target of KSC-56. The overexpression of GLRX3-FLAG was confirmed by western blot with an anti-FLAG antibody (Cell Signaling Technologies) (Figure 4.11A).

In an effort to elucidate the site of labeling of GLRX3 by KSC-56, the two nucleophilic cysteine residues in the Grx domains (Cys159 and Cys261) were mutated to serine residue to afford GLRX3 mutants C159S and C261S. HEK293T cells overexpressing GLRX3 WT, C159S, or C261S were treated with DMSO or KSC-56 (20 μM) for 3 hours at 37 °C. Following cell lysis, a fluorophore was appended to probe-labeled proteins via CuAAC and visualized with in-gel fluorescence. The presence of a robust fluorescent band in the GLRX3 WT and C159S samples indicate that KSC-56 is labeling these proteins, and clearly not targeting Cys159 in the first Grx domain of GLRX3 (Figure 4.11B). However, a clear loss of fluorescence labeling in the GLRX3 C261S sample indicate that KSC-56 is in targeting the second Grx domain and covalently binding C261 of GLRX3.

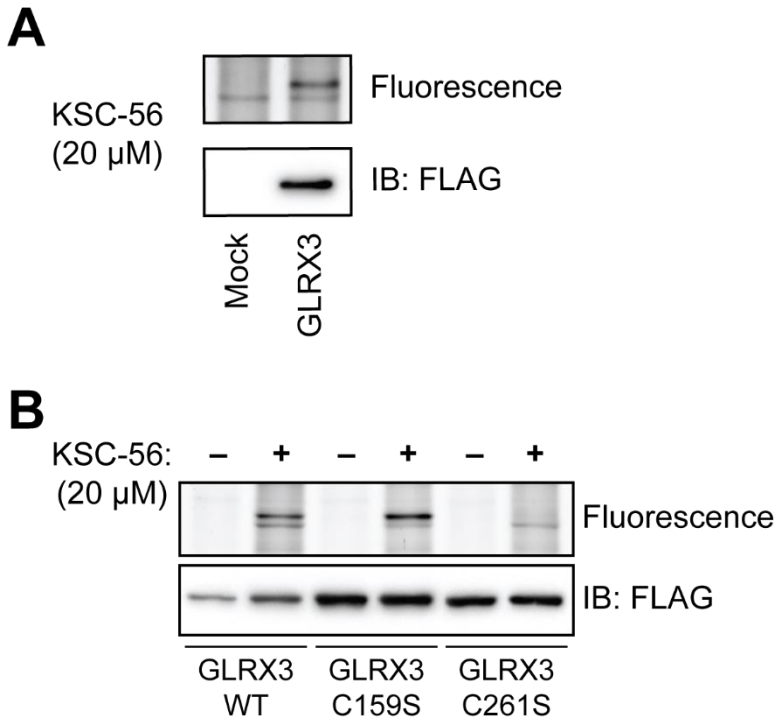

Figure 4.11. (A) GLRX3 was overexpressed in HEK293T cells via transient transfection using pcDNA3.1(+). Cells were subsequently treated with KSC-56 (20 μM) for 3 hours at 37 °C, following analysis by in-gel fluorescence. Overexpression of GLRX3 was confirmed by anti-FLAG western blot. (B) GLRX3 WT, C159S, and C261S were overexpressed in HEK293T cells via transient transfection using pcDNA3.1(+). Cells were subsequently treated with KSC-56 (20 μM) for 3 hours at 37 °C, following analysis by in-gel fluorescence. Overexpression of GLRX3 was confirmed by anti-FLAG western blot.

4.2.10 Validation of PFKP as the Protein Target of KSC-65 and Identification of the Site-of-Labeling

In order to verify the protein target of KSC-65 identified by mass spectrometry, PFKP, we overexpressed the wild-type form of the protein with a C-terminal FLAG-tag using transient transfection in HEK293T cells using pcDNA3.1(+). Briefly, HEK293T cells overexpressing PFKP were treated with DMSO or KSC-65 (20 μM) for 3 hours at 37 °C. Following cell lysis, a fluorophore was appended to probe-labeled proteins via CuAAC and visualized with in-gel fluorescence. The presence of a fluorescent band in the PFKP-FLAG overexpressed sample, which is absent in the mock-transfected control confirms that PFKP is the protein target of KSC-56. The overexpression of PFKP was confirmed by western blot with an anti-FLAG antibody (Figure 4.12A).

Previous work in the Weerapana lab by Alex Shannon identified five reactive cysteine residues on PFKP: Cys179, Cys360, Cys411, Cys529, and Cys641. In an effort to identify the site of labeling on PFKP by KSC-65, four of the five reactive cysteine residues (Cys179, Cys411, Cys529, and Cys641) were mutated to serine residue to afford the PFKP mutants C179S, C411S, C529S, and C641S. HEK293T cells overexpressing PFKP C179S, C411S, C529S, and C641S were treated with DMSO or KSC-65 (20 μM) for 3 hours at 37 °C. Following cell lysis, a fluorophore was appended to probe-labeled proteins via CuAAC and visualized with in-gel fluorescence. The presence of a robust fluorescent band in each of the PFKP transfected samples treated with probe that KSC-565 is not targeting any of these four previously identified reactive cysteine residues (Figure 4.12B). Future work will initially need focused on the identification of the site-of-labeling of KSC-65 on PFKP as there are a total of 15 cysteine residues in total on PFKP.

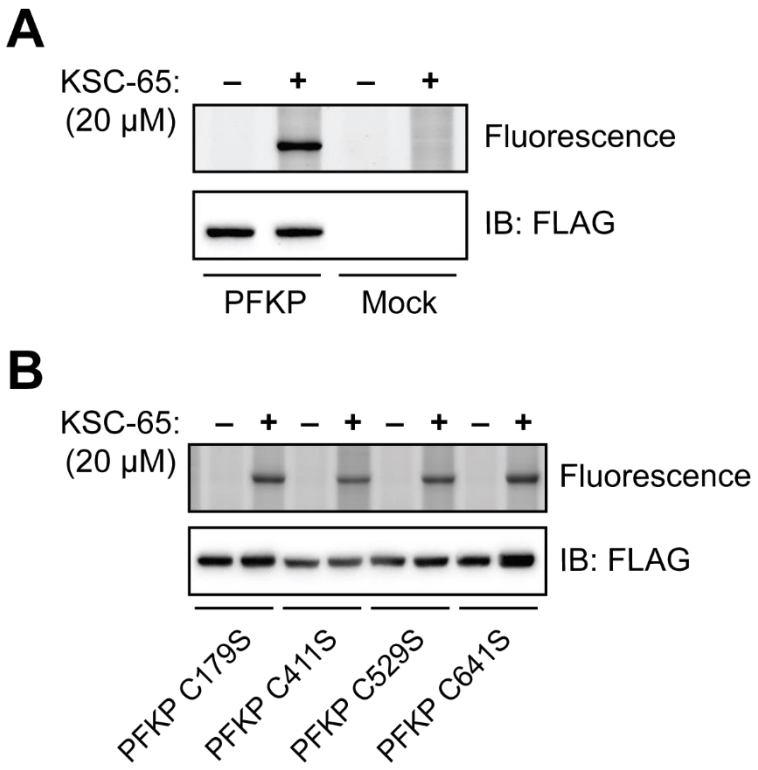

Figure 4.12. (A) PFKP was overexpressed in HEK293T cells via transient transfection using pcDNA3.1(+). Cells were subsequently treated with KSC-65 (20 μM) for 3 hours at 37 °C, following analysis by in-gel fluorescence. Overexpression of PFKP was confirmed by anti-FLAG western blot. (B) PFKP C179S, C411S, C529S, and C641S were overexpressed in HEK293T cells via transient transfection using pcDNA3.1(+). Cells were subsequently treated with KSC-65 (20 μM) for 3 hours at 37 °C, following analysis by in-gel fluorescence. Overexpression of PFKP was confirmed by anti-FLAG western blot.

4.3 Conclusion

In summary, we report the discovery and characterization of a class on chlorotriazine-based electrophiles in which the reactivities are tuned by varying the EWG and EDG 'tuning elements' to modulate the electronics of the triazine ring system. KSC-46, which contains a *p*-chlorothiophenol tuning element for optimized reactivity in the complex proteome. KSC-46 demonstrated a unique reactivity profile, in an IA competition based assay, demonstrates that KSC-46 preferentially binds nucleophilic cysteine residues, but also labels other nucleophilic residues in the proteome as well. KSC-46 and the other second generation library members also contain a biorthogonal alkyne handle, which facilitated the rapid screening of this library of electrophiles *in vitro* and in live cells. Furthering on this, a library of small-molecule probes utilizing the *p*-chlorothiophenol tuning element was synthesized with varying directing groups to direct the library to different subsets of the proteome. Screening of this library *in situ* afforded two compounds, KSC-56 which contains a furfurylamine diversity element and KSC-65 which contains a phenylsulfonylpyrrolidine diversity element, that selectively target proteins in the complex proteome. Identification of these protein targets by LC/LC-MS/MS revealed the target of KSC-56 is glutaredoxin 3 (GLRX3) and the target of KSC-65 is 6-phosphofructo-1-kinase (PFKP). Overexpression of each target in HEK239T cells via transient transfection and subsequent labeling with each probe confirmed the target identification provided by the mass spectrometry studies. Mutation of the two nucleophilic cysteine residues in the Grx domains of GLRX3 followed by subsequent labeling with KSC-56 identified the site-of-labeling of the probe was Cys261 in the C-terminal Grx domain. In the future it will be interesting to use KSC_56 to modulate the ability of GLRX3 to transfer Fe/S cluster to

partner proteins and in turn interrogate the effect on cysteine reacitivity on a global scale. Previous work in the Weerapana lab identified five reactive cysteine residues on PFKP. Following up on four of the five cysteine through site directed mutation revealed that none of the four cysteines investigated were the site-of-labeling of KSC-65. Future work with PFKP will begin with identification of the site-of-labeling of the probe. Also, in collaboration with the Nomura lab at UC Berkeley, we are investigating PFKP inhibition through polar metabolomics studies and isotope tracing, focused around glycolytic intermediates.

4.4 Materials and Methods

4.4.1 General Information

All materials were obtained from Sigma-Aldrich, Fisher Scientific, Combi-Blocks, or Oakwood Chemicals, unless otherwise noted. Phosphate buffered saline (PBS) buffer, RPMI 1640 media, Trypsin-EDTA and Anti-Anti were purchased from Fisher Scientific (Pittsburgh, PA). Fetal bovine serum was purchased from Atlanta Biologicals (Flowery Branch, GA). All protein concentrations were determined using the DC Protein Assay kit from Bio-Rad (Hercules, CA). Analytical thin layer chromatography (TLC) was performed on EMD Millipore F_{254} glass-backed TLC plates (250 µm, Billerica, MA). All compounds were visualized on TLC under UV light and by potassium permanganate staining. Column chromatography was carried out using forced flow of solvent on Sorbent Technologies (Norcross, GA) standard grade silica gel, 40-63 µm particle size, 60 Å pore size. Proton and carbon NMR spectra were carried out on Varian (Palo Alto,

CA) 500 MHz and 600 MHz NMR spectrometers. Chemical shifts (δ) are reported in parts per million (ppm) with chemical shifts reported to internal standards: $CDCl_3$ (7.26 ppm for ^1H, 77.23 ppm for ^{13}C), $(CD_3)_2CO$ (2.05 ppm for ^1H, 29.92 ppm for ^{13}C), CD_3OD (3.31 ppm for ^1H, 49.15 ppm for ^{13}C). Coupling constants (*J*) are reported in Hertz (Hz) and multiplicities are abbreviated as singlet (s), doublet (d), triplet (t), multiplet (m), doublet of doublets (dd), and doublet of triplets (dt). High resolution Mass Spectra (HRMS) were obtained at the Mass Spectrometry Facility at Boston College (Chestnut Hill, MA).

4.4.2 Cell culture and preparation of MCF-7 cell lysates

MCF-7 cells were cultured at 37 °C under an atmosphere of 5% CO_2 in RPMI 1640 media (Corning) supplemented with 10% fetal bovine serum (FBS, Atlanta Biologicals) and 25 μg/mL of Amphotericin B, 10,000 units/mL of penicillin, and 10,000 μg/mL streptomycin (Gibco Anti-Anti). The cells were then harvested and the pellets washed with phosphate buffered saline (PBS). After washing, the pellets were resuspended in an appropriate amount of PBS and then sonicated with an ultrasonic tip sonicator (Cole Parmer, Vernon Hills, IL). The lysates were separated by centrifugation at 45,000 rpm for 45 minutes at 4 °C to obtain soluble and insoluble lysate fractions. The soluble fraction was collected and the pellet discarded. Protein concentrations were determined using the DC Protein Assay kit (Bio-Rad, Hercules, CA).

4.4.3 Fluorescent Gel Analysis

MCF-7 cell lysates (50 µL, 2 mg mL^{-1}) in PBS were treated with probe (1 µL of 50x stock in DMSO) for one hour. Rhodamine-azide (Click Chemistry Tools) was then appended to probe labeled proteins via CuAAC; Rhodamine-azide (25 µM, 100x stock in DMSO), TCEP (1 mM, 50x stock in water), TBTA (100 µM, 17x stock in t-BuOH:DMSO 4:1), and copper (II) sulfate (1 mM, 50x stock in water) were added to the cell lysate. Samples were then incubated at room temperature for one hour to allow for the cycloaddition reaction to occur. An equal volume of SDS-PAGE loading buffer (2x, reducing) was added to each reaction and 20 µL of this solution was separated on a 10% SDS-PAGE gel. Gels were visualized for rhodamine fluorescence on a ChemiDoc MP imaging system (BioRad, Hercules, CA). Gels were then coomassie stained following a standard procedure and visualized on the same imager.

4.4.4 *In situ* labeling experiments

MCF-7 cells were grown to ~90% confluence in 10 cm tissue culture plates. Growth media was removed and replaced with 5 mL RPMI. Probes in an appropriate DMSO stock was then added to the media to achieve the desired labeling concentration and incubated at 37 °C under an atmosphere of 5% CO_2 for 3 hours. Cells were then harvested and were then prepared as lysates as described above.

4.4.5 KSC-56 or KSC-65 Mass Spectrometry Sample Preparation and Data Analysis

MCF-7 cells were grown to ~90% confluence in 15 cm tissue culture plates. Growth media was removed and replaced with 10 mL RPMI. KSC-56 or KSC-65 (10 µL, 1000x stock) or DMSO was then added to the media to achieve the desired labeling concentration

and incubated at 37 °C under an atmosphere of 5% CO_2 for 3 hours. Cells were then harvested and were then prepared as lysates as described above.

Probe-labeled MCF-7 cell lysates (500 µL, 2 mg mL-1) in PBS were subjected to CuAAC. Biotin azide (200 µM from 100x stock in DMSO), TCEP (1 mM, 50x stock in water), TBTA (100 µM, 17x stock in t-BuOH:DMSO 4:1), and copper (II) sulfate (1 mM, 50x stock in water) were added to the cell lysate. Samples were incubated at room temperature for 1 hour to allow for the cycloaddition reaction to occur. Samples were then centrifuged for 10 minutes at 4 °C to pellet the precipitated proteins. Protein pellets were then resuspended in cold methanol by tip sonication followed by centrifugation. Following a second methanol wash, pelleted proteins were solubilized in a 1.2% SDS/PBS solution via tip sonication and incubation at 85 °C for 5 minutes. Samples were then diluted with 5 mL PBS to lower the concentration of SDS to 0.2%. Next, samples were incubated with 100 µL streptavidin agarose beads (Thermo Fisher Scientific, Waltham, MA) at 4 °C for 16 hours. Samples were then washed with 0.2% SDS/PBS (5 mL), PBS (3 x 5 mL), and water (3 x 5 mL). The streptavidin agarose beads were pelleted between each wash step by centrifugation (1,400 g, 3 minutes).

The beads were suspended in a solution of 6 M Urea/PBS (500 µL) and 10 mM dithiothreitol (DTT, 20x stock in water), followed by incubation at 65 °C for 20 minutes. Next, iodoacetamide (20 mM, from 50x stock in water) was added to each sample and incubated at room temperature for 30 minutes. The beads were pelleted (1,400 g, 3 minutes) and resuspended in 200 µL of 2 M Urea/PBS, 1 mM CaCl2 (100x stock in water), and 2 µg trypsin (Promega, Madison, WI). On-bead trypsin digestion was allowed to proceed overnight at 37 °C with agitation. The beads were pelleted (1,400 g, 3 min) and the

supernatant collected. The beads were washed with water (2 x 50 µL) and the washes were combined with the supernatant. Formic acid (15 µL, Thermo Fisher Scientific, Waltham, MA) was then added to each sample and the samples were stored at -20 °C until mass spectrometry analysis.

LC/LC-MS/MS analysis was performed on an LTQ Orbitrap Discovery mass spectrometer (Thermo Fisher Scientific, Waltham, MA) coupled to an Agilent 1200 series HPLC (Agilent Technologies, Santa Clara, CA). Tryptic digests were pressure loaded onto a 250 µm fused silica desalting column packed with 4 cm of Aqua C18 reversed phase resin (Phenomenex, Torrance, CA). Peptides were then eluted onto a biphasic 100 µm fused silica column with a 5 µm tip, packed with 10 cm of C18 and 4 cm of Partisphere SCX (Whatman, Pittsburgh, PA). Elution of the peptides from the desalting column into the biphasic column occurred using a gradient of 5-100% Buffer B in Buffer A (Buffer A: 95% water, 5% acetonitrile, 0.1% formic acid; Buffer B: 20% water, 80% acetonitrile, 0.1% formic acid). The peptides were eluted from the SCX onto the C18 resin and then into the mass spectrometer using four salt pushes[66]. The flow rate of buffer through the fused silica column was set to 0.25 µL min^{-1} and the spray voltage was set 2.75 kV. One full MS scan (400 – 1800 MW) was followed by 8 data dependent scans of the n^{th} most intense ions with dynamic exclusion enabled.

Two biological replicates each of KSC-56 (5 µM), KSC-65 (5 µM), or DMSO treated MCF-7 cells were subjected to LC/LC-MS/MS analysis as outlined above. The generated tandem MS data was searched using the SEQUEST algorithm against the human UniProt database. A static modification of +57.0215 on cysteine was added to account for alkylation of cysteine residues with iodoacetamide. The SEQUEST output files were then

filtered using DTASelect v2.0 to generate a list of proteins identified with a false-discovery rate of < 5%. The resulting peptides were then further filtered to display proteins identified in KSC-34 treated samples with an average of 10 spectral counts or greater across the biological replicates. For each of these proteins, the change in spectral counts between probe-treated samples and DMSO samples was calculated and the data was ranked by those proteins displaying the highest change in spectral counts in the probe-treated samples relative to the DMSO treated samples.

4.4.6 Cloning

The cDNA for GLRX3 and PFKP were obtained from GE Life Sciences. The genes were subcloned into a pcDNA3.1(+) mammalian expression vector. The constructur for subcloning into the vector was generated by polymerase chain reaction (PCR) from the corresponding cDNA using the following primers:

GLRX3-WT-FLAG pcDNA3.1 (+): Forward - 5' ATCCAAGCTCGGATCCACCATGGCGGCGGGGGC 3'; Reverse with FLAG - 5' CGGCCAGCGGGTTTAAACTCACTTGTCGTCATCGTCTTTGTAGTCATTTTCTCC TCTCAGTA 3'

PFKP-WT-FLAG pcDNA3.1 (+): Forward - 5' ATCCAAGCTCGGATCCACCATGGACGCGGACGACTCCCG 3'; Reverse - 5' ATATTAGCGGGTTTAAACTCACTTGTCGTCATCGTCTTTGTAGTCGACACTCC AGGGCTGCACAT 3'.

Site directed mutagenesis was performed to obtain the cysteine to serine mutants used in the site-of-labeling experiments, using the following primers:

GLRX3-C159S-FLAG pcDNA3.1 (+): Forward - 5' CGGTTTCAGCAAGCAGATGG 3'; Reverse - 5' CTGCGTGGTTCTTGAGGAGTTC 3'

GLRX3-C261S-FLAG pcDNA3.1 (+): Forward - 5' CGGATTCAGCAAACAAATTCTG 3'; Reverse - 5' CTTTTTGCTTCCTGTTTGTTTCC 3'

PFKP-C179S-FLAG pcDNA3.1 (+): Forward - 5' CGGCACCGACATGACC 3'; Reverse - 5' CTGAAATCATTGTCGATGGAGC 3'

PFKP-C411S-FLAG pcDNA3.1 (+): Forward - 5' CAACGTAGCTGTCATCAACGTG 3'; Reverse - 5' CTATTGGTCTTTGGGATCTGATCA 3'

PFKP-C529S-FLAG pcDNA3.1 (+): Forward - 5' CGTCCCCATGGTCATGG 3'; Reverse - 5' CTGAACTCCTCGTGCTTCTCC 3'

PFKP-C641S-FLAG pcDNA3.1 (+): Forward - 5' CAGTGAAAACTACACCACCGACTT 3'; Reverse - 5' CTGCTCTCATTTCTGAGCACAAG 3'. All constructs were verified

by DNA sequencing (Genewiz, Cambridge, MA).

4.4.7 Synthetic Methods and Characterization

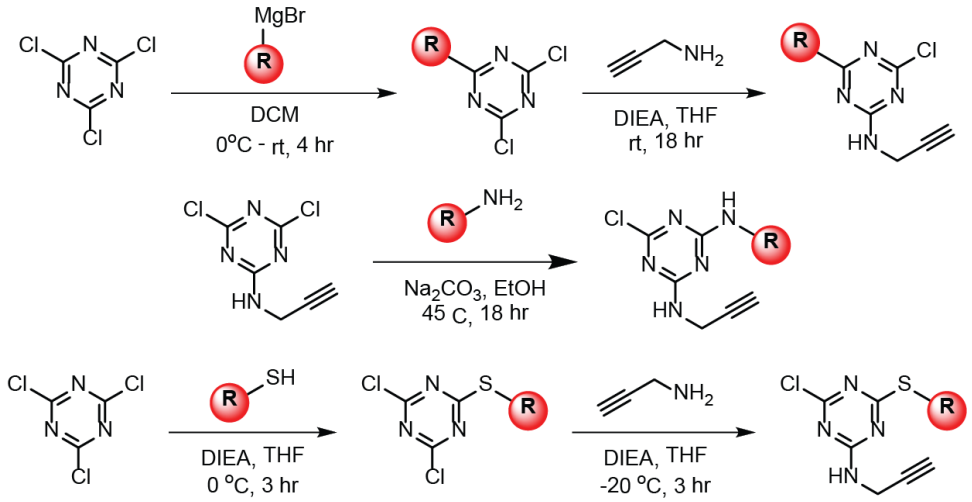

Scheme 4.1. General synthetic scheme for the synthesis of second generation chlorotriazine electrophiles.

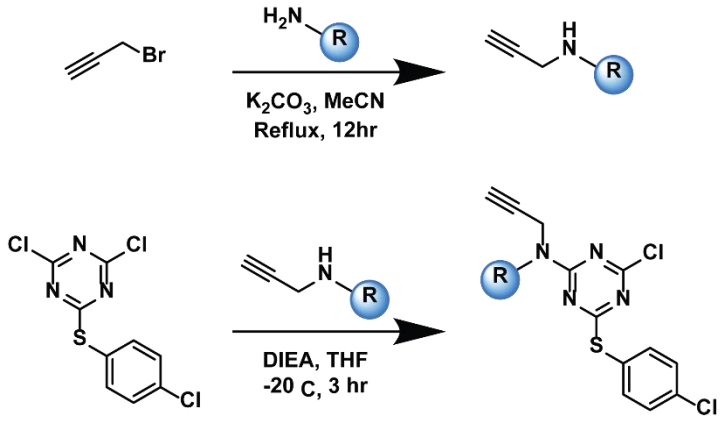

Scheme 4.2. General synthetic scheme for the synthesis of chlorotriazine targeted library.

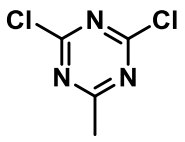

2,4-dichloro-6-methyl-1,3,5-triazine (KSC-3-int): To a solution of cyanuric chloride (561.7 mg mg, 3.045 mmol) in dichloromethane (10 mL), methylmagnesium bromide (3 M, 4.06 mL) was added at -20 °C and stirred for 4h, then stirred 4h at room temperature. Crude residue was extracted via liquid-liquid extraction. Solvents were removed *in vacuo* and crude product was purified with flash chromatography to afford the desired compound, **KSC-3-int**, as a yellow solid (234.8 mg, 47%). ^{1}H NMR (500 MHz, Chloroform-*d*) δ 2.70 (s, 3H).

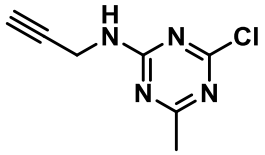

4-chloro-6-methyl-*N*-(prop-2-yn-1-yl)-1,3,5-triazin-2-amine (KSC-3): To a solution of **KSC-3-int** (122.8 mg, 0.7488 mmol) and diisopropylethylamine (145.2 mg, 1.1232 mmol) in THF (10 mL), propargylamine (61.9 µL, 1.1232 mmol) was added at room temperature and stirred overnight. The solvent was removed *in vacuo* and the crude product was purified with flash chromatography to afford the desired compound, **KSC-3**, as a white

solid (136.7 mg, 61%). ^{1}H NMR (500 MHz, Chloroform-*d*) δ 5.65 (s, 1H), 4.28 (ddd, *J* = 11.0, 5.6, 2.5 Hz, 2H), 2.46 (s, 3H), 2.17 (s, 1H).

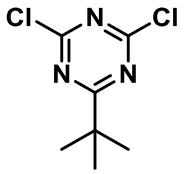

2-(*tert*-butyl)-4,6-dichloro-1,3,5-triazine (KSC-38-int): To a solution of cyanuric chloride (492.5 mg, 2.6707 mmol) and copper iodide (25.4 mg, 0.1335 mmol) in THF (3 mL), 1.7 M *tert*-Butylmagnesium chloride (1.65 mL, 2.8042 mmol) was added at -10 °C. Upon addition of the Grignard, the flask was removed from ice bath and allowed to warm to room temperature. The reaction was stirred for 30 minutes. Crude residue was extracted via liquid-liquid extraction. Solvent was removed *in vacuo* and crude product was purified with flash chromatography to afford the desired compound, **KSC-38-int**, as a colorless oil (215.7 mg, 39%). ^{1}H NMR (600 MHz, Chloroform-d) δ 1.34 (d, J = 2.7 Hz, 9H). ^{13}C NMR (151 MHz, cdcl$_3$) δ 190.27, 171.51, 76.95, 40.07. HRMS for **KSC-38-int**: m/z calcd. 206.0174; obsd. 206.0246.

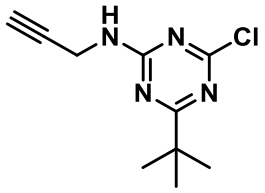

4-(*tert*-butyl)-6-chloro-*N*-(prop-2-yn-1-yl)-1,3,5-triazin-2-amine (KSC-38): To a solution of **KSC-38-int** (185.9 mg, 0.9021 mmol) and diisopropylethylamine (152.6 mg, 1.1810 mmol) in THF (3 mL), propargylamine (59.6 µL, 1.0825 mmol) was added at -20 °C and stirred for 3h. After 3h, the solvent was removed *in vacuo* and the crude product was purified with flash chromatography to afford the desired compound, **KSC-38**, as a white solid (178.8 mg, 86%). ^{1}H NMR (600 MHz, Chloroform-d) δ 4.26 (ddd, J = 33.7, 5.7, 2.5 Hz, 2H), 2.33 – 2.06 (m, 1H), 1.27 (d, J = 34.0 Hz, 9H). ^{13}C NMR (151 MHz, Chloroform-d) δ 190.58, 189.73, 173.47, 172.51, 168.32, 168.21, 81.92, 81.42, 79.94, 79.72, 79.51, 74.83, 73.92, 42.20, 41.77, 33.55, 33.46, 33.38, 32.30, 31.16, 31.14. HRMS for **KSC-38**: m/z calcd. 225.0829; obsd. 225.1033.

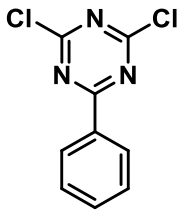

2,4-dichloro-6-phenyl-1,3,5-triazine (KSC-35-int): To a solution of cyanuric chloride (503.9 mg, 2.7325 mmol) in a 1:1 v/v mixture of THF and diethyl ether (30 mL) and benzene (31 mL), phenylmagnesium bromide (3 M, 1.08 mL) was added at 0 °C and stirred for 4h, then stirred 4h at room temperature. Crude residue was extracted via liquid-liquid extraction. Solvents were removed *in vacuo* and crude product was purified with flash chromatography to afford the desired compound, **KSC-35-int**, as a white solid (33.5 mg, 6%). ^{1}H NMR (500 MHz, Chloroform-*d*) δ 8.51 (dd, *J* = 8.2, 1.5 Hz, 2H), 7.66 (td, *J* = 7.4,

1.4 Hz, 1H), 7.58 – 7.47 (m, 2H). ^{13}C NMR (151 MHz, Chloroform-*d*) δ 175.17, 172.40, 135.08, 132.99, 130.28, 129.41, 77.58, 77.37, 77.16. HRMS for **KSC-35-int**: m/z calcd. 225.9861; obsd. 225.9944.

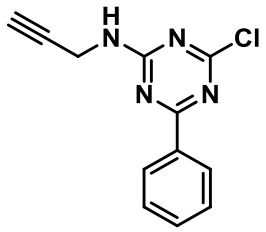

4-chloro-6-phenyl-*N*-(prop-2-yn-1-yl)-1,3,5-triazin-2-amine (KSC-35): To a solution of **KSC-35-int** (50.0 mg, 0.2212 mmol) and diisopropylethylamine (31.4 mg, 0.2433 mmol) in THF (2.5 mL), propargylamine (14.6 μL, 0.2654 mmol) was added. The reaction mixture was stirred at -20 °C (dry ice bath of 9:1 ethylene glycol/ethanol) for 3h. After 3h, the solvent was removed *in vacuo* affording a crude white solid. The crude product was purified by flash chromatography (1:1 dichloromethane/pentane) to give 40.4 mg (0.1651 mmol, 71%) of the desired compound, **KSC-35**, as a white solid. ^{1}H NMR (600 MHz, Acetone-d6) δ 8.43 (ddt, J = 63.6, 7.2, 1.4 Hz, 2H), 7.92 (d, J = 82.8 Hz, 1H), 7.76 – 7.46 (m, 3H), 4.38 (ddd, J = 72.8, 5.9, 2.5 Hz, 2H), 2.75 (q, J = 2.6 Hz, 1H); ^{13}C NMR (151 MHz, Acetone-d6) δ 136.04, 133.97, 133.83, 129.90, 129.65, 129.62, 129.60, 72.78, 72.68, 31.41, 31.22, 30.52, 30.39, 30.26, 30.13, 30.00, 29.88, 29.75, 29.62. HRMS for **KSC-35**: m/z calcd. 245.0516; obsd. 245.0593.

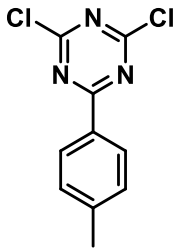

2,4-dichloro-6-(*p*-tolyl)-1,3,5-triazine (KSC-39-int): To a solution of cyanuric chloride (500.1 mg, 2.7119 mmol) in a 1:1 v/v mixture of THF and diethyl ether (30 mL) and benzene (31 mL), *p*-tolylmagnesium bromide (0.5 M, 6.51 mL) was added at 0 °C and stirred for 4h, then stirred 4h at room temperature. Crude residue was extracted via liquid-liquid extraction. Solvents were removed *in vacuo* and crude product was purified with flash chromatography to afford the desired compound, **KSC-39-int**, as a white solid (217.4 mg, 33%). ^{1}H NMR (600 MHz, Chloroform-d) δ 8.41 – 8.22 (m, 2H), 7.27 (d, J = 8.0 Hz, 2H), 2.42 (s, 3H). ^{13}C NMR (151 MHz, cdcl$_3$) δ 174.66, 172.52, 171.85, 146.06, 129.98, 129.86, 21.97. HRMS for **KSC-39-int**: m/z calcd. 240.0017; obsd. 240.0084.

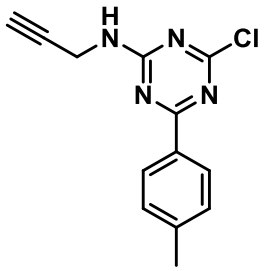

4-chloro-*N*-(prop-2-yn-1-yl)-6-(p-tolyl)-1,3,5-triazin-2-amine (KSC-39): To a solution of **KSC-39-int** (45.0mg, 0.1874 mmol) and diisopropylethylamine (26.6 mg, 0.2061 mmol) in THF (3 mL), propargylamine (7.0 µL, 0.1280 mmol) was added at -20 °C and stirred for 3h. After 3h, the solvent was removed *in* vacuo and the crude product was purified with flash chromatography to afford the desired compound, **KSC-39**, as a white solid (13.2 mg, 27%). ^{1}H NMR (600 MHz, DMSO-d6) δ 8.36 – 8.16 (m, 2H), 7.38 (td, J = 5.7, 5.1, 2.6 Hz, 2H), 4.21 (ddd, J = 79.4, 5.8, 2.5 Hz, 2H), 2.41 (d, J = 5.4 Hz, 3H), 2.10 (s, 1H). HRMS for **KSC-39**: m/s calcd. 259.0672

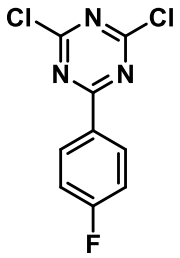

2,4-dichloro-6-(4-fluorophenyl)-1,3,5-triazine (KSC-40-int): To a solution of cyanuric chloride (520.2 mg, 2.8209 mmol) in a 1:1 v/v mixture of THF and diethyl ether (30 mL) and benzene (31 mL), 4-Fluorophenylmagnesium bromide (2 M, 1.69 mL) was added at 0 °C and stirred for 4h, then stirred 4h at room temperature. Crude residue was extracted via liquid-liquid extraction. Solvents were removed *in vacuo* and crude product was purified with flash chromatography to afford the desired compound, **KSC-40-int**, as a white solid (380.1 mg, 55%). ^{1}H NMR (500 MHz, Chloroform-*d*) δ 8.59 – 8.51 (m, 2H), 7.24 – 7.17 (m, 2H). ^{13}C NMR (126 MHz, Chloroform-*d*) δ 171.95, 167.96, 132.53, 132.45, 128.80,

116.38, 116.21, 77.16, 76.91, 76.65. HRMS for **KSC-40-int**: m/z calcd. 243.9766; obsd. 243.9847.

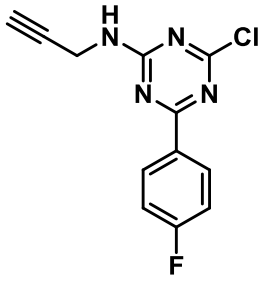

4-chloro-6-(4-fluorophenyl)-*N*-(prop-2-yn-1-yl)-1,3,5-triazin-2-amine (KSC-40): To a solution of **KSC-40-int** (49.6 mg, 0.2032 mmol) and diisopropylethylamine (28.9 mg, 0.2236 mmol) in THF (3 mL), propargylamine (13.4 μL, 0.2439 mmol) was added at -20 °C and stirred for 3h. After 3h, the solvent was removed *in vacuo* and the crude product was purified with flash chromatography to afford the desired compound, **KSC-40**, as a white solid (28.8 mg, 54%). ^{1}H NMR (600 MHz, Acetone-d_6) δ 8.60 – 8.33 (m, 2H), 7.39 – 7.18 (m, 2H), 4.37 (ddd, J = 70.1, 5.9, 2.5 Hz, 2H), 2.81 (s, 1H). ^{13}C NMR (151 MHz, acetone) δ 172.52, 172.15, 171.49, 167.73, 167.28, 166.06, 132.58, 116.66, 80.62, 80.52, 72.81, 72.71, 31.40, 31.21. HRMS for **KSC-40**: m/z calcd. 263.0422; obsd. 263.0500.

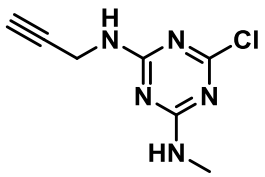

6-chloro-N^2-methyl-N^4-(prop-2-yn-1-yl)-1,3,5-triazine-2,4-diamine (KSC-37): To a solution of RB7 (102.2 mg, 0.5029 mmol) and sodium carbonate (117.3 mg, 1.1014 mmol) in ethanol (7 mL), aniline (56.4µL 0.5532 mmol) was added at room temperature. The reaction mixture was heated to 45 °C for 18h. Crude residue was extracted via liquid-liquid extraction. Solvent was removed *in vacuo* and crude residue was purified with flash chromatography to afford the desired compound, **KSC-37**, as a white solid (22.4 mg, 23%). ^{1}H NMR (600 MHz, Acetone-d_6) δ 4.27 (ddd, J = 34.1, 6.0, 2.5 Hz, 2H), 2.70 (dt, J = 6.6, 2.5 Hz, 1H), 1.31 (s, 3H). ^{13}C NMR (151 MHz, acetone) δ 187.95, 187.36, 171.28, 170.87, 166.94, 166.82, 72.28, 72.13, 39.87, 39.56, 30.94, 30.72, 28.67, 28.62. HRMS for **KSC-37**: m/z calcd. 198.0468; obsd. 198.0547.

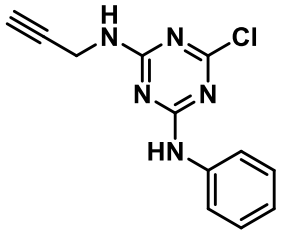

6-chloro-N^2-phenyl-N^4-(prop-2-yn-1-yl)-1,3,5-triazine-2,4-diamine (KSC-36): To a solution of RB7 (103.3 mg, 0.5088 mmol) and sodium carbonate (119 mg, 1.1194 mmol) in ethanol (6 mL), aniline (51.1µL 0.5597 mmol) was added at room temperature. The reaction mixture was heated to 45 °C for 18h. Crude residue was extracted via liquid-liquid extraction. Solvent was removed *in vacuo* and crude residue was purified with flash

chromatography to afford the desired compound, **KSC-36**, as a white solid (48.9 mg, 37%). ^{1}H NMR (600 MHz, Acetone-d_6) δ 8.93 (d, J = 84.3 Hz, 1H), 8.03 – 7.70 (m, 2H), 7.34 (dt, J = 25.2, 7.8 Hz, 2H), 7.08 (dt, J = 15.0, 7.4 Hz, 1H), 4.34 – 4.09 (m, 2H), 2.83 (s, 1H). HRMS for **KSC-36**: m/z calcd. 260.0625; obsd. 260.0703.

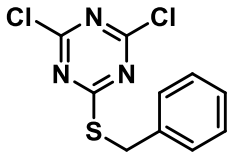

2-(benzylthio)-4,6-dichloro-1,3,5-triazine (KSC-41-int): To a solution of cyanuric chloride (1.01 g, 5.4601 mmol) and diisopropylethylamine (776.2 mg, 6.0061 mmol) in THF (5 mL), a solution of benzyl mercaptan (678.2 mg, 5.4601 mmol) in THF (5 mL) was added dropwise by addition funnel at 0 °C over 30 minutes followed by stirring at 0 °C for 3h. The solvent was removed *in vacuo* and the crude product was purified with flash chromatography to afford the desired compound, **KSC-41-int**, as a white solid (931.7 mg, 63%) ^{1}H NMR (600 MHz, Chloroform-d) δ 7.42 – 7.38 (m, 2H), 7.36 – 7.31 (m, 2H), 7.30 – 7.26 (m, 1H), 4.41 (s, 2H). ^{13}C NMR (151 MHz, Chloroform-d) δ 185.79, 170.20, 135.26, 129.39, 128.99, 128.88, 128.07, 77.58, 77.37, 77.16, 35.70. HRMS for **KSC-41-int**: m/z calcd. 271.9738; obsd. 271.98287.

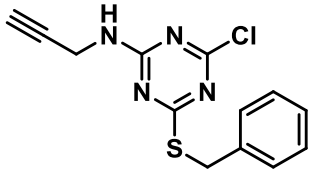

4-(benzylthio)-6-chloro-*N*-(prop-2-yn-1-yl)-1,3,5-triazin-2-amine (KSC-41): To a solution of **KSC-41-int** (389.1 mg, 1.4927 mmol) and diisopropylethylamine (203.3 mg, 1.5727 mmol) in THF (10 mL), propargylamine (274 µL, 1.7157 mmol) was added at -20 °C and stirred for 3h. After 3h, the solvent was removed *in vacuo* and the crude product was purified with flash chromatography to afford the desired compound, **KSC-41**, as a white solid (195.4 mg, 47%). ^{1}H NMR (500 MHz, Acetone-d_6, mixture of rotamers) δ 7.87 (dt, J = 44.5, 5.8 Hz, 1H), 7.53 – 7.37 (m, 2H), 7.36 – 7.28 (m, 2H), 7.28 – 7.22 (m, 1H), 4.41 (d, J = 47.2 Hz, 2H), 4.28 (ddd, J = 22.9, 5.9, 2.5 Hz, 2H), 2.75 (dt, J = 11.9, 2.5 Hz, 1H). ^{13}C NMR (126 MHz, Acetone-d_6, mixture of rotamers) δ 183.46, 182.66, 169.78, 169.22, 165.44, 165.27, 138.36, 138.28, 129.99, 129.94, 129.42, 129.37, 128.18, 80.38, 80.26, 72.79, 35.05, 34.86, 31.29, 31.02. HRMS for **KSC-41**: m/z calcd. 291.0393; obsd. 291.0471.

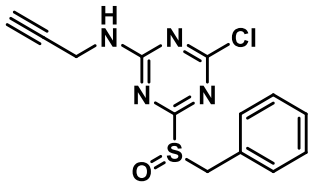

4-(benzylsulfinyl)-6-chloro-*N*-(prop-2-yn-1-yl)-1,3,5-triazin-2-amine (KSC-45): To a solution of **KSC-41** (28.7 mg, 0.0970 mmol) was dissolved in DCM (3 mL) at room temperature. mCPBA (25.5 mg, 1.4806 mmol) was added in one portion. The reaction was stirred at 25 °C for 30 minutes. The solvent was removed *in* vacuo and the crude product

was purified via flash chromatography to afford the desired compound, **KSC-45**, as a white solid (13.8 mg, 46%). ^{1}H NMR (600 MHz, DMSO-d_6, mixture of rotamers) δ 7.35 (dt, J = 4.8, 2.1 Hz, 3H), 7.23 (ddd, J = 12.9, 6.5, 2.9 Hz, 2H), 4.58 – 4.22 (m, 2H), 4.14 (ddd, J = 10.2, 5.5, 2.7 Hz, 2H), 3.26 (dt, J = 19.8, 2.5 Hz, 1H). ^{13}C NMR (151 MHz, DMSO-d_6, mixture of rotamers) δ 183.30, 182.65, 169.32, 169.05, 164.66, 164.36, 130.24, 130.18, 128.43, 128.38, 128.19, 128.15, 79.51, 79.33, 74.14, 73.98, 58.41, 58.23, 30.26, 30.21. HRMS for **KSC-45**: m/z calcd. 307.0342; obsd. 307.0420.

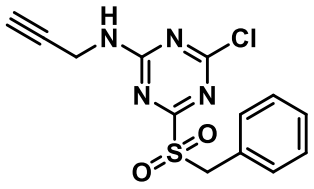

4-(benzylsulfonyl)-6-chloro-*N*-(prop-2-yn-1-yl)-1,3,5-triazin-2-amine (KSC-42): **KSC-41** (44.0 mg, 0.1513 mmol) was dissolved in DCM (0.3M), and allowed to cool to 0 °C while stirring. mCPBA (60.1 mg, 0.3480 mmol) was added in one portion. The reaction was allowed to stir for 12 hr while warming to room temperature. Crude residue was extracted via liquid-liquid extraction and the solvent removed *in vacuo*. The product was purified via flash chromatography to yield a white solid, **KSC-42**, as a white solid (26.4 mg, 0.0818 mmol, 54%). ^{1}H NMR (500 MHz, Chloroform-*d*, mixture of rotamers) δ 7.51 – 7.39 (m, 2H), 7.36 (qd, J = 2.9, 1.6 Hz, 3H), 6.74 – 6.37 (m, 1H), 4.73 (d, J = 16.4 Hz, 2H), 4.31 (ddd, J = 14.6, 5.7, 2.6 Hz, 2H), 2.31 (dt, J = 6.5, 2.5 Hz, 1H). ^{13}C NMR (126 MHz, Chloroform-*d*, mixture of rotamers) δ 174.55, 173.86, 172.48, 171.66, 166.12,

165.90, 131.90, 131.88, 131.31, 129.99, 129.63, 129.33, 129.29, 126.34, 126.14, 73.58, 73.46, 60.21, 57.25, 32.07, 31.94. HRMS for **KSC-42**: m/z calcd. 323.0291; obsd. 323.0370.

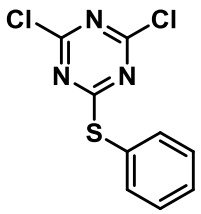

2,4-dichloro-6-(phenylthio)-1,3,5-triazine (KSC-43-int): To a solution of cyanuric chloride (1.05 g, 5.6696 mmol) and diisopropylethylamine (580 µL, 6.2366 mmol) in THF (60 mL), a solution of thiophenol (624.7 mg, 5.6696 mmol) in THF (5 mL) was added dropwise by addition funnel at 0 °C over 30 minutes followed by stirring at 0 °C for 3h. The solvent was removed *in vacuo* and the crude product was purified with flash chromatography to afford the desired compound, **KSC-43-int**, as a white solid (1.1918 g, 81%). ^{1}H NMR (600 MHz, Chloroform-*d*) δ 7.58 – 7.54 (m, 2H), 7.53 – 7.48 (m, 2H), 7.48 – 7.45 (m, 1H). ^{13}C NMR (151 MHz, Chloroform-*d*) δ 186.77, 170.74, 135.43, 130.95, 129.97, 125.72. HRMS for **KSC-43-int**: m/z calcd. 257.9581; obsd. 257.9660.

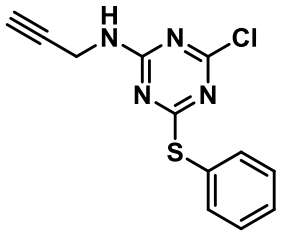

4-chloro-6-(phenylthio)-*N*-(prop-2-yn-1-yl)-1,3,5-triazin-2-amine (KSC-43): To a solution of **KSC-43-int** (197.4 mg, 0.7648 mmol) and diisopropylethylamine (108.7 mg, 0.8412 mmol) in THF (11 mL), propargylamine (59 µL, 0.9177 mmol) was added at -20 °C and stirred for 3h. After 3h, the solvent was removed *in vacuo* and the crude product was purified with flash chromatography to afford the desired compound, **KSC-43**, as a white solid (169.5 mg, 80%). ^{1}H NMR (500 MHz, Chloroform-*d*, mixture of rotamers) δ 7.62 – 7.52 (m, 2H), 7.45 – 7.39 (m, 3H), 7.07 (t, *J* = 5.9 Hz, 1H), 4.05 (ddd, *J* = 126.1, 5.8, 2.5 Hz, 2H), 2.28 – 2.11 (m, 1H). ^{13}C NMR (126 MHz, Chloroform-*d*, mixture of rotamers) δ 183.53, 182.45, 169.33, 168.25, 164.07, 163.70, 135.20, 129.59, 129.56, 129.00, 128.84, 127.13, 126.96, 78.64, 78.28, 72.15, 71.33, 30.65, 30.45, 29.52. HRMS for **KSC-43**: m/z calcd. 277.0236; obsd. 277.0318.

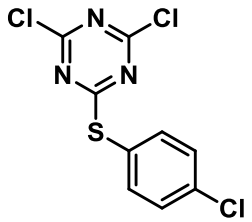

2,4-dichloro-6-((4-chlorophenyl)thio)-1,3,5-triazine (KSC-46-int): To a solution of cyanuric chloride (211.8 mg, 1.0845 mmol) and diisopropylethylamine (208 µL, 1.1930 mmol) in THF (11 mL), a solution of *p*-chlorothiophenol (172.5 mg, 1.1930 mmol) in THF (5 mL) was added dropwise by addition funnel at 0 °C over 30 minutes followed by stirring at 0 °C for 3h. The solvent was removed *in vacuo* and the crude product was purified with

flash chromatography to afford the desired compound, **KSC-46-int**, as a white solid (317.3 mg, 58%). ^{1}H NMR (500 MHz, DMSO-d_6) δ 7.62 – 7.58 (m, 2H), 7.58 – 7.54 (m, 2H). ^{13}C NMR (126 MHz, DMSO-d_6) δ 169.00, 137.53, 135.51, 129.40, 124.07. HRMS for **KSC-46-int**: m/z calcd. 291.9192; obsd. 291.9265.

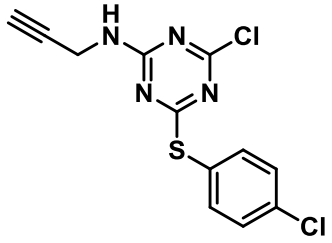

4-chloro-6-((4-chlorophenyl)thio)-*N*-(prop-2-yn-1-yl)-1,3,5-triazin-2-amine (KSC-46): To a solution of **KSC-46-int** (51.4 mg, 0.1757 mmol) and diisopropylethylamine (25.0 mg, 0.1933 mmol) in THF (5 mL), propargylamine (13.5 µL, 0.2108 mmol) was added at -20 °C and stirred for 3h. After 3h, the solvent was removed *in vacuo* and the crude product was purified with flash chromatography to afford the desired compound, **KSC-46**, as a white solid (54.7 mg, 89%). ^{1}H NMR (500 MHz, Chloroform-*d*, mixture of rotamers) δ 8.38 – 8.21 (m, 1H), 8.15 – 8.02 (m, 2H), 8.02 – 7.90 (m, 2H), 4.56 (ddd, J = 92.2, 5.9, 2.3 Hz, 2H), 3.29 – 3.11 (m, 1H). ^{13}C NMR (126 MHz, Chloroform-*d*, mixture of rotamers) δ 192.73, 192.10, 179.67, 179.20, 175.23, 174.98, 147.52, 147.41, 146.03, 139.82, 139.75, 136.98, 89.76, 82.36, 82.23, 40.71, 40.60. HRMS for **KSC-46**: m/z calcd. 310.9847; obsd. 310.9925.

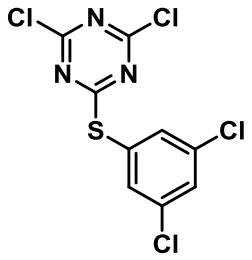

2,4-dichloro-6-((3,5-dichlorophenyl)thio)-1,3,5-triazine (KSC-47-int): To a solution of cyanuric chloride (222.3 mg, 1.2093 mmol) and diisopropylethylamine (232 μL, 1.3302 mmol) in THF (12 mL), a solution of *m,m*-dichlorothiophenol (238.2 mg, 1.3302 mmol) in THF (5 mL) was added dropwise by addition funnel at 0 °C over 30 minutes followed by stirring at 0 °C for 3h. The solvent was removed *in vacuo* and the crude product was purified with flash chromatography to afford the desired compound, **KSC-47-int**, as a white solid (395.4 mg, 45%). ^{1}H NMR (500 MHz, DMSO-d_6) δ 7.86 – 7.78 (m, 1H), 7.76 – 7.70 (m, 2H). ^{13}C NMR (126 MHz, DMSO-d_6) δ 168.41, 151.69, 134.24, 133.92, 130.05, 128.93. HRMS for **KSC-47-int**: m/z calcd.325.8802; obsd. 325.8873.

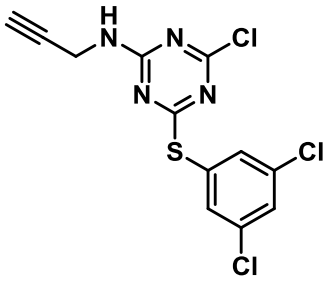

4-chloro-6-((3,5-dichlorophenyl)thio)-*N*-(prop-2-yn-1-yl)-1,3,5-triazin-2-amine (KSC-47): To a solution of **KSC-47-int** (47.2 mg, 0.1443 mmol) and diisopropylethylamine (20.5 mg, 0.1588 mmol) in THF (5 mL), propargylamine (11 μL, 0.1732 mmol) was added at -20 °C and stirred for 3h. After 3h, the solvent was removed *in vacuo* and the crude product was purified with flash chromatography to afford the desired compound, **KSC-47**, as a white solid (13.5 mg, 27%). ^{1}H NMR (500 MHz, Acetone-d_6, mixture of rotamers) δ 8.06 – 7.84 (m, 1H), 7.68 (dd, J = 25.4, 2.0 Hz, 2H), 7.62 (dt, J = 3.7, 1.9 Hz, 1H), 4.37 – 3.93 (m, 2H), 2.70 (dt, J = 23.6, 2.5 Hz, 1H). ^{13}C NMR (126 MHz, Acetone-d_6, mixture of rotamers) δ 182.20, 181.57, 170.05, 165.31, 135.68, 135.64, 134.25, 134.21, 132.13, 130.39, 80.03, 79.83, 72.76, 72.58, 31.09, 30.97. HRMS for **KSC-47**: m/z calcd. 344.9457; obsd. 344.9528.

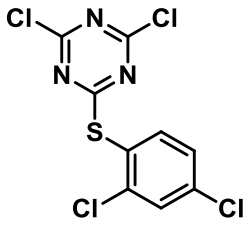

2,4-dichloro-6-((2,4-dichlorophenyl)thio)-1,3,5-triazine (KSC-48-int): To a solution of cyanuric chloride (978.0 mg, 5.3036 mmol) and diisopropylethylamine (1.02 mL, 5.8339 mmol) in THF (50 mL), a solution of *o*,*p*-dichlorothiophenol (1044.7 mg, 5.8339 mmol) in THF (5 mL) was added dropwise by addition funnel at 0 °C over 30 minutes followed by stirring at 0 °C for 3h. The solvent was removed *in vacuo* and the crude product was purified with flash chromatography to afford the desired compound, **KSC-48-int**, as a

white solid (317.3 mg, 58%). ^{1}H NMR (500 MHz, Acetone-d_6) δ 7.84 (d, J = 8.4 Hz, 1H), 7.80 (d, J = 2.2 Hz, 1H), 7.60 – 7.56 (m, 1H). ^{13}C NMR (126 MHz, Acetone-d_6) δ 198.10, 171.16, 140.97, 139.71, 138.59, 131.09, 129.37, 125.12.

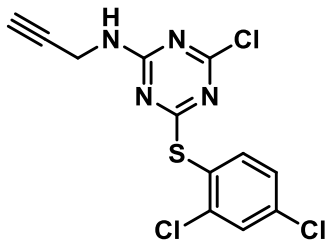

4-chloro-6-((2,4-dichlorophenyl)thio)-*N*-(prop-2-yn-1-yl)-1,3,5-triazin-2-amine (KSC-48): To a solution of **KSC-48-int** (64.0 mg, 0.1957 mmol) and diisopropylethylamine (27.8 mg, 0.2153 mmol) in THF (5 mL), propargylamine (15 µL, 0.2349 mmol) was added at -20 °C and stirred for 3h. After 3h, the solvent was removed *in vacuo* and the crude product was purified with flash chromatography to afford the desired compound, **KSC-48**, as a white solid (66.3 mg, 98%). ^{1}H NMR (600 MHz, Chloroform-*d,* mixture of rotamers) δ 7.63 – 7.57 (m, 1H), 7.55 (dd, J = 8.5, 2.3 Hz, 1H), 7.30 (ddd, J = 8.4, 6.3, 2.2 Hz, 1H), 4.07 (ddd, J = 160.7, 5.7, 2.5 Hz, 2H), 2.23 (dt, J = 50.4, 2.5 Hz, 1H). ^{13}C NMR (151 MHz, Chloroform-*d*, mixture of rotamers) δ 181.75, 180.80, 169.56, 168.70, 164.16, 163.86, 140.56, 138.30, 138.24, 137.09, 130.15, 130.01, 127.67, 127.55, 125.43, 125.25, 78.22, 72.47, 71.78, 30.86, 30.74, 29.63. HRMS for **KSC-48**: m/z calcd. 344.9457; obsd. 344.9525.

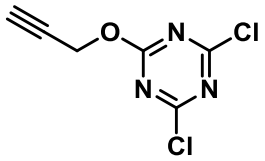

2,4-dichloro-6-(prop-2-yn-1-yloxy)-1,3,5-triazine (KSC-44): To a solution of cyanuric chloride (1.1788 g, 6.3925 mmol) and potassium carbonate (971.9 mg, 7.0317 mmol) in THF (60 mL), propargyl alcohol (394.2 mg, 7.0317 mmol) was added dropwise at 0 °C followed by stirring at 0 °C for 30h. Crude residue was extracted via liquid-liquid extraction. The solvent was removed *in vacuo* and the crude product was purified with flash chromatography to afford the desired compound, **KSC-44**, as a white solid (1.135 g, 87%). ^{1}H NMR (500 MHz, Chloroform-*d*) δ 5.07 (d, *J* = 2.5 Hz, 2H), 2.57 (t, *J* = 2.4 Hz, 1H). ^{13}C NMR (126 MHz, Chloroform-*d*) δ 172.28, 171.26, 170.19, 75.47, 57.10. HRMS for **KSC-44**: m/z calcd. 203.9653; obsd. 203.9731.

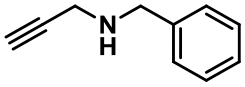

***N*-benzylprop-2-yn-1-amine (KSC-50-int):** To a suspension of (Bromomethyl)benzene (1.03 g, 6.0263 mmol) and potassium carbonate (999.4 mg, 7.2316 mmol) in acetonitrile (20 mL), propargylamine (995.8 mg, 18.0789 mmol) was added in one addition and the reaction was heated to reflux while stirring for 24h. Crude residue was extracted via liquid-liquid extraction. The solvent was removed *in vacuo* and the crude product was purified

with flash chromatography to afford the desired compound, **KSC-50-int**, as a solid (439.5 mg, 50%). ^{1}H NMR (600 MHz, Chloroform-*d*) δ 7.41 – 7.35 (m, 2H), 7.34 (dd, *J* = 8.4, 6.7 Hz, 2H), 7.30 – 7.24 (m, 1H), 3.87 (d, *J* = 1.6 Hz, 2H), 3.40 (dd, *J* = 2.5, 1.1 Hz, 2H), 2.30 (t, *J* = 2.4 Hz, 1H). ^{13}C NMR (151 MHz, Chloroform-*d*) δ 139.46, 128.33, 127.04, 82.20, 71.65, 52.25, 52.11, 37.21. HRMS for **KSC-50-int**: m/z calcd. 146.0891; obsd. 146.0970.

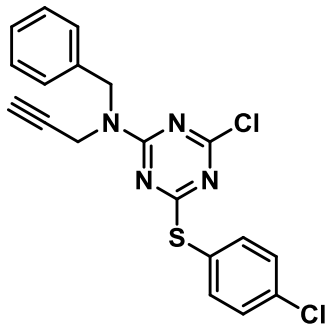

***N*-benzyl-4-chloro-6-((4-chlorophenyl)thio)-*N*-(prop-2-yn-1-yl)-1,3,5-triazin-2-amine (KSC-50):** To a solution of **KSC-46-int** (49.6 mg, 0.2000 mmol) and diisopropylethylamine (24.1 mg, 0.1865 mmol) in THF (5 mL), **KSC-50-int** (29.5 mg, 0.2034 mmol) was added at -20 °C and stirred for 3h. After 3h, the solvent was removed *in vacuo* and the crude product was purified with flash chromatography to afford the desired compound, **KSC-50**, as a white solid (61.4 mg, 90%). ^{1}H NMR (600 MHz, Chloroform-*d*, mixture of rotamers) δ 7.77 – 6.94 (m, 8H), 5.12 – 4.66 (m, 2H), 4.43 – 4.09 (m, 2H), 2.31 – 2.08 (m, 1H). ^{13}C NMR (151 MHz, Chloroform-*d*, mixture of rotamers) δ 179.61, 163.76, 163.67, 137.22, 137.09, 136.70, 136.63, 134.94, 129.12, 128.55, 128.39,

128.35, 128.07, 127.88, 127.80, 127.74, 127.32, 127.24, 79.28, 79.17, 71.34, 71.22, 48.64, 48.43, 34.85, 34.71, 30.24. HRMS for **KSC-50**: m/z calcd. 401.0316; obsd. 401.0381.

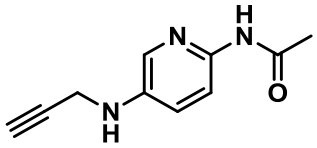

***N*-(5-(prop-2-yn-1-ylamino)pyridin-2-yl)acetamide (KSC-52-int):** To a suspension of 2-Acetamido-5-Aminopyridine (391.5 mg, 2.9590 mmol), sodium iodide (194.1 mg, 1.290 mmol), and potassium carbonate (894.7 mg, 6.470 mmol) in acetonitrile (7 mL), tosylated propargyl alcohol (598.9 mg, 2.8500 mmol) was added dropwise and the reaction was heated to reflux while stirring for 12h. Crude residue was extracted via liquid-liquid extraction. The solvent was removed *in vacuo* and the crude product was purified with flash chromatography to afford the desired compound, **KSC-52-int**, as a yellow solid (161.5 mg, 33%). HRMS for **KSC-52-int**: m/z calcd. 190.0902; obsd. 190.0980.

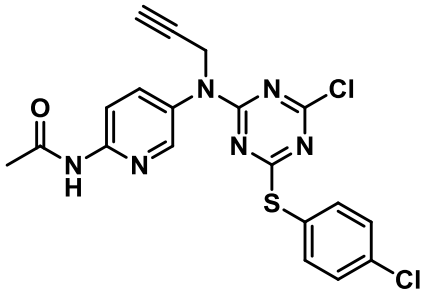

***N*-(5-((4-chloro-6-((4-chlorophenyl)thio)-1,3,5-triazin-2-yl)(prop-2-yn-1-yl)amino)pyridin-2-yl)acetamide (KSC-52):** To a solution of **KSC-46-int** (50.4 mg, 0.1723 mmol) and diisopropylethylamine (24.5 mg, 0.1895 mmol) in THF (5 mL), **KSC-52-int** (39.1 mg, 0.2067 mmol) was added at -20 °C and stirred for 3h. After 3h, the solvent was removed *in vacuo* and the crude product was purified with flash chromatography to afford the desired compound, **KSC-52**, as a white solid (68.4 mg, 89%). ^{1}H NMR (600 MHz, Acetone-d_6, mixture of rotamers) δ 9.68 – 9.55 (m, 1H), 8.35 – 8.07 (m, 2H), 7.85 – 7.50 (m, 2H), 7.40 – 7.17 (m, 2H), 4.65 (dd, J = 127.8, 2.5 Hz, 2H), 2.83 (td, J = 7.7, 3.7 Hz, 1H), 2.23 (d, J = 29.6 Hz, 3H). ^{13}C NMR (151 MHz, Acetone-d_6, mixture of rotamers) δ 182.94, 169.84, 165.22, 152.32, 147.85, 137.95, 137.87, 137.29, 136.24, 133.73, 130.36, 130.00, 126.76, 114.24, 114.10, 79.07, 74.93, 74.70, 40.98, 40.29, 30.74, 30.49, 24.62, 24.45. HRMS for **KSC-50**: m/z calcd. 401.0316; obsd. 401.0381.

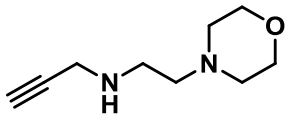

***N*-(2-morpholinoethyl)prop-2-yn-1-amine (KSC-53-int):** To a suspension of propargylbromide (600.0 mg, 4.0350 mmol) and potassium carbonate (613.4 mg, 4.4385 mmol) in acetonitrile (10 mL), 4-(2-Aminoethyl)morpholine (1.576 g, 12.1049 mmol) was added in one addition and the reaction was heated to reflux while stirring for 24h. Crude residue was extracted via liquid-liquid extraction. The solvent was removed *in vacuo* and the crude product was purified with flash chromatography to afford the desired compound,

KSC-53-int, as a solid (517.6 mg, 61%). ^{1}H NMR (500 MHz, Chloroform-*d*) δ 3.54 (t, *J* = 4.7 Hz, 4H), 3.29 (d, *J* = 2.6 Hz, 2H), 2.64 (t, *J* = 6.1 Hz, 2H), 2.35 (t, *J* = 6.1 Hz, 2H), 2.30 (t, *J* = 4.5 Hz, 4H), 2.10 (s, 1H). ^{13}C NMR (126 MHz, Chloroform-*d*) δ 81.82, 70.96, 66.46, 57.54, 53.14, 44.02, 37.63. HRMS for **KSC-53-int**: m/z calcd. 169.1263; obsd. 169.1341.

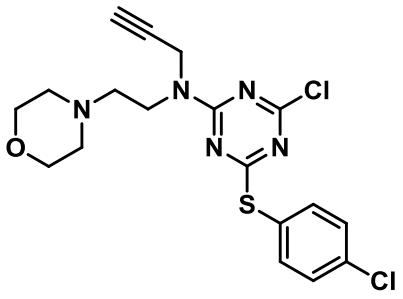

4-chloro-6-((4-chlorophenyl)thio)-*N*-(2-morpholinoethyl)-*N*-(prop-2-yn-1-yl)-1,3,5-triazin-2-amine (KSC-53): To a solution of **KSC-46-int** (50.4 mg, 0.1723 mmol) and diisopropylethylamine (24.5 mg, 0.1895 mmol) in THF (5 mL), **KSC-53-int** (34.8 mg, 0.2067 mmol) was added at -20 °C and stirred for 3h. After 3h, the solvent was removed *in vacuo* and the crude product was purified with flash chromatography to afford the desired compound, **KSC-53**, as a white solid (62.1 mg, 85%). ^{1}H NMR (600 MHz, Acetone-d_6, mixture of rotamers) δ 8.12 (dd, *J* = 8.6, 0.8 Hz, 2H), 7.99 (dd, *J* = 19.4, 8.6 Hz, 2H), 4.86 (dd, *J* = 118.4, 2.5 Hz, 3H), 4.08 – 3.95 (m, 5H), 3.25 (dt, *J* = 22.2, 2.5 Hz, 1H). HRMS for **KSC-53**: m/z calcd. 424.0687; obsd. 424.0766.

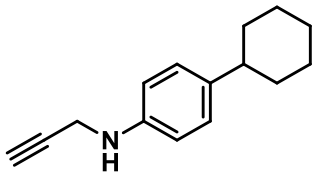

4-cyclohexyl-*N*-(prop-2-yn-1-yl)aniline (KSC-55-int): To a suspension of propargylbromide (119.5 mg, 1.0045 mmol) and potassium carbonate (157.7 mg, 1.105 mmol) in acetonitrile (4 mL), 4-Cyclohexylaniline (528.2 g, 3.0136 mmol) was added in one addition and the reaction was heated to reflux while stirring for 24h. Crude residue was extracted via liquid-liquid extraction. The solvent was removed *in vacuo* and the crude product was purified with flash chromatography to afford the desired compound, **KSC-55-int**, as a solid (99.9 mg, 47%). ^{1}H NMR (600 MHz, Chloroform-*d*) δ 7.11 – 7.06 (m, 2H), 6.69 – 6.63 (m, 2H), 3.93 (d, *J* = 2.4 Hz, 2H), 3.78 (s, 1H), 2.51 – 2.36 (m, 1H), 2.23 (t, *J* = 2.4 Hz, 1H), 1.95 – 1.79 (m, 4H), 1.75 (dddd, *J* = 12.6, 4.5, 3.0, 1.4 Hz, 1H), 1.47 – 1.32 (m, 4H), 1.31 – 1.19 (m, 1H). ^{13}C NMR (151 MHz, Chloroform-*d*) δ 144.75, 138.41, 127.39, 113.45, 81.21, 71.10, 43.55, 34.62, 33.81, 26.91, 26.14. HRMS for **KSC-53-int**: m/z calcd. 214.3240; obsd. 214.1560.

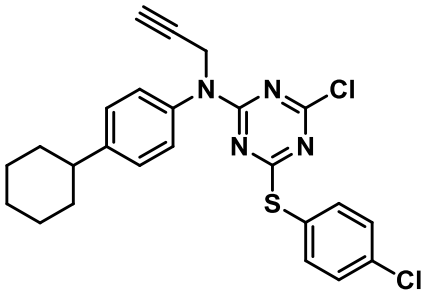

4-chloro-6-((4-chlorophenyl)thio)-*N*-(4-cyclohexylphenyl)-*N*-(prop-2-yn-1-yl)-1,3,5-triazin-2-amine (KSC-55): To a solution of **KSC-46-int** (32.8 mg, 0.1121 mmol) and diisopropylethylamine (15.9 mg, 0.1233 mmol) in THF (3 mL), **KSC-55-int** (28.7 mg, 0.1345 mmol) was added at -20 °C and stirred for 3h. After 3h, the solvent was removed *in vacuo* and the crude product was purified with flash chromatography to afford the desired compound, **KSC-55**, as a white solid (53.1 mg, 100%). ^{1}H NMR (600 MHz, Chloroform-*d*, mixture of rotamers) δ 7.51 (dd, *J* = 109.9, 8.1 Hz, 2H), 7.28 – 7.17 (m, 3H), 7.13 – 6.99 (m, 3H), 4.47 (dd, *J* = 191.4, 2.4 Hz, 2H), 2.26 – 2.18 (m, 1H), 2.01 – 1.72 (m, 5H). ^{13}C NMR (151 MHz, Chloroform-*d*, mixture of rotamers) δ 182.26, 182.05, 169.32, 169.08, 167.85, 163.72, 147.82, 147.57, 138.49, 138.38, 136.83, 136.15, 136.07, 135.46, 132.57, 130.99, 129.37, 128.98, 128.92, 127.88, 127.39, 126.42, 126.37, 126.28, 126.04, 78.82, 78.62, 77.37, 77.16, 76.95, 72.65, 72.11, 68.27, 44.29, 44.18, 41.03, 40.35, 38.86, 34.56, 34.46, 30.50, 29.83, 29.06, 26.99, 26.96, 26.24, 23.88, 23.11, 14.19, 11.10. HRMS for **KSC-53**: m/z calcd. 469.0942; obsd. 469.1021.

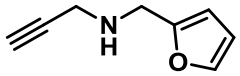

***N*-(furan-2-ylmethyl)prop-2-yn-1-amine (KSC-56-int):** To a suspension of propargylbromide (225.0 mg, 1.8900 mmol) and potassium carbonate (287.5 mg, 2.0800 mmol) in acetonitrile (6 mL), Furfurylamine (551.1 g, 5.6700 mmol) was added in one addition and the reaction was heated to reflux while stirring for 24h. Crude residue was extracted via liquid-liquid extraction. The solvent was removed *in vacuo* and the crude

product was purified with flash chromatography to afford the desired compound, **KSC-56-int**, as a solid (103.7 mg, 41%). ^{1}H NMR (600 MHz, Chloroform-*d*) δ 7.33 (dd, *J* = 1.9, 0.9 Hz, 1H), 6.27 (dd, *J* = 3.2, 1.8 Hz, 1H), 6.23 – 6.09 (m, 1H), 3.84 (d, *J* = 0.8 Hz, 2H), 3.38 (d, *J* = 2.4 Hz, 2H), 2.22 (t, *J* = 2.4 Hz, 1H). ^{13}C NMR (151 MHz, Chloroform-*d*) δ 152.74, 141.82, 109.92, 107.26, 81.45, 71.51, 44.36, 36.90. HRMS for **KSC-53-int**: m/z calcd. 136.0684; obsd. 136.0762.

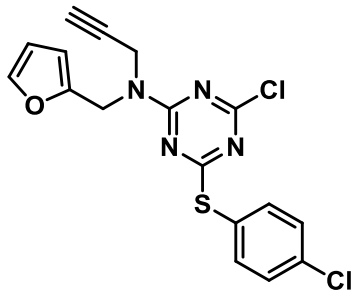

4-chloro-6-((4-chlorophenyl)thio)-*N*-(furan-2-ylmethyl)-*N*-(prop-2-yn-1-yl)-1,3,5-triazin-2-amine (KSC-56): To a solution of **KSC-46-int** (86.2 mg, 0.2947 mmol) and diisopropylethylamine (41.9 mg, 0.3242 mmol) in THF (9 mL), **KSC-56-int** (47.8 mg, 0.3536 mmol) was added at -20 °C and stirred for 3h. After 3h, the solvent was removed *in vacuo* and the crude product was purified with flash chromatography to afford the desired compound, **KSC-56**, as a yellow solid (97.5 mg, 85%). ^{1}H NMR (600 MHz, Acetone-d_6, mixture of rotamers) δ 7.74 – 7.59 (m, 2H), 7.58 – 7.49 (m, 2H), 7.48 (ddd, *J* = 3.5, 1.9, 0.8 Hz, 1H), 6.48 – 6.37 (m, 1H), 6.37 – 6.06 (m, 1H), 4.78 (d, *J* = 137.4 Hz, 2H), 4.31 (dd, *J* = 153.6, 2.5 Hz, 2H), 2.75 (dt, *J* = 35.5, 2.5 Hz, 1H). ^{13}C NMR (151 MHz, Acetone-d_6, mixture of rotamers) δ 183.10, 183.06, 169.95, 169.92, 164.45, 164.41,

150.50, 150.42, 143.91, 143.75, 138.07, 137.97, 137.91, 136.71, 136.61, 130.31, 130.29, 127.45, 127.42, 111.48, 111.40, 110.41, 109.87, 78.69, 78.67, 74.19, 73.84, 43.34, 43.24, 36.71. HRMS for **KSC-56**: m/z calcd. 391.0109; obsd. 391.0187.

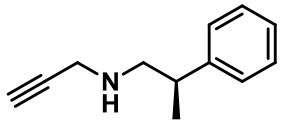

(*R*)-*N*-(2-phenylpropyl)prop-2-yn-1-amine (KSC-57-int): To a suspension of propargylbromide (183.3 mg, 1.2327 mmol) and potassium carbonate (187.4 mg, 1.3560 mmol) in acetonitrile (6 mL), (*R*)-2-phenylpropan-1-amine (500.0 mg, 3.6980 mmol) was added in one addition and the reaction was heated to reflux while stirring for 24h. Crude residue was extracted via liquid-liquid extraction. The solvent was removed *in vacuo* and the crude product was purified with flash chromatography to afford the desired compound, **KSC-57-int**, as a solid (121.8 mg, 57%). ^{1}H NMR (500 MHz, Chloroform-*d*) δ 7.32 (t, *J* = 7.5 Hz, 2H), 7.23 (dd, *J* = 12.5, 7.3 Hz, 3H), 3.39 (t, *J* = 2.7 Hz, 2H), 2.94 (dd, *J* = 7.5, 4.3 Hz, 2H), 2.84 (dd, *J* = 9.5, 5.9 Hz, 1H), 2.19 (d, *J* = 2.4 Hz, 1H), 1.29 (d, *J* = 6.1 Hz, 3H). ^{13}C NMR (126 MHz, Chloroform-*d*) δ 144.91, 128.42, 127.01, 126.26, 82.00, 71.06, 55.59, 39.90, 38.10, 20.03. HRMS for **KSC-57-int**: m/z calcd. 174.1204; obsd. 174.1283.

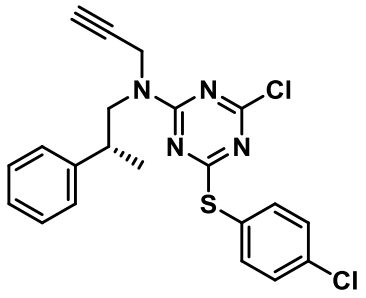

(*R*)-4-chloro-6-((4-chlorophenyl)thio)-*N*-(2-phenylpropyl)-*N*-(prop-2-yn-1-yl)-1,3,5-triazin-2-amine (KSC-57): To a solution of **KSC-46-int** (46.8 mg, 0.1600 mmol) and diisopropylethylamine (22.7 mg, 0.1760 mmol) in THF (5 mL), **KSC-57-int** (33.3 mg, 0.1920 mmol) was added at -20 °C and stirred for 3h. After 3h, the solvent was removed *in vacuo* and the crude product was purified with flash chromatography to afford the desired compound, **KSC-57**, as a yellow solid (48.0 mg, 70%).

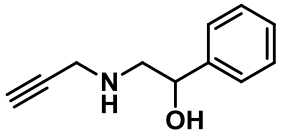

1-phenyl-2-(prop-2-yn-1-ylamino)ethan-1-ol (KSC-58-int): To a suspension of propargylbromide (96.0 mg, 0.6458 mmol) and potassium carbonate (214.2 mg, 1.5499 mmol) in acetonitrile (6 mL), 2-amino-1-phenylethan-1-ol (265.8 mg, 1.9373 mmol) was added in one addition and the reaction was heated to reflux while stirring for 24h. Crude residue was extracted via liquid-liquid extraction. The solvent was removed *in vacuo* and the crude product was purified with flash chromatography to afford the desired compound,

KSC-58-int, as a solid (44.9 mg, 40%). ^{1}H NMR (600 MHz, Chloroform-*d*) δ 7.39 – 7.31 (m, 4H), 7.30 – 7.23 (m, 1H), 4.75 (dd, *J* = 8.9, 3.6 Hz, 1H), 3.42 (d, *J* = 2.4 Hz, 2H), 2.95 (dd, *J* = 12.1, 3.6 Hz, 1H), 2.81 (dd, *J* = 12.2, 8.9 Hz, 1H), 2.21 (t, *J* = 2.5 Hz, 1H). ^{13}C NMR (151 MHz, Chloroform-*d*) δ 142.31, 128.29, 128.23, 127.46, 125.82, 125.72, 81.54, 71.80, 71.64, 55.75, 37.72. HRMS for **KSC-58-int**: m/z calcd. 176.0997; obsd. 176.1075.

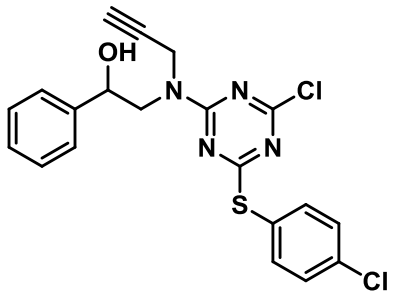

2-((4-chloro-6-((4-chlorophenyl)thio)-1,3,5-triazin-2-yl)(prop-2-yn-1-yl)amino)-1-phenylethan-1-ol (KSC-58): To a solution of **KSC-46-int** (62.5 mg, 0.2135 mmol) and diisopropylethylamine (30.4 mg, 0.2349 mmol) in THF (6 mL), **KSC-58-int** (44.9 mg, 0.2349 mmol) was added at -20 °C and stirred for 3h. After 3h, the solvent was removed *in vacuo* and the crude product was purified with flash chromatography to afford the desired compound, **KSC-58**, as a white solid (69.2 mg, 78%). ^{1}H NMR (600 MHz, Acetone-d_6, mixture of rotamers) δ 7.73 – 7.62 (m, 2H), 7.58 – 7.49 (m, 2H), 7.48 – 7.40 (m, 1H), 7.35 (td, *J* = 7.7, 1.5 Hz, 2H), 7.30 – 7.23 (m, 1H), 7.14 – 7.07 (m, 1H), 5.18 – 4.78 (m, 1H), 4.79 – 4.55 (m, 1H), 4.54 – 4.14 (m, 1H), 3.98 – 3.47 (m, 2H), 2.77 (dt, *J* = 20.8, 2.5 Hz, 1H). ^{13}C NMR (151 MHz, Acetone-d_6, mixture of rotamers) δ 206.26, 182.80, 169.49, 164.73, 164.60, 143.71, 143.43, 137.88, 137.86, 136.75, 136.52, 130.54, 130.24,

129.25, 129.21, 128.47, 128.37, 127.49, 126.85, 126.70, 79.27, 79.23, 73.89, 73.65, 72.42, 72.03, 55.02, 54.59, 54.56, 38.61, 38.51, 30.36, 30.23, 30.10, 29.97, 29.85, 29.72, 29.59. HRMS for **KSC-58**: m/z calcd. 431.0422; obsd. 431.0500.

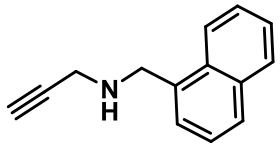

***N*-(naphthalen-1-ylmethyl)prop-2-yn-1-amine (KSC-59-int):** To a suspension of propargylbromide (64.5 mg, 0.4338 mmol) and potassium carbonate (143.9 mg, 1.0412 mmol) in acetonitrile (6 mL), Naphthalen-1-ylmethanamine (204.6 mg, 1.3015 mmol) was added in one addition and the reaction was heated to reflux while stirring for 24h. Crude residue was extracted via liquid-liquid extraction. The solvent was removed *in vacuo* and the crude product was purified with flash chromatography to afford the desired compound, **KSC-59-int**, as a solid. ^{1}H NMR (600 MHz, Acetone-d_6) δ 8.31 – 8.26 (m, 1H), 7.92 – 7.87 (m, 1H), 7.81 (d, J = 8.2 Hz, 1H), 7.54 – 7.48 (m, 3H), 7.43 (dd, J = 8.2, 6.9 Hz, 1H), 4.31 (s, 2H), 3.47 (d, J = 2.4 Hz, 2H), 2.73 (t, J = 2.4 Hz, 1H). ^{13}C NMR (151 MHz, Acetone-d_6) δ 136.58, 134.82, 133.00, 129.21, 128.43, 127.05, 126.54, 126.36, 126.12, 125.18, 83.33, 72.74, 50.52, 38.08. HRMS for **KSC-59-int**: m/z calcd. 196.1048; obsd. 196.1126.

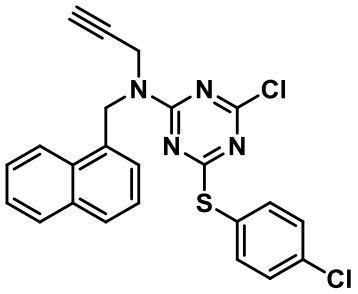

4-chloro-6-((4-chlorophenyl)thio)-*N*-(naphthalen-1-ylmethyl)-*N*-(prop-2-yn-1-yl)-1,3,5-triazin-2-amine (KSC-59): To a solution of **KSC-46-int** (61.3 mg, 0.2335 mmol) and diisopropylethylamine (33.2 mg, 0.2568 mmol) in THF (7 mL), **KSC-59-int** (54.7 mg, 0.2802 mmol) was added at -20 °C and stirred for 3h. After 3h, the solvent was removed *in vacuo* and the crude product was purified with flash chromatography to afford the desired compound, **KSC-59**, as a white solid (56.5 mg, 78%). ^{1}H NMR (600 MHz, Acetone-d_6, mixture of rotamers) δ 8.22 – 7.77 (m, 3H), 7.71 – 7.63 (m, 1H), 7.62 – 7.53 (m, 2H), 7.53 – 7.48 (m, 1H), 7.48 – 7.36 (m, 3H), 7.29 (dd, J = 7.0, 1.2 Hz, 1H), 7.04 – 6.93 (m, 1H), 5.28 (d, J = 154.2 Hz, 2H), 4.30 (dd, J = 168.0, 2.5 Hz, 2H), 2.77 (dt, J = 35.6, 2.5 Hz, 1H). ^{13}C NMR (151 MHz, Acetone-d_6, mixture of rotamers) δ 184.79, 184.66, 171.80, 171.55, 166.33, 166.28, 139.50, 139.14, 138.20, 138.00, 136.65, 136.56, 134.13, 133.92, 133.56, 133.40, 131.90, 131.60, 131.43, 131.37, 131.19, 130.91, 129.22, 129.18, 129.06, 128.72, 128.70, 128.65, 128.60, 127.99, 127.91, 127.83, 127.78, 125.90, 125.68, 80.49, 76.02, 75.63, 50.28, 49.89. HRMS for **KSC-59**: m/z calcd. 451.0473; obsd. 451.0550.

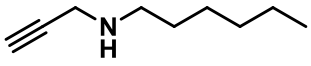

***N*-(prop-2-yn-1-yl)hexan-1-amine (KSC-60-int):** To a suspension of propargylbromide (323.3 mg, 2.7180 mmol) and potassium carbonate (819 mg, 5.9290 mmol) in acetonitrile (8 mL), hexylamine (250 mg, 2.4710 mmol) was added in one addition and the reaction was heated to reflux while stirring for 24h. Crude residue was extracted via liquid-liquid extraction. The solvent was removed *in vacuo* and the crude product was purified with flash chromatography to afford the desired compound, **KSC-60-int**, as a solid (192.3 mg, 51%). ^{1}H NMR (500 MHz, Chloroform-*d*) δ 3.40 (d, *J* = 2.4 Hz, 2H), 2.66 (t, *J* = 7.2 Hz, 2H), 2.21 – 2.10 (m, 1H), 1.52 – 1.39 (m, 2H), 1.37 – 1.15 (m, 6H), 0.86 (t, *J* = 6.8 Hz, 3H). ^{13}C NMR (126 MHz, Chloroform-*d*) δ 82.72, 71.45, 49.10, 38.54, 32.11, 30.17, 27.35, 22.97, 14.39. HRMS for **KSC-60-int**: m/z calcd. 178.1517; obsd. 178.1600.

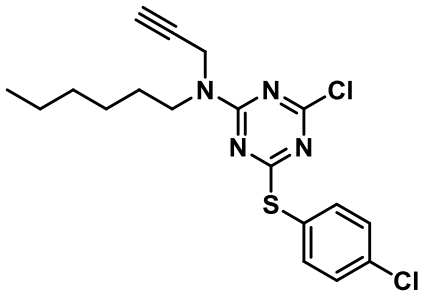

4-chloro-6-((4-chlorophenyl)thio)-*N*-hexyl-*N*-(prop-2-yn-1-yl)-1,3,5-triazin-2-amine (KSC-60): To a solution of **KSC-46-int** (70.0 mg, 0.2394 mmol) and diisopropylethylamine (34.0 mg, 0.2633 mmol) in THF (3 mL), **KSC-60-int** (40 mg, 0.2873 mmol) was added at -20 °C and stirred for 3h. After 3h, the solvent was removed *in vacuo* and the crude product was purified with flash chromatography to afford the

desired compound, **KSC-60**, as a an oil (69.0 mg, 73%). ^{1}H NMR (600 MHz, Acetone-d_6, mixture of rotamers) δ 7.72 – 7.61 (m, 2H), 7.59 – 7.48 (m, 2H), 4.31 (dd, J = 124.3, 2.5 Hz, 2H), 3.74 – 3.26 (m, 2H), 2.76 (dt, J = 17.8, 2.5 Hz, 1H), 1.48 – 1.26 (m, 6H), 1.25 – 1.01 (m, 3H), 0.90 – 0.84 (m, 3H). ^{13}C NMR (151 MHz, Acetone-d_6, mixture of rotamers) δ 206.05, 182.81, 182.23, 169.67, 169.35, 164.11, 163.95, 138.15, 137.73, 136.56, 136.32, 130.15, 130.06, 127.47, 127.43, 79.27, 73.59, 73.33, 48.43, 47.74, 37.20, 37.00, 32.34, 32.13, 27.71, 27.57, 27.11, 26.94, 23.31, 23.18, 14.34, 14.28. HRMS for **KSC-60**: m/z calcd. 395.0786; obsd. 395.0864.

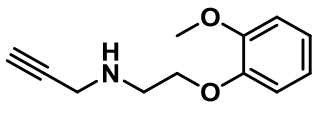

***N*-(2-(2-methoxyphenoxy)ethyl)prop-2-yn-1-amine (KSC-61-int):** To a suspension of propargylbromide (100 mg, 0.8406 mmol) and potassium carbonate (139.4 mg, 0.1008 mmol) in acetonitrile (8 mL), 2-(2-Methoxy)ethylamine (281.1 mg, 1.6812 mmol) was added in one addition and the reaction was heated to reflux while stirring for 24h. Crude residue was extracted via liquid-liquid extraction. The solvent was removed *in vacuo* and the crude product was purified with flash chromatography to afford the desired compound, **KSC-61-int**, as a solid (100.3 mg, 58%). ^{1}H NMR (600 MHz, Chloroform-*d*) δ 6.96 – 6.90 (m, 2H), 6.88 (ddd, J = 7.9, 6.1, 1.7 Hz, 2H), 4.13 (t, J = 5.3 Hz, 2H), 3.84 (s, 3H), 3.50 (d, J = 2.5 Hz, 2H), 3.09 (t, J = 5.3 Hz, 2H), 2.22 (t, J = 2.4 Hz, 1H). ^{13}C NMR (151 MHz,

Chloroform-*d*) δ 149.66, 148.13, 121.47, 120.70, 114.19, 111.76, 81.87, 71.33, 68.74, 55.67, 47.52, 38.06. HRMS for **KSC-61-int**: m/z calcd. 206.1103; obsd. 206.1181.

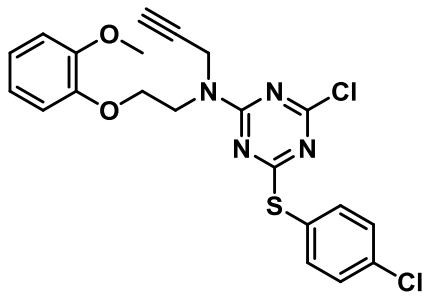

4-chloro-6-((4-chlorophenyl)thio)-*N*-(2-(2-methoxyphenoxy)ethyl)-*N*-(prop-2-yn-1-yl)-1,3,5-triazin-2-amine (KSC-61): To a solution of **KSC-46-int** (55.3 mg, 0.1890 mmol) and diisopropylethylamine (26.8. mg, 0.2079 mmol) in THF (5 mL), **KSC-61-int** (46.5 mg, 0.2268 mmol) was added at -20 °C and stirred for 3h. After 3h, the solvent was removed *in vacuo* and the crude product was purified with flash chromatography to afford the desired compound, **KSC-61**, as a white solid (83.0 mg, 95%). ^{1}H NMR (600 MHz, Acetone-d_6, mixture of rotamers) δ 7.69 – 7.62 (m, 2H), 7.55 – 7.45 (m, 2H), 7.00 – 6.81 (m, 4H), 4.54 (dd, *J* = 122.7, 2.5 Hz, 2H), 4.15 (dt, *J* = 106.0, 5.5 Hz, 2H), 3.91 (dt, *J* = 107.2, 5.5 Hz, 3H), 3.79 (d, *J* = 15.3 Hz, 4H), 2.79 (dt, *J* = 22.0, 2.5 Hz, 1H). ^{13}C NMR (151 MHz, Acetone-d_6, mixture of rotamers) δ 206.08, 182.76, 182.50, 169.70, 169.55, 164.39, 164.30, 150.68, 150.60, 149.09, 137.94, 137.76, 136.52, 136.40, 130.10, 130.08, 127.45, 127.35, 122.46, 122.36, 121.58, 121.54, 114.74, 114.35, 113.11, 113.02, 79.23, 79.18, 73.88, 73.60, 67.32, 66.88, 56.13, 56.09, 47.05, 46.63, 38.20, 37.97. HRMS for **KSC-61**: m/z calcd. 461.0528; obsd. 461.0606.

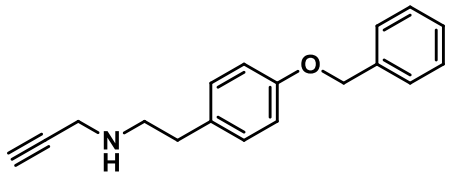

***N*-(4-(benzyloxy)phenethyl)prop-2-yn-1-amine (KSC-62-int):** To a suspension of propargylbromide (88.1 mg, 0.5928 mmol) and potassium carbonate (163.9 mg, 1.1856 mmol) in acetonitrile (4 mL), 2-(4-(benzyloxy)phenyl)ethan-1-amine (112.2 mg, 0.4940 mmol) was added in one addition and the reaction was heated to reflux while stirring for 24h. Crude residue was extracted via liquid-liquid extraction. The solvent was removed *in vacuo* and the crude product was purified with flash chromatography to afford the desired compound, **KSC-62-int**, as a solid (31.4 mg, 24%). ^{1}H NMR (600 MHz, Chloroform-*d*) δ 7.48 – 7.42 (m, 2H), 7.43 – 7.36 (m, 2H), 7.36 – 7.30 (m, 1H), 7.18 – 7.11 (m, 2H), 6.97 – 6.89 (m, 2H), 5.05 (s, 2H), 3.44 (dd, *J* = 2.5, 1.0 Hz, 2H), 2.95 (t, *J* = 7.1 Hz, 2H), 2.77 (t, *J* = 7.1 Hz, 2H), 2.25 – 2.17 (m, 1H). ^{13}C NMR (151 MHz, Chloroform-*d*) δ 157.64, 137.47, 132.39, 129.96, 128.88, 128.22, 127.77, 115.22, 82.43, 71.64, 70.36, 50.27, 38.46, 35.57. HRMS for **KSC-62-int**: m/z calcd. 266.14667; obsd. 266.1545.

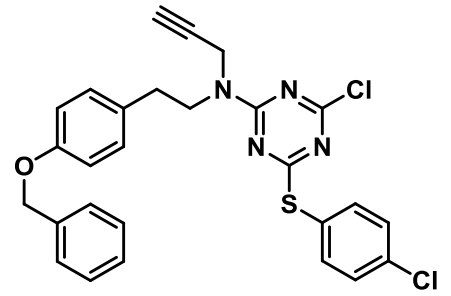

***N*-(4-(benzyloxy)phenethyl)-4-chloro-6-((4-chlorophenyl)thio)-*N*-(prop-2-yn-1-yl)-1,3,5-triazin-2-amine (KSC-62):** To a solution of **KSC-46-int** (27.8 mg, 0.0952 mmol) and diisopropylethylamine (13.5. mg, 0.1047 mmol) in THF (3 mL), **KSC-62-int** (30.3 mg, 0.1142 mmol) was added at -20 °C and stirred for 3h. After 3h, the solvent was removed *in vacuo* and the crude product was purified with flash chromatography to afford the desired compound, **KSC-62**, as a white solid (43.0 mg, 87%). ^{1}H NMR (600 MHz, Acetone-d_6, mixture of rotamers) δ 7.73 – 7.63 (m, 2H), 7.58 – 7.50 (m, 2H), 7.50 – 7.42 (m, 2H), 7.39 (q, J = 7.8 Hz, 2H), 7.35 – 7.28 (m, 1H), 7.22 – 7.17 (m, 1H), 6.97 – 6.92 (m, 2H), 6.92 – 6.86 (m, 1H), 5.10 (d, J = 12.5 Hz, 2H), 4.29 (dd, J = 144.9, 2.5 Hz, 2H), 3.90 – 3.57 (m, 2H), 2.80 (ddd, J = 20.5, 4.7, 2.0 Hz, 1H), 2.73 – 2.66 (m, 2H). ^{13}C NMR (151 MHz, Acetone-d_6, mixture of rotamers) δ 169.36, 164.14, 158.46, 138.51, 137.96, 137.74, 131.42, 130.69, 130.54, 130.36, 130.11, 129.28, 128.57, 128.35, 115.80, 81.38, 79.19, 73.90, 70.46, 49.65, 37.14, 32.83. HRMS for **KSC-62**: m/z calcd. 521.0891; obsd. 521.0970.

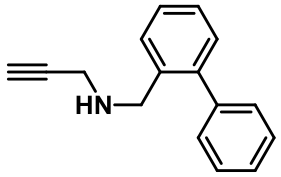

***N*-([1,1'-biphenyl]-2-ylmethyl)prop-2-yn-1-amine (KSC-63-int):** To a suspension of propargylbromide (104.3 mg, 0.8771 mmol) and potassium carbonate (243 mg, 1.7543

mmol) in acetonitrile (3.5 mL), 2-phenylbenzylamine hydrochloride (160.6 mg, 0.7310 mmol) was added in one addition and the reaction was heated to reflux while stirring for 24h. Crude residue was extracted via liquid-liquid extraction. The solvent was removed *in vacuo* and the crude product was purified with flash chromatography to afford the desired compound, **KSC-63-int**, as a solid (32 mg, 20%). ^{1}H NMR (600 MHz, Chloroform-*d*) δ 7.50 (dd, *J* = 7.5, 1.5 Hz, 1H), 7.45 – 7.30 (m, 7H), 7.29 – 7.24 (m, 1H), 3.81 (s, 2H), 3.33 (d, *J* = 2.4 Hz, 2H), 2.13 (t, *J* = 2.4 Hz, 1H). ^{13}C NMR (151 MHz, Chloroform-*d*) δ 142.16, 141.21, 136.94, 130.28, 129.47, 129.29, 128.26, 127.63, 127.20, 127.17, 82.14, 71.45, 50.12, 37.71. HRMS for **KSC-63-int**: m/z calcd. 222.1204; obsd. 222.1283.

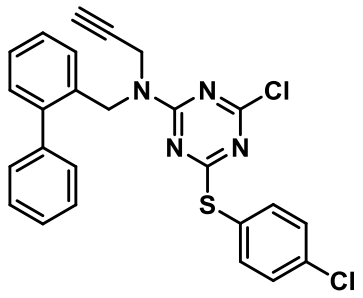

***N*-([1,1'-biphenyl]-2-ylmethyl)-4-chloro-6-((4-chlorophenyl)thio)-*N*-(prop-2-yn-1-yl)-1,3,5-triazin-2-amine (KSC-63):** To a solution of **KSC-46-int** (35.3 mg, 0.1205 mmol) and diisopropylethylamine (17.1. mg, 0.1325 mmol) in THF (3 mL), **KSC-63-int** (35.3 mg, 0.1205 mmol) was added at -20 °C and stirred for 3h. After 3h, the solvent was removed *in vacuo* and the crude product was purified with flash chromatography to afford the desired compound, **KSC-63**, as a white solid (55.0 mg, 96%). ^{1}H NMR (600 MHz, Acetone-d_6, mixture of rotamers) δ 8.12 – 7.92 (m, 2H), 7.87 – 7.74 (m, 7H), 7.69 – 7.59

(m, 3H), 5.23 (d, J = 147.0 Hz, 2H), 4.54 (dd, J = 156.4, 2.5 Hz, 2H), 3.08 (dt, J = 25.3, 2.5 Hz, 1H). ^{13}C NMR (151 MHz, Acetone-d_6, mixture of rotamers) δ 192.41, 191.97, 179.33, 179.14, 174.14, 173.97, 152.82, 152.47, 151.10, 151.05, 147.41, 147.37, 146.03, 143.67, 143.24, 140.70, 140.67, 139.77, 139.68, 139.40, 139.25, 138.87, 138.72, 138.67, 138.25, 138.23, 138.16, 138.07, 137.69, 137.05, 136.97, 88.09, 83.70, 83.37, 58.08, 57.79, 45.67, 45.49. HRMS for **KSC-63**: m/z calcd. 477.0629; obsd. 477.0708.

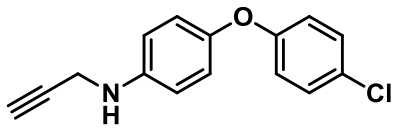

4-(4-chlorophenoxy)-*N*-(prop-2-yn-1-yl)aniline (KSC-64-int): To a suspension of propargylbromide (161.7 mg, 1.3590 mmol) and potassium carbonate (375.7 mg, 2.7182 mmol) in acetonitrile (5 mL), 4-amino-4-chlorodiphenylether (248.8 mg, 1.1326 mmol) was added in one addition and the reaction was heated to reflux while stirring for 24h. Crude residue was extracted via liquid-liquid extraction. The solvent was removed *in vacuo* and the crude product was purified with flash chromatography to afford the desired compound, **KSC-64-int**, as a solid (73 mg, 25%). ^{1}H NMR (600 MHz, Acetone-d_6) δ 7.34 – 7.24 (m, 2H), 6.94 – 6.84 (m, 4H), 6.82 – 6.73 (m, 2H), 5.25 (t, J = 6.4 Hz, 1H), 3.96 (dd, J = 6.3, 2.4 Hz, 2H), 2.63 (t, J = 2.4 Hz, 1H). ^{13}C NMR (151 MHz, Acetone-d_6) δ 159.08, 147.96, 145.89, 130.27, 127.05, 121.80, 119.10, 114.98, 82.41, 72.05, 33.78. HRMS for **KSC-64-int**: m/z calcd. 258.7170; obsd. 258.0686.

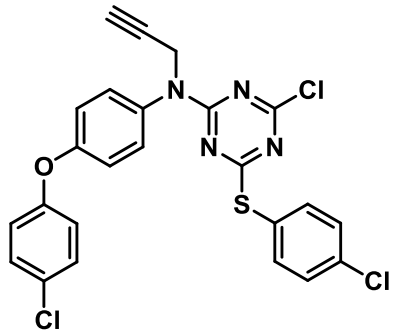

4-chloro-*N*-(4-(4-chlorophenoxy)phenyl)-6-((4-chlorophenyl)thio)-*N*-(prop-2-yn-1-yl)-1,3,5-triazin-2-amine (KSC-64): To a solution of **KSC-46-int** (22.4 mg, 0.0766 mmol) and diisopropylethylamine (10.9. mg, 0.0843 mmol) in THF (2 mL), **KSC-64-int** (23.7 mg, 0.0920 mmol) was added at -20 °C and stirred for 3h. After 3h, the solvent was removed *in vacuo* and the crude product was purified with flash chromatography to afford the desired compound, **KSC-64**, as a white solid (27.9 mg, 71%). ^{1}H NMR (500 MHz, Acetone-d_6, mixture of rotamers) δ 7.64 (dd, J = 81.3, 8.0 Hz, 2H), 7.44 (ddd, J = 21.4, 12.7, 8.4 Hz, 4H), 7.31 (dd, J = 32.9, 8.3 Hz, 2H), 7.18 – 6.93 (m, 4H), 4.62 (dd, J = 120.3, 2.5 Hz, 2H), 2.86 – 2.75 (m, 1H). ^{13}C NMR (126 MHz, Acetone-d_6, mixture of rotamers) δ 181.84, 163.86, 156.18, 155.55, 136.92, 136.34, 129.94, 129.29, 129.05, 128.96, 128.71, 126.35, 126.14, 120.88, 118.81, 118.56, 101.37, 87.77, 78.38, 73.45, 73.25, 40.36, 39.80.

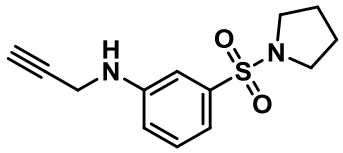

***N*-(prop-2-yn-1-yl)-3-(pyrrolidin-1-ylsulfonyl)aniline (KSC-65-int):** To a suspension of propargylbromide (100 mg, 0.8406 mmol) and potassium carbonate (139.4 mg, 0.1009 mmol) in acetonitrile (5 mL), (aminophenyl)sulfonyl pyrrolidine (380.4 mg, 0.1681 mmol) was added in one addition and the reaction was heated to reflux while stirring for 24h. Crude residue was extracted via liquid-liquid extraction. The solvent was removed *in vacuo* and the crude product was purified with flash chromatography to afford the desired compound, **KSC-65-int**, as a solid (100.9 mg, 45%). ^{1}H NMR (600 MHz, Chloroform-*d*) δ 7.31 (t, *J* = 7.9 Hz, 1H), 7.17 (dd, *J* = 7.9, 1.4 Hz, 1H), 7.10 (t, *J* = 2.0 Hz, 1H), 6.85 (dd, *J* = 8.2, 2.4 Hz, 1H), 4.34 (t, *J* = 6.1 Hz, 1H), 3.96 (dd, *J* = 6.0, 2.4 Hz, 2H), 3.30 – 3.17 (m, 4H), 2.21 (t, *J* = 2.4 Hz, 1H), 1.76 – 1.69 (m, 4H). ^{13}C NMR (151 MHz, Chloroform-*d*) δ 147.63, 137.75, 130.04, 117.64, 117.30, 111.90, 80.49, 71.98, 48.26, 33.63, 25.51. HRMS for **KSC-65-int**: m/z calcd. 265.0932; obsd. 265.1011.

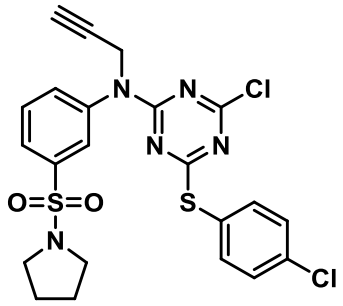

4-chloro-6-((4-chlorophenyl)thio)-*N*-(prop-2-yn-1-yl)-*N*-(3-(pyrrolidin-1-ylsulfonyl)phenyl)-1,3,5-triazin-2-amine (KSC-65): To a solution of **KSC-46-int** (48.6

mg, 0.1661 mmol) and diisopropylethylamine (23.6. mg, 0.1827 mmol) in THF (5 mL), **KSC-65-int** (52.7 mg, 0.1993 mol) was added at -20 °C and stirred for 3h. After 3h, the solvent was removed *in vacuo* and the crude product was purified with flash chromatography to afford the desired compound, **KSC-65**, as a white solid (58.7 mg, 68%). ^{1}H NMR (500 MHz, Acetone-d_6, mixture of rotamers) δ 8.21 – 7.10 (m, 8H), 4.73 (d, J = 109.3 Hz, 2H), 3.22 (d, J = 5.9 Hz, 4H), 2.90 – 2.73 (m, 1H), 1.81 – 1.66 (m, 4H). ^{13}C NMR (126 MHz, Acetone-d_6, mixture of rotamers) δ 169.73, 164.72, 142.37, 137.76, 137.35, 132.73, 130.88, 130.12, 127.98, 127.28, 78.99, 74.79, 74.57, 48.85, 25.85. HRMS for **KSC-65**: m/z calcd. 520.0357; obsd. 520.0436.

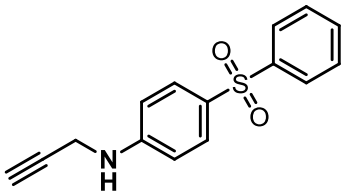

4-(phenylsulfonyl)-*N*-(prop-2-yn-1-yl)aniline (KSC-66-int): To a suspension of propargylbromide (175.8 mg, 1.1821 mmol) and potassium carbonate (178.2 mg, 1.2896 mmol) in acetonitrile (5 mL), 4-(phenylsulfonyl)aniline (250.7 mg, 1.0746 mmol) was added in one addition and the reaction was heated to reflux while stirring for 24h. Crude residue was extracted via liquid-liquid extraction. The solvent was removed *in vacuo* and the crude product was purified with flash chromatography to afford the desired compound, **KSC-66-int**, as a solid (71.8 mg, 25%). ^{1}H NMR (500 MHz, Chloroform-*d*) δ 7.92 – 7.81 (m, 2H), 7.80 – 7.68 (m, 2H), 7.55 – 7.36 (m, 3H), 6.69 – 6.58 (m, 2H), 3.93 (dd, J = 6.0,

2.5 Hz, 2H), 2.23 (t, J = 2.4 Hz, 1H). ^{13}C NMR (126 MHz, Chloroform-*d*) δ 150.87, 143.00, 132.60, 129.75, 129.18, 127.14, 112.69, 79.61, 72.06, 32.97. HRMS for **KSC-66-int**: m/z calcd. 271.0667; obsd. 272.0742.

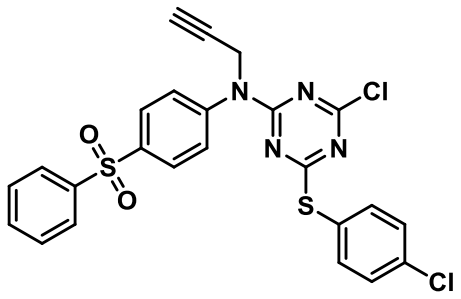

4-chloro-6-((4-chlorophenyl)thio)-*N*-(4-(phenylsulfonyl)phenyl)-*N*-(prop-2-yn-1-yl)-1,3,5-triazin-2-amine (KSC-66): To a solution of **KSC-46-int** (64.3 mg, 0.2199 mmol) and diisopropylethylamine (31.3. mg, 0.2419 mmol) in THF (5 mL), **KSC-66-int** (71.6 mg, 0.2639 mol) was added at -20 °C and stirred for 3h. After 3h, the solvent was removed *in vacuo* and the crude product was purified with flash chromatography to afford the desired compound, **KSC-65**, as a white solid. ^{1}H NMR (600 MHz, Acetone-d_6, mixture of rotamers) δ 8.12 – 7.95 (m, 5H), 7.77 – 7.52 (m, 8H), 2.81 (t, J = 2.5 Hz, 2H), 2.05 (p, J = 2.2 Hz, 1H). ^{13}C NMR (151 MHz, Acetone-d_6, mixture of rotamers) δ 183.37, 169.88, 164.64, 146.28, 142.84, 137.70, 136.71, 134.60, 130.66, 130.33, 129.56, 128.76, 127.06, 79.15, 74.72, 60.68, 40.72. HRMS for **KSC-65**: m/z calcd. 527.0092; obsd. 527.0195.

References

1. Singh, J.; Petter, R. C.; Baillie, T. A.; Whitty, A., The resurgence of covalent drugs. *Nat Rev Drug Discov* **2011,** *10* (4), 307-17.
2. Johnson, D. S.; Weerapana, E.; Cravatt, B. F., Strategies for discovering and derisking covalent, irreversible enzyme inhibitors. *Future Med Chem* **2010,** *2* (6), 949-64.
3. Bauer, R. A., Covalent inhibitors in drug discovery: from accidental discoveries to avoided liabilities and designed therapies. *Drug Discov Today* **2015,** *20* (9), 1061-73.
4. Edgington, L. E.; Verdoes, M.; Bogyo, M., Functional imaging of proteases: recent advances in the design and application of substrate-based and activity-based probes. *Curr Opin Chem Biol* **2011,** *15* (6), 798-805.
5. Fonovic, M.; Bogyo, M., Activity-based probes as a tool for functional proteomic analysis of proteases. *Expert Rev Proteomics* **2008,** *5* (5), 721-30.
6. Cravatt, B. F.; Wright, A. T.; Kozarich, J. W., Activity-based protein profiling: from enzyme chemistry to proteomic chemistry. *Annu Rev Biochem* **2008,** *77*, 383-414.
7. Weerapana, E.; Simon, G. M.; Cravatt, B. F., Disparate proteome reactivity profiles of carbon electrophiles. *Nat Chem Biol* **2008,** *4* (7), 405-7.
8. Weerapana, E.; Wang, C.; Simon, G. M.; Richter, F.; Khare, S.; Dillon, M. B.; Bachovchin, D. A.; Mowen, K.; Baker, D.; Cravatt, B. F., Quantitative reactivity profiling predicts functional cysteines in proteomes. *Nature* **2010,** *468* (7325), 790-5.
9. Shin, N. Y.; Liu, Q.; Stamer, S. L.; Liebler, D. C., Protein targets of reactive electrophiles in human liver microsomes. *Chem Res Toxicol* **2007,** *20* (6), 859-67.
10. Patricelli, M. P.; Szardenings, A. K.; Liyanage, M.; Nomanbhoy, T. K.; Wu, M.; Weissig, H.; Aban, A.; Chun, D.; Tanner, S.; Kozarich, J. W., Functional interrogation of the kinome using nucleotide acyl phosphates. *Biochemistry* **2007,** *46* (2), 350-8.
11. Gu, C.; Shannon, D. A.; Colby, T.; Wang, Z.; Shabab, M.; Kumari, S.; Villamor, J. G.; McLaughlin, C. J.; Weerapana, E.; Kaiser, M.; Cravatt, B. F.; van der Hoorn, R. A., Chemical proteomics with sulfonyl fluoride probes reveals selective labeling of functional tyrosines in glutathione transferases. *Chem Biol* **2013,** *20* (4), 541-8.

12. Shannon, D. A.; Gu, C.; McLaughlin, C. J.; Kaiser, M.; van der Hoorn, R. A.; Weerapana, E., Sulfonyl fluoride analogues as activity-based probes for serine proteases. *Chembiochem* **2012,** *13* (16), 2327-30.
13. Kidd, D.; Liu, Y.; Cravatt, B. F., Profiling serine hydrolase activities in complex proteomes. *Biochemistry* **2001,** *40* (13), 4005-15.
14. Greenbaum, D.; Medzihradszky, K. F.; Burlingame, A.; Bogyo, M., Epoxide electrophiles as activity-dependent cysteine protease profiling and discovery tools. *Chem Biol* **2000,** *7* (8), 569-81.
15. Evans, M. J.; Morris, G. M.; Wu, J.; Olson, A. J.; Sorensen, E. J.; Cravatt, B. F., Mechanistic and structural requirements for active site labeling of phosphoglycerate mutase by spiroepoxides. *Mol Biosyst* **2007,** *3* (7), 495-506.
16. Bachovchin, D. A.; Ji, T.; Li, W.; Simon, G. M.; Blankman, J. L.; Adibekian, A.; Hoover, H.; Niessen, S.; Cravatt, B. F., Superfamily-wide portrait of serine hydrolase inhibition achieved by library-versus-library screening. *Proc Natl Acad Sci U S A* **2010,** *107* (49), 20941-6.
17. Kato, D.; Boatright, K. M.; Berger, A. B.; Nazif, T.; Blum, G.; Ryan, C.; Chehade, K. A.; Salvesen, G. S.; Bogyo, M., Activity-based probes that target diverse cysteine protease families. *Nat Chem Biol* **2005,** *1* (1), 33-8.
18. Verdoes, M.; Oresic Bender, K.; Segal, E.; van der Linden, W. A.; Syed, S.; Withana, N. P.; Sanman, L. E.; Bogyo, M., Improved quenched fluorescent probe for imaging of cysteine cathepsin activity. *J Am Chem Soc* **2013,** *135* (39), 14726-30.
19. Shannon, D. A.; Banerjee, R.; Webster, E. R.; Bak, D. W.; Wang, C.; Weerapana, E., Investigating the proteome reactivity and selectivity of aryl halides. *J Am Chem Soc* **2014,** *136* (9), 3330-3.
20. Miller, J., The S_N Mechanism in Aromatic Compounds. Part XXVII.[1] A Quantitative Approach to Aromatic Nucleophilic Substitution. *J Am Chem Soc* **1963,** *85* (11), 1628-1635.
21. Bernasconi, C. F., *Chimia* **1980,** *34*.
22. Crawford, L. A.; Weerapana, E., A tyrosine-reactive irreversible inhibitor for glutathione S-transferase Pi (GSTP1). *Mol Biosyst* **2016,** *12* (6), 1768-71.

23. Nebert, D. W.; Vasiliou, V., Analysis of the glutathione S-transferase (GST) gene family. *Hum Genomics* **2004,** *1* (6), 460-4.
24. Senger, N. A.; Bo, B.; Cheng, Q.; Keeffe, J. R.; Gronert, S.; Wu, W., The element effect revisited: factors determining leaving group ability in activated nucleophilic aromatic substitution reactions. *J Org Chem* **2012,** *77* (21), 9535-40.
25. El Guesmi, N.; Berionni, G.; Asghar, B. H., Electronic and solvent effects on kinetics of SNAr substitution reactions of substituted anilines with 2,6-bis(trifluoromethanesulfonyl)-4-nitroanisole in MeOH-Me2SO mixtures of varying composition: one reaction with two mechanistic pathways. *Monatsh Chem* **2013,** *144* (10), 1537-1545.
26. M. J. Frisch, G. W. T., H. B. Schlegel, G. E. Scuseria, M. A. Robb, J. R. Cheeseman, G. Scalmani, V. Barone, B. Mennucci, G. A. Petersson, H. Nakatsuji, M. Caricato, X. Li, H. P. Hratchian, A. F. Izmaylov, J. Bloino, G. Zheng, J. L. Sonnenberg, M. Hada, M. Ehara, K. Toyota, R. Fukuda, J. Hasegawa, M. Ishida, T. Nakajima, Y. Honda, O. Kitao, H. Nakai, T. Vreven, J. A. Montgomery, Jr., J. E. Peralta, F. Ogliaro, M. Bearpark, J. J. Heyd, E. Brothers, K. N. Kudin, V. N. Staroverov, R. Kobayashi, J. Normand, K. Raghavachari, A. Rendell, J. C. Burant, S. S. Iyengar, J. Tomasi, M. Cossi, N. Rega, J. M. Millam, M. Klene, J. E. Knox, J. B. Cross, V. Bakken, C. Adamo, J. Jaramillo, R. Gomperts, R. E. Stratmann, O. Yazyev, A. J. Austin, R. Cammi, C. Pomelli, J. W. Ochterski, R. L. Martin, K. Morokuma, V. G. Zakrzewski, G. A. Voth, P. Salvador, J. J. Dannenberg, S. Dapprich, A. D. Daniels, Ö. Farkas, J. B. Foresman, J. V. Ortiz, J. Cioslowski, and D. J. Fox *Gaussian 09*, Wallingford, CT, 2009.
27. Speers, A. E.; Adam, G. C.; Cravatt, B. F., Activity-based protein profiling in vivo using a copper(i)-catalyzed azide-alkyne [3 + 2] cycloaddition. *J Am Chem Soc* **2003,** *125* (16), 4686-7.
28. Speers, A. E.; Cravatt, B. F., Profiling enzyme activities in vivo using click chemistry methods. *Chem Biol* **2004,** *11* (4), 535-46.
29. Frey, A. G.; Palenchar, D. J.; Wildemann, J. D.; Philpott, C. C., A Glutaredoxin.BolA Complex Serves as an Iron-Sulfur Cluster Chaperone for the Cytosolic Cluster Assembly Machinery. *J Biol Chem* **2016,** *291* (43), 22344-22356.

30. Maio, N.; Rouault, T. A., Iron-sulfur cluster biogenesis in mammalian cells: New insights into the molecular mechanisms of cluster delivery. *Biochim Biophys Acta* **2015,** *1853* (6), 1493-512.
31. Lill, R., Function and biogenesis of iron-sulphur proteins. *Nature* **2009,** *460* (7257), 831-8.
32. Rodriguez-Manzaneque, M. T.; Tamarit, J.; Belli, G.; Ros, J.; Herrero, E., Grx5 is a mitochondrial glutaredoxin required for the activity of iron/sulfur enzymes. *Mol Biol Cell* **2002,** *13* (4), 1109-21.
33. Wingert, R. A.; Galloway, J. L.; Barut, B.; Foott, H.; Fraenkel, P.; Axe, J. L.; Weber, G. J.; Dooley, K.; Davidson, A. J.; Schmid, B.; Paw, B. H.; Shaw, G. C.; Kingsley, P.; Palis, J.; Schubert, H.; Chen, O.; Kaplan, J.; Zon, L. I., Deficiency of glutaredoxin 5 reveals Fe-S clusters are required for vertebrate haem synthesis. *Nature* **2005,** *436* (7053), 1035-39.
34. Li, H.; Mapolelo, D. T.; Dingra, N. N.; Naik, S. G.; Lees, N. S.; Hoffman, B. M.; Riggs-Gelasco, P. J.; Huynh, B. H.; Johnson, M. K.; Outten, C. E., The yeast iron regulatory proteins Grx3/4 and Fra2 form heterodimeric complexes containing a [2Fe-2S] cluster with cysteinyl and histidyl ligation. *Biochemistry* **2009,** *48* (40), 9569-81.
35. Muhlenhoff, U.; Molik, S.; Godoy, J. R.; Uzarska, M. A.; Richter, N.; Seubert, A.; Zhang, Y.; Stubbe, J.; Pierrel, F.; Herrero, E.; Lillig, C. H.; Lill, R., Cytosolic monothiol glutaredoxins function in intracellular iron sensing and trafficking via their bound iron-sulfur cluster. *Cell Metab* **2010,** *12* (4), 373-85.
36. Rouhier, N.; Couturier, J.; Johnson, M. K.; Jacquot, J. P., Glutaredoxins: roles in iron homeostasis. *Trends Biochem Sci* **2010,** *35* (1), 43-52.
37. Lillig, C. H.; Berndt, C.; Holmgren, A., Glutaredoxin systems. *Biochim Biophys Acta* **2008,** *1780* (11), 1304-17.
38. Herrero, E.; de la Torre-Ruiz, M. A., Monothiol glutaredoxins: a common domain for multiple functions. *Cell Mol Life Sci* **2007,** *64* (12), 1518-30.
39. Haunhorst, P.; Berndt, C.; Eitner, S.; Godoy, J. R.; Lillig, C. H., Characterization of the human monothiol glutaredoxin 3 (PICOT) as iron-sulfur protein. *Biochem Biophys Res Commun* **2010,** *394* (2), 372-6.

40. Banci, L.; Camponeschi, F.; Ciofi-Baffoni, S.; Muzzioli, R., Elucidating the Molecular Function of Human BOLA2 in GRX3-Dependent Anamorsin Maturation Pathway. *J Am Chem Soc* **2015,** *137* (51), 16133-43.
41. Banci, L.; Brancaccio, D.; Ciofi-Baffoni, S.; Del Conte, R.; Gadepalli, R.; Mikolajczyk, M.; Neri, S.; Piccioli, M.; Winkelmann, J., [2Fe-2S] cluster transfer in iron-sulfur protein biogenesis. *Proc Natl Acad Sci U S A* **2014,** *111* (17), 6203-8.
42. Banci, L.; Ciofi-Baffoni, S.; Gajda, K.; Muzzioli, R.; Peruzzini, R.; Winkelmann, J., N-terminal domains mediate [2Fe-2S] cluster transfer from glutaredoxin-3 to anamorsin. *Nat Chem Biol* **2015,** *11* (10), 772-8.
43. Haunhorst, P.; Hanschmann, E. M.; Brautigam, L.; Stehling, O.; Hoffmann, B.; Muhlenhoff, U.; Lill, R.; Berndt, C.; Lillig, C. H., Crucial function of vertebrate glutaredoxin 3 (PICOT) in iron homeostasis and hemoglobin maturation. *Mol Biol Cell* **2013,** *24* (12), 1895-903.
44. Witte, S.; Villalba, M.; Bi, K.; Liu, Y.; Isakov, N.; Altman, A., Inhibition of the c-Jun N-terminal kinase/AP-1 and NF-kappaB pathways by PICOT, a novel protein kinase C-interacting protein with a thioredoxin homology domain. *J Biol Chem* **2000,** *275* (3), 1902-9.
45. Cha, H.; Kim, J. M.; Oh, J. G.; Jeong, M. H.; Park, C. S.; Park, J.; Jeong, H. J.; Park, B. K.; Lee, Y. H.; Jeong, D.; Yang, D. K.; Bernecker, O. Y.; Kim, D. H.; Hajjar, R. J.; Park, W. J., PICOT is a critical regulator of cardiac hypertrophy and cardiomyocyte contractility. *J Mol Cell Cardiol* **2008,** *45* (6), 796-803.
46. Jeong, D.; Cha, H.; Kim, E.; Kang, M.; Yang, D. K.; Kim, J. M.; Yoon, P. O.; Oh, J. G.; Bernecker, O. Y.; Sakata, S.; Le, T. T.; Cui, L.; Lee, Y. H.; Kim, D. H.; Woo, S. H.; Liao, R.; Hajjar, R. J.; Park, W. J., PICOT inhibits cardiac hypertrophy and enhances ventricular function and cardiomyocyte contractility. *Circ Res* **2006,** *99* (3), 307-14.
47. Voet, D.; Voet, J., *Biochemistry*. 3rd ed.; John Wiley & Sons: 2004; p 1616.
48. Dunaway, G. A.; Kasten, T. P.; Sebo, T.; Trapp, R., Analysis of the phosphofructokinase subunits and isoenzymes in human tissues. *Biochem J* **1988,** *251* (3), 677-83.

49. Van Schaftingen, E.; Jett, M. F.; Hue, L.; Hers, H. G., Control of liver 6-phosphofructokinase by fructose 2,6-bisphosphate and other effectors. *Proc Natl Acad Sci U S A* **1981,** *78* (6), 3483-6.
50. Van Schaftingen, E.; Hue, L.; Hers, H. G., Fructose 2,6-bisphosphate, the probably structure of the glucose- and glucagon-sensitive stimulator of phosphofructokinase. *Biochem J* **1980,** *192* (3), 897-901.
51. Chesney, J., 6-phosphofructo-2-kinase/fructose-2,6-bisphosphatase and tumor cell glycolysis. *Curr Opin Clin Nutr Metab Care* **2006,** *9* (5), 535-9.
52. Hesterberg, L. K.; Lee, J. C., Self-association of rabbit muscle phosphofructokinase: effects of ligands. *Biochemistry* **1982,** *21* (2), 216-22.
53. Costa Leite, T.; Da Silva, D.; Guimaraes Coelho, R.; Zancan, P.; Sola-Penna, M., Lactate favours the dissociation of skeletal muscle 6-phosphofructo-1-kinase tetramers down-regulating the enzyme and muscle glycolysis. *Biochem J* **2007,** *408* (1), 123-30.
54. Webb, B. A.; Forouhar, F.; Szu, F. E.; Seetharaman, J.; Tong, L.; Barber, D. L., Structures of human phosphofructokinase-1 and atomic basis of cancer-associated mutations. *Nature* **2015,** *523* (7558), 111-4.
55. Hanahan, D.; Weinberg, R. A., Hallmarks of cancer: the next generation. *Cell* **2011,** *144* (5), 646-74.
56. Yalcin, A.; Telang, S.; Clem, B.; Chesney, J., Regulation of glucose metabolism by 6-phosphofructo-2-kinase/fructose-2,6-bisphosphatases in cancer. *Exp Mol Pathol* **2009,** *86* (3), 174-9.
57. Moon, J. S.; Kim, H. E.; Koh, E.; Park, S. H.; Jin, W. J.; Park, B. W.; Park, S. W.; Kim, K. S., Kruppel-like factor 4 (KLF4) activates the transcription of the gene for the platelet isoform of phosphofructokinase (PFKP) in breast cancer. *J Biol Chem* **2011,** *286* (27), 23808-16.
58. Sheng, H.; Tang, W., Glycolysis Inhibitors for Anticancer Therapy: A Review of Recent Patents. *Recent Pat Anticancer Drug Discov* **2016,** *11* (3), 297-308.
59. Chand, P.; Tapolsky, G. H. PFKFB33 inhibitor and methods of use as an anti-cancer therapeutic. 2013.
60. Lee, Y. H.; Jim, J. D. Inhibitors of PFKFB3 for cancer therapy. US9492418 B2, 2012.

61. Tapolsky, G. H.; Chand, P.; Trent, J. O.; Telang, S.; Clem, B. F.; Chesney, J. Family of PFKFB3 inhibitors with anti-neoplastic activities US8557823 B2, 2013.
62. Styrbjörn, B.; Katarina, F.; Charles, H.; Evert, H.; Mattias, J.; Thomas, L.; Jessica, M.; Meral, S. Preparation of (hetero) aryl sulfonamides for treating inflammation and cancer. 2012.
63. Johan, A.; Evert, H.; Thomas, L.; Jessica, M.; Meral, S.; Mattias, J.; Katarina, F.; Kenth, H. Preparation of bisarylsulfonamides as inhibitors of 6-phosphofructo-2-kinase/ fructose-2,6-bisphosphatase PFKFB3 and PFKFB4 isoforms useful in the treatment of inflammation and cancer. 2011.
64. Chand, P.; Chesney, J. A.; Clem, B. F.; Tapolsky, G. H.; Telang, S.; Trent, J. O. Small molecule inhibitors of 6-phosphofructo-2-kinase/fructose-2, 6-biphosphatase 3 and glycolytic flux and their methods of use as anti-cancer therapeutics. 2011.
65. Chesney, J.; Trent, J. O.; Telang, S.; Clem, B.; Meier, J. Family of PFKFB3 inhibitors with anti-neoplastic activities. 2008.
66. Weerapana, E.; Speers, A. E.; Cravatt, B. F., Tandem orthogonal proteolysis-activity-based protein profiling (TOP-ABPP)--a general method for mapping sites of probe modification in proteomes. *Nat Protoc* **2007,** *2* (6), 1414-25.

Appendix. Mass Spectometry Tables

Appendix Table 4.1. Mass Spectrometry data for KSC-56 treated samples. The proteins shown are those that displayed an average spectral count of 10 or greater in the KSC-56 treated sample. The data is sorted by the spectral count difference between the KSC-56 treated and the DMSO (no probe) samples.

ID	Protein	Description	pI	Length (aa)	Mass(Da)	DMSO Avg	KSC 56 Avg	Change in SC
O76003	GLRX3	GLRX3 Glutaredoxin-3	5.4	335	37432	0	312	312
P49327	FASN	FASN Fatty acid synthase	6.4	2511	273424	17	283	266
P08238	HSP90AB1	HSP90AB1 Heat shock protein HSP 90-beta	5	724	83264	11	224	214
Q71U36	TUBA1A	TUBA1A Tubulin alpha-1A chain	5.1	451	50136	16	189	173
P60709	ACTB	ACTB Actin, cytoplasmic 1	5.5	375	41737	28	188	160
P68366	TUBA4A	TUBA4A Tubulin alpha-4A chain	5.1	448	49924	26	177	152
P07900	HSP90AA1	HSP90AA1 Heat shock protein HSP 90-alpha	5	732	84660	7	157	150
P78527	PRKDC	PRKDC DNA-dependent protein kinase catalytic subunit	7.1	4128	469093	0	135	135
P21333	FLNA	FLNA Filamin-A	6.1	2647	280737	29	161	132
Q00610	CLTC	CLTC Clathrin heavy chain 1	5.7	1675	191613	7	125	118
P05165	PCCA	PCCA Propionyl-CoA carboxylase alpha chain, mitochondrial	7.5	728	80059	94	199	105
Q9BVA1	TUBB2B	TUBB2B Tubulin beta-2B chain	4.9	445	49953	0	105	105
P13639	EEF2	EEF2 Elongation factor 2	6.8	858	95338	17	117	100
Q96RQ3	MCCC1	MCCC1 Methylcrotonoyl-CoA carboxylase subunit alpha, mitochondrial	7.8	725	80473	157	247	90
P15924	DSP	DSP Desmoplakin	6.8	2871	331774	4	91	87
P14618	PKM	PKM Pyruvate kinase isozymes M1/M2	7.8	531	57937	36	123	87
P07437	TUBB	TUBB Tubulin beta chain	4.9	444	49671	63	149	86
P68371	TUBB4B	TUBB4B Tubulin beta-4B chain	4.9	445	49831	64	146	82
P04075	ALDOA	ALDOA Fructose-bisphosphate aldolase A	8.1	364	39420	10	84	74

Q01813	PFKP	PFKP 6-phosphofructokinase type C	7.6	784	85596	2	73	72
P07339	CTSD	CTSD Cathepsin D	6.5	412	44552	0	68	68
Q9NY65	TUBA8	TUBA8 Tubulin alpha-8 chain	5.1	449	50094	19	82	63
Q05639	EEF1A2	EEF1A2 Elongation factor 1-alpha 2	9	463	50470	0	61	61
P21266	GSTM3	GSTM3 Glutathione S-transferase Mu 3	5.5	225	26560	0	59	59
Q92616	GCN1L1	GCN1L1 Translational activator GCN1	7.5	2671	292756	2	59	58
Q15365	PCBP1	PCBP1 Poly(rC)-binding protein 1	7.1	356	37498	1	58	57
Q15149	PLEC	PLEC Plectin	6	4684	531796	9	65	56
Q8TEX9	IPO4	IPO4 Importin-4	5	1081	118715	2	57	55
Q16881	TXNRD1	TXNRD1 Thioredoxin reductase 1, cytoplasmic	7.4	649	70756	0	51	51
O75369	FLNB	FLNB Filamin-B	5.7	2602	278162	11	62	51
H7C469	Uncharacterized	Uncharacterized protein	5.7	379	40447	0	51	51
Q14204	DYNC1H1	DYNC1H1 Cytoplasmic dynein 1 heavy chain 1	6.4	4646	532412	4	48	44
Q9HCC0	MCCC2	MCCC2 Methylcrotonoyl-CoA carboxylase beta chain, mitochondrial	7.7	563	61333	3	47	44
Q8TCU6	PREX1	PREX1 Phosphatidylinositol 3,4,5-trisphosphate-dependent Rac exchanger 1 protein	6.4	1659	186202	1	45	44
P35579	MYH9	MYH9 Myosin-9	5.6	1960	226530	7	50	44
P27708	CAD	CAD CAD protein	6.5	2225	242981	0	42	42
P08107	HSPA1B	HSPA1B Heat shock 70 kDa protein 1A/1B	5.6	641	70052	8	50	42
P11142	HSPA8	HSPA8 Heat shock cognate 71 kDa protein	5.5	646	70898	14	55	42
O43175	PHGDH	PHGDH D-3-phosphoglycerate dehydrogenase	6.7	533	56651	4	44	40
P08243	ASNS	ASNS Asparagine synthetase	6.9	561	64370	0	39	39
P11413	G6PD	G6PD Glucose-6-phosphate 1-dehydrogenase	6.8	515	59257	2	39	38
Q7Z6Z7	HUWE1	HUWE1 E3 ubiquitin-protein ligase HUWE1	5.2	4374	481896	0	37	37
Q13085	ACACA	ACACA Acetyl-CoA carboxylase 1	6.4	2346	265551	243	280	37
P22314	UBA1	UBA1 Ubiquitin-like modifier-activating enzyme 1	5.8	1058	117849	8	44	37

Q13509	TUBB3	TUBB3 Tubulin beta-3 chain	4.9	450	50433	62	98	37
P42704	LRPPRC	LRPPRC Leucine-rich PPR motif-containing protein, mitochondrial	6.1	1394	157904	6	42	36
Q14980	NUMA1	NUMA1 Nuclear mitotic apparatus protein 1	5.8	2115	238257	0	35	35
Q09666	AHNAK	AHNAK Neuroblast differentiation-associated protein AHNAK	6.1	5890	629114	0	35	35
Q14145	KEAP1	KEAP1 Kelch-like ECH-associated protein 1	6.4	624	69666	0	34	34
P23528	CFL1	CFL1 Cofilin-1	8.1	166	18502	0	33	33
P17858	PFKL	PFKL 6-phosphofructokinase, liver type	7.5	780	85018	3	36	33
P06733	ENO1	ENO1 Alpha-enolase	7.4	434	47169	6	38	33
P68104	EEF1A1	EEF1A1 Elongation factor 1-alpha 1	9	462	50141	54	87	33
Q06830	PRDX1	PRDX1 Peroxiredoxin-1	8.1	199	22110	1	33	32
P04792	HSPB1	HSPB1 Heat shock protein beta-1	6.4	205	22783	12	43	31
O00410	IPO5	IPO5 Importin-5	4.9	1097	123630	2	32	31
Q15021	NCAPD2	NCAPD2 Condensin complex subunit 1	6.6	1401	157182	0	30	30
Q15366	PCBP2	PCBP2 Poly(rC)-binding protein 2	6.8	365	38580	0	30	30
P30519	HMOX2	HMOX2 Heme oxygenase 2	5.4	316	36033	0	29	29
Q6AI08	HEATR6	HEATR6 HEAT repeat-containing protein 6	7	1181	128781	0	28	28
P68133	ACTA1	ACTA1 Actin, alpha skeletal muscle	5.4	377	42051	0	28	28
P62736	ACTA2	ACTA2 Actin, aortic smooth muscle	5.4	377	42009	0	28	28
P42224	STAT1	STAT1 Signal transducer and activator of transcription 1-alpha/beta	6.1	750	87335	1	28	27
Q86VP6	CAND1	CAND1 Cullin-associated NEDD8-dissociated protein 1	5.8	1230	136375	2	28	27
O14980	XPO1	XPO1 Exportin-1	6.1	1071	123386	0	26	26
P10809	HSPD1	HSPD1 60 kDa heat shock protein, mitochondrial	5.9	573	61055	10	35	25
P38646	HSPA9	HSPA9 Stress-70 protein, mitochondrial	6.2	679	73681	4	26	23
Q9Y490	TLN1	TLN1 Talin-1	6.1	2541	269765	2	23	22
O00299	CLIC1	CLIC1 Chloride intracellular channel protein 1	5.2	241	26923	0	22	22

Q14974	KPNB1	KPNB1 Importin subunit beta-1	4.8	876	97170	2	23	22
P60174	TPI1	TPI1 Triosephosphate isomerase	5.9	286	30791	4	25	22
P07737	PFN1	PFN1 Profilin-1	8.3	140	15054	6	27	21
P49588	AARS	AARS Alanine--tRNA ligase, cytoplasmic	5.5	968	106810	3	23	21
Q9Y5L0	TNPO3	TNPO3 Transportin-3	5.6	923	104203	0	21	21
P60842	EIF4A1	EIF4A1 Eukaryotic initiation factor 4A-I	5.5	406	46154	2	23	21
Q13395	TARBP1	TARBP1 Probable methyltransferase TARBP1	7.1	1621	181674	0	20	20
P53396	ACLY	ACLY ATP-citrate synthase	7.3	1101	120839	1	21	20
P46940	IQGAP1	IQGAP1 Ras GTPase-activating-like protein IQGAP1	6.5	1657	189251	3	23	20
Q9HAV4	XPO5	XPO5 Exportin-5	5.8	1204	136311	0	20	20
P55060	CSE1L	CSE1L Exportin-2	5.8	971	110417	3	23	20
Q02790	FKBP4	FKBP4 Peptidyl-prolyl cis-trans isomerase FKBP4	5.4	459	51805	2	22	20
Q9UL46	PSME2	PSME2 Proteasome activator complex subunit 2	5.7	239	27402	0	20	20
Q92598	HSPH1	HSPH1 Heat shock protein 105 kDa	5.4	858	96865	3	22	20
Q5TH69	ARFGEF3	ARFGEF3 Brefeldin A-inhibited guanine nucleotide-exchange protein 3	5.8	2177	240649	0	19	19
P52209	PGD	PGD 6-phosphogluconate dehydrogenase, decarboxylating	7.2	483	53140	0	18	18
P19174	PLCG1	PLCG1 1-phosphatidylinositol 4,5-bisphosphate phosphodiesterase gamma-1	6	1290	148532	0	18	18
Q15393	SF3B3	SF3B3 Splicing factor 3B subunit 3	5.3	1217	135577	0	18	18
Q14697	GANAB	GANAB Neutral alpha-glucosidase AB	6.1	944	106874	0	18	18
E9PPU0	EPPK1	EPPK1 Epiplakin	6	2420	264622	3	20	18
P26641	EEF1G	EEF1G Elongation factor 1-gamma	6.7	437	50119	8	25	18
P11498	PC	PC Pyruvate carboxylase, mitochondrial	6.8	1178	129634	516	533	17
P14625	HSP90B1	HSP90B1 Endoplasmin	4.8	803	92469	4	21	17
O95671	ASMTL	ASMTL N-acetylserotonin O-methyltransferase-like protein	6.1	621	68857	0	17	17

P04406	GAPDH	GAPDH Glyceraldehyde-3-phosphate dehydrogenase	8.5	335	36053	6	23	17
P15559	NQO1	NQO1 NAD(P)H dehydrogenase	8.9	274	30868	0	17	17
Q96T76	MMS19	MMS19 MMS19 nucleotide excision repair protein homolog	6.4	1030	113289	0	16	16
P07814	EPRS	EPRS Bifunctional glutamate/proline--tRNA ligase	7.3	1512	170590	1	17	16
P38606	ATP6V1A	ATP6V1A V-type proton ATPase catalytic subunit A	5.5	617	68304	0	16	16
P78417	GSTO1	GSTO1 Glutathione S-transferase omega-1	6.6	241	27566	0	16	16
P30153	PPP2R1A	PPP2R1A Serine/threonine-protein phosphatase 2A 65 kDa regulatory subunit A alpha isoform	5.1	589	65309	0	15	15
P34932	HSPA4	HSPA4 Heat shock 70 kDa protein 4	5.2	840	94331	3	18	15
Q7L576	CYFIP1	CYFIP1 Cytoplasmic FMR1-interacting protein 1	6.9	1253	145182	0	15	15
Q06323	PSME1	PSME1 Proteasome activator complex subunit 1	6	249	28723	0	14	14
O15067	PFAS	PFAS Phosphoribosylformylglycinamidine synthase	5.8	1338	144734	1	15	14
Q13200	PSMD2	PSMD2 26S proteasome non-ATPase regulatory subunit 2	5.2	908	100200	0	14	14
Q06210	GFPT1	GFPT1 Glucosamine--fructose-6-phosphate aminotransferase	7.1	699	78806	0	14	14
P48506	GCLC	GCLC Glutamate--cysteine ligase catalytic subunit	6.1	637	72766	0	14	14
P09429	HMGB1	HMGB1 High mobility group protein B1	5.7	215	24894	0	13	13
Q53FA3	HSPA1L	HSPA1L Heat shock 70kDa protein 1-like variant	6.3	641	70404	3	16	13
Q6PJG6	BRAT1	BRAT1 BRCA1-associated ATM activator 1	5.3	821	88119	0	13	13
P31948	STIP1	STIP1 Stress-induced-phosphoprotein 1	6.8	543	62639	4	17	13
Q5TFE4	NT5DC1	NT5DC1 5'-nucleotidase domain-containing protein 1	6.3	455	51845	0	13	13
Q8WXH0	SYNE2	SYNE2 Nesprin-2	5.4	6885	796457	0	13	13
Q13263	TRIM28	TRIM28 Transcription intermediary factor 1-beta	5.8	835	88550	2	15	13
P07237	P4HB	P4HB Protein disulfide-isomerase	4.9	508	57116	2	15	13
P04080	CSTB	CSTB Cystatin-B	7.6	98	11140	0	13	13
P37802	TAGLN2	TAGLN2 Transgelin-2	8.2	199	22391	2	14	13

P15170	GSPT1	GSPT1 Eukaryotic peptide chain release factor GTP-binding subunit ERF3A	5.6	499	55756	0	12	12
O00170	AIP	AIP AH receptor-interacting protein	6.3	330	37636	0	12	12
P46109	CRKL	CRKL Crk-like protein	6.7	303	33777	0	12	12
O60610	DIAPH1	DIAPH1 Protein diaphanous homolog 1	5.4	1272	141347	0	12	12
P30876	POLR2B	POLR2B DNA-directed RNA polymerase II subunit RPB2	6.9	1174	133896	0	12	12
P11586	MTHFD1	MTHFD1 C-1-tetrahydrofolate synthase, cytoplasmic	7.3	935	101559	0	12	12
P54886	ALDH18A1	ALDH18A1 Delta-1-pyrroline-5-carboxylate synthase	7.1	795	87302	0	12	12
P30046	DDT	DDT D-dopachrome decarboxylase	7.3	118	12712	0	12	12
P31939	ATIC	ATIC Bifunctional purine biosynthesis protein PURH	6.7	592	64616	4	15	12
B0V043	VARS	VARS Valyl-tRNA synthetase	7.6	1264	140466	0	12	12
Q9BTE3	MCMBP	MCMBP Mini-chromosome maintenance complex-binding protein	5.9	642	72980	0	12	12
P50990	CCT8	CCT8 T-complex protein 1 subunit theta	5.6	548	59621	2	14	12
P53618	COPB1	COPB1 Coatomer subunit beta	6	953	107142	1	12	11
Q9ULA0	DNPEP	DNPEP Aspartyl aminopeptidase	7.4	475	52428	0	11	11
Q5T4S7	UBR4	UBR4 E3 ubiquitin-protein ligase UBR4	6	5183	573849	0	11	11
Q8N1F7	NUP93	NUP93 Nuclear pore complex protein Nup93	5.7	819	93488	0	11	11
P50991	CCT4	CCT4 T-complex protein 1 subunit delta	7.8	539	57924	0	11	11
P48735	IDH2	IDH2 Isocitrate dehydrogenase	8.7	452	50909	1	12	11
Q99873	PRMT1	PRMT1 Protein arginine N-methyltransferase 1	5.4	361	41516	0	11	11
O95373	IPO7	IPO7 Importin-7	4.8	1038	119516	0	11	11
P41250	GARS	GARS Glycine--tRNA ligase	7	739	83166	0	11	11
Q9H0W8	SMG9	SMG9 Protein SMG9	7	520	57651	0	11	11
P29401	TKT	TKT Transketolase	7.7	623	67878	3	13	11
O15327	INPP4B	INPP4B Type II inositol 3,4-bisphosphate 4-phosphatase	6.3	924	104738	0	10	10
Q86X55	CARM1	CARM1 Histone-arginine methyltransferase CARM1	6.7	608	65854	0	10	10

P61978	HNRNPK	HNRNPK Heterogeneous nuclear ribonucleoprotein K	5.5	463	50976	0	10	10
P52597	HNRNPF	HNRNPF Heterogeneous nuclear ribonucleoprotein F	5.6	415	45672	0	10	10
P00966	ASS1	ASS1 Argininosuccinate synthase	8	412	46530	3	13	10
Q9NR09	BIRC6	BIRC6 Baculoviral IAP repeat-containing protein 6	6	4857	530260	0	10	10
O75153	KIAA0664	KIAA0664 Clustered mitochondria protein homolog	6.1	1309	146669	0	10	10
P41252	IARS	IARS Isoleucine--tRNA ligase, cytoplasmic	6.1	1262	144498	0	10	10
P22102	GART	GART Trifunctional purine biosynthetic protein adenosine-3	6.7	1010	107767	0	10	10
P55072	VCP	VCP Transitional endoplasmic reticulum ATPase	5.3	806	89322	3	13	10
E7EVH7	KLC1	KLC1 Kinesin light chain 1	7.3	732	83695	0	10	10
Q12931	TRAP1	TRAP1 Heat shock protein 75 kDa, mitochondrial	8.2	704	80110	1	11	10
Q07866	KLC1	KLC1 Kinesin light chain 1	6.2	573	65310	0	10	10
P23443	RPS6KB1	RPS6KB1 Ribosomal protein S6 kinase beta-1	6.7	525	59140	0	10	10
P06744	GPI	GPI Glucose-6-phosphate isomerase	8.3	558	63147	2	11	10
O15027	SEC16A	SEC16A Protein transport protein Sec16A	5.6	2179	233515	0	10	10
Q9P2J5	LARS	LARS Leucine--tRNA ligase, cytoplasmic	7.3	1176	134466	1	11	10
P16615	ATP2A2	ATP2A2 Sarcoplasmic/endoplasmic reticulum calcium ATPase 2	5.3	1042	114757	0	10	10
P13010	XRCC5	XRCC5 X-ray repair cross-complementing protein 5	5.8	732	82705	0	10	10
Q13572	ITPK1	ITPK1 Inositol-tetrakisphosphate 1-kinase	6.2	414	45621	0	10	10
P12814	ACTN1	ACTN1 Alpha-actinin-1	5.4	892	103058	4	13	10
P00558	PGK1	PGK1 Phosphoglycerate kinase 1	8.1	417	44615	3	12	10
Q9H3U1	UNC45A	UNC45A Protein unc-45 homolog A	6.1	944	103077	2	11	9
P11940	PABPC1	PABPC1 Polyadenylate-binding protein 1	9.5	636	70671	1	10	9
P62826	RAN	RAN GTP-binding nuclear protein Ran	7.5	216	24423	1	10	9
P18206	VCL	VCL Vinculin	5.7	1134	123799	1	10	9
P55786	NPEPPS	NPEPPS Puromycin-sensitive aminopeptidase	5.7	919	103276	2	10	9

Q9Y678	**COPG1**	**COPG1 Coatomer subunit gamma-1**	**5.5**	**874**	**97718**	**2**	**10**	**9**
Q8WUM4	**PDCD6IP**	**PDCD6IP Programmed cell death 6-interacting protein**	**6.5**	**868**	**96023**	**1**	**10**	**9**
P78371	**CCT2**	**CCT2 T-complex protein 1 subunit beta**	**6.4**	**535**	**57488**	**2**	**11**	**9**
P50395	**GDI2**	**GDI2 Rab GDP dissociation inhibitor beta**	**6.5**	**445**	**50663**	**2**	**11**	**9**
P53621	**COPA**	**COPA Coatomer subunit alpha**	**7.7**	**1224**	**138345**	**3**	**11**	**9**
O43592	**XPOT**	**XPOT Exportin-T**	**5.4**	**962**	**109964**	**2**	**10**	**9**
P11021	**HSPA5**	**HSPA5 78 kDa glucose-regulated protein**	**5.2**	**654**	**72333**	**3**	**11**	**8**
P62937	**PPIA**	**PPIA Peptidyl-prolyl cis-trans isomerase A**	**7.8**	**165**	**18012**	**7**	**15**	**8**
O43707	**ACTN4**	**ACTN4 Alpha-actinin-4**	**5.4**	**911**	**104854**	**4**	**11**	**7**
P63104	**YWHAZ**	**YWHAZ 14-3-3 protein zeta/delta**	**4.8**	**245**	**27745**	**3**	**10**	**7**
P40926	**MDH2**	**MDH2 Malate dehydrogenase, mitochondrial**	**8.7**	**338**	**35503**	**7**	**12**	**6**
P05166	**PCCB**	**PCCB Propionyl-CoA carboxylase beta chain, mitochondrial**	**7.6**	**539**	**58216**	**8**	**12**	**4**
P14174	**MIF**	**MIF Macrophage migration inhibitory factor**	**7.9**	**115**	**12476**	**9**	**11**	**3**
O00763	**ACACB**	**ACACB Acetyl-CoA carboxylase 2**	**6.5**	**2458**	**276539**	**26**	**28**	**2**
Q9BUF5	**TUBB6**	**TUBB6 Tubulin beta-6 chain**	**4.9**	**446**	**49857**	**41**	**32**	**-9**

Appendix Table 4.2. Mass Spectrometry data for KSC-65 treated samples. The proteins shown are those that displayed an average spectral count of 10 or greater in the KSC-65 treated sample. The data is sorted by the spectral count difference between the KSC-65 treated and the DMSO (no probe) samples.

ID	**Protein**	**Description**	**pI**	**Length(aa)**	**Mass(Da)**	**DMSO Avg**	**KSC65 Avg**	**Change in SC**
Q01813	**PFKP**	**PFKP 6-phosphofructokinase type C**	**7.6**	**784**	**85596**	**2**	**546**	**545**
P11498	**PC**	**PC Pyruvate carboxylase, mitochondrial**	**6.8**	**1178**	**129634**	**516**	**973**	**457**
P60709	**ACTB**	**ACTB Actin, cytoplasmic 1**	**5.5**	**375**	**41737**	**28**	**320**	**293**
Q71U36	**TUBA1A**	**TUBA1A Tubulin alpha-1A chain**	**5.1**	**451**	**50136**	**16**	**220**	**204**

P08238	HSP90AB1	HSP90AB1 Heat shock protein HSP 90-beta	5	724	83264	11	203	192
P05165	PCCA	PCCA Propionyl-CoA carboxylase alpha chain, mitochondrial	7.5	728	80059	94	264	170
Q96RQ3	MCCC1	MCCC1 Methylcrotonoyl-CoA carboxylase subunit alpha, mitochondrial	7.8	725	80473	157	321	164
P07900	HSP90AA1	HSP90AA1 Heat shock protein HSP 90-alpha	5	732	84660	7	153	146
O43175	PHGDH	PHGDH D-3-phosphoglycerate dehydrogenase	6.7	533	56651	4	133	129
P07437	TUBB	TUBB Tubulin beta chain	4.9	444	49671	63	180	118
P49327	FASN	FASN Fatty acid synthase	6.4	2511	273424	17	130	113
P14618	PKM	PKM Pyruvate kinase isozymes M1/M2	7.8	531	57937	36	124	88
P68371	TUBB4B	TUBB4B Tubulin beta-4B chain	4.9	445	49831	64	151	88
Q9HCC0	MCCC2	MCCC2 Methylcrotonoyl-CoA carboxylase beta chain, mitochondrial	7.7	563	61333	3	84	82
Q99536	VAT1	VAT1 Synaptic vesicle membrane protein VAT-1 homolog	6.3	393	41920	0	71	71
Q15365	PCBP1	PCBP1 Poly(rC)-binding protein 1	7.1	356	37498	1	69	68
Q13509	TUBB3	TUBB3 Tubulin beta-3 chain	4.9	450	50433	62	129	67
O76003	GLRX3	GLRX3 Glutaredoxin-3	5.4	335	37432	0	65	65
P13639	EEF2	EEF2 Elongation factor 2	6.8	858	95338	17	81	64
P68366	TUBA4A	TUBA4A Tubulin alpha-4A chain	5.1	448	49924	26	86	61
Q16881	TXNRD1	TXNRD1 Thioredoxin reductase 1, cytoplasmic	7.4	649	70756	0	55	55
P17858	PFKL	PFKL 6-phosphofructokinase, liver type	7.5	780	85018	3	55	52
P04075	ALDOA	ALDOA Fructose-bisphosphate aldolase A	8.1	364	39420	10	62	52
P21333	FLNA	FLNA Filamin-A	6.1	2647	280737	29	68	39
P10809	HSPD1	HSPD1 60 kDa heat shock protein, mitochondrial	5.9	573	61055	10	41	31
P11142	HSPA8	HSPA8 Heat shock cognate 71 kDa protein	5.5	646	70898	14	42	28
P42704	LRPPRC	LRPPRC Leucine-rich PPR motif-containing protein, mitochondrial	6.1	1394	157904	6	33	27
Q9BUF5	TUBB6	TUBB6 Tubulin beta-6 chain	4.9	446	49857	41	65	24
P15924	DSP	DSP Desmoplakin	6.8	2871	331774	4	27	23
P08243	ASNS	ASNS Asparagine synthetase	6.9	561	64370	0	22	22
Q9NQC3	RTN4	RTN4 Reticulon-4	4.5	1192	129931	0	21	21

P22314	UBA1	UBA1 Ubiquitin-like modifier-activating enzyme 1	5.8	1058	117849	8	28	21
Q00610	CLTC	CLTC Clathrin heavy chain 1	5.7	1675	191613	7	27	20
Q05639	EEF1A2	EEF1A2 Elongation factor 1-alpha 2	9	463	50470	0	19	19
P11413	G6PD	G6PD Glucose-6-phosphate 1-dehydrogenase	6.8	515	59257	2	21	19
P14625	HSP90B1	HSP90B1 Endoplasmin	4.8	803	92469	4	23	19
P35579	MYH9	MYH9 Myosin-9	5.6	1960	226530	7	26	19
Q9NY65	TUBA8	TUBA8 Tubulin alpha-8 chain	5.1	449	50094	19	38	19
P30519	HMOX2	HMOX2 Heme oxygenase 2	5.4	316	36033	0	18	18
Q06830	PRDX1	PRDX1 Peroxiredoxin-1	8.1	199	22110	1	19	18
Q8TEX9	IPO4	IPO4 Importin-4	5	1081	118715	2	19	17
O00299	CLIC1	CLIC1 Chloride intracellular channel protein 1	5.2	241	26923	0	17	17
P06733	ENO1	ENO1 Alpha-enolase	7.4	434	47169	6	22	17
P07737	PFN1	PFN1 Profilin-1	8.3	140	15054	6	23	17
P61978	HNRNPK	HNRNPK Heterogeneous nuclear ribonucleoprotein K	5.5	463	50976	0	16	16
P50990	CCT8	CCT8 T-complex protein 1 subunit theta	5.6	548	59621	2	18	16
P07237	P4HB	P4HB Protein disulfide-isomerase	4.9	508	57116	2	18	16
P04792	HSPB1	HSPB1 Heat shock protein beta-1	6.4	205	22783	12	28	16
Q8WUM4	PDCD6IP	PDCD6IP Programmed cell death 6-interacting protein	6.5	868	96023	1	16	15
P63104	YWHAZ	YWHAZ 14-3-3 protein zeta/delta	4.8	245	27745	3	17	14
Q15366	PCBP2	PCBP2 Poly(rC)-binding protein 2	6.8	365	38580	0	14	14
Q9UL46	PSME2	PSME2 Proteasome activator complex subunit 2	5.7	239	27402	0	14	14
Q14974	KPNB1	KPNB1 Importin subunit beta-1	4.8	876	97170	2	15	14
Q8TCU6	PREX1	PREX1 Phosphatidylinositol 3,4,5-trisphosphate-dependent Rac exchanger 1 protein	6.4	1659	186202	1	13	12
P60174	TPI1	TPI1 Triosephosphate isomerase	5.9	286	30791	4	16	12
P16615	ATP2A2	ATP2A2 Sarcoplasmic/endoplasmic reticulum calcium ATPase 2	5.3	1042	114757	0	12	12
O95671	ASMTL	ASMTL N-acetylserotonin O-methyltransferase-like protein	6.1	621	68857	0	11	11

Q96N66	MBOAT7	MBOAT7 Lysophospholipid acyltransferase 7	9	472	52765	0	11	11
P38646	HSPA9	HSPA9 Stress-70 protein, mitochondrial	6.2	679	73681	4	15	11
Q86VP6	CAND1	CAND1 Cullin-associated NEDD8-dissociated protein 1	5.8	1230	136375	2	12	11
P27348	YWHAQ	YWHAQ 14-3-3 protein theta	4.8	245	27764	2	12	11
P08107	HSPA1B	HSPA1B Heat shock 70 kDa protein 1A/1B	5.6	641	70052	8	19	11
Q09666	AHNAK	AHNAK Neuroblast differentiation-associated protein AHNAK	6.1	5890	629114	0	10	10
P78417	GSTO1	GSTO1 Glutathione S-transferase omega-1	6.6	241	27566	0	10	10
P78527	PRKDC	PRKDC DNA-dependent protein kinase catalytic subunit	7.1	4128	469093	0	10	10
Q53FA3	HSPA1L	HSPA1L Heat shock 70kDa protein 1-like variant	6.3	641	70404	3	12	9
O00410	IPO5	IPO5 Importin-5	4.9	1097	123630	2	10	9
P17066	HSPA6	HSPA6 Heat shock 70 kDa protein 6	6.1	643	71028	5	14	9
P49588	AARS	AARS Alanine--tRNA ligase, cytoplasmic	5.5	968	106810	3	11	8
P34932	HSPA4	HSPA4 Heat shock 70 kDa protein 4	5.2	840	94331	3	10	7
P14174	MIF	MIF Macrophage migration inhibitory factor	7.9	115	12476	9	12	3
O00763	ACACB	ACACB Acetyl-CoA carboxylase 2	6.5	2458	276539	26	28	2
P68104	EEF1A1	EEF1A1 Elongation factor 1-alpha 1	9	462	50141	54	20	-35
Q13085	ACACA	ACACA Acetyl-CoA carboxylase 1	6.4	2346	265551	243	188	-56